BNWL-1551 Vol. II
Part 1
UC-53

Battelle
Pacific Northwest Laboratories
Richland, Washington 99352

AEC Research and Development Report

PACIFIC NORTHWEST LABORATORY ANNUAL REPORT FOR 1970 TO THE USAEC DIVISION OF BIOLOGY AND MEDICINE

VOLUME II: PHYSICAL SCIENCES
PART 1. ATMOSPHERIC SCIENCES

June 1971

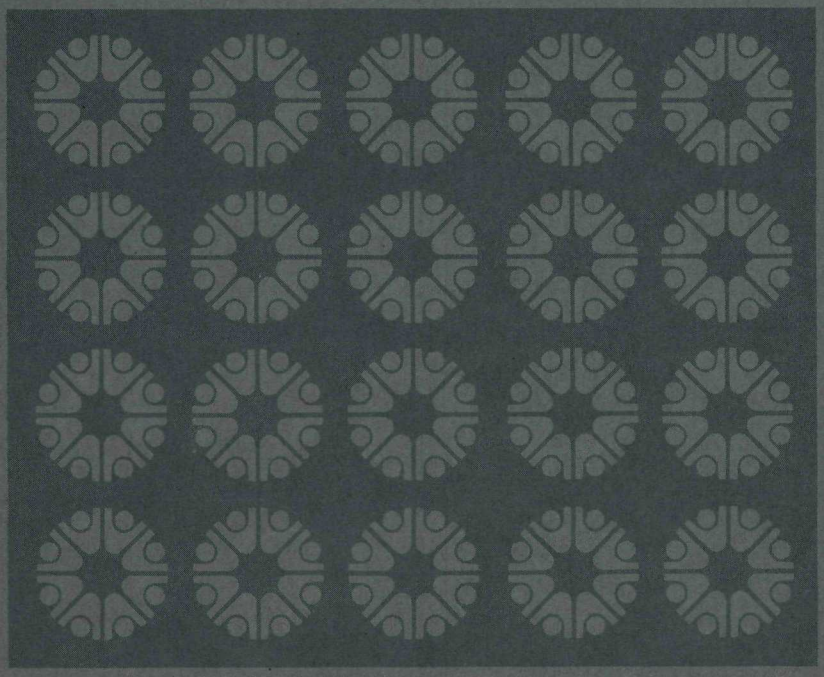

BNWL-1551 Vol. II Part 1

DISCLAIMER

PACIFIC NORTHWEST LABORATORY
operated by
BATTELLE
for the
U.S. ATOMIC ENERGY COMMISSION
Under Contract AT(45-1)-1830

BNWL-1551
Part 1
UC-53, Meteorology

PACIFIC NORTHWEST LABORATORY
ANNUAL REPORT FOR 1970
to the
USAEC Division of Biology and Medicine
VOLUME II: PHYSICAL SCIENCES
Part 1. Atmospheric Sciences

By

C. L. Simpson, Manager
and
Staff Members

of the
Atmospheric Resources Department

June 1971

BATTELLE
PACIFIC NORTHWEST LABORATORIES
RICHLAND, WASHINGTON 99352

Volume I of this report to the USAEC Division of Biology and Medicine, covering work in the Biological and Ecological Sciences, is issued as BNWL-1550, Parts 1 and 2, respectively. Volume II of the report covers work in the physical sciences and is issued in this present part, Atmospheric Sciences, and in Part 2, Radiological Sciences, BNWL-1551.

Printed in the United States of America
Available from
National Technical Information Service
U.S. Department of Commerce
5285 Port Royal Road
Springfield, Virginia 22151
Price: Printed Copy $3.00; Microfiche $0.95

FOREWORD

The series of papers in this year's ANNUAL REPORT represent substantial progress in summarizing results obtained in interdisciplinary research in atmospheric sciences. As this report is being published, a number of very important new experiments are either underway or in their final planning stages because of the developments made during the year.

In studies of atmospheric diffusion, the expansion of the ^{85}Kr diffusion grid will now permit additional tests to be conducted investigating effects of diffusion and deposition. Of particular interest is the study of transport in near calm wind conditions and in conditions of extreme atmospheric stability. Reports in this volume document the development of methodology that now makes possible the conduct of these important experiments.

In studies of precipitation scavenging, field experiments involving in-cloud and below cloud measurements were initiated on the western Washington coast. Data pertaining to the synoptic and microphysical description of the storms are being obtained to assist in interpreting artificial tracer and cosmogenic radionuclide analyses. The conduct of these tests and their subsequent analyses are a major contribution to furthering our understanding of an important mechanism for removing radioactivity from the atmosphere.

One of the major events during 1970 was the Precipitation Scavenging Symposium in Richland, jointly sponsored by the Atomic Energy Commission and the Pacific Northwest Laboratories. Approximately one hundred scientists contributed to the first international scientific meeting devoted to precipitation scavenging.

The papers summarized here give the results from last year's studies and provide a basis for furthering the understanding of atmospheric processes as they relate to the United States Atomic Energy Commission programs.

C. L. Simpson, Manager
Atmospheric Resources Department

Reports previously issued in this series are as follows:

HW-63824	July 1, 1959 - December 31, 1959
HW-70050	Period Ending December 31, 1960
HW-73337	Period Ending December 31, 1961
HW-77609	Period Ending December 31, 1962
HW-81746	Period Ending December 31, 1963
BNWL-36	Period Ending December 31, 1964
BNWL-235 Part 1	Period Ending December 31, 1965
BNWL-481 Part 1	Period Ending December 31, 1966
BNWL-715 Part 3	Period Ending December 31, 1967
BNWL-1051 Part 1	Period Ending December 31, 1968
BNWL-1307 Part 1	Period Ending December 31, 1969

BLANK

CONTENTS

BNWL-1551
Part 1

PACIFIC NORTHWEST LABORATORY
ANNUAL REPORT FOR 1970
to the
USAEC Division of Biology and Medicine
VOLUME II: PHYSICAL SCIENCES
Part 1. Atmospheric Sciences

PRECIPITATION SCAVENGING STUDIES

In the accompanying papers we report on some of the accomplishments made during 1970 in the precipitation scavenging programs. If these reports are compared with those in last year's annual report, then some of the changes in the directions of the studies become evident. Thus we are attempting to bridge the gap between results of scavenging research and the practical problems of safety analysis, and we are intensifying our efforts to understand in-cloud scavenging. Another accomplishment during 1970 was our hosting of the 1970 Precipitation Scavenging Meeting.

There are other goals toward which we are working and on which we have made progress, that are not reported here. Foremost among these is to perform in-cloud scavenging, field-research experiments, to elucidate cloud- and micro-physical aspects of scavenging. One of the experiments, which is in progress in the Cascade Range, has the objective of comparing ice-nucleation with post-nucleation scavenging; another is to determine cloud physics parameters and determine the rainout rates for pyrotechnic tracers in the maritime atmosphere at Quillayute. We are very grateful to individuals at the University of Washington, the State Department of Natural Resources, the National Weather Service station at Quillayute and the 758 U.S. Air Force Radar Squadron, at Neah Bay, without whose assistance these experiments would not be in progress. Other goals toward which we are working are to determine the snow scavenging rate as a function of the characteristics of the snow and of the contaminant, and to initiate an atmospheric aerosols experimental study, utilizing the department's recently acquired aircraft.

Looking farther into the future, we cannot help but conclude that precipitation scavenging research must become inextricably interwoven with atmospheric transport and diffusion, cloud physics, aerosol physics and chemistry, air pollution research, weather modification, and safety analysis. This conclusion follows from even the most cursory look at a practical problem. Thus, if there were a release: what are the physical and chemical

properties of the aerosol; to where will it be transported and how will it diffuse; how will it be entrained in clouds; how will it be scavenged; how will its properties, both chemical and physical, be modified in the atmosphere; and further, what, if anything, can be done (for example by modifying the weather) to decrease the potential danger of the release? It is important to tackle all these questions and with continuing support, we shall proceed to attempt to answer them.

BNWL-1551
Part 1

AEROSOL PARTICLE SIZE DEPENDENCE OF THE "RAINOUT RATE"*

W. G. N. Slinn

The concept is introduced that in-cloud scavenging of aerosol particles should be viewed as a multi-rate process. The two rates considered are: the rate of attachment of aerosol particles to cloud water and, secondly, the cloud water removal rate. Estimates of both are given and a qualitative plot is constructed, which indicates the dependence of the "rainout rate" on aerosol particle size.

Although the aerosol particle size dependence of the below-cloud scavenging (washout) rate has been evaluated theoretically in a number of papers,[1,2,3] there have been virtually no investigations of the corresponding in-cloud (rainout) problem. Following Greenfield,[4] Byutner and Gisina[5] and Zimin[1] have studied the rate of coagulation of aerosol particles with cloud droplets but, as we shall discuss below, such studies do not lead to a definitive prediction of a "rainout rate." Various authors[3,6,7,8] have looked at specific physical processes involved in the rainout process, but their results have not yet been fitted into a comprehensive model of in-cloud scavenging. Junge's,[9] Engelmann's[10] and Makhon'ko's[11] formalisms appear to be most appropriate for the prediction of the nucleation scavenging of fission product debris.

We wish to propose here that one of the reasons why the dependence of the "rainout rate" on aerosol particle size (and other properties) has not been treated adequately, is that the available conceptual framework for in-cloud scavenging was inadequate; specifically, an unequivocal "rainout rate" does not exist. Previously it has been assumed that the in-cloud scavenging process was a first-order rate process. This leads to the result that if the initial concentration of the pollutant within the cloud is χ_o (e.g., dpm m^{-3}) then subsequently

$$\chi = \chi_o \exp(-\sigma t) \qquad (1)$$

where σ is the "rainout rate." However, in this note we shall introduce the concept that, unlike the below-cloud case, in-cloud scavenging is a multi-order rate process. In particular, we shall discuss the simplest in-cloud scavenging process; that is, when only two definite events occur.

The two stages of the rainout process that we wish to discuss are: (1) the attachment of the aerosol particles to cloud droplets, and (2) the removal of the cloud droplets to the ground. Let α (sec^{-1})

*Based on a paper submitted for publication in The Journal of the Atmospheric Sciences.

be the rate of attachment of the aerosol particles to the cloud droplets. For example, for Brownian diffusional coagulation of aerosol particles with diffusivity, D (cm^2 sec^{-1}) to cloud droplets of mean radius R (cm) and number density N (cm^{-3}), then (see Junge,[9] p. 292)

$$\alpha = 4\pi \text{ DRN}. \qquad (2)$$

Further, let β (sec^{-1}) be the rate at which contaminant in the cloud water is transported to the ground (β might be interpreted also as a cloud water removal rate). An estimate of β will be given below. These two stages of the scavenging process are illustrated schematically in Figure 1. For now we shall ignore the complications that in reality, both α and β can be expected to be time dependent.

What we desire to determine is the time variation of the total concentration, χ_T, of the pollutant that resides in the cloud. First, let us identify that component of χ_T which is unattached to cloud water (i.e., that component which is in the air): χ_A. Also, let χ_{CW} be the concentration of the contaminant which is in the cloud water. By definition

$$\chi_T = \chi_A + \chi_{CW}. \qquad (3)$$

Now, χ_A varies because of its attachment to cloud water:

$$\chi_A = \chi_o \exp(-\alpha t) \qquad (4)$$

where for now we ignore other possible causes of variation of χ_A such as production, radioactive decay, evaporation of droplets, etc. and where we have assumed that initially,

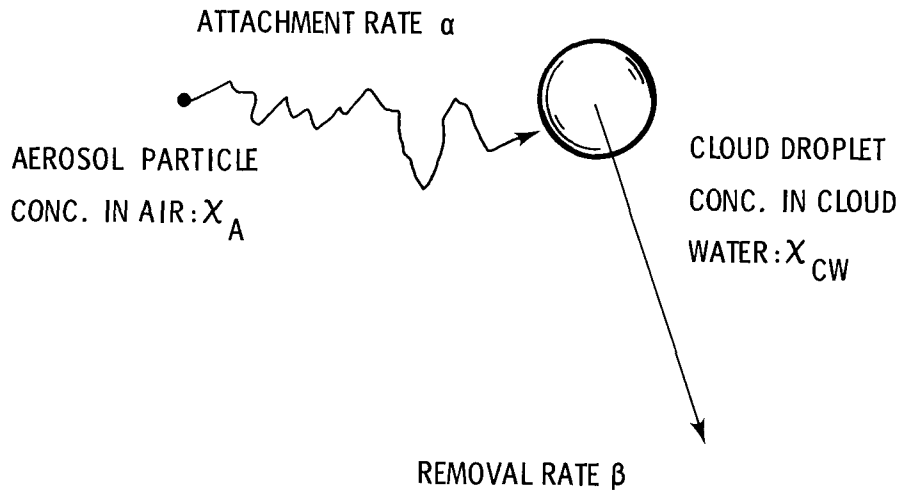

Neg 710763-1

FIGURE 1. An Illustration of Two Stages of the Rainout Process; Attachment of Aerosol Particles to the Cloud Droplets (rate, α) and Removal of the Cloud Droplets (rate, β).

$\chi_T = \chi_A = \chi_o$. On the other hand, χ_{CW} increases because of attachment of χ_A to the cloud droplets and decreases because of its removal from the cloud to the ground:

$$\frac{d\chi_{CW}}{dt} = \alpha \chi_A - \beta \chi_{CW} \qquad (5)$$

where, again, we propose to ignore other effects. Substituting (4) into (5) and assuming $\chi_{CW}(0) = 0$, and also, substituting the solution of (5) into (3) leads to the desired result

$$\chi_T = \frac{\chi_o}{\beta-\alpha} [\beta e^{-\alpha t} - \alpha e^{-\beta t}]. \qquad (6)$$

The result (6) is to be contrasted with the usual formalism (1). It demonstrates our contention that in general, a single "rainout rate" can not be identified. However, in the limiting case $\alpha >> \beta$, i.e., when the attachment rate is very rapid compared with the cloud water removal rate (e.g., for nucleation scavenging) then (6) leads to

$$\chi_T = \chi_o \exp(-\beta t) \quad , \quad (\alpha >> \beta) \qquad (7)$$

so that in this case β can be identified as the "rainout rate." On the other hand, for $\alpha << \beta$, i.e., the attachment rate is slow compared with the cloud water removal rate (e.g., as we shall see below, for Brownian diffusional coagulation scavenging of aerosol particles of radii, a $\gtrsim 0.01\ \mu$) then (6) leads to

$$\chi_T = \chi_o \exp(-\alpha t) \quad , \quad (\alpha << \beta) \qquad (8)$$

in which case α can be identified as the "rainout rate." Thus, in general, the process with the slowest rate is the rate-limiting process, and can be identified as the "rainout rate."

To obtain further appreciation of this conceptual framework for in-cloud scavenging, we must estimate β, the rate at which contaminant in the cloud water is transported to the ground. Toward this end, consider the schematic representation in Figure 2. The amount of contaminant in the cloud water within some "active volume of precipitation development," AT (where A is an arbitrary area) is χ_{CW} AT (e.g., dpm). T is an admittedly poorly-defined thickness of the region from which precipitation is emanating and if desired, χ_{CW} can be considered as an average value for this region. During dt, the amount of cloud water which is transported to the ground via a rainfall of intensity J_o (e.g., mm hr^{-1}) is $\rho J_o A\, dt$, where ρ is the density of water. If, during the growth of the cloud droplets and their subsequent transport to the ground, the contaminant is neither diluted nor concentrated, from its concentration in the cloud water of χ_{CW} (dpm per m^3 of air) or χ_{CW}/w (dpm per g of cloud water) where $w(g\ m^{-3})$ is the condensed water in the cloud, then

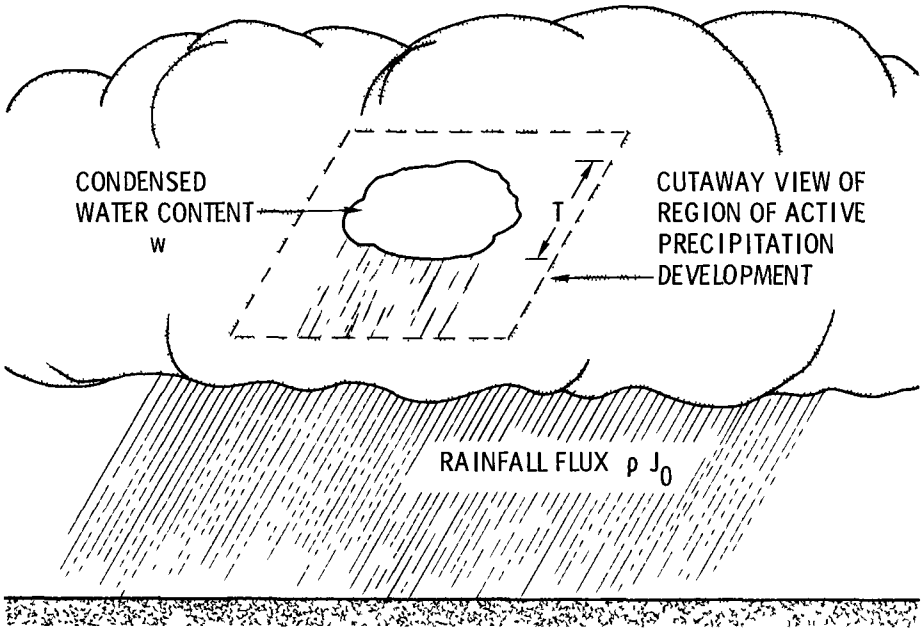

Neg 710763-3

FIGURE 2. A Schematic Identification of the Quantities Which Determine the Cloud Water Removal Rate, β.

$$\frac{d}{dt}\,(\chi_{CW}\,AT) = \alpha\,\chi_A\,AT - \frac{\rho J_o A}{w}\,\chi_{CW}. \qquad (9)$$

Thus, from this qualitative argument we can identify a removal rate

$$\beta \sim \frac{\rho J_o}{w\,T}\ (\mathrm{sec}^{-1}). \qquad (10)$$

We wish to emphasize that the above estimate of β is at best only qualitative. It would appear that both for precipitation scavenging and cloud physics research in general, further theoretical and extensive experimental study of β is justified. For example, it is desirable to know the interrelations between w,T and J_o. If we use J_o = 1 mm hr^{-1}, T = 1 km and w = 1 g m^{-3}, then (10) provides the estimate:

$$\beta \sim 1\ \mathrm{hr}^{-1}. \qquad (11)$$

Schematic results of this conceptual framework for in-cloud scavenging as a multi-rate process are illustrated in Figure 3. The dotted horizontal line is the cloud water removal rate β as given by (11). The dashed line is the attachment rate for Brownian diffusional coagulation of aerosol particles to cloud droplets with mean radius 10 μ and number density of 200 cm^{-3}. In this case [see Equation (2)], $\alpha\ (\mathrm{sec}^{-1}) \simeq D\ (\mathrm{cm}^2\ \mathrm{sec}^{-1})$. The solid curve gives the resulting "rainout

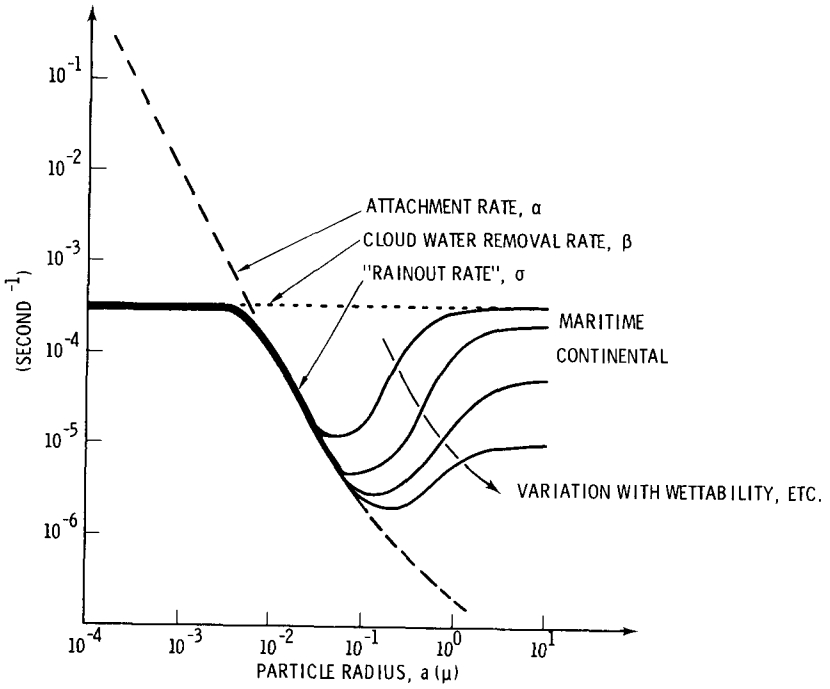

Neg 710763-2

FIGURE 3. A Qualitative Plot of the Dependence of the "Rainout Rate" on Aerosol Particle Size.

rate" - by which we mean the rate of the stage of the rainout process which limits the speed of the scavenging. For aerosol particles larger than about 0.1 μ, the curves are only qualitative. What we wish to suggest for this particle size range is that (as discussed elsewhere in this volume*) the probability that an individual aerosol particle acts as a cloud droplet nucleus, depends not only on the particle's chemical and physical characteristics, but also on the competition that it experiences with other aerosol particles, to become the favored nucleus on which water condenses. One should similarly modify the curves for smaller aerosol particles, if they act as (reverse) sublimation ice crystal nuclei. Actually, for ice crystal nuclei in a mixed cloud, then perhaps even β should be modified if the Bergeron process is operating.

In conclusion, we wish to suggest that even in its simplest form, in-cloud scavenging should be viewed as a multi-rate process. In this way, a more satisfactory conceptual framework of rainout can be obtained. For

*See "An Inquiry Into the Causes of the Variations in the Bomb Debris Scavenging Ratios" by the same author.

example, we suggest that the reason why both nucleation and natural radionuclide scavenging yield "rainout rates" in the range of 10^{-4} to 10^{-3} sec^{-1} is because, in both cases, the "rainout rate" is actually the cloud water removal rate, β.

There are a number of aspects of this analysis which require further study, especially a more adequate evaluation of β. Thus, in addition to improving on Equation (10), an attempt should be made to introduce the concepts discussed by Davis,[12] of the distinction between attachment to cloud droplets in precipitating versus nonprecipitating clouds. This could be accomplished by using time dependent rate coefficients α and β in Equations (4) and (5).

ACKNOWLEDGEMENTS

The author wishes to thank B. C. Scott and W. E. Davis for their contributions to the concepts presented here.

REFERENCES

1. *A. G. Zimin. "Mechanisms of Capture and Precipitation of Atmospheric Contaminants by Clouds and Precipitation." Problems of Nuclear Meteorology, edited by I. L. Karol' and S. G. Malakhov. Translated from a publication of the State Publishing House, Moscow, 1962. AEC-tr-6128, 1964.*

2. *W.G.N. Slinn. "Numerical Explorations of Washout of Aerosol Particles." See this volume. 1971.*

3. *W.G.N. Slinn and J. M. Hales. "Phoretic Processes in Scavenging," Precipitation Scavenging (1970), R. J. Engelmann and W.G.N. Slinn, coords., No. 22 of A.E.C. Symposium Series, available from NTIS as CONF-700601. 1970.*

4. *S. M. Greenfield. "Rain Scavenging of Radioactive Particulate Matter from the Atmosphere," J. Meteor., vol. 14, pp. 115-125, 1957.*

5. *E. K. Byutner and F. A. Gisina. "Effective Coefficient of Capture of Aerosol Particles by Rain and Cloud Droplets," JPRS-24, 490, pp. 133-151; transl. from Trudy, Leningradskii Gidrometeorologicheskii Institut, Vypusk 15. 1963.*

6. *P. Goldsmith, H. J. Delafield and L. C. Cox. "The Role of Diffusiophoresis in the Scavenging of Radioactive Particles from the Atmosphere," Quart. J. Roy. Met. Soc., vol. 89, pp. 43-61, 1963.*

7. *O. A. Vittori and V. Prodi. "Scavenging of Atmospheric Particles by Ice Crystals," J. Atmos. Sciences, vol. 24, pp. 533-538, 1967.*

8. *B. B. Hicks. "Nucleation and Wet Removal of Fallout." J. Applied Meteor., vol. 5, pp. 169-174. 1966.*

9. *C. E. Junge. Air Chemistry and Radioactivity, Academic Press, New York, 1963.*

10. *R. J. Engelmann. "The Calculation of Precipitation Scavenging," Meteorology and Atomic Energy 1968, D. H. Slade, ed., available from NTIS as TID-24190. 1968.*

11. *K. P. Makhon'ko. "Simplified Theoretical Notion of Contaminant Removal by Precipitation from the Atmosphere," Tellus XIX, pp. 467-476. 1967.*

12. *W. E. Davis. "An Interpretation of the In-Cloud Scavenging of Particulates," Pacific Northwest Laboratory Annual Report for 1969, Volume II: Physical Sciences, Part 1. Atmospheric Sciences, BNWL-1307. Battelle-Northwest, Richland, Washington, June 1970.*

BNWL-1551
Part 1

STUDIES OF IN-CLOUD SCAVENGING RATES AND MECHANISMS USING SHORT-LIVED COSMOGENIC RADIONUCLIDES

J. A. Young,* R. W. Perkins,* C. W. Thomas,*
N. A. Wogman* and B. C. Scott

Rainwater concentrations of the cosmogenic radionuclides ^{24}Na, ^{38}Cl and ^{39}Cl and their production rates from argon were measured in studies of the rates and mechanisms of in-cloud processes such as raindrop nucleation and precipitation scavenging.

The production rates of the cosmogenic radionuclides are known to increase by 2 to 3 orders of magnitude between ground level and near the top of the atmosphere, and it appears that the atom production rates of ^{24}Na:^{38}Cl:^{39}Cl are about 1:20:30 at precipitation formation altitudes. Assuming that these production ratios are correct, it can be shown that the ^{39}Cl:^{38}Cl disintegration rate ratio would be restricted to a range of 1:1 to 1.5:1 and the ^{24}Na:^{38}Cl ratios would be restricted between 0.0021:1 and 0.05:1 for a steady state production with no vertical movement of air but with precipitation scavenging allowed. Thus, the ratio of the relatively long-lived ^{24}Na to the short-lived ^{38}Cl in rainwater provides a means of determining the time period between any previous atmospheric cleansing, due to precipitation scavenging, and the present in-cloud nucleation while the ^{39}Cl:^{38}Cl ratio can be utilized to determine the raindrop development time. The short-lived cosmogenic radionuclides ^{24}Na, ^{38}Cl and ^{39}Cl were separated from 61 rainwater samples collected during the winter and spring of 1969-1970 at Richland and Quillayute, Washington, by passing the water through a fiberglass filter to remove particulates, an Al_2O_3 bed to remove ^{214}Pb and ^{214}Bi, a cation bed to remove ^{24}Na, and an anion bed to remove ^{38}Cl and ^{39}Cl. The filter and the resin beds were analyzed immediately using multidimensional gamma-ray spectrometers.

The cosmogenic radionuclide activities in the rainwater samples showed an inverse relationship between precipitation rate and activity. This indicates that at high rainfall rates the raindrops grew significantly more by condensation, which would dilute the radionuclides already present in the droplet, than in the case of light rains. In light rains growth by coalescence may be relatively more important. There is also an inverse relationship between the ratio of the long-lived to the short-lived cosmogenic radionuclides and the precipitation rate. The $^{39}Cl/^{38}Cl$ and $^{24}Na/^{38}Cl$ ratios are higher at lower precipitation rates. After

*Radiological Sciences Department

incorporation in a raindrop, the cosmogenic radionuclides decay away, with the longer-lived radionuclide decaying slower, so the ratio of the long-lived to the short-lived radionuclide increases with time. Therefore, the higher $^{24}Na/^{38}Cl$ and $^{39}Cl/^{38}Cl$ ratios in light rains indicate a longer time between drop formation and arrival at ground level in light rains than in heavy ones. If it is assumed that essentially all the radionuclides present in a raindrop are incorporated at the time of the original nucleation of the droplet around an aerosol particle, it can be calculated that times of 20 to 120 minutes are required to reach ground level. If significant amounts of cosmogenic radionuclides are incorporated after nucleation, then the times to reach ground level would be longer than calculated.

The heights and bases of the rain clouds were estimated using ceilometer and radiosonde data, therefore the total cosmogenic radionuclide content in the cloud could be calculated using the measured atmospheric concentrations. From the radionuclide concentrations in clouds and rain arriving at ground level, rainout coefficients of 10^{-4} sec^{-1} to 5×10^{3} sec^{-1} were calculated, where the rainout coefficient is defined as the fraction of the radionuclides scavenged per unit time. These high rainout coefficients indicate that scavenging is very rapid, with the radionuclide bearing aerosol being scavenged within a few minutes at the location of raindrop nucleation.

The findings are shown in Figures 1 and 2.

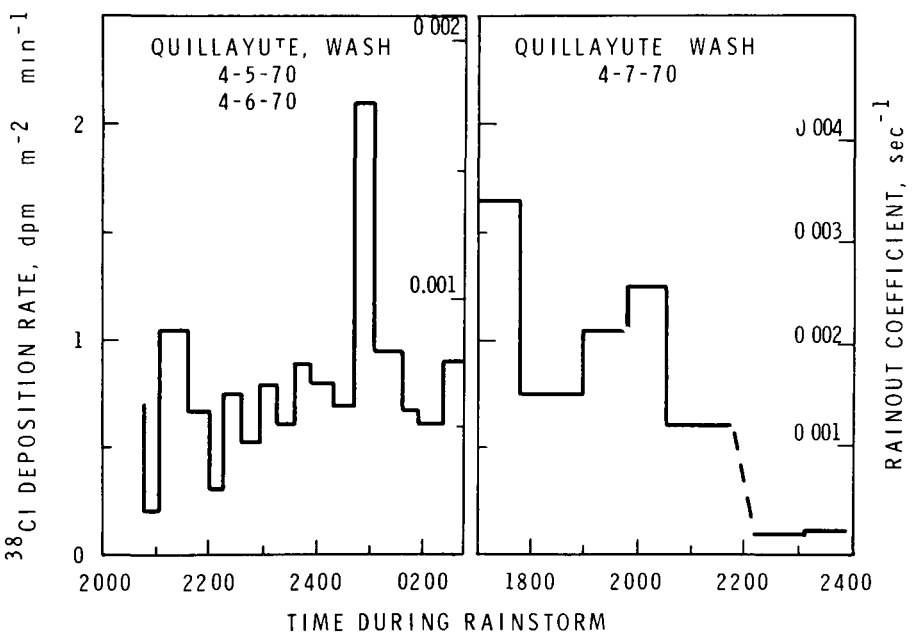

Neg 702613-8

FIGURE 1. ^{38}Cl Deposition Rates, Decay Corrected to Nucleation Times and Rainout Coefficients

FIGURE 8b

TIME PERIOD BETWEEN PREVIOUS ATMOSPHERIC CLEANSING AND PRESENT IN-CLOUD NUCLEATION

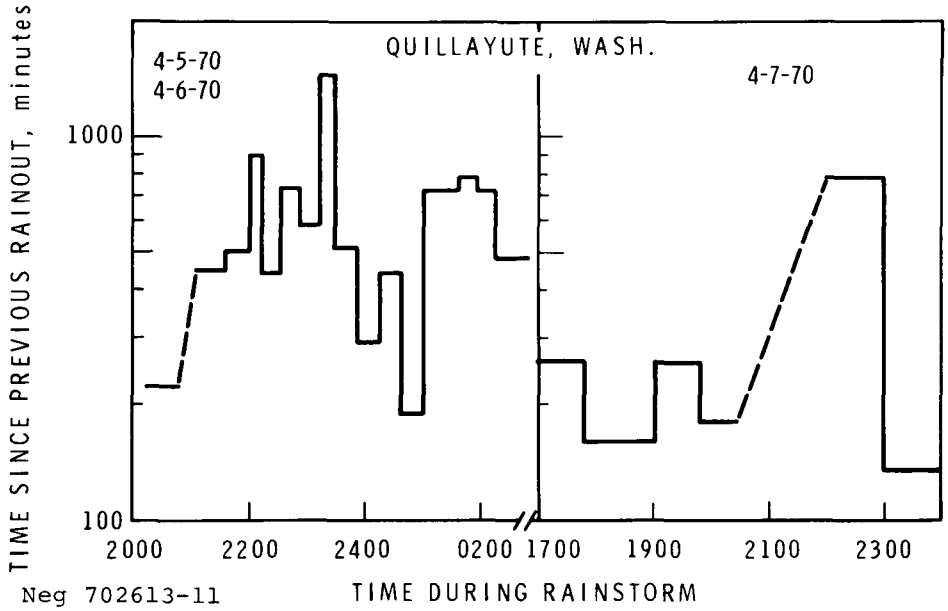

Neg 702613-11

FIGURE 2. Time Period Between Previous Atmospheric Cleansing and Present In-Cloud Nucleation

BNWL-1551
Part 1

A PRELIMINARY ANALYSIS OF COSMOGENIC RADIONUCLIDE SCAVENGING*

W. G. N. Slinn

A preliminary analysis is presented of two microphysical processes which could be responsible for the precipitation scavenging of cosmogenic radionuclides. It is tentatively concluded that the dominant mechanism responsible for the in-cloud scavenging of ^{38}Cl in continental convective clouds may be Brownian diffusional coagulation of the radionuclides directly with the precipitation embryos, whereas for ^{24}Na in maritime stratus clouds it may be cloud droplet nucleation scavenging. An approximate, time dependent scavenging ratio (κ/χ) is derived and some qualitative comparisons are made with experimental results. However, it is suggested that more aerosol and cloud physics data are needed before quantitative predictions can be made.

Perkins and co-workers[1,2] have recently reported some interesting results of the measurement of the concentration in rain water of the cosmogenic radionuclides (CRN): ^{38}Cl (37.3 min half-life), ^{39}Cl (55 min) and ^{24}Na (15 hrs). As a conceptual model for the interpretation of their data, they assumed that the dominant scavenging mechanism is the attachment of the CRN to aerosol particles which subsequently act as cloud droplet nuclei. The purpose of this present brief inquiry is to attempt to analyze the microphysical processes involved in the scavenging and thereby to assess the relative magnitudes of cloud droplet nucleation (CDN) scavenging, ice crystal nucleation (ICN) scavenging, and Brownian diffusional coagulation (BDC) scavenging. By BDC scavenging is meant the direct attachment by Brownian diffusion of the CRN to cloud droplets or ice crystals.

A necessary first step in the analysis is to consider the attachment of the CRN to natural aerosol particles in cloud free air, since it is these aerosol particles which subsequently act as cloud droplet and ice crystal nuclei. It is assumed that the CRN behave similarly to radon and thoron daughters in that, almost immediately after their creation, they exist as "primary ions;" i.e., as a cluster of about 10 atoms with a Brownian diffusion coefficient, D, of approximately 0.05 cm^2 sec^{-1} (see Reference 3, p.220). It will be seen below that an exact value for D is not needed so long as we can be sure of its order of magnitude. Via the diffusion of the CRN, they become attached to natural aerosol particles and our first goal is to determine their distribution on the aerosol particles according

Based on an article submitted for presentation at the U.S.-Australia Weather Modification Conference, September 6-16, 1971

to aerosol particle size; i.e., to determine the attachment spectrum.

We shall present first an outline of the theory used to derive the attachment spectra. Aspects of the problem have been studied by Lassen,[4] Brock[5] and others and experimental confirmation of the theory is available in the results of Chamberlain and Dyson,[6] Jacobi, et al.,[7] Soilleux[8] and others (for a review see Junge,[3] pp. 220-230). If the aerosol particles have radii r, large enough so that their diffusion can be ignored compared with the diffusion of the CRN (corrections for this and other effects will be mentioned later) and if the shortest time interval of interest is large compared with $r^2/4\ D$ (e.g., if r is as large as 100 μ, then $r^2/4\ D \lesssim 10^{-3}$ sec) then the rate of attachment of the CRN to aerosol particles can be obtained by solving the steady-state diffusion equation

$$D\ \nabla^2 n = 0 \qquad (1)$$

where n is the number density of CRN. Assuming that there is perfect retention of the CRN by the aerosol particles, then from (1) we obtain that the flux of CRN to each aerosol particle of radius r is (Dn_f/r), where n_f is the average number density of unattached CRN in the cloud-free air. Consequently, the number of CRN picked up by each aerosol particle of radius r, during dt is

$$4\pi D\ r\ n_f\ dt. \qquad (2)$$

Consider now the attachment to all aerosol particles. If the average distance between aerosol particles ($\sim N_T^{-1/3} \sim 1$ mm, for a total number density of aerosol particles, N_T, of the order of 10^3 cm^{-3}) is large compared with their average radius, $\bar{r}_f$, then interactions between the diffusion fields around each can be ignored. In this case, if there are F(r) dr aerosol particles per unit volume whose radius is between r to r + dr, then the rate of attachment of CRN to all such particles is

$$\alpha(r) \equiv 4\pi D\ r\ F(r)\ dr$$

$$\equiv K(r)\ F(r)\ dr \qquad (3)$$

where we have introduced the symbols: $\alpha(r)$ for the rate of attachment (sec^{-1}) of CRN to aerosol particles of radius r and number density F(r) dr, and K(r) for the coefficient (cm^3 sec^{-1}) for Brownian diffusional coagulation (BDC) of CRN to aerosol particles of radius r.

Before determining the attachment spectra in cloud-free air, we should consider the number of CRN available for attachment; i.e., n_f. During dt, this number changes because: Pdt are produced (where P is the production rate, CRN m^{-3} sec^{-1}); $\lambda\ n_f$ dt radioactively decay; and $\bar{\alpha}\ n_f$ dt become attached to aerosol particles, where $\bar{\alpha}$ is the average attachment rate:

$$\bar{\alpha} = 4\pi D \int_0^\infty r\ F(r)\ dr \equiv 4\pi D\ \bar{r}_f\ N_T \qquad (4)$$

in which N_T is the total number density and $\bar{r}_f$ is the average radius of the aerosol particles in the cloud-free

air. For example if $N_T = 10^3$ /cm^3 and $\bar{r}_f = 0.1\ \mu$, then $\bar{\alpha} \simeq (1\ \text{min})^{-1}$. Thus the number of aerosol particles in the cloud-free air satisfies

$$\frac{dn_f}{dt} = P - \lambda n_f - \bar{\alpha} n_f. \qquad (5)$$

If initially n_f is n_{fo}, then subsequently

$$n_f = n_{fo} e^{-(\lambda+\bar{\alpha})t} + \frac{P}{(\lambda+\bar{\alpha})} [1 - e^{-(\lambda+\bar{\alpha})t}]. \qquad (6)$$

Since for the CRN of interest $\lambda << \bar{\alpha}$, then in a time of the order of $\bar{\alpha}^{-1} \simeq 1$ min, n_f reaches a steady-state value of

$$n_f\ [t >> (\lambda+\bar{\alpha})^{-1}] \to P/\bar{\alpha}. \qquad (7)$$

The number of CRN per unit volume that are attached to aerosol particles of radius r to r + dr, say f(r) dr, where f(r) is the attachment spectrum, can be determined as follows. During dt, this number changes because an additional αn_f dt CRN attach to the aerosol particles and because λ f(r) dr dt decay. Thus from (3) and (7),

$$\frac{df}{dt} = 4\pi D\ r\ F \frac{P}{\bar{\alpha}} - \lambda f. \qquad (8)$$

If initially the spectrum is f_o, then subsequently

$$f = f_o e^{-\lambda t} + \frac{P}{\lambda} \frac{rF}{\bar{r}_f N_T} (1 - e^{-\lambda t}). \qquad (9)$$

For t large compared with the half-life of the radioactivity, there is attained the steady-state attachment spectrum

$$f\ (t >> \lambda^{-1}) \to \frac{P}{\lambda} \frac{rF}{\bar{r}_f N_T} \qquad (10)$$

or, using (3) and (4)

$$f\ dr \to \frac{P}{\lambda} \frac{\alpha}{\bar{\alpha}} \qquad (11)$$

In Figure 1 (from Brock[5]) are shown the steady-state attachment spectra for different model aerosol particle size distributions for urban, maritime and upper tropospheric aerosols. All curves have been normalized to the value unity, at r = 1 μ and they have been corrected for the noncontinuum aspects of the attachment process, which are important for the attachment to aerosol particles of radii smaller than about 0.1 μ. This correction yields[4,5] that in the general case, the attachment rates and therefore the attachment spectra are not proportional to r [see Equation (10)] but are proportional to $hr^2/(1+hr)$, where $h \simeq 7\ \mu^{-1}$. Since our major concern will be with the attachment of the CRN to aerosol particles larger than 1 μ (especially, to cloud droplets and ice crystals) we have chosen not to discuss this complication and shall use the simpler and sufficiently accurate Smoluchowski theory which we have been discussing. However, in the remaining discussion, we shall label, where appropriate, the radius r with an asterisk, r*, to remind us of this potential correction. From Figure 1 it is seen that for a low ($\lesssim$ 1 km) altitude maritime atmosphere, the bulk of the radioactivity will be attached to aerosol particles in the size range: $0.1 \lesssim r \lesssim 10\ \mu$. For urban and upper tropospheric environments (and,

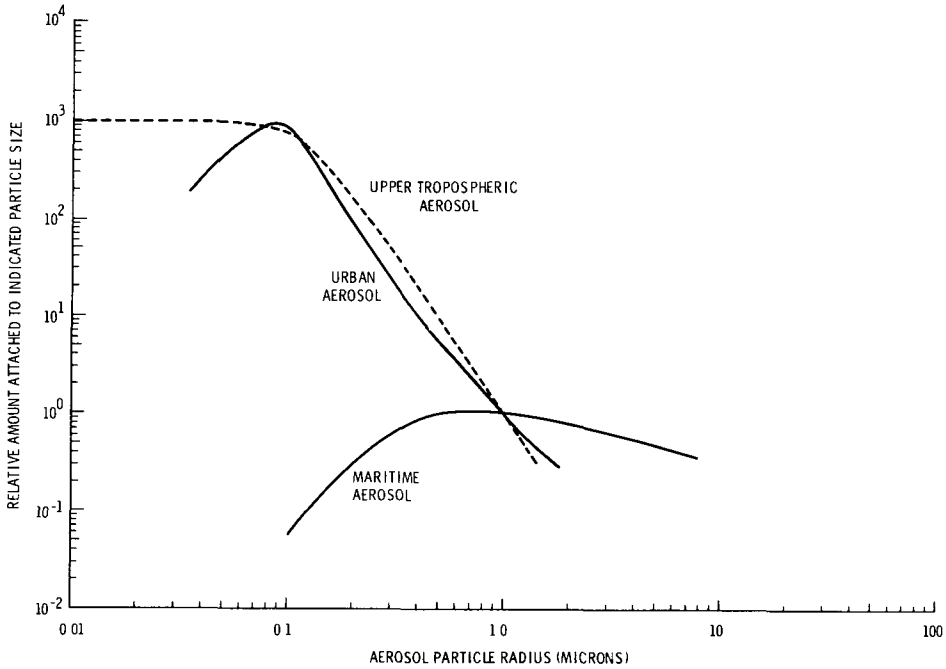

Neg 710247-8

FIGURE 1. Relative Attachment Spectra in Different Atmospheric Aerosol Environments. All curves have been normalized to the value unity, for a particle radius of 1 μ. From Brock.[5]

as will be seen later, also for continental aerosols) the bulk of the CRN will dwell predominately on aerosol particles whose radii are near or less than 0.1 μ.

What is of most concern to us in the present investigation is not the total distribution of the radioactivity according to particle size, but the activity, A, of an individual aerosol particle which subsequently, i.e., after entering a cloud, will act as a cloud droplet (CD) or ice crystal (IC) nucleus. To obtain this, we divide (10) (the steady-state radioactive burden on all aerosol particles of radius r to r+dr) by the number of aerosol particles of radius r, F(r) dr. Thus the burden of radioactivity on a single aerosol particle is

$$A = \frac{r^*}{\bar{r}_f^* N_T} \frac{P}{\lambda} \qquad (12)$$

Equation (12) is quite transparent in that it predicts that, except for the weighting factor $(r^*/\bar{r}_f^*)$, each aerosol particle shares $(1/N_T)$ parts of the total activity. Qualitatively, from the very approximate date[3,9,10] in Table 1, for similar low altitudes,

the steady-state burden of CRN on CDN in a maritime atmosphere is an order of magnitude greater than that on CDN in a continental atmosphere. Consequently the large updrafts in connective storms would probably result in CDN with a relatively small burden of CRN.

We now consider the similar problem of the attachment of CRN to all aerosol particles (i.e., including cloud droplets and ice crystals) within a cloud. We shall concentrate specifically on the case of a warm cloud but it is clear that except for a numerical factor (replacing 4π by a factor more appropriate to a non-spherical particle) the theory for the case of ice crystals is the same. As in (5), the number of CRN in the cloudy air, n_c, available for attachment, satisifies

$$\frac{dn_c}{dt} = P(z) - \lambda n_c - \bar{\alpha}_c n_c \qquad (13)$$

where $\bar{\alpha}_c$ is defined as in (4), the integral extending over the radii for all aerosol particles. In (13) we have used the symbol P(z) for the production rate, to indicate its dependence on altitude. As in (7), the steady-state value for the number of CRN available for attachment is approximately

$$n_c \left[t >> (\lambda + \bar{\alpha}_c)^{-1}\right] \rightarrow P(z)/\bar{\alpha}_c. \qquad (14)$$

Similarly, the attachment spectrum within the cloud will be

$$f_c = f_{co} e^{-\lambda t} + \frac{P(z)}{\lambda} \frac{r^* F}{\bar{r}_c^* N_T} (1 - e^{-\lambda t}) \qquad (15)$$

where $\bar{r}_c^*$ is the average radius of all aerosol particles and N_T has not changed since condensation on some aerosol particles does not change their total number, assuming that there is no natural multiplication mechanism operating in a subfreezing cloud.[11]

The corresponding steady-state attachment spectra (i.e., $t >> \lambda^{-1}$) are shown in Figure 2. Since, in general the attachment spectra are proportional to the attachment rate [see Equation (11)], the attachment rate is plotted, for then: the shapes of the curves show the distribution of the CRN according to aerosol particle size, while the magnitudes give the rate of attachment (values are given on the right hand side of Figure 2). For convenience in plotting the curves, a logarithmic scale for r is used and cumulative distributions are introduced according to

$$fdr = \frac{df}{d \log r} d \log r = \frac{r^*}{\bar{r}_f^* N_T} \frac{P}{\lambda} \frac{dF}{d \log r} d \log r. \qquad (16)$$

In Figure 2, curve 1a is a plot of Junge's[3] model aerosol particle size distribution for a ground level continental atmosphere. Curve 1c gives the corresponding attachment spectrum as given by the Smoluchowski theory, Equation (16). Curve 1b shows the

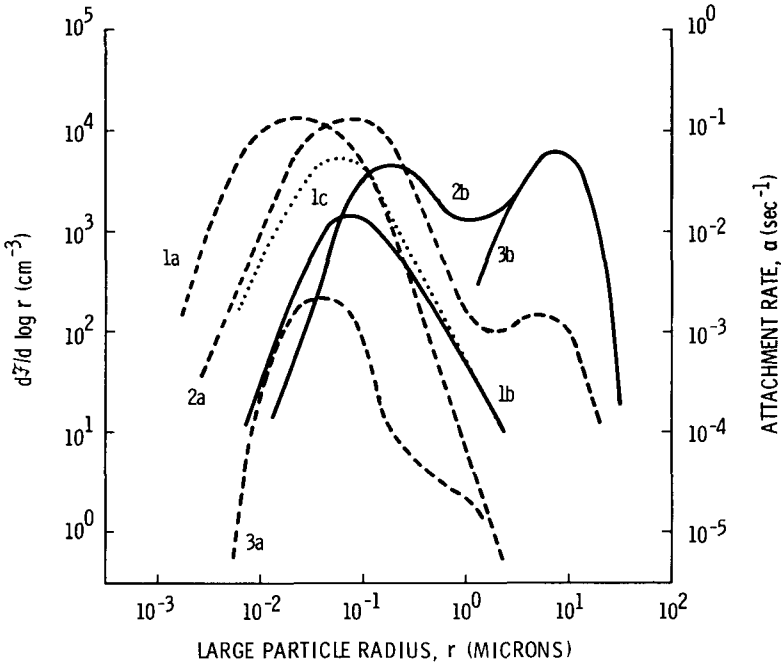

Neg 710247-3

FIGURE 2. The Attachment Spectra and Rates of Attachment (see ordinate on right hand side) for Cosmogenic Radionuclides in Different Aerosol Environments. Curve 1a: Junge's model aerosol size distribution for a continental atmosphere; Curve 2a, the modification of 1a because of condensation; 3a, schematic size distribution of aerosols in a maritime atmosphere. Curve 1b: attachment spectrum for continental aerosols (1c is obtained from the Smoluchowski theory). Curve 2b: the attachment spectrum corresponding to the aerosol distribution 2a (the large contribution at $r \gtrsim 10$ μ corresponds to attachment to cloud droplets). Curve 3b schematically indicates the attachment spectrum in a maritime cloud.

correction for the noncontinuum aspects of the attachment process as given by Lassen and Rau (see Junge,[3] p. 224). Curve 2a shows Moordy's prediction (see Junge,[3] p. 136) of the modification of the continental spectrum, arising from condensation. The "hump" at about 10 μ, corresponds to the presence in the cloud of about 200 cloud droplets per cm^3. Curve 2b gives an estimate of the corresponding attachment spectrum and demonstrates that in the steady state, a significant number of CRN would be attached to the cloud droplets. Curves 3a and 3b show qualitatively the corresponding aerosol size distribution and attachment spectrum for a maritime atmosphere.

We wish to emphasize that although these curves are useful since they demonstrate that there is rapid

attachment of the CRN to cloud droplets, they are misleading, since they are steady-state spectra and, for example, for ^{24}Na, they would not be attained unless the cloud droplet lifetime, τCD, was of the order of 15 hours. However, the spectra are quite likely to be attained by the short-lived chlorine isotopes, which suggests that for them, there is significant BDC scavenging.

To determine the burden of radioactivity on an individual cloud droplet, we proceed as before and, in addition, take the initial activity to be that of the steady-state activity on the CDN. For an average cloud droplet we obtain, as in (12),

$$A_{cd} = \frac{P(\bar{z}_{CD})}{\lambda N_T}\left[\frac{P(\bar{z}_f)\ \bar{r}^*_{CDN}}{P(\bar{z}_{CD})\ \bar{r}^*_f} e^{-\lambda t} + \frac{\bar{r}^*_{CD}}{\bar{r}^*_c}(1 - e^{-\lambda t})\right] \quad (17)$$

where $\bar{z}_{CD}$ and $\bar{z}_f$ represent average heights at which the CRN are attached to cloud droplets and their nuclei, respectively;

- $\bar{r}^*_{CDN}$ is the average radius of a CDN;
- $\bar{r}^*_f$ is the average radius of the aerosol particles in the cloud free air;
- $\bar{r}^*_{CD}$ is the average radius of the cloud drops, and
- $\bar{r}^*_c$ is the average of all aerosol particles in the cloud,

and again, the asterisk is used to indicate that the r's should be corrected for the kinetic regime of the attachment process. Actually, the second term on the RHS of (17) should also be an average over the lifetime of the cloud droplet: during its condensational growth and subsequent trajectory. This could be especially important for convective storms. However, we do not propose to pursue this complication at the present time.

To transpose (17) into more customary notation we introduce the following variables:

- $\chi(z_{CD}) = P(z_{CD})/\lambda$, (dpm/m^3) - the equilibrium concentration of CRN in the atmosphere at "cloud droplet" altitudes,
- $\kappa_{CD} = A_{CD}/(4\pi\rho\ r^3_{CD}/3)$, $(dpm/g\ H_2O)$ - the concentration of radioactivity in the cloud water;
- $w = N_{CD}\ \frac{4}{3}\pi\rho\ r^3_{CD}$, (g/m^3) - the condensed water content in the cloud, where
- $N_{CD} = \varepsilon^*\ N_T$ (cm^{-3}) - the number density of cloud droplets and ε^* - the fraction of the total number of aerosol particles which are activated as CDN.

We also introduce:

- τ_{CD} - the average lifetime of a cloud droplet, from its nucleation through the condensation process, until there is no longer significant pickup of CRN either because the drop is at a lower elevation or because, through coalescence with other cloud droplets, its area to volume ratio results in negligible κ change, or both, and
- τ_h - the average time during which there is no longer significant pickup of CRN; i.e.,

an estimate of the time for coalescence growth and subsequent fallout from the cloud of the hydrometeor.

Finally, if we ignore: concentration of the radionuclides within the precipitation arising from its evaporation; dilution because of coalescence with purer drops (which could be quite important!), and the contribution from other modes of scavenging, then from (17) we obtain that the precipitation scavenging concentration ratio for CRN will be

$$\frac{\kappa}{\chi(\bar{z}_{CD})} = \frac{\epsilon^*}{w}\left[\frac{P(\bar{z}_f)}{P(\bar{z}_{CD})}\frac{\bar{r}^*_{CDN}}{\bar{r}^*_f}e^{-\lambda\tau_{CD}} + \frac{\bar{r}^*_{CD}}{\bar{r}^*_c}(1 - e^{-\lambda\tau_{CD}})\right]e^{-\lambda\tau_h} \quad (18)$$

Conservatively, we should stop the analysis here, especially because of the many uncertainties in the cloud and aerosol physics data and because of the assumptions we have introduced. However, based on the rough data of Tables 1 and 2 we shall proceed to make the approximate estimates for the parameters in

$$\frac{\kappa}{\chi} = \mathcal{A}\left[p_s e^{-\lambda\tau_{CD}} + (1 - e^{-\lambda\tau_{CD}})\right]e^{-\lambda\tau_h}. \quad (19)$$

TABLE 1. Qualitative Aerosol Physics Data

	r^*_{CDN} (μ)	$\bar{r}^*_f$ (μ)	N_T (cm^{-3})	$A\lambda/P$ (cm^3)
Maritime (z = 0)	0.14	0.07	2×10^2	10^{-2}
Continental (z = 0)	0.25	0.05	10^4	5×10^{-4}
Altitude of ∿2 km	0.05	0.05	10^2	10^{-2}

TABLE 2. Qualitative Cloud Physics Data

	N_{CD} (cm^{-3})	$\bar{r}_{CD}$ (μ)	$\bar{r}^*_{CD}/\bar{r}^*_c$	w ($g\ m^{-3}$)	ϵ^*
Maritime (z = 0)	10^2	8	1	0.2	0.5
Continental (z = 0)	2×10^2	6	50	0.2	0.01
Altitude of ∿2 km	10^2	8	1	0.2	1

Thus, for different cloud types, we might expect order of magnitude values such as:

	$\mathcal{C}$	$\mathcal{P}$	$\mathcal{r}$
Ns	10	0.3	1
Cb	1	0.03	0.1

In addition to the above mentioned uncertainties, it should be mentioned also that there remains some uncertainty concerned with the radiological data. Thus the parameter p in (19) [$p \equiv P(\bar{z}_f)/P(\bar{z}_{CD})$] may be different for different CRN, because of the $^{40}Ar(\mu^-, n)^{39}Cl$ reaction. It has been suggested[12,13] that this reaction could contribute significantly to the ^{39}Cl production below 5 km, which would be specially important for storms with large updrafts.

Although quantitative comparisons cannot yet be made with the experimental data nevertheless, some qualitative comparisons are available. Toward this end, we show in Figure 3 a plot of the κ ratios: $\kappa(^{24}Na)/\kappa(^{38}Cl)$ and $\kappa(^{39}Cl)/\kappa(^{38}Cl)$, as given by (19),

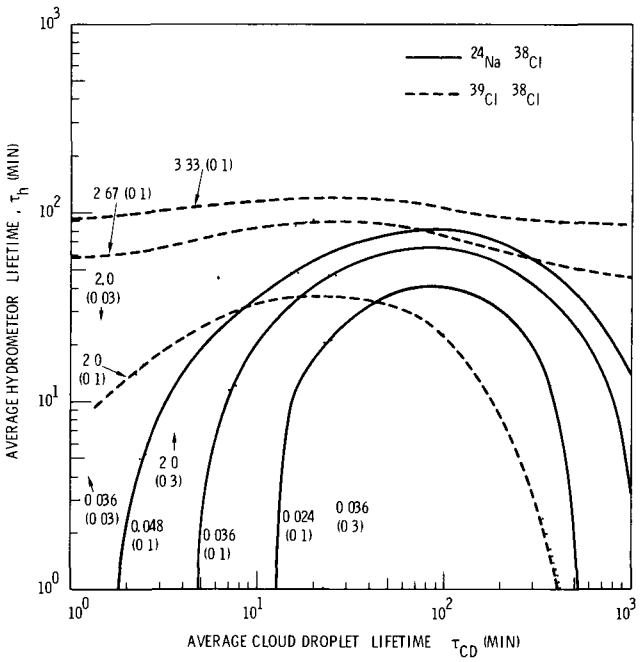

Neg 710973-3

FIGURE 3. The Ratio of Cosmogenic Radionuclide Concentrations in Precipitation as Given by Equation (18) for ^{24}Na:^{38}Cl (solid curves) and ^{39}Cl:^{38}Cl (dashed curves) as a Function of Cloud Droplet "Lifetime" and Hydrometeor "Lifetime." Assumed ratios of production rates are 1:17:35 for ^{24}Na:^{38}Cl:^{39}Cl. Values chosen for the parameters in Equation (19) are: $\mathcal{r}\mathcal{p} = 0.1$. Some curves (shown dotted) are also given for the case $\mathcal{r}\mathcal{p} = 0.3$, 0.03. Observed values for these ratios are typically 0.04 for ^{24}Na:^{38}Cl and 2.0 for ^{39}Cl:^{38}Cl. For $\mathcal{r}\mathcal{p} = 0.1$ the curves intersect for a cloud droplet "lifetime" of about 15 minutes and hydrometeor "lifetime of about 30 minutes.

as a function of the cloud droplet "lifetime" and the hydrometeor "lifetime" (see discussion above for the more exact meanings). Most curves shown in Figure 3 correspond to $\gamma_p = 0.1$ but, for comparison, some have $\gamma_p = 0.3$ and 0.03. The ratio of production rates for ^{24}Na:^{38}Cl:^{39}Cl is taken to be 1:17:35. These production rates differ from those suggested by Perkins, et al.[1,2] (1:20:30) both because of the recent measurements by Young, et al.[14] and because an attempt was made, based on the calculated rates of Bhandrai, et al.,[12] to account for the μ^- production of ^{39}Cl at elevations of about 1 km. If the ratios should, in fact, be 1:20:30, then the numbers labeling the ^{39}Cl:^{38}Cl curves should be reduced by a factor of 0.75 (e.g., 2.0 → 1.5) and those labeling the ^{24}Na:^{38}Cl should be reduced by a factor $\simeq 5/6$ (e.g., 0.048 → 0.040).

From the curves in Figure 3 and from the values for the ratios measured by Perkins, et al.[1,2] [of, typically, 2 for the $\kappa(^{39}Cl)/\kappa(^{38}Cl)$ ratio and 0.04 for $\kappa(^{24}Na)/\kappa(^{38}Cl)$] it is seen that the curves intersect for cloud droplet life times of the order of 15 minutes and average hydrometeor growth times of about 30 minutes. When it is recalled[15] that the e-fold time for coalescence growth of cloud droplets is about (2.5/w) minutes, where w is the condensed water content of the cloud in g m^{-3}, so that growth from, say, a 50 μ to a 500 μ cloud droplet would take of the order of 30 minutes if w ∿0.2 g m^{-3}, then it can be concluded that the theory is capable of predicting the observed ratios of concentrations for different radionuclides.

Other comparisons with experimental data follow more directly. Using the above values for γ_p, τ_{CD} and τ_h and using $\epsilon = 10$, leads to a κ/χ prediction, for example for ^{24}Na, of-the-order-of 1 (dpm/g H_2O)/(dpm/m^3, air). Similar predictions are easily made for the other radionuclides. These κ/χ ratios are in reasonable agreement with the experimental results. Finally, in line with our comments* that for both nucleation and Brownian diffusional coagulation scavenging of "particles" (viz., CRN) with large diffusivity, the in-cloud scavenging rate is dictated by the cloud water removal rate, then it is predicted that the "rainout rate" for CRN is in the range 10^{-3} to 10^{-4} sec^{-1}.

In summary, we sigh to suggest that, in spite of the obvious difficulties involved in predicting CRN scavenging, the potential applications of CRN in cloud physics research is significant. Thus it may be possible that the CRN can provide cloud physics research with a "clock" to measure events on the microphysical scale. Thus, even if the absolute vlues of the concentrations of CRN and the ratio of their concentrations are difficult to interpret, it may be possible to identify during an

---

*See in this volume: "Aerosol Particle Size Dependence of the 'Rainout Rate'," by the same author.

individual storm the effect of, for example, cloud seeding or orographic lift on the two "lifetimes" discussed above (see Figure 3). This potential warrants the continuation of further measurements, subject to the criterion that the experiments be designed to identify the practical applications of CRN.

REFERENCES

1. *R. W. Perkins, C. W. Thomas, J. A. Young. "Application of Short-Lived Cosmogenic Radionuclides as Tracers of In-Cloud Scavenging Processes," J. Geophys. Res., Vol. 75, pp. 3076-3087. 1970.*

2. *R. W. Perkins, C. W. Thomas, J. A. Young, B. C. Scott. "In-Cloud Scavenging Analysis From Cosmogenic Radionuclide Measurements," Precipitation Scavenging (1970), R. J. Engelmann and W.G.N. Slinn, coords., AEC Symposium Series, No. 22. Available from NTIS as CONF-700601. 1970.*

3. *C. E. Junge. Air Chemistry and and Radioactivity, Academic Press, New York, 1963.*

4. *L. Lassen. "The Distribution of Natural Radioactivity on the Different Particle Sizes in Atmospheric Aerosols," Z. Physik, Vol. 163, p. 363. 1961.*

5. *J. R. Brock. "Attachment of Trace Systems on Atmospheric Aerosols," Ibid, Reference 2, p. 339-45.*

6. *A. C. Chamberlain and A. E. Dyson. 1956. See Reference 3.*

7. *W. Jacobi, A. Schraub, K. Aurand and H. Muth. 1959. See Reference 3.*

8. *P. J. Soilleux. "A Measurement of the Size Spectrum and Charge to Total Ratio of Condensation Nuclei and Naturally Occurring Radon Daughters Attached to Them." Health Physics, Vol. 18, pp. 245-254. 1970.*

9. *I. H. Blifford. "Tropospheric Aerosols," J. Geophys. Res., Vol. 75, pp. 3099-3103. 1970.*

10. *E. S. Selezneva. "Main Features of Condensation Nuclei Distribution in the Free Atmosphere Over the European Territory of the USSR," Tellus, Vol. 18, pp. 525-531. 1966.*

11. *S. C. Mossop. "Concentrations of Ice Crystals in Clouds," Bul. Am. Met. Soc., Vol. 51, pp. 474-478. 1970.*

12. *N. Bhandri, S. G. Bhat, D. P. Kharkar, S. Krishna Swamy, D. Lal and A. S. Tamhane. "Cosmic Ray Produced Mg^{28}, Si^{31}, S^{38}, Cl^{38}, Cl^{34a} and Other Short-Lived Radioisotopes in Wet Precipitation," Tellus, Vol. 18, pp. 504-515. 1966.*

13. *D. Lal, B. Peters. "Cosmic Ray Produced Radioisotopes and Their Application to Problems in Geophysics," Progress in Elementary Particle and Cosmic Ray Physics, Vol. 6, J. G. Wilson and S. A. Wouthuysen, eds., pp. 3-74, North Holland, Pub. So., Amsterdam. 1962.*

14. *J. A. Young, C. W. Thomas and N. A. Wogman. "Cosmogenic Radionuclide Production Rates in Argon in the Stratosphere," Nature, Vol. 227, July 11, pp. 160-161, 1970, in the 1970 Annual Report to the Division of Biology and Medicine from the Radiological Sciences Department.*

A CASE STUDY OF IN-CLOUD SCAVENGING OR DIRECT PICKUP OF COSMOGENIC RADIONUCLIDES BY CLOUD WATER OR ICE

W. E. Davis

A case study was carried out for the storm of February 6, 1970 over Oregon and Washington. Results from the case study were input into a model for in-cloud scavenging of cosmogenic radionuclides and compared with ground measurements of these radionuclides. The model results indicated an in-cloud scavenging coefficient of 10^{-4} sec^{-1} to 10^{-3} sec^{-1} for ^{24}Na, ^{38}Cl and ^{39}Cl.

In order to evaluate measurements of radionuclide deposited in rainfall at Hanford through a model of in-cloud scavenging, a study was made of the February 6, 1970 storm over Washington and Oregon. Required inputs to the model study were: time of precipitation, heights of cloud base and top, cloud water content and precipitation rate along the storm's path. Diabatic trajectories[1] along with FAA reports of cloud observations were utilized to estimate cloud height. For cloud bases, surface reports of measurements or estimates of cloud base were used. The trajectories were also utilized to estimate the cloud's path and hence to determine the appropriate hourly precipitation measurements to utilize for input to the model.

The results of this study were: cloud top at 6.7 to 7.5 km with some layering expected, base of cloud at approximately 1.5 km, a time of 3 hours or more since precipitation began, and a mean precipitation rate of 0.06 in./hour. Cloud water content was estimated from the results of cloud water content studies by Ponomarenko and Zabolotskaia.[2] From the cloud water estimates and the observed surface precipitation, along the path of the storm, a dilution coefficient, i.e., the fraction of the cloud water removed by rainfall per unit time of 4×10^{-3} sec^{-1}, was calculated.

The model,[3] reported in last year's annual report, relates production of the radionuclides, their decay and their removal by scavenging to cloud water. The radionuclides in the cloud water were in turn dependent on the rate of scavenging as well as decay and dilution by rain leaving the cloud. Once the parameters affecting the dependency had been determined, the model could be utilized. The results from the model were then compared with the surface deposition after they were corrected for fall time. The results are indicated in Figures 1, 2, and 3. From these plots, the following can be concluded. An in-cloud scavenging coefficient range of 10^{-3} sec^{-1} to 10^{-4} sec^{-1} was determined for the three radionuclides, although there is not strict agreement of ^{24}Na results with compatible results of ^{38}Cl and ^{39}Cl.

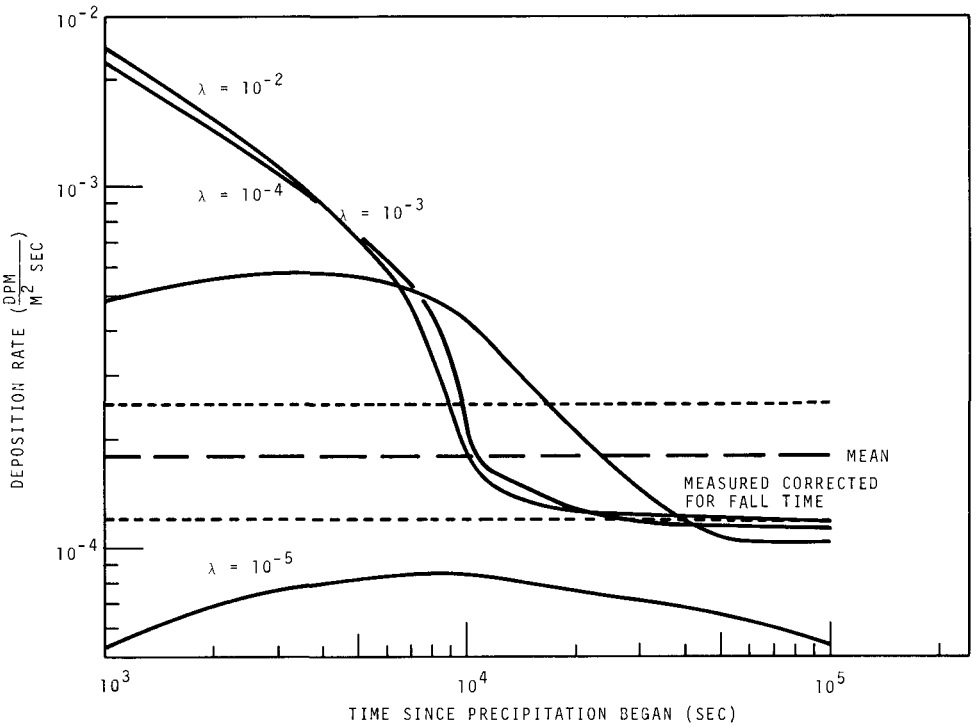

Neg 710923-2

FIGURE 1. Indirect Pickup of ^{24}Na by Water Droplets or Ice Particles

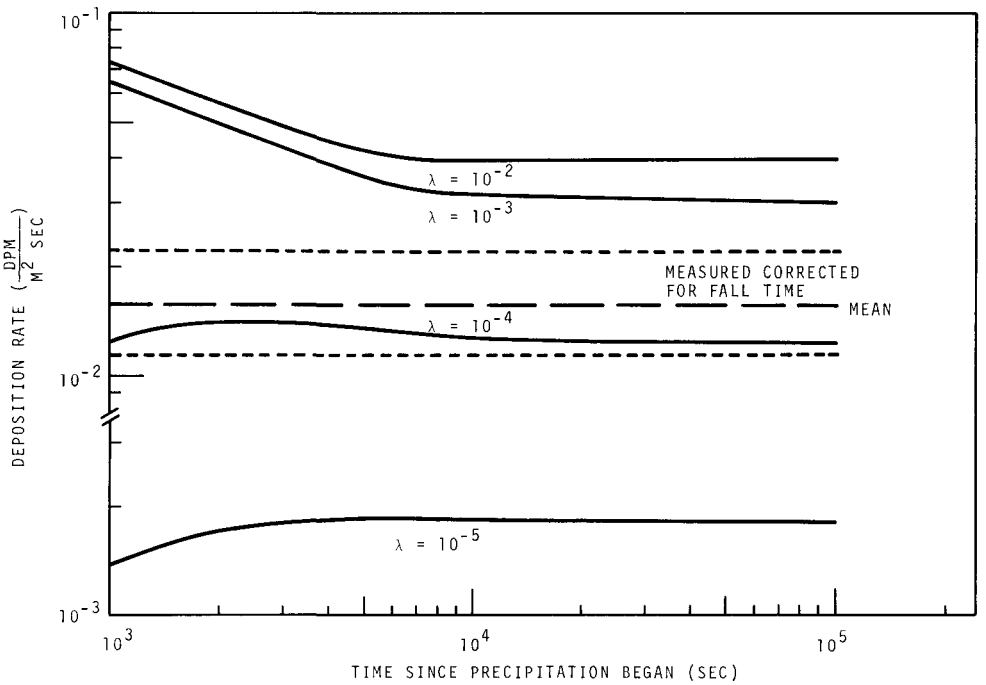

Neg 710972-3

FIGURE 2. Indirect Pickup of ^{39}Cl by Water Droplets or Ice Particles

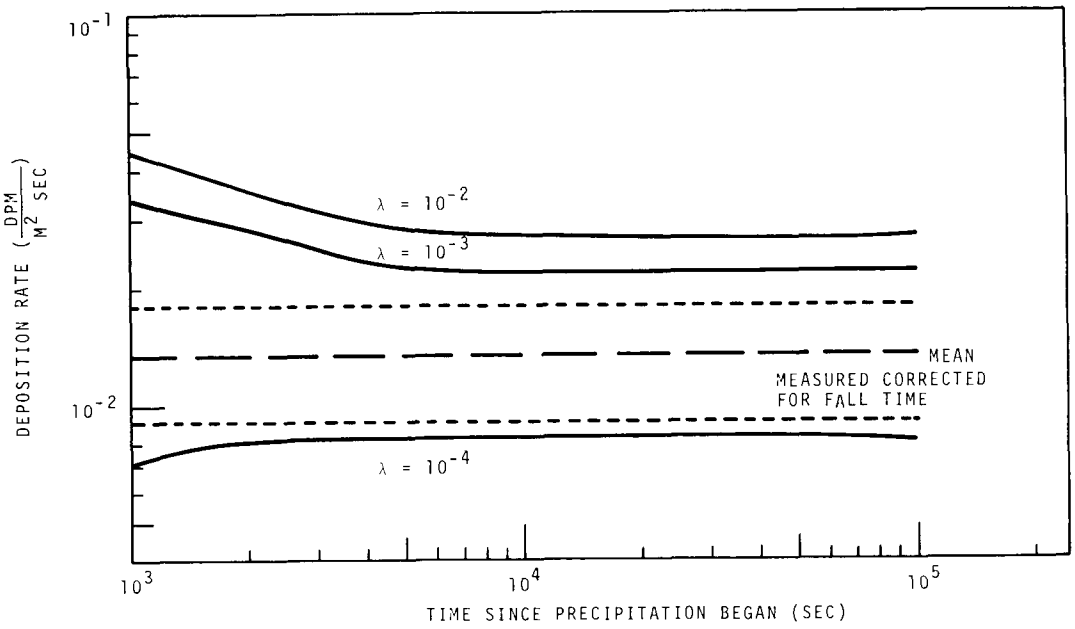

Neg 710972-4

FIGURE 3. Indirect Pickup of ^{38}Cl by Water Droplets or Ice Particles

The deposition of the three radionuclides were also computed from the model which was modified for direct pickup by the cloud droplets and ice particles of the newly produced radionuclides. All newly produced radionuclides were hypothesized to immediately attach directly to the cloud elements. In order to test this hypothesis, the model was rerun with the production term adding radionuclides directly to the cloud elements and with all other parameters the same as indicated previously. With this assumption, only ^{24}Na observations were explained by the results of the model while ^{38}Cl and ^{39}Cl deposition was overestimated. Direct attachement to cloud droplets could still be an effective removal mechanism if errors in cloud height or in the radionuclide clear air concentrations were present in this analysis. Improved understanding of the mechanism of radionuclides attachment to cloud water as well as better measurements of cloud height and liquid water content of the clouds will offer increased confidence in the results of the model presented.

REFERENCES

1. *W. E. Davis and B. C. Scott. "Diabatic Trajectories and a Trajectory Cast Study of the Effluent from Phoebus 1B EP-IV February 23, 1967," Pacific Northwest Laboratory Annual Report for 1968 to the USAEC Division of Biology and Medicine, Volume II: Physical Sciences, Part 1. Atmospheric Sciences, BNWL-1051, Part 1, UC-48, pp. 35-45, November 1969.*

2. *I. N. Ponomarenko and T. N. Zabolotskaia. Experimental Data on the Liquid-Water Content of Frontal Clouds over the Steppe Portion of the Ukraine, June 1967.*

3. *W. E. Davis. "An Interpretation of the In-Cloud Scavenging of Particulates," Pacific Northwest Laboratory Annual Report for 1969 to the USAEC Division of Biology and Medicine, Volume II: Physical Sciences, Part 1. Atmospheric Sciences, BNWL-1307, Part 1, UC-48, pp. 107-110, June 1970.*

✓ TIME CONSTANTS FOR CLOUD SEEDING AND TRACER EXPERIMENTS*

W. G. N. Slinn

Estimates are derived for some appropriate time constants for weather modification and cloud physics tracer experiments. Under the assumption that ice-nucleation proceeds via contact nucleation (rather than by reverse-sublimation) estimates are made for the recommended number densities of AgI particles that should be released and for the time intervals that should be allotted, to affect both precipitation augmentation and hail suppression. Similar estimates are given for cloud physics experiments which use tracers generated by pyrotechnic flares.

The purpose of this note is to comment on the time constants for the attachment to cloud droplets of submicron aerosol particles such AgI particles released by pyrotechnic flares and acetone generators. The experimental problem of concern is that a sufficient quantity of tracer is released and that a sufficient time is allotted, between release of the aerosol particles and their incorporation into the cloud water, so that the desired objective (be it augmenting precipitation, suppressing hail, or tracing cloud physics processes) is attained. It is expected that estimates of these time constants have been made previously and that they appear elsewhere in the literature. However, even if this is the case, it appears in the light of recent discussions at workshop meetings, that a reiteration of the results is appropriate.

For the present we seek only order-of-magnitude estimates of the appropriate time constants; the symbol $\mathcal{O}$ is used for: "of the order of magnitude of." It is assumed that the dominant attachment process is the Brownian diffusion of the aerosol particles to the hydrometeor surfaces. Thus we assume, for example, that the ice nucleation of water droplets by AgI proceeds via contact nucleation (Weickmann et al., 1970).

*Submitted for publication in The Journal of the Atmospheric Sciences.

First, consider the reduction in the number density (particles cm^{-3}) of aerosol particles which are unattached to cloud droplets; that is the reduction in n_f the number density of aerosol particles that at time t are still "free." During a time interval dt, each cloud droplet of radius R picks up (see for example, Junge, 1963, p. 292)

$$4\pi DR\, n_f\, dt \qquad (1)$$

aerosol particles, where D is their diffusion coefficient. Equation (1) describes the attachment to one cloud droplet; if there are N cloud droplets per cm^3, then the number of "free" aerosol particles will evolve according to

$$\frac{dn_f}{dt} = -(4\pi DRN)\, n_f \quad . \qquad (2)$$

$$\text{Thus } n_f = n_{fo} \exp(-t/\tau_r) \quad , \qquad (3)$$

where τ_r is the desired time constant for the reduction of the aerosol concentration:

$$\tau_r = \frac{1}{4\pi DRN} . \qquad (4)$$

If the dominant attachment is to cloud droplets (see further comments below) and if we assume that their number density is $\sigma(10^2)$ cm^{-3} and their average radius is $\sigma(10)$ μ, then (4) becomes

$$\tau_r = \sigma(D^{-1}) \qquad (5)$$

with τ_r in sec and D in cm^2 sec^{-1}. Some numerical values are given in Table 1. Typically the peak of the aerosol size distribution from acetone generators and pyrotechnic flares is between 0.01 and 0.1 μ. In this case, $\tau_r = \sigma(10)$ hours!

TABLE 1. Order-of-Magnitude of the Time Constant, τ_r, for the Reduction of the "Free" Aerosol Particle Concentration Via Attachment to Cloud Droplets

Aerosol Particle Radius, μ	10^{-3}	10^{-2}	10^{-1}
Diffusion Coefficient, cm^2 sec^{-1}	10^{-2}	10^{-4}	10^{-6}
Time Constant, τ_r, sec	10^2	10^4	10^6

Before proceeding further with this development, we should comment on other effects; for example, there could be attachment to natural aerosol particles and to hydrometeors. However, even if we ignore the kinetic correction to the diffusion process (Junge, 1963, pp. 220-225), the attachment to 10^4 natural aerosol particles per cm^3 of average radius 0.1 would result in a value for τ_r which is the same as for 10^2 cloud drops of average radius 10 μ. Thus (4) would change only by a factor of about 2. Also, even if we include the ventilation term (Slinn and Shen, 1970) which accounts for the increase in the attachment rate of aerosol particles arising from the hydrometeor's motion, the increase in the rate by a factor of about

10^3 will not compensate for its decrease by a factor of about 10^5, arising from the different number densities of 10 μ versus, say, 1 mm water drops in the cloud.

It does not follow from the above that $\mathcal{O}(10)$ hours is required for cloud seeding releases to be effective. In this case we are not so interested in the time required for the reduction in the air concentration of the aerosol particles as we are in the time required for the attachment of one AgI particle to a single cloud droplet (or raindrop). There appears to be considerable confusion about this point to which, in private discussions, this author has perhaps contributed.

To determine the time required for attachment to a single cloud drop or hydrometeor, we assume that the number density of unattached aerosol particles, n_f, is a constant. Based on the large time constant, τ_r, for their reduction, (4), this is a reasonable assumption although account should be taken of the variation in n_f because of release mechanisms, cloud updraft speeds, turbulent diffusion and so on. From (1), the number of aerosol particles picked up during a time T by a single cloud drop of radius R is

$$4\pi DR\, n_f\, T \quad . \tag{6}$$

If we include ventilation terms, then we have that (6) predicts that any sized water droplet will pick up a single submicron aerosol particle in the attachment time

$$\tau_a \simeq \frac{1}{4\pi DR\, n_f\, [1+Re^{1/2}\, Sc^{1/3}]} \tag{7}$$

where $Re = V_t\, R/\nu$ is the Reynolds number and V_t is the terminal velocity of the hydrometeor, and where $Sc = \nu/D$ is the particle's Schmidt number, in which $\nu \simeq 0.1$ cm^2 sec^{-1} is the kinematic viscosity of air.

It is clear from (7) that the time required for cloud seeding to be effective hinges on the magnitude of n_f, the number density of "free" AgI particles. Approximate relations from (7) are:

$$\text{Cloud drop } (R = 10\ \mu): \quad \tau_a \simeq \frac{10^2}{D\, n_f} \tag{8}$$

$$\text{Raindrop } (R = 1\ mm): \quad \tau_a \simeq \frac{10^{-2}}{D\, n_f} \tag{9}$$

for τ in seconds, D in cm^2 sec^{-1} and n_f in cm^{-3}. Some numerical values are given in Table 2.

The questions that now arise are concerned with how many cloud droplets or raindrops is it desirable to seed. For augmenting precipitation it may be desirable to seed only one cloud droplet per liter (for then each seeded embryo's mass might grow by the Bergeron mechanism to $\mathcal{O}(0.1)$ mg if the liquid water content of the cloud is $\mathcal{O}(0.1)$ g/m^3. In this case only one cloud droplet out of every 10^5 (if there are 10^2/cm^3) need be seeded. Thus the time required for attachment to cloud drops (Line 2 of Table 2) can be reduced by a factor of 10^5 (Line 4, Table 2). Consequently, if an attachment time $\mathcal{O}(10^3)$ seconds is allotted, then seeding should be effective (other conditions being suitable) using $\mathcal{O}(100)$ AgI particles per liter. On the other hand, if

for hail suppression it is desirable to seed all large hydrometeors (R $\simeq$ 1 mm) - there apparently being little change of seeding all cloud droplets (see Line 2, Table 2) - then to perform effective seeding in the $\mathcal{O}(10^2)$ seconds available (for updraft speeds $\mathcal{O}(10)$ m sec^{-1}), effective seeding should be possible if there are $\gtrsim \mathcal{O}(10)$ AgI particles/cm^3. This could be accomplished if $\mathcal{O}(10^{16})$ ice nuclei were dispersed within an appropriate region of the cloud, of characteristic dimension $\mathcal{O}(10)$ km.

TABLE 2. Order-of-Magnitude of the Time Constant, τ_a, for the Attachment to a Hydrometeor of a Single Aerosol Particle of Radius 0.05 μ ($D \simeq 10^{-5}$ cm^2 sec^{-1})

Number density of aerosol particles, cm^{-3}	10^5	10^3	10^1	10^{-1}	10^{-3}
Time (sec) for attachment to a 10μ cloud droplet	10^2	10^4	10^6	10^8	10^{10}
Time (sec) for attachment to a 1 mm raindrop	10^{-2}	10^0	10^2	10^4	10^6
τ_a (sec) for one of every 10^5 cloud drops	10^{-3}	10^{-1}	10^1	10^3	10^5

To obtain estimates of the required concentrations and time intervals for tracer experiments, we return to Equation (4). The amount of tracer incorporated into the cloud water during time T will be approximately

$$n = n_o (1 - e^{-T/\tau_r}) \simeq n_o \, T \, 4\pi DRN . \quad (10)$$

Therefore its concentration in cloud water will be approximately

$$n_o \, T \, 4\pi DRN/w \quad (11)$$

where w is the liquid water content of the cloud. If this concentration also appears in the precipitation reaching the ground (which would correspond to an optimum experimental situation!) then for a release of 1 kg of tracer, with $D = 10^{-5}$ cm^2 sec^{-1} in a volume of $(1 \text{ km})^3$ and for $N = 10^2$ cm^{-3} and R = 10 μ, the concentration in the rain would be $\mathcal{O}(T)$ nanograms of tracer/liter of water with T in seconds. For $T = 10^2$ to 10^3 seconds, the tracer should be detectable by activation or other analyses, provided the sampling network on the ground is sufficiently dense.

In conclusion it appears that even if electric, phoretic and turbulence

influences on the attachment rate are ignored and, especially, even if AgI acts as a contact rather than a (reverse) sublimation nucleus, rain augmentation, hail suppression, and tracer experiments are theoretically feasible.

REFERENCES

1. *C. E. Junge. Air Chemistry and Radioactivity, Academic Press, New York, 1963.*

2. *W. G. N. Slinn and S. F. Shen. "Anisotropic Brownian Diffusion and Precipitation Scavenging of Submicron Particles," J. Geophys. Res., 75, pp. 2267-2270, 1970.*

3. *H. K. Weickmann, U. Katz, and R. Steele. "Silver Iodide - Sublimation or Contact Nucleus?," Proc. of Second National Conference on Weather Modification, Am. Met. Soc., pp. 332-336, 1970.*

A NUMERICAL MODEL TO DESCRIBE OROGRAPHIC PRECIPITATION IN THE PACIFIC NORTHWEST

B. C. Scott

A two-dimensional numerical model is being developed to describe the meteorological events occurring as moisture laden air is orographically lifted over the coastal mountain ranges. The basic equations defining cloud and precipitation formation are presently being included in the model. These equations are presented and discussed.

The airflow-precipitation model is being developed in two independent segments: airflow-trajectory description, and cloud and precipitation production. The airflow segment is essentially complete, and has been described in detail elsewhere.(1) Briefly, this segment of the model calculates the steady-state trajectories of moisture laden air being orographically lifted over a mountain barrier. Data output includes vertical and horizontal wind components, and initial estimates of the cloud density at interior points within the cloud.

In the past year, some minor modifications have been made in the description of the wind field (V). Previously, d ln P/dx was assumed to vary linearly along the base streamline. Here P is pressure and x is the horizontal coordinate. This assumption resulted in large accelerations of the wind along the base streamline,

and large vertical velocities throughout much of the lower segments of the model. If the lower boundary condition specifies dV/dx to be constant along the base streamline, the model equations can also be solved. With this assumption, the pressure surfaces bow slightly and the vertical velocity profile is moderated. Hopefully, field measurements will provide some insight into which boundary condition is more appropriate. Until such a time, the model will calculate the wind field utilizing each condition, and output a velocity difference field for comparison.

An additional minor improvement includes considering a rawinsonde's horizontal motion as it rises and moves with the wind over the mountain. Thus, a slanted profile describing already perturbed values of temperature, wind and moisture is now input into the model.

Although these two changes were relatively minor in importance, they necessitated re-writing the computer program describing the first segment of the model. The program, called AIRFLOW, is now more compact and subject to easy modification. In addition, the data output is now on a rectangular grid, thus facilitating an easy transferal of data to the cloud and precipitation production routines.

CLOUD AND PRECIPITATION PRODUCTION

The airflow segment of the model merely provides an initial estimate of the cloud densities. Another set of equations will be necessary to achieve more realistic approximations. The following two-dimensional cloud and precipitation equations are presently being incorporated into the airflow model. Their derivation closely parallels the work of Kessler.[2]

Consider the continuity equation for any quantity q

$$\frac{\partial q}{\partial t} = -\left[\frac{\partial}{\partial x}(qu) + \frac{\partial}{\partial z}(qw)\right], \qquad (1)$$

where x, z, t, u, w are the horizontal distance, vertical distance, time, horizontal wind speed, and vertical wind speed, respectively. Here, let the quantity q be defined to equal the combined density of all water substance except precipitation. Thus $q = l_c + Q_s$ where l_c is the condensed water content of the cloud (g cm^{-3}), which hereafter we shall call the "cloud density" and Q_s is the saturation vapor density. The use of (1) requires that q share the motion of the air. Thus, (1) controls the distribution of the q already formed but makes no allowance for any depletion of q.

The motion of air itself is also suitably governed by the continuity equation

$$\frac{\partial \rho}{\partial t} = -\left[\frac{\partial}{\partial x}(\rho u) + \frac{\partial}{\partial z}(\rho w)\right] = 0, \qquad (2)$$

where ρ is the air density. Here, the air density is taken to be locally steady, but ρ is not required to be horizontally uniform as in Kessler's development. By substituting (2) into (1) all derivatives of the wind components are eliminated.

Further simplification is achieved by substituting r_s = mixing ratio = Q_s/ρ and noting that $\partial Q_s/\partial t$ is locally zero in the steady-state AIRFLO segment of the model. Thus, the cloud production equation to be used in the model is

$$\frac{\partial l_c}{\partial t} = -\left[u \frac{\partial l_c}{\partial x} + w \frac{\partial l_c}{\partial z}\right] + K_2 l_c + K_1. \quad (3)$$

The terms K_1 and K_2 are locally steady and specified at each grid point by the AIRFLO segment

$$K_1 = -\rho\left[u \frac{\partial r_s}{\partial x} + w \frac{\partial r_s}{\partial z}\right],$$

$$K_2 = u \frac{\partial \ln\rho}{\partial x} + w \frac{\partial \ln\rho}{\partial z}.$$

The compressibility term K_2 is on the order of 10^{-5} (sec^{-1}), and is generally 1 to 2 orders-of-magnitude smaller than the generation term K_1. As shown in (3), the change in cloud density at a point occurs because cloud advects, air compresses or expands, and air rises and saturates.

Equation (3) will be numerically integrated until a steady-state cloud density is achieved at each grid point. This particular equilibrium condition will be a description of the cloud density obtained when no condensed water is removed during cloud formation.

The initial conditions for the numerical integration will be obtained from the cloud density field produced by AIRFLO. Should the actual airflow at the upwind side of the model be initially saturated, the cloud content at the boundary will be specified either with some assumed value or with a measured value.

The mathematical description of the density of precipitation content (M) can be obtained in a manner similar to the preceding paragraphs. M is assumed to share the horizontal motion of the air, but also M is allowed to have a vertical component V relative to the air. Here V is negative since it is downwind and it is also a kind of average speed since the precipitation content at a point is distributed over particles of different sizes and fall speeds. Thus the continuity equation governing the motion of precipitation <u>already</u> formed is

$$\frac{\partial M}{\partial t} = -\left\{\frac{\partial}{\partial x}(Mu) + \frac{\partial}{\partial z} M\left[(V + w)\right]\right\}. \quad (4)$$

By using (2) to simplify, and by grouping the steady-state terms, (4) reduces to

$$\frac{\partial M}{\partial t} = -\left[u \frac{\partial M}{\partial x} + w \frac{\partial M}{\partial z}\right] - \frac{\partial}{\partial z}(MV) + M K_2. \quad (5)$$

Thus, neglecting any production or depletion, the local change of precipitation content at a point occurs because the wind advects precipitation to and from that point, because material falls from above, and because the air containing precipitation expands and contracts.

Equations (3) and (5) govern the unrelated changes of cloud and precipitation content. In the real atmosphere

the interaction of the tiny cloud droplets will eventually produce a spectrum of raindrops; i.e., Equation (3) should have depletion; Equation (5) should have production. The microphysics of this cloud-rain interaction can be broken into principally three processes: autoconversion, cloud collection, and evaporation. Autoconversion is the changing of cloud droplets to precipitation through some process such as diffusion or coalescence. Once larger drops have formed, their fall velocities carry them through a large population of cloud particles and facilitate the growth of precipitation in the cloud by the sweeping out or "collecting" of cloud particles.

The third microphysical process, evaporation, is presently not being considered. Autoconversion and cloud collection have been empirically described by Kessler.[2] His approximations are gross simplifications of the processes occurring in clouds, but they do provide a first guess of cloud physics, and establish a basis for the description of the cloud-precipitation interactions occurring in the AIRFLO model. Kessler's expressions are given without proof or derivation because the complete descriptions are available in his original work.

Autoconversion: The rate of cloud conversion into precipitation is given by

$$\frac{dM}{dt} = - \frac{dl_c}{dt} = K_3 (l_c - a)$$

$$K_3 > 0 \text{ when } l_c > a$$

$$K_3 = 0 \text{ when } l_c < a \qquad (6)$$

where K_3 is a constant, and a is some threshold value below which cloud conversion does not occur.

Cloud collection: The rate of accumulation of cloud by falling precipitation

$$\frac{dM}{dt} = K_4 \, E \, N_o^{1/8} \, l_c \, M^{7/8} \, \text{Exp} \, (K_5 z), \qquad (7)$$

where K_4 and K_5 are constants, E is the collection efficiency (presently assumed to be independent of drop diameter), and N_o is the number of rain-drops per unit volume per unit diameter range. Additional necessary relationships are

$$D_o = 8.7 \, N_o^{-1/4} \, M^{1/4} \quad [\text{cm}]$$

$$V_o = - 3830 \, N_o^{-1/8} \, M^{1/8} \, \text{Exp} \, (K_5 z) \quad [\text{cm/sec}]$$

where V_o is the terminal velocity of the raindrop of median diameter D_o. The expression for cloud collection assumes (i) that the precipitation particles are size distributed according to an inverse exponential law, and (ii) that the vertical mass transport of precipitation is based on the fall speed of the median diameter precipitation particle.

By inserting these microphysical terms into Equations (3) and (5) a description of the interaction between the two processes results:

$$\frac{\partial l_c}{\partial t} = -\left[u \frac{\partial l_c}{\partial x} + w \frac{\partial l_c}{\partial z}\right] + l_c\left[K_2 - K_3 - K_6 M^{7/8}\right] + K_1 + K_3 a,$$

$$\frac{\partial M}{\partial t} = -\left[u \frac{\partial M}{\partial z} + w \frac{\partial M}{\partial z} + \frac{\partial}{\partial z}\left(M V_o\right)\right] + M K_2 + M^{7/8} l_c K_6 + K_3 (l_c - a). \quad (9)$$

These equations will be iterated until equilibrium is achieved. The model rainfall rate will then be computed at the surface boundary points via

$$J_o = M_{SFC} V_o$$

The winter sampling of 1970-1971 in the Olympic Peninsula will provide an opportunity for some field verification of the model's accuracy, and some valuable input data. The model requires as data input a vertical sounding of the atmosphere at the inflow side and the pressure at the model mountain top. To satisfy these needs, rawinsonde data will be taken as frequently as possible during sampling periods. Additionally, a barograph has been installed on a 2000 foot high mountain to provide mountain top data near the sampling site. Aircraft measurements are expected to provide drop size distributions, inflow liquid water contents, and cloud ice distributions.

Data for model verification will come from aircraft measurements of air temperature, cloud water content, and from visual and radar observations of cloud boundaries. A ground based air defense radar will be utilized in an attempt to delineate regions of precipitation, and to obtain estimates of vertical cloud extent. Additional model verification will include measurements of surface precipitation rates.

NUMERICAL CALCULATIONS

The evaluation of Equation (9) requires numerical integration. Several finite-difference schemes are presently being tested with primary emphasis being placed upon accuracy after several iterations. Extreme care and caution is necessary in numerical modeling, especially when little definite information is available about the true solutions of the equations as is the case for Equation (9). The pseudo-diffusion introduced by many differencing schemes can eventually swamp the true solution with numerical noise or truncation error. Some compromise is necessary however. The desire for accuracy may require so much computer storage and computation time that it would be unreasonable to attempt a numerical solution.

Preliminary results of the accuracy tests indicate that a two-step modified centered difference scheme[3] will provide acceptable approximations for the advection terms. A Taylor series expansion of the production

(sink) terms appears adequate to describe their true rates of change.

REFERENCES

1. B. C. Scott. "A Numerical Model to Describe Orographic Precipitation in the Pacific Northwest," Pacific Northwest Laboratory Annual Report for 1969, Vol. II: Physical Sciences, Part 1. Atmospheric Sciences, BNWL-1307. Battelle-Northwest, Richland, Washington, June, 1970.

2. E. Kessler. "On the Distribution and Continuity of Water Substance in Atmospheric Circulations," Meteorological Monographs, Vol. 10, No. 32, published by the American Meteorological Monographs, Vol. 10, No. 32, published by the American Meteorological Society. November, 1969.

3. C. R. Molenkamp. "Accuracy of Finite-Difference Methods Applied to the Advection Equation," Journal of Applied Meteorology, Vol. 7, No. 2, pp. 160-167, American Meteorological Society, April, 1968.

THE STOCHASTIC GROWTH OF A RAIN DROPLET*

W. G. N. Slinn and A. G. Gibbs**

Two approaches are used in this theoretical analysis of the stochastic growth by a coalescence of a single, large cloud droplet (rain droplet) as it falls through cloud droplets whose sizes and spatial locations are specified statistically. In the first approach, moments are taken of a linearized, difference-kernel, coalescence equation. The first and second moments are used to predict the mean and variance of the statistical density function for the mass of the rain droplet. The results are compared with a recent numerical prediction. In the second approach, an appropriate Fokker-Planck equation is obtained. This equation is derived both from the linearized coalescence equation and from an elementary statistical model. An exact solution to the Fokker-Planck equation is derived and plots of the evolution of the statistical density function for the mass of the rain droplet are presented. These results are compared with those based on a Gaussian distribution.

In this paper we study the stochastic growth of a single, large cloud droplet (which herein we call a rain droplet) as it falls through and coalesces with smaller cloud droplets. The growth is stochastic since the size and spatial location of the cloud droplets are specified only statistically. The impetus for our work was the recent report by Chin[1] of numerical studies of the same process. Using the Monte Carlo method, he generated thirty-two computor simulations

---

* *This report is abstracted from an article with the same title which has been accepted for publication in The Journal of Atmospheric Sciences. A portion of the financial support for this work was obtained from Battelle Memorial Institute's Physical Sciences Program.*

** *Mathematics and Physics Research Department*

of a rain-droplet's growth and from these, obtained an estimate of the mean growth rate.

Our analytical study starts from the coalescence equation which, contrary to some opinions, does contain the statistical influence of both the size distribution and the random location (Poisson distribution) of the cloud droplets. If $\mathcal{F}(m,t)\,dm$ is the average number of cloud droplets per unit volume that at time t have mass between m and m + dm (or $\mathcal{F}dm$ can be interpreted as the probability per unit volume that at time t a specific droplet has mass between m and m + dm) then the time evolution of $\mathcal{F}$ arising from collisions between cloud droplets is governed by[2,3]

$$\frac{\partial \mathcal{F}}{\partial t} = 1/2 \int_0^m K(m',\, m-m')\, \mathcal{F}(m',t)\, \mathcal{F}(m - m',t)\, dm' - \int_0^\infty K(m',m)\, \mathcal{F}(m',t)\, \mathcal{F}(m,t)\, dm' \qquad (1)$$

where K(m,m') is the collection kernel which describes the physics of the collision and coalescence of cloud droplets of mass m and m'. The first term on the rhs of (1) describes the increase in the number of droplets with mass m arising from collisions between smaller droplets, and the second term describes the loss of droplets of mass m through collisions with droplets of any size.

The restriction of the analysis to the study of the growth of a rain droplet ($r \gtrsim 30\ \mu$) is utilized to justify two approximations of (1). First, if the size distribution of cloud droplets can be separated into two distinct classes as indicated in Figure 1, then (as shown in the complete manuscript) (1) can be reduced to the linear integro-differential equation:

$$\frac{\partial F(M,t)}{\partial t} = \int_0^M K(M - m,\, m)\, F(M-m)\, f(m)\, dm - \int_0^\infty K(M,m)\, F(M)\, f(m)\, dm \qquad (2)$$

where we have used the suggestive notation: F(M) for the rain droplet's size distribution function and f(m) for the cloud droplet's. Secondly, we have demonstrated that for a rain droplet interacting with cloud droplets, it is adequate to approximate the collection kernel. Two approximations studied in detail are:

$$K = a\, M \quad (cm^3\ sec^{-1}) \qquad (3)$$

and

$$K = M\, g(m) - h(m) \qquad (4)$$

where a is a constant and g and h are essentially arbitrary functions of m.

Using the kernel, (4), we have shown that the moments of the rain droplet's size distribution function must satisfy

$$\frac{dF_n}{dt} = \sum_{j=o}^{n-1} \binom{n}{j} \left[I_{n-j} F_{j+1} - J_{n-j} F_j \right] \quad (5)$$

where the parenthetical expression is the binomial coefficient and I_n and J_n are known moments of the cloud droplet's size distribution function

$$\left[I_n, J_n \right] = \int_o^\infty dm\, m^n f(m) \left[g(m), h(m) \right]. \quad (6)$$

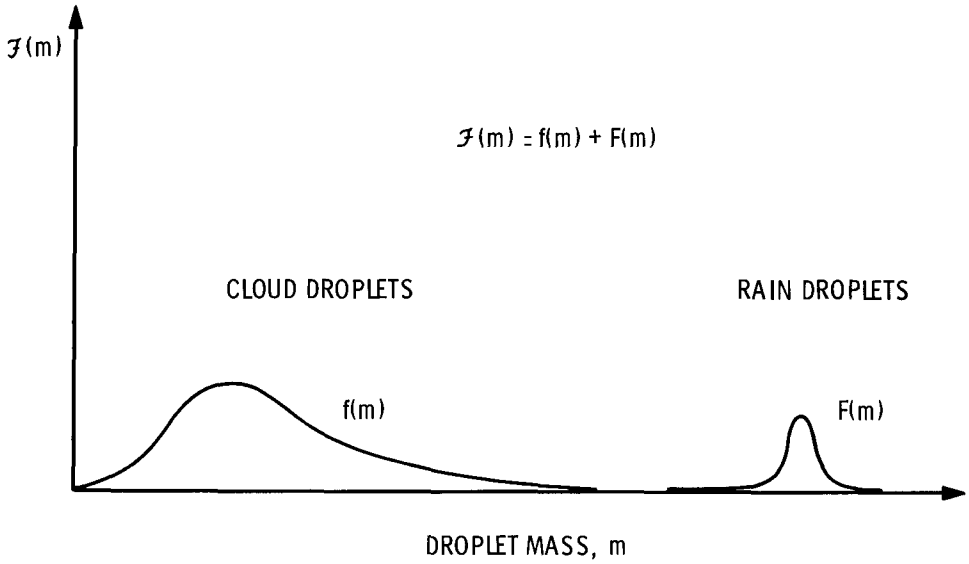

Neg 710068-2

FIGURE 1. Assumed Decomposition of ℱ(the Statistical Density Function for the Mass, for all Water Droplets) into f (the Density Function for the Cloud Droplets) and F (for the Rain Droplets).

As an example of the solutions to (5), we have considered the case with g(m) = b and h(m) = bm, where b is a constant, and with f(m) given by the Khrgian-Mazin[4] spectrum:

$$f(r) = c\, r^2 \exp\left(-\frac{3r}{\langle r \rangle}\right) \quad (7)$$

where $$c = \frac{3}{4\pi\rho} \frac{L}{5!} \left(\frac{3}{\langle r \rangle}\right)^6 \quad (8)$$

and where r is the radius of a cloud droplet; <r> is their average radius, and L is the liquid water content of the cloud measured in g cm^{-3}. For this case the mean mass of a rain droplet is given by

$$\langle M \rangle - F_1 = \frac{28}{5} \langle m \rangle + \left(M_o - \frac{28}{5} \langle m \rangle\right) e^{bLt} \quad (9)$$

where <m> is the mean mass of the cloud droplets. Thus for large time the mass grows exponentially with time constant of approximately (2.5/L')

minutes, where L' is the liquid water content in g m^{-3}. For large time the variance of the mass distribution becomes

$$\sigma^2 \equiv F_2 - F_1^2 \sim \frac{28}{5} \langle m \rangle (M_o - 10 \langle m \rangle) e^{2bLt}. \quad (10)$$

A comparison of our results with Chin's[1] is shown in Figure 2. The mean growth of the mass, (9), is shown by the center curve. We have chosen the same data as used by Chin; in particular, the specific value for b was chosen so that our curve for the mean mass would agree with Chin's at t = 1000 sec. The pair of outer curves (i.e., the top and bottom curves) give the interval, symmetric about the mean, which contains 95% ($\simeq \pm 2\sigma$) of the area under an assumed Gaussian distribution for the mass, with variance given by Equation (10). The "error bar" at t = 1000 sec is Chin's result for the interval of 95% confidence of his value for the mean. Our results for this interval ($\pm 1.96\sigma/32^{1/2}$, where the number 32 arises from the number of simulations performed by Chin) are shown by the pair of inner curves. In Figure 3 we have shown the evolution of the radius of a rain droplet whose initial radius is 50 μ. The outer curves give the range within which resides 95% of the probability distribution for the mass.

In addition to studying the evolution of the moments, we have studied also the evolution of the entire statistical density function for the mass. From (2) using the kernel (3), and also from an elementary statistical model, we derived the Fokker-Planck equation:

$$\frac{\partial P}{\partial t} + \beta(t) \frac{\partial MP}{\partial M} = \gamma(t) \frac{\partial^2 MP}{\partial M^2} \quad (11)$$

where

$$(\beta, \gamma) = a \int_o^\infty dm\, f(m,t)\, (m, m^2/2) \quad (12)$$

are moments of the (assumed time dependent) cloud droplet size distribution function, and where we have changed notation from F to P to emphasize that different approximations are involved. The solution to (12) subject to the initial condition

$$P(M, t \to o) = \delta(M - M_o) \quad (13)$$

was found to be

$$\phi(M',\tau) = \left(\frac{M'M_o}{\tau^2}\right)^{1/2} I_1\left[2\left(\frac{M'M_o}{\tau^2}\right)^{1/2}\right] \exp\left[\frac{-(M'+M_o)}{\tau}\right] \quad (14)$$

where $\phi = MP$ (15)

$$M' = M \exp\left[-\int_o^t \beta(t)\, dt'\right] \quad (16)$$

$$\tau = \int_o^t \gamma(t') \exp\left[-\int_o^{t'} \beta(t'')\, dt''\right] dt' \quad (17)$$

and I_1 is the modified Bessel function of first order. This solution, along with a Gaussian distribution G(M,t) whose mean and variance were

found by taking moments of (11), are plotted in Figure 4. It is seen that the two functions, P and G, are almost indistinguishable.

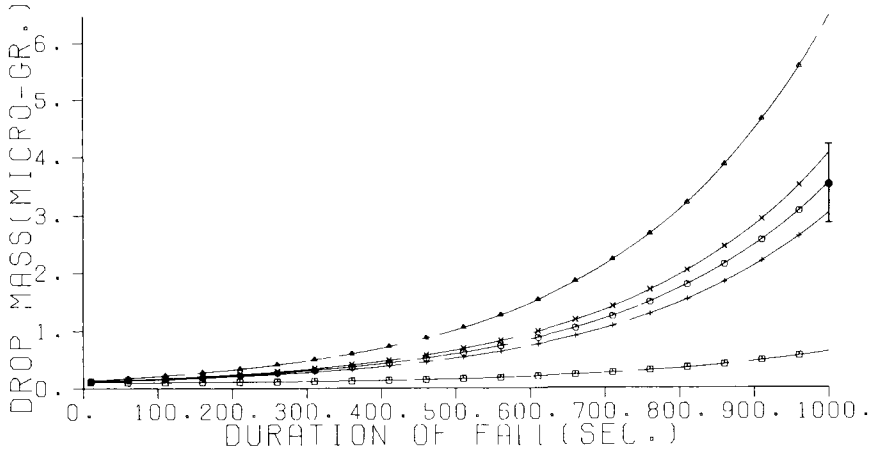

Neg 710068-4

FIGURE 2. The Mean Growth of the Mass (center curve) and Variation About the Mean, for a Rain Droplet of Initial Radius 30 μ. Cloud physics data: $L = 1$ g m^{-3}, $\langle r \rangle = 7.5$ μ and (see text) $b = 3.66 \times 10^3$ g^{-1} sec^{-1}. The two outer curves (△ and □) contain 95% of the area under an assumed Gaussian distribution for the mass. The two inner curves (X and +) show our prediction of Chin's estimate for the mean. His result is shown as the "error bar" at 1000 sec.

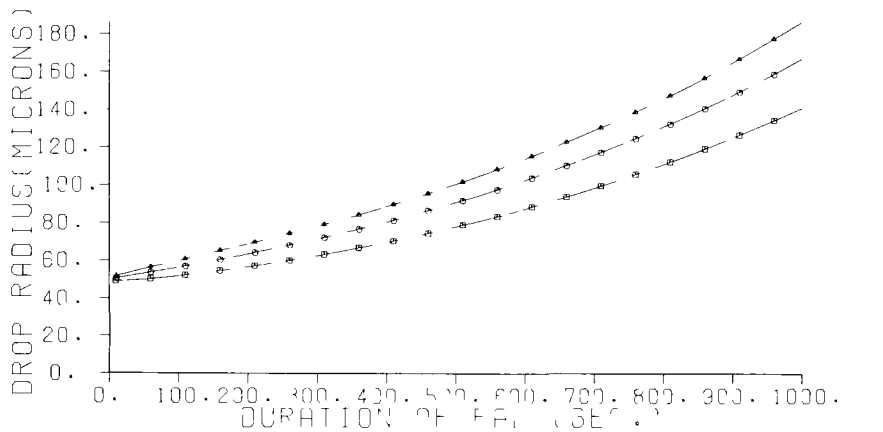

Neg 710068-3

FIGURE 3. The Mean Growth of the Radius (center curve) for a Rain Droplet of Initial Radius 50 μ, Growing in the Same Cloud as for Figure 2. The two outer curves show the range of R values, in which is contained 95% probability for the mass.

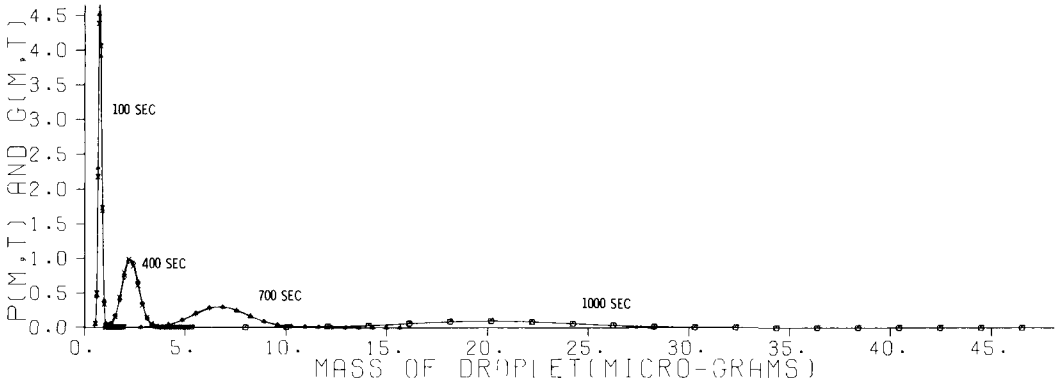

Neg 710068-1

FIGURE 4. The Time Evolution of the Statistical Density Function for the Mass of a Rain Droplet, Initial Radius 50 μ, Growing in a Cloud with L = 1 g m^{-3}, $\langle r \rangle$ = 7.5 μ and (see text) a = 3.66 × 10^3 cm^3 g^{-1} sec^{-1}. Both the solution to the Fokker-Planck equation (P) and a Gaussian distribution (G) are plotted, but the curves are almost indistinguishable.

These calculations have generated a number of interesting results. The comparison of (14) with a Gaussian distribution, G, suggests that the true solution to (2), for a delta function initial condition, is close to G. What is certain is that it is much more reasonable to use G than the cumbersome formula (14). Furthermore, we thereby gain more confidence in our assumption, used for Figures 2 and 3, that the distribution is Gaussian.

Our comparison with Chin's result is quite satisfactory in view of the assumptions we have made, especially about the form of the collection efficiency. In addition our results have the standard advantages of analytical solution (over numerical solutions) that different cloud physics and rain droplet data may easily be used. Also, from (5), we can proceed to obtain higher moments of the distribution and thereby obtain estimates of its skewness, kurtosis, etc.

A further result of this analysis is that, hopefully, we have been able to shed a little light on the foundations of the coalescence theory. For example, Scott[5] states: "Warshaw[6] has claimed that the usual kinetic equation for cloud droplet growth by coalescence treats only the average behavior of droplets and not the deviation from it. This conclusion is erroneous." That Scott is correct, that is, "that solutions to the kinetic coalescence equation contain the probabilities of all possible histories of droplet growth, and not just their average behavior" is demonstrated in our Figure 4. Thus, we obtained the Fokker-Planck equation from the coalescence equation; if it described

only the average behavior of a droplet, then the delta function initial condition would have remained a delta function.

As another example, Chin's wording. "previous investigations of the cloud droplet growth process were usually based on the assumption of a homogeneous and isotropic cloud. In this study this restriction is temporarily removed by introducing random positioning of cloud droplets..." suggests that the coalescence equation does not contain this information. That this is not true (and also, confer Scott,[5]) can be seen from our two derivations that led to the identical Fokker-Planck equation. one, directly from the coalescence equation, and the other (not described here) from an elementary statistical model in which was used a Poisson distribution for the spatial distribution of the cloud drops.

Finally, our ability to solve for the moments of F, or to obtain the solution to the Fokker-Planck equation, for the case of a time dependent cloud droplet distribution allows us to investigate the resulting change in the growth rate of a rain droplet. Thus Berry[2] has determined that compared with the stochastic model, the continuous model underestimates the mean growth rate by a factor of about 6. He states: "the major reason for this is that all the water mass moves with the mode in the stochastic model, whereas in the continuous model, most water mass must remain on the small droplets." We have not been able to determine this factor of 6, mentioned by Berry, since in our case f(m,t) must be specified, but perhaps it is useful to have the formalism available into which experimental values for β and γ (Equation 12) or I_n and J_n (Equation 6) can be substituted, in the event that the factor, 6, is not realistic.

REFERENCES

1. *H. C. Chin. "Simulation of the Cloud Droplet Collection Process," Proc. Conf. on Cloud Physics, Aug. 24-27, 1970, Ft. Collins. Amer. Met. Soc., pp. 119-120. 1970.*

2. *E. X. Berry. "Cloud Droplet Growth by Collection," J. Atmos. Sc., Vol. 24, pp. 688-701. 1967.*

3. *W. T. Scott. "Analytic Studies of Cloud Droplet Coalescence I," J. Atmos. Sc., Vol. 25, pp. 54-65. 1968.*

4. *A. M. Borovikov, A. Kh. Khrgian and Others. Cloud Physics. Clearinghouse, OTS-63-11141. 1961.*

5. *W. T. Scott. "Comments on 'Cloud Droplet Coalescence Statistical Foundations and a One-Dimensional Sedimentation Model'." J. Atmos. Sc., Vol. 25, p. 150. 1968.*

6. *M. Warshaw. "Cloud Droplet Coalescence: Statistical Foundations and a One-Dimensional Sedimentation Model." J. Atmos. Sc., Vol. 24, pp. 278-286. 1967.*

A FINITE-DIFFERENCE APPROXIMATION FOR EQUATIONS DESCRIBING THE FORMATION OF CLOUD AND PRECIPITATION

B. C. Scott

A set of partial differential equations can be used to describe the formation and growth of cloud and precipitation. The complex spatial dependence of the coefficients in the equations makes an analytic solution intractable and requires that the solutions be obtained numerically. A finite-difference approximation of the general equations has been developed and used to compute solutions for trial cases where the analytic solutions were known. The numerical results are presented and compared with the analytic solutions. In general, the numerical approximations produced quite acceptable results.

The development of a numerical airflow model by Scott* has resulted in a set of partial differential equations which govern the formation and growth of cloud and precipitation. Specifically these equations are of the general form

$$\frac{\partial A}{\partial t} = - u \frac{\partial A}{\partial x} - w \frac{\partial A}{\partial z} - k_1 A + k_2 \qquad (1)$$

where A is any property, and u, w, x, z, t are the horizontal wind, vertical wind, horizontal coordinate, vertical coordinate, and time respectively. The properties u, w, k_1 and k_2 are independent of time and specified at each point. The terms k_1 and k_2 are generally positive but <<1, and represent decay and production of A, respectively.

A numerical integration is required in order to solve Equation (1). The selected procedure must satisfy three basic requirements; i.e., the initial distribution of A must be properly advected, the boundary conditions must be specified in a manner that allows the passage of A through the boundaries without introducing distortions or oscillations in A, and finally, the terms k_1 and k_2 must properly operate on the advecting A distribution.

Several finite-differencing schemes have been used to approximate advection terms. Molenkamp[1] has demonstrated that the extensively used upstream-differencing scheme produces highly unsatisfactory results. His studies also indicated that the two-step process of Lax-Wendroff[2] and the Arakawa approximations[1,3,4] are poor approximators of advection. Schemes which produce excellent results are available, but they require excessive computor storage and

*See, "A Numerical Model to Describe the Orographic Precipitation in the Pacific Northwest," by B. C. Scott in this report.

computation time. See, for example, Roberts-Weiss.[5] The present discussion concentrates on the results of approximating the advection terms of (1) with a two-step centered-difference scheme.

In general, if only the advection terms are considered in (1), the centered-difference approximation would be

$$A^{n+1}_{j\,k} = A^{n-1}_{j\,k} - \mu_{j\,k}\,(A^{n}_{j+1\,k} - A^{n}_{j-1\,k}) - \xi_{j\,k}\,(A^{n}_{j\,k+1} - A^{n}_{j\,k-1})$$

$$\mu_{jk} = \frac{u_{j\,k}\,\Delta t}{\Delta x},\quad \xi_{j\,k} = \frac{w_{j\,k}\,\Delta t}{\Delta z} \qquad (2)$$

where $A^{n}_{j\,k}$ is the value of A at grid point j, k and at time n. If Δx and Δz are the horizontal and vertical spacing between adjacent rows or columns of grid points and Δt is the time increment, $x = j\,\Delta x$, $z = k\,\Delta z$, and $t = n\,\Delta t$. The steady-state velocity components at the j, k grid point are given by $u_{j\,k}$ and $w_{j\,k}$.

Equation (2) can be extended to a two-step process by halving the time step[1]

$$A^{n+1/2}_{j\,k} = A^{n-1/2}_{j\,k} - \frac{\mu_{j\,k}}{2}\left[A^{n}_{j+1\,k} - A^{n}_{j-1\,k}\right] - \frac{\xi_{j\,k}}{2}\left[A^{n}_{j\,k+1} - A^{n}_{j\,k-1}\right],$$

$$A^{n+1}_{j\,k} = A^{n}_{j\,k} - \frac{\mu_{j\,k}}{2}\left[A^{n+1/2}_{j+1\,k} - A^{n+1/2}_{j-1\,k}\right] - \frac{\xi_{j\,k}}{2}\left[A^{n+1/2}_{j\,k+1} - A^{n+1/2}_{j\,k-1}\right]. \qquad (3)$$

The number of computations is reduced if the points with <u>both</u> j and k even or odd, $A^{n}_{j\,k}$ is evaluated at integral times, and at the other points $A^{n}_{j\,k}$ is evaluated at half-integral times.

The finite-difference approximation (3) was applied to several trial problems in order to test its accuracy, and to provide some understanding of the scheme's numerical characteristics. The first problem defined an initial circular distribution of A such that

$$A(x,z,o) = 1 - \frac{r}{8\Delta} \qquad \text{for } r < 8\Delta$$

$$A(x,z,o) = 0 \qquad \text{for } r \geq 8\Delta,$$

where Δ is the grid spacing, and r is the distance from the maximum value of A. This distribution of A was placed in a velocity field which was rotating with constant angular velocity Ω about an axis normal to the grid points. The solution to (1), (advection only) when governed by these conditions, is then merely a pure displacement about the axis of rotation (see Figure 1).

Figure 2 shows the calculated A distribution after 40 time iterations.* Isolines of A have been advected at a velocity less than Ω and the amplitude of A has been damped near the center. There has

Forty time steps used in all trial cases because 40 is roughly the number of iterations needed to advect the slowest air parcel through the grid of Scott's numerical airflow model. A strict stability criterion has been assumed; i.e.,

$$\frac{u\Delta t}{\Delta x} < 1 \text{ and } \frac{w\Delta t}{\Delta z} < 1.$$

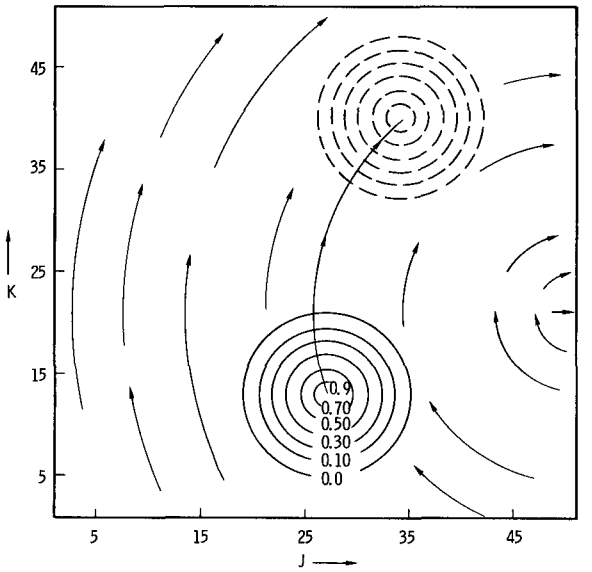

Neg 710923-3

FIGURE 1. The Displacement of the Property A in a Rotating Velocity Field. The axis of rotation is perpendicular to the solid arrow. The direction of motion is indicated by the remaining arrows. The dashed figure marks the time location of A after a movement corresponding to 40 time iterations.

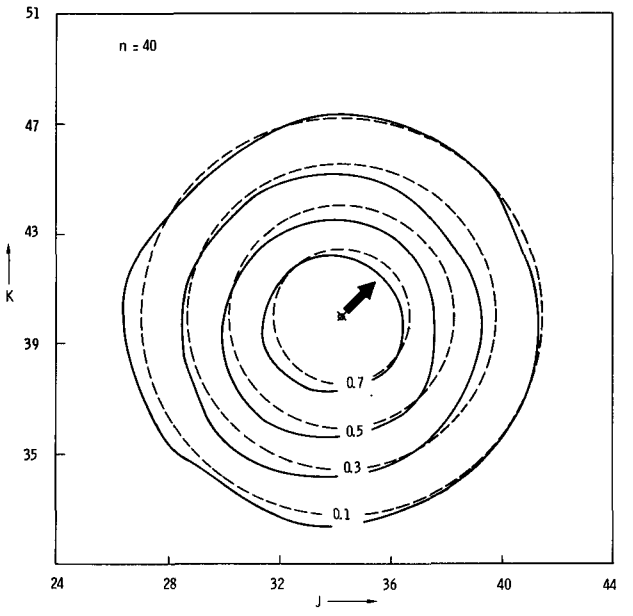

Neg 710923-7

FIGURE 2. The Computed A Distribution. Solid isolines are calculated values of A. The dashed curves represent the correctly advected A field and have values equal to the nearest solid curve. The arrow marks the present direction of movement.

also been some distortion of the initial circular A which most likely results from the inability of the difference scheme to handle the discontinuities in the A gradient at the center and at the edge of the initial distribution. An irregular oscillation of A occurs over the entire grid with maximum amplitude near the region where A was initially nonzero. Negative values of A have not been allowed, and this appears to prevent the oscillations from growing significantly with time. In spite of those shortcomings, A has been advected quite satisfactorily.

For the second case study, a rectangular initial A distribution was selected to determine how accurately the two-step difference scheme would advect and rotate the A distribution in the sheared wind field of case study one (see Figure 3). Figure 4 presents the results after 40 iterations. Although A was damped and was advected with a velocity slightly less than Ω, the rotation of A was accomplished satisfactorily. This same trial case was run for 80 time steps with a step interval equal to one-half the original size; i.e., the rectangle advects the same total distance in both cases. Truncation error appeared to be equivalent for both cases and only very minor differences were observed.

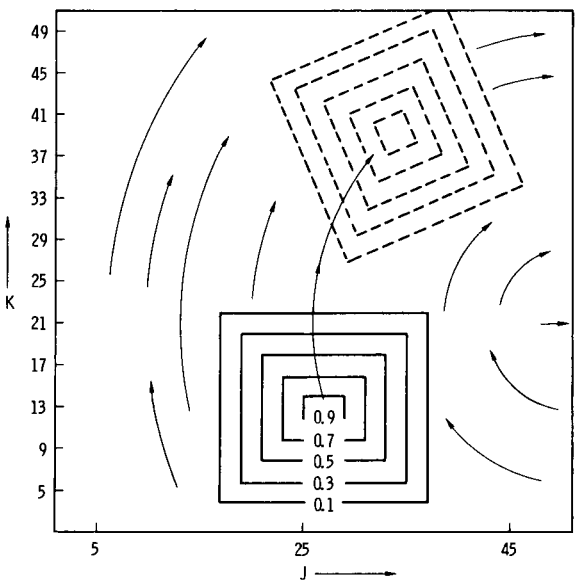

Neg 710923-2

FIGURE 3. The Advection of a Rectangular A Field. The displacement of the property A in a rotating velocity field. The axis of rotation is perpendicular to the solid arrow. The direction of motion is indicated by the remaining arrows. The dashed figure marks the time location of A after a movement corresponding to 40 time iterations.

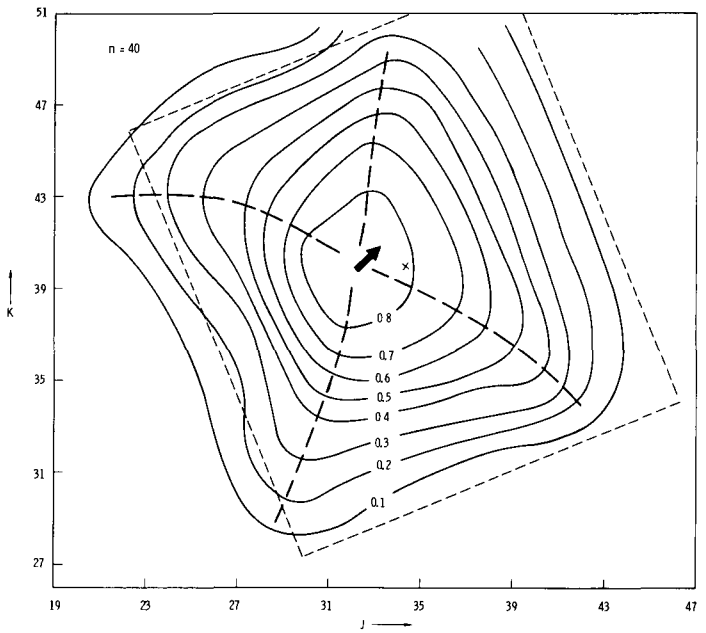

Neg 710923-10

FIGURE 4. The Computed Rectangular A Distribution. The dashed rectangle marks the 0.1 isopleth of the correctly advected rectangle. The remaining two dashed curves mark the diagonals of the computed rectangle. Solid isolines are calculated values of A. The dashed curves represent the correctly advected A field and have values equal to the nearest solid curve. The arrow marks the present direction of movement.

In the above two case studies, the property A was not allowed to touch the grid boundaries. In the airflow model, cross boundary flow must be specified. Several boundary schemes have been tried, most of which either were poor approximations, or became unstable when the sink and production terms were added. The scheme finally selected takes the average of the three slopes shown in Figure 5. Thus a value outside the grid, say $A^n_{j+1\ k}$ for example, is defined as

$$A^n_{j+1\ k} = \left[2\ (A^n_{j\ k-1} + A^n_{j\ k+1} + A^n_{j-1\ k}) - A^n_{j-1\ k-2} - A^n_{j-1\ k+2} - A^n_{j-3\ k}\right]/3$$

Figure 6 shows the sequence of events as the circular A distribution of the first case study is advected through the boundary. Again, distortion and damping take place, but the general features of A remain clearly distinguishable.

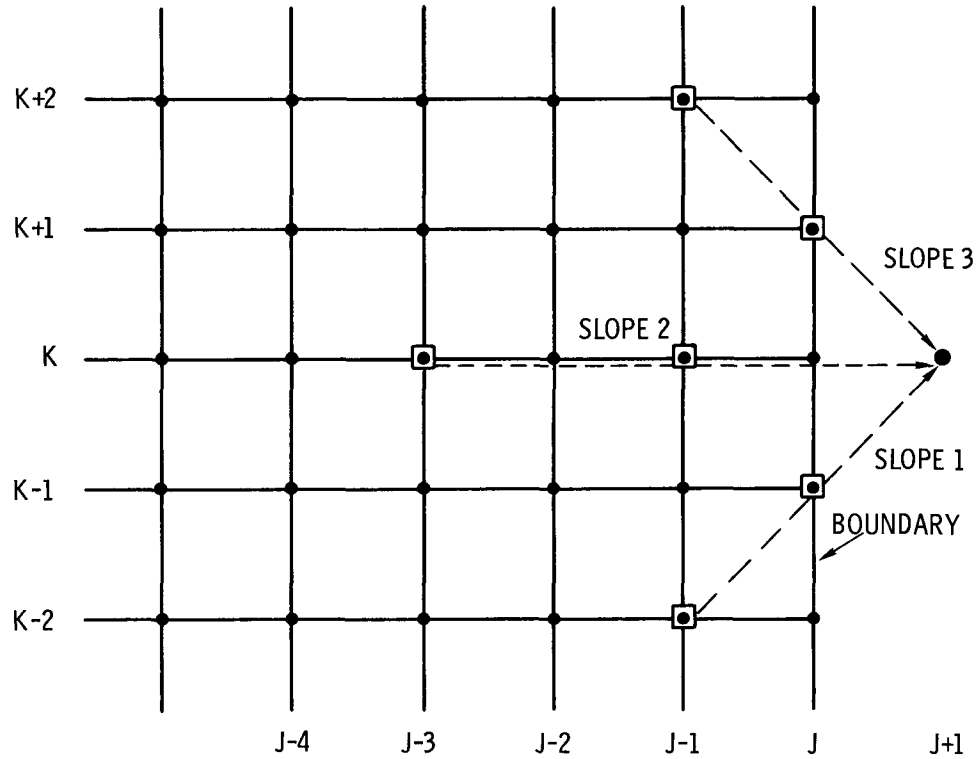

Neg 710923-1

FIGURE 5. The Scheme Used to Approximate the Value of a Point Outside the Numerical Grid.

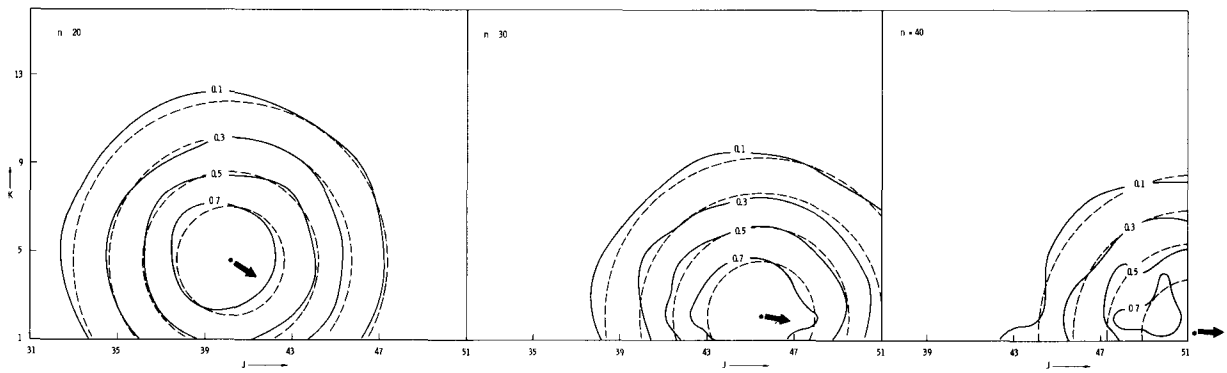

Neg 710923-11

FIGURE 6. The Advection of a Circular A Distribution Through the Boundaries. Figure 6-a is at 20 iterations, 6-b at 30 iterations, and 6-c at 40 iterations. Solid isolines are calculated values of A. The dashed curves represent the correctly advected A field and have values equal to the nearest solid curve. The arrow marks the present direction of movement.

Now by ignoring the advection terms in (1), there results an equation describing the growth* of A

$$\frac{\partial A}{\partial t} = - k_1 A (x,z,t) + k_2. \qquad (4)$$

If the spatial dependence of A is neglected, then the function A(t) can be approximated with a one-dimensional Taylor's series expansion

$$A(t) = A(t_o) + \frac{dA}{dt}\Big|_{t_o} (t - t_o) + \frac{d^2A}{dt^2}\Big|_{t_o} \frac{(t - t_o)^2}{2!} + \ldots \qquad (5)$$

Utilizing (4) and rewriting in finite-difference notation, (5) can be expressed as**

$$A_{j\,k}^{n+1} = A_{j\,k}^{n} + (k_2 - k_1 A_{j\,k}^{n}) \Delta t + (k_1^2 A_{j\,k}^{n} - k_1 k_2) \frac{\Delta t^2}{2} \qquad (6)$$

with truncation error E of

$$E = \frac{d^3A}{dt^3}\Big|_{\tau} \frac{(t - t_o)^3}{3!} = \frac{(k_1^2 k_2 - k_1^3 A)\Delta t^3}{6}\Big|_{\tau}, \quad t_o < \tau < t.$$

Needless to say, in the absence of advection, (6) is an extremely accurate expression when $k_i \Delta t$ (i = 1,2) is small.

To provide a complete approximation of (1), the growth expression (6) has been inserted into the two step advection approximation (3). There result equations of the form

$$A_{j\,k}^{n+1/2} = A_{j\,k}^{n-1/2} - \frac{\mu_{j\,k}}{2} (A_{j+1\,k}^{n} - A_{j-1\,k}^{n}) - \frac{\xi_{j\,k}}{2} (A_{j\,k+1}^{n} - A_{j\,k-1}^{n}) + (k_2 - k_1 A_{j\,k}^{n-1/2}) \Delta t + (k_1^2 A_{j\,k}^{n-1/2} - k_1 k_2) \frac{\Delta t^2}{2},$$

$$A_{j\,k}^{n+1} = A_{j\,k}^{n} - \frac{\mu_{j\,k}}{2} (A_{j+1\,k}^{n+1/2} - A_{j-1\,k}^{n+1/2}) - \frac{\xi_{j\,k}}{2} (A_{j\,k+1}^{n+1/2} - A_{j\,k-1}^{n+1/2}) + (k_2 - k_1 A_{j\,k}^{n}) \Delta t + (k_1^2 A_{j\,k}^{n} - k_1 k_2) \frac{\Delta t^2}{2}. \qquad (7)$$

*The quantity, A, Grows when $k_2/k_1 > A$ and dies when $k_2/k_1 < A$.

**In this and following expressions, k_1 and k_2 are defined at each point j, k, n.

In order to provide an accuracy test for (7), it was decided to calculate what change in A would have occurred in the first trial case had the k_i terms been nonzero. Intuitively the answer is simple; i.e., A is advected and A also grows or dies. The change of A as a function of time results from the solution of (4)

$$A = \frac{1}{k_1}\left[(k_1 A_o - k_2)e^{-k_1 t} + k_2\right] \quad (8)$$

where A = A(t) only.

There is only one minor complication. The equations advecting A tend also to damp and distort A. Thus, for accuracy comparisons, the growth correction (8) should be applied to the final damped, distorted, advected A field. The errors in (7) can then be estimated by integrating (7) for some time interval, and then comparing these results with the "growth corrected" values from trial case one. Table 1 shows the results of this comparison for row j = 35 of the 50 × 50 grid. The number of iterations is again equal to 40, and k_1 and k_2 have both been set equal to 10^{-3}. The maximum error of (7) is quite acceptable.

TABLE 1. The Numerical Integration of Equation (1): A Comparison Between the True Solution and Computed Values

(1)	(2)	(3)	(4)	(5)
k-grid Number	Advection Only (Equation 3)	Advection and Growth (Equation 7)	True Value (Col. 2 Corrected with Equation 8)	Error (Col. 3- Col. 4)
31	0.01273	0.68293	0.69358	-0.011
33	0.16238	0.73168	0.74003	-0.008
35	0.40010	0.80422	0.81381	-0.001
37	0.65179	0.88469	0.89193	-0.007
39	0.81252	0.94328	0.94181	+0.001
41	0.77661	0.94319	0.93067	+0.013
43	0.55977	0.88109	0.86337	+0.018
45	0.29874	0.79641	0.78235	+0.014
47	0.11644	0.73279	0.72577	+0.007
49	0.03333	0.70239	0.70000	+0.002

The results of the trial case studies have shown that Equation (1) can be successfully approximated by expression (7). The major portion of the observed errors can be attributed to the fact that a centered-difference scheme has difficulty approximating derivatives in a region where the gradient of A is changing rapidly. There is little doubt that the accuracy could be improved by increasing the grid density. While the change of the gradient A used in the case studies may have been severe, it could very well be typical of distributions found in the atmosphere where A could represent, for example, cloud droplet density or rainwater content.

REFERENCES

1. *C. R. Molenkamp. "Accuracy of Finite-Difference Methods Applied to the Advection Equation," J. Applied Meteorology, Vol. 7, No. 2, pp. 160-167. 1968.*

2. *P. D. Lax and B. Wendroff. "Systems of Conservation Laws," Comm. Pure Appl. Math., Vol. 13, pp. 217-237. 1960.*

3. *A. Arakawa. "Computational Design for Long-Term Numerical Integration of the Equations of Fluid Motion: Two-Dimensional Incompressible Flow. Part I." J. Comp. Phys., Vol. 1, pp. 119-143. 1966.*

4. *D. K. Lilly. "On the Computational Stability of Numerical Solutions of Time-Dependent Non-Linear Geophysical Fluid Dynamics Problems," Mon. Wea. Rev., Vol. 93, pp. 11-26. 1965.*

5. *K. V. Roberts and N. O. Weiss. "Convective Difference Schemes," Math. Comp., Vol. 20, pp. 272-299. 1966.*

BNWL-1551
Part 1

AN INQUIRY INTO THE CAUSES OF THE VARIATIONS IN THE BOMB DEBRIS SCAVENGING RATIOS

W. G. N. Slinn

A preliminary survey is made of the variability of each of the terms in the expression for the precipitation scavenging concentration ratios: $\kappa/\chi = \varepsilon/w$, where κ is the concentration of the pollutant in the precipitation at ground level; χ is its concentration in the region of the atmosphere where the debris enters the precipitation; ε is the fraction of the radioactivity which enters the cloud water, and w is the condensed water content of the cloud. It is seen that the variability of χ and w could account for some of the observed variations in the scavenging ratios but it appears that the major causes are the variations in ε and κ. In particular, it is suggested that variations in κ arise from different average cloud droplet radii.

Engelmann[1,2] has recently emphasized the utility of precipitation scavenging concentration ratios (or rainout ratios) for predicting in-cloud scavenging of bomb debris. These ratios, for a specific pollutant, are just the ratio of its concentration, κ, in the precipitation at ground level, to its air concentration, χ, in the region of the atmosphere where the pollutant enters the precipitation. The utility of these κ/χ ratios can be deduced from Figure 1 where some recent compilations[2,3] for fission-product debris are displayed. Their relatively small variation, in the range

$$0.2 \lesssim \frac{\kappa}{\chi} \lesssim 2.0 \left(\frac{\text{dpm/g } H_2O}{\text{dpm/m}^3 \text{ in air}} \right), \quad (1)$$

is the essence of their utility.

As small as the variation is, nevertheless there is a variation of about an order of magnitude. The purpose of this short report is to inquire into the causes of some of the systematic variations and to attempt to identify some of the variables whose determination might assist us in better understanding the scavenging of bomb debris. We hasten to add that this is an exploratory study and makes no pretense of being exhaustive or complete.

Following Junge[10] we propose to interpret the scavenging ratios within the simple formalism outlined in Figure 2. A certain fraction ε of the pollutant enters the cloud water. Thereby its concentration in the cloud water is $\varepsilon\chi$ (dpm/m^3) or, upon introducing the symbol w for the condensed water in the cloud per m^3, the concentration can also be written as

$$\frac{\varepsilon\chi}{w} \frac{\text{dpm/m}^3}{\text{g/m}^3}.$$

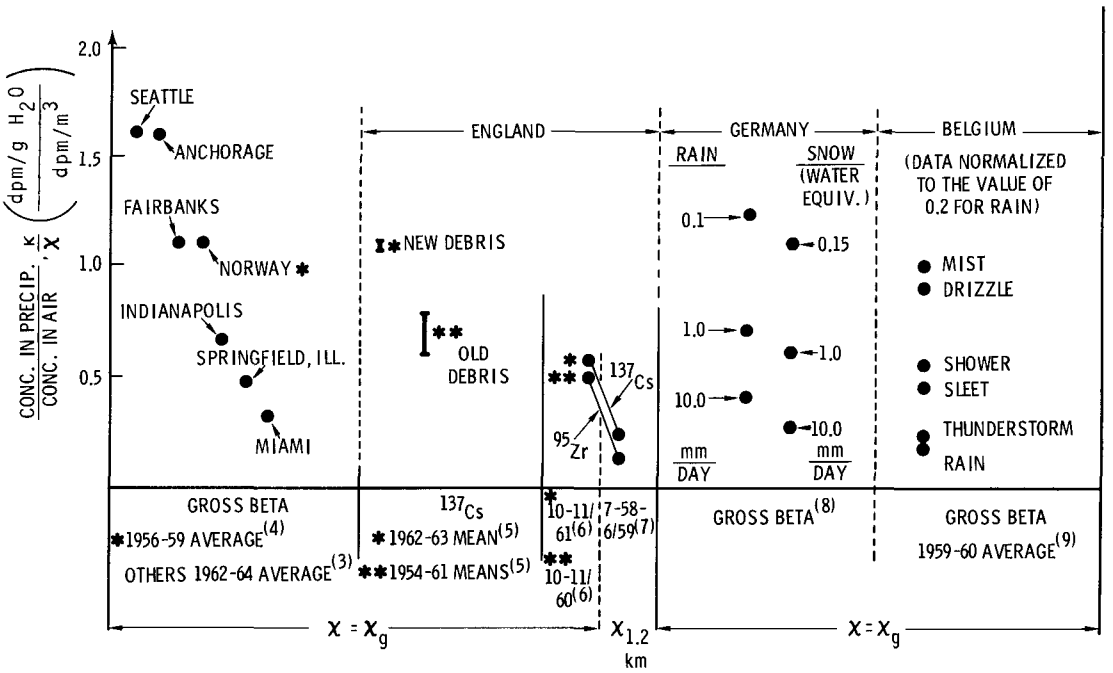

Neg 710247-5

FIGURE 1. The Ratio of the Concentration of Fission Product Debris in Precipitation, κ (dpm/g H_2O) to the Concentration in the Atmosphere χ (dpm/m^3).

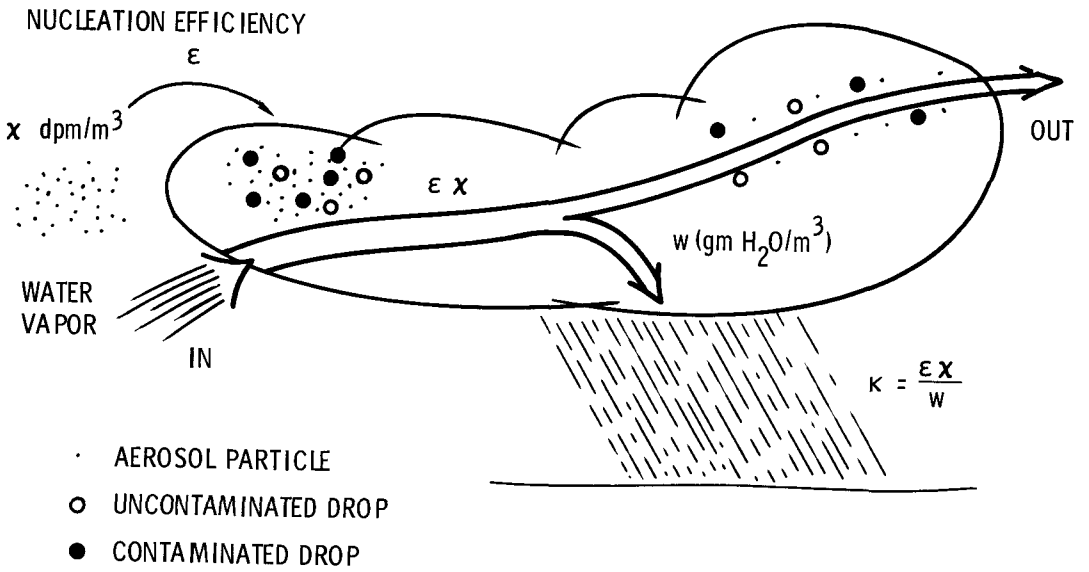

Neg 710247-2

FIGURE 2. A Schematic Representation of the Aspects of the Derivation of the Relation $\kappa/\chi = \varepsilon/w$.

Finally, if the contaminated water is neither concentrated by evaporation nor diluted by condensation (or by coalescence with purer cloud drops) then the concentration, κ, of the pollutant in the precipitation reaching the groud will be $\varepsilon\chi/w$ or

$$\frac{\kappa}{\chi} = \frac{\varepsilon}{w} . \qquad (2)$$

For $\varepsilon = \mathcal{O}(1)$ and $w = \mathcal{O}(1)$ g/m^3, then $\kappa/\chi = \mathcal{O}(1)$.

Using this formalism we need not digress from our interpretation of the scavenging ratios, to describe the various physical mechanisms which could be responsible for the incorporation of the pollutant into the precipitation. Some of these processes are discussed in other contributions to this volume. However, it is likely that the dominant mechanism of bomb debris scavenging is cloud droplet nucleation and we shall proceed as if this were known with certainty. In the event that this were incorrect, most of our comments would need to be only slightly modified.

Immediately we can see that with plausible values for ε and w, (2) has the capability to explain the range of values of the bomb-debris ratios given in Figure 1. However, rather than choosing these values at random, we shall now proceed to explore each of the terms in (2) (in the order: χ, ε, w and then κ) to determine what values are reasonable.

χ: One of the variables we need is $\chi(z)$, the air concentration of the pollutant as a function of height. In the analysis, χ is the concentration at the height at which the pollutant enters the precipitation, whereas in Figure 1 it is to be noticed that all but one of the data points correspond to χ_g, the concentration at ground elevation. Since most bomb debris enters the troposphere from the stratosphere, its concentration increases with height. It appears[11,12] that at least within the lowest 5 (or so) km of the troposphere, χ may be represented by

$$\chi = \chi_g \, e^{z/z^*} \qquad (3)$$

with

$$1 \lesssim z^* \lesssim 4 \text{ km}.$$

Admittedly this is a wide range for the e-fold distance, but it can be appreciated that the variation reflects the potentially large variations of the trajectories of different air masses.

It is seen that the difference within the two pairs of data for ^{95}Zr and ^{137}Cs in Figure 1 could be attributed to the variation in χ values, using the value 4/3 km for the e-fold distance in (3). It is not suggested that this does in fact explain the difference, but at least the change is in the correct direction. In a similar manner, all the ratios given in Figure 1 and based on χ_g should be reduced according to

$$\frac{\kappa}{\chi} = \frac{\chi_g}{\chi}\frac{\kappa}{\chi_g} = e^{-z/z^*}\frac{\kappa}{\chi_g}. \qquad (4)$$

However, the question that comes to mind immediately is: what z values

are appropriate? That is, what are the average heights at which precipitation forms, for the various geographical locations shown in Figure 1?

It is tempting to generalize from the observations that for cumulus clouds, maritime are more unstable than continental and, on the average, will produce rain (with a specified probability) with cloud base at about 1 km whereas the continental cumuli bases must reach to about twice this height.[13] If the majority of the precipitation at Springfield and Indianapolis, and at Miami were produced by cumulus clouds (which we are not necessarily suggesting) and other things being equal (which is not necessarily so) then for an assumed maritime atmosphere at Miami and using $z^* = 2$ km, we obtain (see Figure 1)

$$\left.\frac{\kappa}{\chi}\right|_{\text{Miami}} = e^{-1/2} \left.\frac{\kappa}{\chi_g}\right|_{M} = 0.2$$

$$= e^{-2/2} \left.\frac{\kappa}{\chi_g}\right|_{c} = \left.\frac{\kappa}{\chi}\right|_{\text{Continental}} . \quad (5)$$

However intriguing this result may be, we are not now in a position to justify such generalizations. The only point we wish to make is that determining average $\chi(z)$ and cloud heights would assist us in understanding the scavenging ratios. For now, it appears that all the κ/χ_g ratios in Figure 1 should be reduced by a factor of about $e^{-1/2} \approx 0.6$.

ε: In an attempt to understand the variability in the fraction, ε, of the total radioactivity that is incorporated into the cloud water, it is necessary to consider the properties of the aerosol particles which host the radioactivity. This is a huge task. Some of the properties of interest are: the distribution of the radioactivity according to size of the aerosol particles; their chemical composition or at least their solubility and/or wettability; their change (aging) within the atmosphere, and the competition that exists between the radioactive versus the other particles, to become the favored nucleus for water condensation. Perforce our comments will be brief.

Immediately, a distinction should be made between new versus old debris. An example of the corresponding distinction in the scavenging ratios is shown in Figure 1, where it is seen (other things being equal!) that ε for old debris is about half that for new debris. Makhon'ko[14] describes cases where the difference is larger than a factor of ten. One of the questions that we should attempt to answer concerns the reason for this difference.

First let us look at some of the characteristics of fresh debris. Among the many interesting properties of fresh debris studied by Sisefsky and Persson[15] we mention only their observation that the radioactivity of individual aerosol particles varies as the mass of the particles. Nathams et al.[16] have reported that the size distribution of the particles is typically log normal with geometric mean radius of about 0.1 μ and geometric standard deviation of about 2.0. From these two results[15,16] we can

conclude that the bulk of fresh debris is on particles which, if soluble or even "sufficiently" wettable, would be good cloud droplet nuclei (CDN). Therefore we expect that the large scavenging ratios for fresh debris correspond to the physical phenomenon that almost all such radioactivity resides on good CDN and the resultant ε values will be near unity.

Continuing with this line of reasoning, one would conclude that the older the debris becomes (old *versus* new being qualitative terms only) the lower would become the scavenging ratios, since continuously the best CDN would be removed, until eventually, ε would become vanishingly small. Since, in fact, the scavenging ratios tend to a relatively invariant value, it would appear that eventually a relatively steady-state situation prevails, wherein the debris residing on small particles (0.01 - 0.1 μ) enters the troposphere from its reservoir in the stratosphere, coagulates with aerosol particles, and eventually is scavenged *via* nucleation. This picture is similar in outline but slightly different in detail from that discussed by Makhon'ko.[17]

One of the important aspects of this proposed chain of events is to determine to what size aerosol particles the debris becomes attached. Brock[18] has recently considered this question theoretically and has emphasized that at least for gaseous trace substances, the attachment spectra have different maxima, for different atmospheric aerosols: a broad maximum near 1 μ for maritime aerosols, and maxima at radii less than 0.1 μ for urban and upper tropospheric aerosols. Similar results would be expected for small aerosol particles whose attachment is governed by Brownian diffusion. Experimental evidence[19,20,21] of such differences is displayed in Figure 3. From these results we can expect that the scavenging ratios will be higher for a maritime than for a continental atmosphere, since the old debris will be attached to larger particles, which, in general, are better CDN.

There is another process that could enhance the differences in the scavenging ratios at different geographical locations, even more, namely: the competition among aerosol particles to become the favored nucleus upon which condensation occurs. Since even old debris would be expected to be distributed on individual aerosol particles in proportion to their mass, we can use Junge's[10] estimate (p. 291) that the ratio of ε's for: maritime and troposphere aerosols with a total particle concentration of less than 200 to 300/cm^3, to continental aerosols of low concentration, to continental aerosols of high concentration, will be in the ratio of 1.0.8:0.5.

Taking into account both these effects it is interesting that from Figure 1, the ratio of the scavenging ratios for: Seattle and Anchorage, to Fairbanks and Norway, to Indianapolis and Springfield, are in the ratio of (approximately) 1:0.7:0.4. However, suggestive this might be, it is not to be taken too seriously until more data

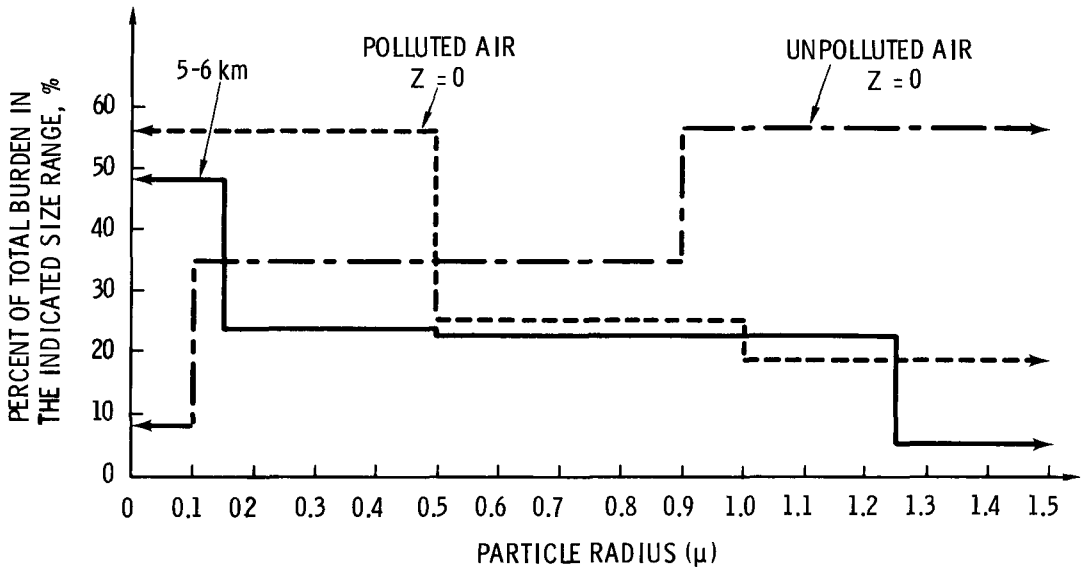

Neg 710247-6

FIGURE 3. The Distribution of Artificial Radioactivity on Aerosol Particles as Obtained on Different Cascade Impactors by: Gasiev et al.,(19) at 5-6 km in December, 1964, Near Moscow (solid curve); Rosinski and Stockham,(20) in Ground Level Air in Chicago, 1960 (dashed curve) and Kalkstein et al.(21) for Ground Level, Unpolluted Air (dotted curve).

(especially meteorological data) are analyzed. One of the reasons for our hesitancy is that the Miami data do not appear to fit this scheme; another reason is obtained from Figure 4 [from Makhon'ko[9]] where it is seen that the geographical variation of the scavenging ratios is much more comlicated than one would conclude from Figure 1. The main conclusion to be

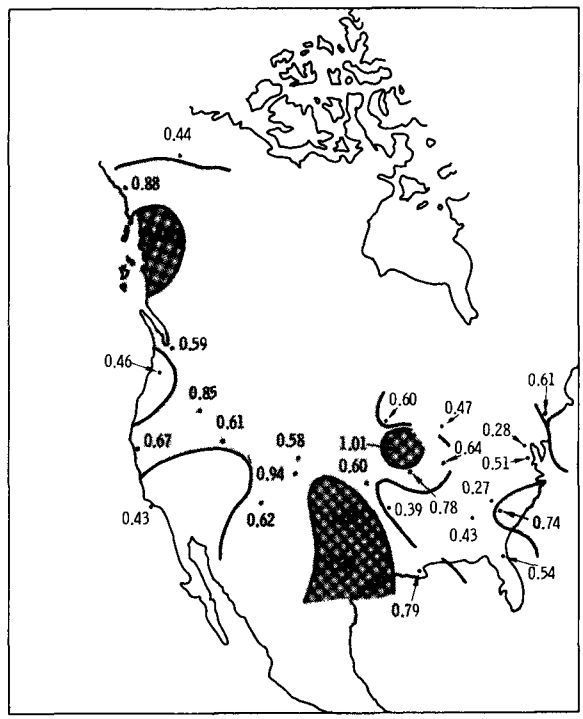

Neg 710247-7

FIGURE 4. An Indication of the Complex Geographical Distribution of κ/χ Values (from Makhon'ko[9]).

made in this section is that determining ε is integrally tied to a thorough study of both aerosol physics and chemistry, and synoptic meteorological data.

w: Another variable that could cause variations in the scavenging ratios, κ/χ, is the average condensed water content of the clouds, w. By average is meant the average for all cloud types that produce precipitation at each geographical location of interest. One of the uncertainties in the available data is the value for the average solid water (ice) content. Otherwise, considerable data are available[13,22] on the liquid water content, including its dependence on cloud temperature. From Figure 5 it is seen that typically the average w for different cloud types falls within the relatively narrow range of 0.1 to 0.6 g/m^3 (larger w's have been measured but, again, those shown are average values). It is interesting that for the range of measured w and κ/χ values, the appropriate ε values can vary between about 0.01 and 1.0.

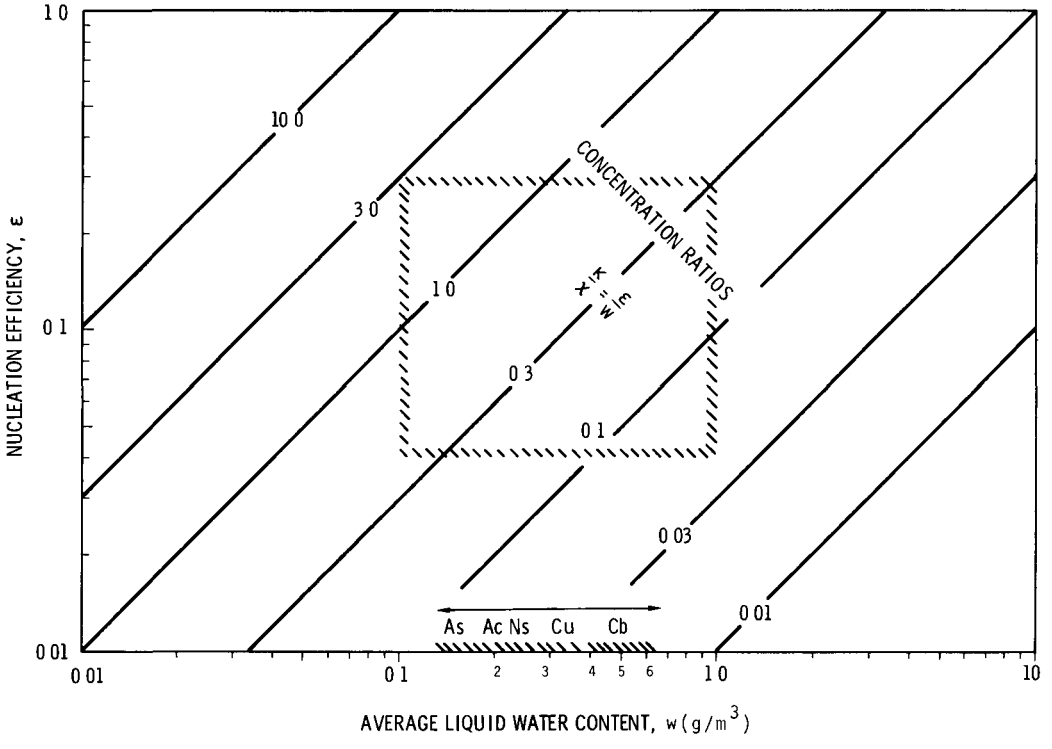

Neg 710247-4

FIGURE 5. An Indication of the Variability of the Average Liquid Water Content for Different Clouds and the Resultant Concentration Ratios for Different ε Values.

κ: The final term in the expression $\kappa/\chi = \varepsilon/w$ to be discussed, is the possible variation in κ because of dilution or concentration of the contaminant, between the time of its incorporation into the cloud drops until its arrival at the ground. It is expected that such processes are responsible for the variations in the κ/χ ratios, seen on the right hand side of Figure 1. Further evidence of the variation can be seen in Figure 6.[23,24,25] There it is seen that the natural α-radioactivity of individual cloud drops falls as r^{-3}, suggesting that the radon daughters were attached to the CDN and that the cloud drops grew by coalescence. For raindrops, it is seen that the natural α-radioactivity per g H_2O, falls as R^{-2} whereas for bomb-debris β-activity falls as R^{-1}. In this last case, R is the mean radius of the raindrops during a given rainfall.

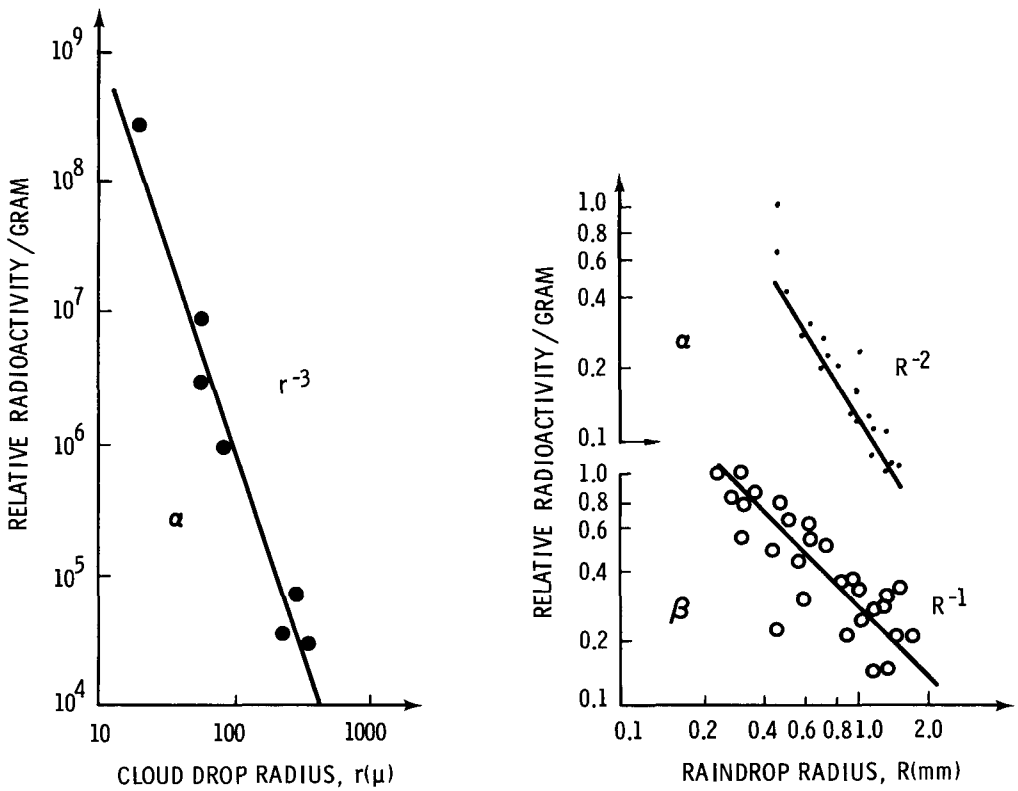

Neg 710247-1

FIGURE 6. The Dependence of κ on Cloud Droplet and Raindrop Size (from Avramenko and Makhon'ko(26)).

There is considerable uncertainty as to the cause of these different dependencies on the size of the water drops. Styro and Vebrene[24] suggested that the R^{-2} variation for their data arose from evaporation, but Avramyenko and Makhon'ko's[25] data (R^{-1}) were obtained under conditions for which evaporation would be negligible and they suggested[26] that it could be explained if the concentration of bomb debris within the cloud drops varied with the cloud drop radius according to r^{-1}. It should be mentioned that if this is correct, then it suggests that bomb debris is picked up not by nucleation or by Brownian diffusion, but by inertial capture. This is not a very palatable concept, since the collection efficiency is so small for $\lesssim 1\ \mu$ aerosol particles impacting on cloud droplets.

An alternative explanation for this phenomenon that the smaller the mean raindrop size, or the smaller the precipitation rate, the greater the concentration, κ, of the pollutant, is the following. Suggestions toward this explanation are also given by Mrose[27] and by Petrenchuk and Drozdova.[28] Consider first the growth of a single raindrop. If we assume that the bomb debris radioactivity enters each cloud droplet only via nucleation, then as water condenses on a specific aerosol particle of activity A_p, say, the concentration within the cloud droplet will be

$$\kappa_{CD} = \frac{A_p}{(4/3)\pi\rho r^3} \frac{dpm}{g\ H_2O} \qquad (6)$$

that is, it falls as r^{-3}. Now if the cloud droplet grows to raindrop size by coalescence with other cloud droplets which on the average have the same concentration κ_{CD}, then the activity of the raindrop will be

$$\kappa_{RD} = \frac{\text{Total Activity}}{\text{Total Mass}} = \frac{\sum A_p}{\sum (4/3)\pi\rho r^3} \qquad (7)$$

which, upon taking an average over N cloud droplets, becomes

$$\kappa_{RD} = \frac{N\ \bar{A}_p}{N\ (4/3)\pi\rho r^3} = \bar{\kappa}_{CD} \qquad (8)$$

that is, we obtain the obvious result that through coalescence of cloud droplets with the same activity, κ will remain constant. (Which, by the way, is the essence of the reason why Avramyenko and Makhon'ko[26] conclude that the cloud droplets must have $\kappa_{CD} \sim r^{1}$ in order to explain $\kappa_{RD} \sim R^{-1}$.)

The above considerations do not produce the desired result that small raindrops have relatively greater radioactivity, but immediately we ask what conditions dictate the size of the raindrops? That is, what conditions are fulfilled to cause precipitation to fall as a drizzle rather than a torrent? If it were dictated by the number of cloud droplets which coalesce with one another, then (by the above reasoning) all precipitation rates should produce precipitation with the same κ. Thus we are forced to reject the hypothesis that it is dictated by the thickness of the cloud. However,

if the intensity of rain is dictated by the size of the cloud droplets, then the observed κ values can be explained. Physically this is a reasonable condition, since the smaller the cloud droplets, the lower the collection efficiency and therefore the slower the growth rate to raindrop size.

To see that this criterion can lead to the correct κ_{RD} ratios, we see from (8) that

$$\frac{\kappa_{RD}\ (R_1)}{\kappa_{RD}\ (R_2)} = \left(\frac{\bar{r}_2}{\bar{r}_1}\right)^3 \qquad (9)$$

where $\bar{r}_i$ is the average radius of the cloud droplets, which lead to raindrops of radius R_i. For example, a ratio of κ values as large as 8 (see Figure 6 for a 0.3 mm and a 2.0 mm raindrop) arises, according to (9), i.e.,

$$\frac{\kappa_{RD}\ (0.3\ mm)}{\kappa_{RD}\ (2.0\ mm)} = 8 = \left(\frac{\bar{r}_{2.0\ mm}}{\bar{r}_{0.3\ mm}}\right)^3, \qquad (10)$$

from a difference in cloud drop sizes of only 2, i.e.

$$\bar{r}_{2.0\ mm} = 2\ \bar{r}_{0.3\ mm}. \qquad (11)$$

This seems to be a highly reasonable result. (Incidently, if it is correct, then it represents a very sensitive and yet simple method for measuring average cloud drop radii.)

Other factors that could influence κ include coalescence with cloud droplets that have condensed at different elevations and therefore at different $\chi(z)$, and also, evaporation below the cloud base. It should be mentioned that it would be useful to see if the variation of κ during an individual convective storm[29,30] can be explained on the basis of variable cloud droplet size: smaller droplets at the beginning and ending of the storm; larger cloud drops during the middle of the storm. Also, it may be that the Miami data in Figure 1 are low, simply because on the average, the cloud droplets are slightly larger than those at the continental sites.

In summary, this has been a preliminary survey. We have inquired after the causes of the observed variations of the precipitation scavenging concentration ratios, and have seen that they could arise from any one of the terms of the equation

$$\frac{\kappa}{\chi} = \frac{\varepsilon}{w}.$$

The variability of ε and κ appears to be especially important.

REFERENCES

1. *R. J. Engelmann. "The Calculation of Precipitation Scavenging," in Meteorology and Atomic Energy 1968, D. H. Slade, ed., U. S. Atomic Energy Commission, Division of Technical Information, available as TID-24190 from the Clearinghouse, 1968.*

2. *R. J. Engelmann. "Scavenging Prediction Using Ratios of Concentrations in Air and Precipitations" in Precipitation Scavenging (1970), R. J. Engelmann and W. G. N. Slinn, coords., No. 22 of AEC Symposium Series, Available from NTIS as CONF-700601. 1970.*

3. W. E. Bradley. "The Relationship Between the Radioactivity in Surface Air and Precipitation," submitted to Atmospheric Environment, 1970.

4. S. H. Small. "Wet and Dry Deposition of Fallout Materials at Kjeller," Tellus, vol. 12, pp. 308-314, 1960.

5. D. H. Peirson and R. S. Cambray. "Fission Product Fallout from the Nuclear Explosions of 1961 and 1962," Nature, vol. 205, pp. 433-440, January 30, 1965.

6. D. H. Peirson and J. R. Keane. "Characteristics of Early Fallout from the Russian Nuclear Explosion of 1961," Nature, vol. 196, pp. 801-807, December 1, 1962.

7. A. C. Chamberlain. "Aspects of the Deposition of Radioactive and Other Gases and Particles," pp. 63-88 of Aerodynamic Capture of Particles, E. G. Richardson, ed. Pergamon Press, New York, 1960.

8. M. Hinzpeter. "The Influence of Meteorological Parameters on the Propogation of Radioactive Fission Products in the Biosphere," Proc. 2nd Int. Conf. on the Peaceful Uses of Atomic Energy, vol. 18, p. 184, 1958.

9. K. P. Makhon'ko. "The Ability of Various Types of Precipitation to Wash Out Fission Products from the Atmosphere and the Respective Washout Characteristics," Izv., Atmos. and Oceanic Phys., vol. 2, pp. 297-304 (transl. pp. 177-182), 1966.

10. C. E. Junge. Air Chemistry and Radioactivity. Academic Press, New York, 1963.

11. P. Kruger. "Influence of Inversions upon Precipitation Deposition of Radioactive Aerosols," Tellus, vol. 18, pp. 516-524, 1966.

12. L. E. Nazarov, A. F. Kuzenkov, S. G. Malakhov, L. A. Volokitina, Ya. I. Gaziyov and A. S. Vasil'yev. "Radioactive Aerosol Distribution in the Middle and Upper Troposphere over the USSR in 1963-68," J. Geophys. Res., vol. 75, pp. 3575-3588, 1970.

13. N. H. Fletcher. The Physics of Rainclouds. Cambridge at the University Press, 1962.

14. K. P. Makhon'ko. "Spontaneous Removal of Radioactive Dust from the Lower Troposphere (Review)," Izv. Atmos. and Oceanic Phys., vol. 2, pp. 508-522 (transl. pp. 304-313), 1966.

15. Jan Sisefsky and Gunnar Persson. "Fractionization Properties of Nuclear Debris from the Chinese Test of 24 December 1967," Health Physics, vol. 18, pp. 347-356, 1970.

16. M. W. Nathans, R. Thews, W. D. Holland, and P. A. Benson. "Particle Size Distribution in Clouds from Nuclear Airbursts," J. Geophys. Res., vol. 75, pp. 7559-7572, 1970.

17. K. P. Makhon'ko. "Simplified Theoretical Notion of Contaminant Removal by Precipitation from the Atmosphere," Tellus, vol. 19, pp. 467-476, 1967.

18. J. M. Brock. "Attachment of Trace Substances on Atmospheric Aerosols," in Precipitation Scavenging (1970), R. J. Engelmann and W. G. N. Slinn, coords., No. 22 of AEC Symposium Series, Available form NTIS as CONF-700601. 1970.

19. Y. I. Gasiev, S. G. Malakhov, L. E. Nazarov and A. N. Silantiev. "The Size Distribution of Radioactive Particles from Nuclear Weapon Tests and Their Transport in the Atmosphere," Tellus, vol. 18, pp. 474-485, 1966.

20. J. Rosinski and J. Stockham. "Preliminary Studies of Scavenging Systems Related to Radioactive Fallout," Summary Report ARF 3127-12, Armour Research Foundation, 1960.

21. M. I. Kalkstein, P. J. Drevinsky, E. A. Martell, C. W. Chagnon, J. E. Manson and C. E. Junge. "Natural Aerosols and Nuclear

Debris Studies," Progress Report II, GRD Research Notes, No. 24, 1959.

22. *A. M. Borovikov, I. I. Gaivoronskii, E. G. Zak, V. V. Kostarev, I. P. Mazin, V. E. Minervin, A. Kh. Khrgian and S. M. Shmeter. Cloud Physics, Gimiz, Gidrometeorologicheskoe Izdatel'stov, Leningrad, 1961. Translated and available from the Clearinghouse as OTS-63-11141, 1963.*

23. *V. Yu. Potsyus. "The Technique for Cloud Element Radioactivity Measurements by the Alpha-Radiographic Technique," Acad. Nauk Lit. SSR, vol. 10, p. 1, 1959.*

24. *B. I. Styra and B. K. Vebrene. "On the Technique of Individual Precipitation Particle Radioactivity Measurements and Some Preliminary Results of Such Investigations," Izv. Acad. Nauk USSR, Atmos. Oceanic Phys., vol. 2, p. 10, 1966.*

25. *A. S. Avramenko and K. P. Makhon'ko. "Radioactivity of Raindrops," Izv. Atmos. and Oceanic. Phys., vol. 5, pp. 647-648 (transl. pp. 375-376), 1969.*

26. *A. S. Avramenko and K. P. Makhon'ko. "Model for Capture of Radioactivity by Precipitation," J. Geophys. Res., vol. 75, pp. 3613-3622, 1970.*

27. *H. Mrose. "Measurement of pH and Chemical Analysis of Rain-, Snow-, and Fog-Water," Tellus, vol. 18, pp. 266-270, 1966.*

28. *O. P. Petrenchuk and V. M. Drozdova. "On the Chemical Composition of Cloud Water," Tellus, vol. 18, pp. 280-286, 1966.*

29. *D. F. Gatz and A. N. Dingle. Deposition of Atmospheric Particulate Matter by Convective Storms: The Role of the Convective Updraft as an Input Mechanism, The University of Michigan, College of Engineering Report, COO-1407-6, 1966.*

30. *F. A. Huff and G. E. Stout. "Distribution of Radioactive Rainout in Convective Rainfall," J. Appl. Met., vol. 3, pp. 707-717, 1964.*

WASHOUT OF SOLUBLE DYE PARTICLES

M. T. Dana

Washout experiments were conducted using soluble rhodamine B particles with aerodynamic equivalent diameters ranging from 1.2 to 11.2 microns. The resulting washout coefficients for the particles larger than 1.8 microns agreed well with theoretical estimates for impactive scavenging. The smaller particle experiments resulted in anomalously high washout coefficients, not immediately explainable in terms of operating conditions or scavenging mechanisms.

The series of washout field experiments at Quillayute Air Base was continued during the 1969-1970 winter field season. The tracer utilized was the soluble dye rhodamine B, which is fluorescent in water solution. The experimental procedure and details of instrumentation have been reported previously.[1-3]

Experimental details of the successful experiments are listed in Table 1. The particle mass median diameter has been converted to aerodynamic equivalent diameter for unit density spheres. This diameter is given[4] by

$$d = d' \, (\rho k)^{1/2}, \qquad (1)$$

where d is the aerodynamic equivalent diameter (cm), ρ is the particle density (1.38 g/cm^3 for rhodamine B), k is the Cunningham slip correction:

$$k = 1 + \frac{0.16 \times 10^{-4}}{d'}$$

d' is the actual rhodamine particle diameter (cm) as determined from the aerosol generator calibration curve.[2]

For the purpose of tabulating washout coefficients and other results, the experiments are divided into four particle size groups, with results shown in Tables 2a-2d. The experimental "apparent" washout coefficients (which include dry deposition, if any) for arcs A (25 m) and B (50 m) are indicated as Λ_A and Λ_B.

Comparison of these results to theory of impactive scavenging has been done in the following way. In a consideration of washout by inertial effects (the "sweeping out" of particles by falling raindrops), the washout coefficient may be expressed as

$$\Lambda = \frac{\pi}{4} F_o D_2^2 E, \qquad (2)$$

where F_o is the flux of raindrops (mm^{-2} hr^{-1}), D_2 is the mean areal raindrop diameter (mm), and E is a gross collection efficiency for the particle spectrum by a given raindrop spectrum. The quantity $\alpha = \frac{\pi}{4} F_o D_2^2$ is a characterization of the raindrop spectrum for a given experiment, and

may be determined from raindrop size spectra alone. Thus, knowledge of α and the experimental washout coefficient Λ_e allows calculation of

$$E_e = \frac{\Lambda_e}{\alpha}. \quad (3)$$

Similarly, if the theoretical washout coefficient Λ_T is computed using published collection efficiencies such as those of Mason,[5] a gross theoretical collection efficiency E_T can be computed:

$$E_T = \frac{\Lambda_T}{\alpha}. \quad (4)$$

These quantities are listed in Tables 2. Since α is generally proportional to the rainfall rate J, the raindrop spectrum is characterized by α/J. The E_e values have been computed using the lower of the two arc washout coefficients. This was done since, in the experiments from which dry deposition data were available, little or no dry deposition was indicated at the first arc.

TABLE 1. Experimental Details

Date	Experiment	Particle Diameter, d(μ)	Mass of Tracer Released-Q, g	Wind Speed $\bar{u}$, $cm\ sec^{-1}$	Rainfall Intensity J, $mm\ hr^{-1}$
12-10-69	UIL-23	1.0	0.04	376	0.6
	24	1.8	0.22	618	1.4
	25	11.2	39.8	670	0.7
12-11-69	UIL-26	1.2	0.13	882	2.7
	27	1.2	0.09	1152	4.4
2-5-70	UIL-31	1.8	0.18	420	1.4
	32	1.8	0.17	354	1.3
	33	4.8	0.65	422	1.4
3-11-70	UIL-34	1.8	0.07	370	3.6
3-12-70	UIL-35	1.8	0.11	800	0.6
	36	4.8	1.31	820	4.4
	37	4.8	1.35	900	1.3
	38	11.2	10.3	900	12 ± 5
3-13-70	UIL-39	1.8	0.11	305	2.3
	40	4.8	1.24	290	3.1
	41	4.8	1.23	325	2.2
	42	11.2	11.4	475	3.9
3-15-70	UIL-43	1.2	0.07	580	6.1
	44	1.2	0.05	575	7.7

TABLE 2a. Washout Results for d = 11.2 μ

Experiment	Λ_A ($sec^{-1} \times 10^4$)	Λ_B ($sec^{-1} \times 10^4$)	α/J, mm^{-1}	E_e	E_T[a]
UIL-25	2.3	5.6	2.2[b]	0.54	0.60
38	20.9	16.8	1.4	0.36 ± 0.3[c]	0.71
42	6.9	10.9	1.8	0.35	0.71

a. Using collection efficiencies of Mason,[5] for d = 12 μ
b. No experimental rain spectra - a typical Quillayute spectrum was used
c. Variation due to uncertainty in J

TABLE 2b. Washout Results for d = 4.8 μ

Experiment	Λ_A ($sec^{-1} \times 10^4$)	Λ_B ($sec^{-1} \times 10^4$)	α/J, mm^{-1}	E_e	E_T[a]
UIL-33	1.3	6.2	1.7	0.20	0.28
36	6.4	12	1.5	0.35	0.33
37	2.2	8.7	1.5	0.41	0.31
40	4.0	4.7	1.7	0.27	0.35
41	3.2	3.3	1.7	0.31	0.35

a. Using collection efficiencies of Mason,[5] d = 6 μ

TABLE 2c. Washout Results for d = 1.8 μ

Experiment	λ_A ($sec^{-1} \times 10^4$)	λ_B ($sec^{-1} \times 10^4$)	α/J (mm^{-1})	E_e	E_T[a]
UIL-24	1.6	5.5	1.9[b]	0.22	0.05
31	1.1	3.2	1.7	0.17	0.06
32	1.3	2.7	1.7	0.21	0.06
39	3.3	2.7	1.5	0.28	0.10

a. Using collection efficiencies of Mason,[5] for d = 2 μ (extrapolated from Mason's calculations)
b. See Note (b), Table 2a

TABLE 2d. Washout Results for d = 1.2 μ

Experiment	λ_A ($sec^{-1} \times 10^4$)	λ_B ($sec^{-1} \times 10^4$)	α/J, (mm^{-1})	E_e	E_T[a]
UIL-23	1.9	1.4	2.2[b]	0.38	0.02
26	7.3	10.4	1.4[b]	0.70	0.03
27	[c]	12.6	1.5[b]	0.69	0.03
43	15.2	18.7	1.8-2.1	0.43-0.50	0.02
44	21.2	14.0	1.6	0.41	0.03

a. Estimated by extrapolation of Mason's[5] values to smaller size
b. See Note (b), Table 2a
c. No data available

The anomalously high experimental gross collection efficiencies--as compared to those expected from the inertial scavenging theory--for particles smaller than five microns cannot be immediately accounted for in terms of aerosol generation conditions or scavenging mechanisms. Scavenging of the aerosol generator output prior to complete evaporation of the solution droplets (whose diameters were about 40 microns) may have led to enhanced λ_e values. But this effect would lead to uniformly higher values of λ_A over λ_B, which was not the case. Another possibility is growth of the particles, once they are formed, by condensation in the high humidity atmosphere. Work is in progress to determine the potential effects of these situations. Notably, a new aerosol generator is being

developed which will produce smaller initial methanol solution droplets.* In addition, particle size measurements will be made during the experiments.

A potential scavenging mechanism for small particles, which is not accounted for in the inertial theory, is an electrostatic charge effect. The extent of the influence of electric charges on the washout of small particles is not known, but raindrop charge measurements at Quillayute indicate that the continuous rain which occurs during the experiments is nearly always positively charged.(6) Also, conditions existed at Quillayute which probably resulted in the formation of a negative space charge near the ground.(7) This space charge may have influenced the aerosol charge such that aerosol and raindrops were of opposite polarity.

REFERENCES

1. *M. T. Dana and M. A. Wolf. "Experimental Studies in Precipitation Scavenging," Pacific Northwest Laboratory Annual Report for 1967, Vol. II: Physical Sciences, Part 3. Atmospheric Sciences, BNWL-715-3, pp. 128-140. Battelle-Northwest, Richland, Washington, October, 1968.*

2. *M. A. Wolf and M. T. Dana. "Experimental Studies in Precipitation Scavenging," Pacific Northwest Laboratory Annual Report for 1968, Vol. II: Physical Sciences, Part 1. Atmospheric Sciences, BNWL-1051-1, pp. 18-25. Battelle-Northwest, Richland, Washington, November 1969.*

3. *M. T. Dana, M. A. Wolf and L. A. du Plessis. "Field Experiments in Precipitation Scavenging," Pacific Northwest Laboratory Annual Report for 1969, Vol II: Physical Sciences, Part 1. Atmospheric Sciences, BNWL-1307-1, pp. 77-81. Battelle-Northwest, Richland, Washington, June 1970.*

4. *J. P. Flesch, C. H. Norris and A. E. Nugent, Jr. "Calibrating Particulate Air Samplers with Monodisperse Aerosols· Application to the Anderson Cascade Impactor," Amer. Ind. Hyg. Assoc. J., Vol. 28, pp. 507-516, 1967.*

5. *B. J. Mason. The Physics of Clouds, Oxford University Press, London, 1957. pp. 422-424.*

6. *M. Terry Dana. "The Electric Charges on Raindrops in Continuous and Showery Rainfall," submitted to J. Atmos. Sci.*

7. *M. Terry Dana. "Rain Scavenging of Soluble Dye Particles," in Precipitation Scavenging (1970), R. J. Engelmann and W. G. N. Slinn, coords., No. 22 of AEC Symposium Series. Available from NTIS as CONF-700601. 1970.*

*See "Calibration of an Ultrasonic Nozzle for Aerosol Generation," this report.

BNWL-1551
Part 1

THE PROPERTIES OF PARTICLES, AIRBORNE UNDER SIMULATED CONDITIONS ACCOMPANYING ACCIDENTS IN NUCLEAR INSTALLATIONS

L. A. du Plessis and L. C. Schwendiman

The efficiency of removal of airborne radioactive particles by scavenging processes and gravitational settling is determined by the size, shape, and chemical and physical properties of the aerosols. A literature review was made primarily for the benefit of scavenging studies to determine the nature of aerosols arising from various nuclear installations during postulated accidents. The results of this survey are presented. A conclusion is reached that sources and conditions are extremely variable and every incident must be treated in more detail to obtain a particle size spectrum. Particularly lacking are data on the nature of aerosols following escape from the structure in which the incident occurred. If scavenging data are to be used most effectively, much more must be known about the nature of aerosols from accidental releases.

Aerosols released into the atmosphere by accidents in nuclear installations may be hazardous when they reach the ground. In order to assess the hazard, it is necessary to know what radioactive isotopes are carried by the aerosols, how soon they reach the ground, and how widely they are dispersed. The distribution of atmospheric aerosols in space and time is controlled by meteorological processes. The effect of such processes on the aerosols depends on particle properties such as size and chemical composition.

This report is a survey of some of the literature on aerosols that may be released in nuclear accidents. Relevant literature was found by searching the subject indexes of Nuclear Safety and Nuclear Science Abstracts. Although not exhaustive, this literature review and the assembled data relating to the nature of aerosols generated in serious nuclear incidents will be of interest and value in washout and deposition investigations.

The course of a nuclear accident may be divided into five stages:
Stage 1: Radioactive materials, some possibly in the form of aerosols, are released from the components in which they are normally contained, e.g., fuel elements or coolant loops. At the time of an accident, such components are usually at a high temperature.
Stage 2: The radioactive materials move from the hot zone where they are released through piping or other conduits to the containment vessel, which is at ambient temperature. In this stage, aerosols may be formed by condensation of vapors.
Stage 3: Aerosols released into or formed in the containment vessel undergo changes such as chemical

reaction, growth, agglomeration, settling to the floor, and plating on the walls.

Stage 4: Aerosols in the containment vessel escape to the outer atmosphere, either through the normal ventilation system (whose operation may be accidentally impaired) or through accidental ruptures.

Stage 5: The aerosols undergo further changes in the atmosphere.

The report literature contains experimental data on stages 1, 2, and 3, and has been searched for information on the following aerosol properties:

Chemical composition
Radioactive elements present
Particle-size distribution
Particle shape.

In the search for data on aerosol properties, attention has been concentrated on fairly close simulations of accidental releases, e.g., melting of clad fuel elements or burning of plutonium-containing waste. Less attention has been given to experiments in which the nature of the aerosol was assumed beforehand, and in which the aerosol was then produced by some process that would not take place in a real accident, such as an electric arc or exploding wire.

The aerosol properties of interest depend on the following factors: type of installation, nature of accident, fuel material, cladding material, percent burnup of fuel, and atmosphere in reactor.

In this report, aerosols are classified according to the type of installation in which they originate, and subclassified according to nature of accident.

WATER-COOLED REACTORS

Information on aerosols has been obtained for accidents in water-cooled reactors. The worst accident foreseen is loss of coolant, followed by melting of the fuel elements (6, p. XVII). The other kind of accident is overheating of the fuel by a reactivity transient.

The fission products from such accidents (other than noble gases) fall into two classes, volatile and non-volatile. The volatile elements are iodine, tellurium, and cesium, while the non-volatile elements are barium, strontium, zirconium, and cerium. Uranium, the fuel, also is non-volatile. Ruthenium is sometimes volatile, and sometimes non-volatile. Of the non-volatile elements released by the fuel, only very small fractions escape from the hot zone and reach the containment vessel. A larger fraction of the volatile elements reaches the containment vessel, where they are largely adsorbed on aerosols, rather than being present in gaseous form.

Loss of Coolant

Loss-of-coolant accidents have been simulated at Oak Ridge by both in-pile and out-of-pile heating of fuel elements containing UO_2 or uranium-aluminum alloy.

These experiments yielded aerosols with particle sizes ranging from 16Å

to 4 μm, which are listed in Table 1. It is interesting that all particle sizes from molecular sizes up to several micrometers have been found.

Not much work has been done on the chemical composition of the aerosols. It is surmised that the aerosol from stainless-steel-clad UO_2 melted in air consists of separate UO_2 and stainless steel particles (3, pp. 48,49). Presumably the stainless steel is present in oxidized forms.

According to photomicrographs, the aerosols generally consist of agglomerates of spherical particles or platelets (1, pp. 12-15) (3, pp. 17-20) (5, pp. 31-39).

The radioactive chemical elements found in the aerosols are listed in Table 2.

TABLE 1. Particle Sizes of Aerosols from Simulated Loss-of-Coolant Accidents in Water-Cooled Reactors

Reference	Pages	Fuel	Aerosol Particle Size
(1)	16	UO_2	0.02 - 0.14 μm
	24	UO_2	0.06 - 1.20 μm
	34,35	UO_2	Two groups around 22Å and 30Å
(2)	13	U-Al	0.04 - 4 μm
(3)	46	UO_2	16 - 39Å
	52,53	UO_2	0.015 - 0.64 μm
(5)	32	UO_2	0.015 - 0.7 μm
	36	UO_2	0.01 - 0.35 μm
(6)	30	UO_2	MMD 0.15 - 0.34 μm

The effect of atmosphere on fission-product release in aerosols from molten UO_2 was studied in experiments with dry helium, moist helium, dry air, and moist air (5, pp. 32,37). "Of the eight elements measured (I, Te, Cs, Ru, Sr, Ba, Zr, Ce), only I and Ru showed significant variations in behavior with changes in atmosphere." Release of I and Ru was greatest in moist air. It is stated that oxygen increases the volatility of Ru by converting it to RuO_4 (1, p. 11). This effect of oxygen on Ru release in aerosols also appears in experiments with U-Al alloy (2, p. 32). The release of I, Te, Cs, and Ru from the alloy was measured in air, helium, and steam-air mixture. Release of Cs was less in air and steam-air mixture, probably because the oxide is less volatile than the metal.

TABLE 2. Radioactive Elements Present in Aerosols from Simulated Loss-of-Coolant Accidents in Water-Cooled Reactors

Reference	Pages	Fuel	Radioactive Elements in Aerosol
(1)	24,30,35	UO_2	^{89}Sr, ^{95}Zr, ^{106}Ru, ^{131}I, ^{132}Te ^{137}Cs, ^{140}Ba, ^{144}Ce, U
(2)	20	UO_2	I, Te, Cs, Ba
	13,32	U-Al	I, Te, Cs, Ru
(3)	22	U-Al	I
	22,45,54	UO_2	^{137}Cs, ^{131}I, ^{132}Te, ^{89}Sr, ^{140}Ba, ^{106}Ru, ^{95}Zr, ^{144}Ce, U
(4)	6, 8, 9	UO_2	I, Cs, Te, Ru, Pu, Sr
	46-50	UO_2	I
(5)	37	UO_2	I, Te, Cs, Ru, Sr, Ba, Zr, Ce
(6)	12,13,16,17	UO_2	Cs, Ru, Te, Ba, I
(7)	118,119	UO_2	I

Release of U, I, Te, Cs, Sr, and Ba from bare, stainless-steel-clad, and Zircaloy-clad UO_2 has been studied (1, pp. 19-25). The most striking effects were produced by the Zircaloy cladding, which decreased the release of Te and increased that of Sr.

The percentage release of fission products from U-Al alloy appears to be insensitive to burnup, except in the case of I, whose release increases with burnup (3, pp. 5-6). Release from UO_2 is also insensitive to burnup, except that percentage release of Te and Cs increases with burnup (4, p. 6) (5, p. 38), while that of Ru decreases (5, p. 38).

Reactor Transients

Except for additional fission products resulting from increased radiation during the transient, there should not be much difference between aerosols released in transient and loss-of-coolant accidents.

Transient experiments on stainless steel-clad UO_2 were made with atmospheres of argon (3, p. 32) and moist air (4, p. 19). The results with argon did not differ markedly from those with moist air. Aerosol particles (mostly agglomerated) ranged in size from 0.02 μm to 0.9 μm (4, pp. 20,22), and contained UO_2, ^{131}I, ^{129}Te, ^{137}Cs, ^{106}Ru, ^{89}Sr, ^{140}Ba, ^{95}Zr, and ^{144}Ce.

GAS-COOLED REACTORS

The accident envisaged in a gas-cooled reactor is a fire in which the UC_2 fuel is burned.

This accident has been simulated by burning UC_2 coated with pyrolytic carbon and embedded in a graphite matrix. Aerosol particles in the size range 13-35A were found to carry ^{131}I, ^{132}Te, ^{137}Cs, ^{95}Zr, and ^{144}Ce (3, p. 46). Filters used in these experiments collected particles in the size range 0.01 to 70 μm (3, pp. 52,53). Particles of diameter 70 μm are large enough to descend rapidly by gravitation.

LIQUID-METAL-COOLED FAST BREEDER REACTORS

In water-cooled reactors, the fission products are the most hazardous materials present. In LMFBR's, on the other hand, the plutonium used as fuel may well overshadow the fission products as a hazard (8, p. 94). It has been stated that "it is very likely that the behavior of nuclear aerosols, particularly those of sodium and plutonium, will be a controlling factor in reactor safety in the event of a catastrophic accident involving the fast breeder reactor (9, p. 8)."

Information has been obtained on two kinds of simulated accident: firstly, loss of coolant, leading to melting and vaporization of the fuel; secondly, burning of radioactive coolant (molten sodium) accidentally released from the primary coolant loop. Sodium fires of two kinds have been studied, burning of a pool of molten sodium and burning of a spray.

Loss-of-Coolant

This accident has been studied by vaporizing PuO_2 and UO_2 into argon, nitrogen, or air.[8] Both oxides condensed in all the atmospheres to form cubic particles from 40 to 400Å on an edge. These particles quickly agglomerated into chains and clusters of equivalent diameter 0.05 to 0.3 μm. When sodium was present together with PuO_2, the aerosol consisted of cubic PuO_2 particles enclosed in spherical particles of some sodium compound.

Sodium Fires

A pool of sodium in a pot at 1000°F was burned in N_2-O_2 mixtures containing 4% and 21% O_2. Aerosols of initial mean particle radius 0.6 μm (standard deviation 1.2 or 1.75 μm) were obtained (10, pp. 20,24). Over the course of several hours' aging, the mean particle radius increased to 1.0 μm and then decreased.

In order to study the fate of ^{131}I present in a sodium fire, a pool of sodium containing NaI was burned. The iodine remained with the sodium in the resulting aerosol, whose mean aerodynamic equivalent diameter varied over the course of hours between the limits 1 and 3 μm.[12] When a pool of sodium not containing NaI was burned in an atmosphere containing I_2, the resulting aerosol scavenged the I_2 from the gas and had an aerodynamic equivalent diameter of 3.8 μm and standard deviation 1.8 μm.[12]

PLUTONIUM-HANDLING FACILITIES

When not incorporated in a reactor core, plutonium is in chemical processing plants, fabricating shops, or storage. It is usually present in these facilities as metal, in the form of powders of its compounds, or in aqueous or non-aqueous solutions. An analysis of accidents in such facilities has shown the major causes to be explosion, fire, and excess pressure.[13] Aerosols containing plutonium often result from the accidents.

References (13) and (14) report particle sizes for aerosols formed in simulations of accidents that may occur in plutonium-handling facilities. The following is a list of such experiments and the particle sizes measured:

Burning of Pu metal in air	MMD 4.2 μm
Entrainment in air drawn past oxide resulting from burning Pu metal	< 0.5 μm
Heating of partially oxidized Pu oxalate powder in air current	MMD 25 μm
Heating of fresh Pu oxalate powder in air current	5 - 60 μm
Heating of Pu fluoride powder in air current	MMD 26 μm
Boiling of aqueous Pu nitrate solution	MMD 4 μm
Entrainment of air drawn past Pu nitrate left after evaporation of aqueous solution	MMD 20.5 μm

Reference (13) also reports that particulate containing Pu could be filtered out of the gases from burning fir shavings, corrugated cardboard, cheesecloth, and surgeon's gloves contaminated with Pu. These materials are typical of those in contaminated waste cartons, and their ash forms the aerosols.

Although there appears to be only fragmentary information on aerosols that may be released by most types of nuclear accident, it is clear that a great variety of aerosols have to be taken into account in atmospheric scavenging studies. Particles range continuously from molecular sizes up to sizes that settle readily. They may be single particles or long chains, and may consist of insoluble oxides or deliquescent sodium hydroxide.

This report concentrates on the properties possessed by aerosols in the early stages of a nuclear accident. These are the properties that the aerosols would have in the atmosphere if they were promptly released from the containment vessel. A more thorough study of the literature on accident stages 3 and 4 (pp. 68 and 69) is necessary to determine the properties of aerosols released after hours or days of aging in the containment vessel.

REFERENCES

1. *Nuclear Safety Program Semiannual Progress Report for Period Ending 31 Dec. 1962, ORNL-3401, Oak Ridge National Laboratory.*

2. *Nuclear Safety Program Semiannual Progress Report for Period Ending 30 June 1963, ORNL-3483, Oak Ridge National Laboratory.*

3. *Nuclear Safety Program Semiannual Progress Report for Period Ending 31 Dec. 1963, ORNL-3547, Oak Ridge National Laboratory.*

4. *Nuclear Safety Program Semiannual Progress Report for Period Ending 30 June 1964, ORNL-3691, Oak Ridge National Laboratory.*

5. *Nuclear Safety Program Semiannual Progress Report for Period Ending 30 June 1964, ORNL-3843, Oak Ridge National Laboratory.*

6. *Nuclear Safety Program Annual Progress Report for Period Ending 31 Dec. 1968, ORNL-4374, Oak Ridge National Laboratory.*

7. *Reactor Chemistry Division Annual Progress Report for Period Ending 31 Dec. 1968, ORNL-4400, Oak Ridge National Laboratory.*

8. *F. L. Horn, A. W. Castleman. "PuO_2-UO_2-Na aerosols produced by vaporization of fast reactor core materials," in Treatment of Airborne Radioactive Wastes, proceedings of a Symposium, New York, 26-30 Aug. 1968, pp. 93-114, IAEA, 1968.*

9. *BNL-14242, Rapporteur's summary of Session No. 4 of International Congress on the Diffusion of Fission Products, Saclay, France, 4-6 Nov. 1969.*

10. *AI-AEC-12878, Characteristics of Aerosols Produced by Sodium Fires, Vol. II, 31 Oct. 1969.*

11. *J. Granger, C. Nelson, M. Silberberg. "Characterization of Energy Release and Aerosol Behavior from Sodium Spray Fires," presented at 11th AEC Air Cleaning Conference, Richland, Washington, Sept. 1970.*

12. *L. Baurmash, C. Nelson, J. Granger, R. Koontz. "Behavior of Iodine in the Presence of Sodium Oxide Aerosols," presented at 11th AEC Air Cleaning Conference, Richland, Washington, Sept. 1970.*

13. *J. Mishima, L. C. Schwendiman. "The Amount and Characteristics of Plutonium Made Airborne under Thermal Stress," BNWL-SA-3379, October 1970.*

14. *L. C. Schwendiman, J. Mishima, C. A. Radasch. "Airborne Release of Particles in Overheating Incidents Involving Plutonium Metal and Compounds," in Treatment of Airborne Radioactive Wastes, Proceedings of a Symposium, New York, 26-30 Aug. 1968, pp. 117-131. IAEA, 1968.*

BNWL-1551
Part 1

NUMERICAL EXPLORATIONS OF WASHOUT OF AEROSOL PARTICLES

W. G. N. Slinn

A theoretical framework is constructed for the applications to safety analyses of below-cloud rain scavenging research results. Semiempirical expressions are presented for the collection efficiency, for the raindrop and particle size distributions, and for the washout rates. Sample calculations are presented to describe the potentials of the analysis. These examples model the simulated reduction in airborne radioactivity and the contamination of the precipitation, that would result from below-cloud rain scavenging.

There have been a considerable number of analyses of the dependence of the rain scavenging (washout) rate on the size of individual aerosol particles. For reviews see References 1, 2, 3. However, to our knowledge there has been only extremely limited application of these results to the prediction of the rain scavenging of realistic aerosol particle size distributions. Toward removing this deficiency, we have initiated a numerical study of the washout of aerosol particles whose size distributions and radioactive burdens more realistically portray those which are of potential concern for safety analyses. The present brief report describes some of our initial progress.

To determine the rain scavenging rate for a polydisperse aerosol, it is necessary first to consider the rate of removal of a single particle (radius, a) by a single raindrop (radius, R). As is well known,[3] the collection efficiency, E, is not known accurately. For the present, we propose to use

$$E(a,R) = \left[1 - \exp\left(\frac{K}{k}\right)\right] + \frac{4}{Pe}\left(1 + 0.4\ Re^{1/2}Sc^{1/3}\right) \qquad (1)$$

which appears to reflect adequately the present state-of-the-art[1,4,5] for collection by inertial (first term) and diffusional (second term) rain scavenging. In (1):

$K = \frac{2}{9}\frac{a^2\rho_p}{R^2\rho_a}$ Re is the Stokes parameter;

$k \simeq 2$ is an empirical constant,

Pe = Re Sc is the Péclét number,

Re = VR/ν is the Reynolds number;

Sc = ν/D is the Schmidt number,

in which ρ_a and ν are the mass density and kinematic viscosity of air, ρ_p, a and D are the mass density, radius and diffusivity of the aerosol particles, and V and R are the terminal velocity and radius of the raindrop.

To determine the rain scavenging (washout) rate, Λ, for a monodisperse aerosol, (1) must be integrated over all raindrop sizes according to

$$\Lambda(a) = \int_0^\infty \pi R^2 \, E(a,R) \, V(R) \, N(R) \, dR \quad (2)$$

where $N(R)\,dR$ is the number of raindrops per cm^3, whose radius is between R to R + dR. For now, we propose to use an extension of the Khrgian-Mazin[1] raindrop size distribution function:

$$N(R) = \left[\frac{(10^{-4} \text{ sec}) \, J_o}{6\pi \, R_m^{\,7}} \right] R^2 \exp\left(-\frac{2R}{R_m}\right) \quad (3)$$

where R_m is the mean raindrop size, and J_o ($cm\ sec^{-1}$) is the rainfall intensity. Substituting (3) into (2) and using $V = 8000\ R\ (sec^{-1})$,[1] leads to

$$\Lambda(a) = \frac{J_o}{2 R_m} \left\{ \left[1 - \exp\left(-\frac{K}{k}\right) \right] + \frac{0.8}{\langle Pe \rangle} \left(1 + 0.8 \langle Re \rangle^{1/2} \, Sc^{1/3} \right) \right\} \quad (4)$$

where $\langle Pe \rangle$ and $\langle Re \rangle$ are based on R_m.

Some interesting results which follow from (4) are the following. First, the plot of this washout rate (Figure 1) demonstrates the familiar slow rate of removal of aerosol particles whose size is in the range 0.01 to 0.1. Also, directly from (4) we see that the washout rate is fairly well directly proportional to the rainfall rate, although there generally is a dependence of R_m on J_o.[6] Further, we see from (4) that for inertial scavenging $\Lambda \propto R_m^{-1}$, whereas for convective diffusional scavenging by large raindrops $\Lambda \propto R_m^{-2}$.

Now, to determine the rate of removal of a polydisperse aerosol, the size distribution of the aerosol particles must be specified. Again for the present, we use, for the number (at time t) of aerosol particles per cm^3 whose radius is between a and a + da, the modified Khrgian-Mazin spectrum[1]

$$f(a,t)\,da = n(t) \frac{4}{a_m^3} a^2 \exp\left(-\frac{2a}{a_m}\right) da, \quad (5)$$

where n(t) is the total number density of aerosol particles, regardless of their size. Plots of f(a) for various mean particle radii, a_m, are shown in Figure 2 where it is to be noticed that the logarithmic scale on the abscissa overemphasizes the rate of decay of the size distribution function for large particles.

Before applying the above outline to realistic problems, it is necessary also to obtain a specification of the attachment spectrum; i.e., the amount of noxious material attached to aerosol particles as a function of their size. For example, if at time t there are f(a,t)da aerosol particles per cm^3 whose radii are between a and a + da, then we introduce an attachment function $\mathcal{A}(a)$ defined so that (for example) the amount of radioactivity per unit volume which at time t is attached to aerosol

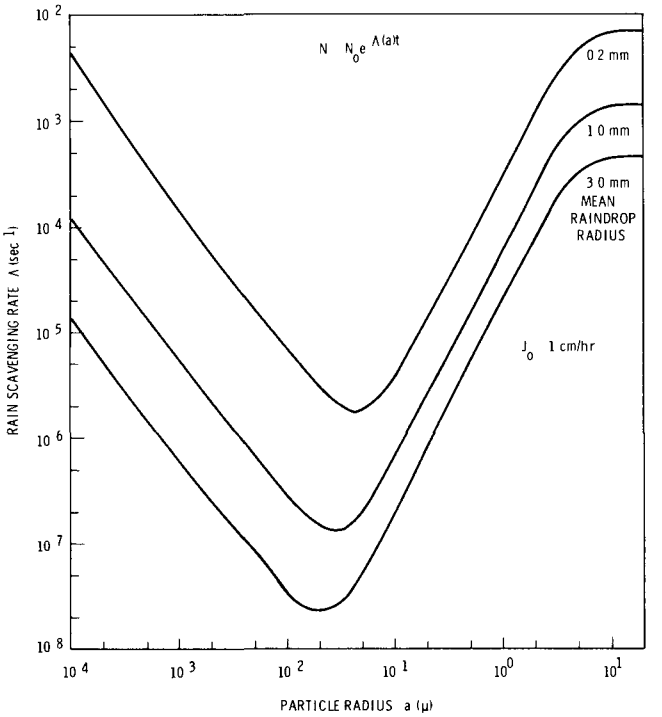

Neg 710973-1

FIGURE 1. The Washout Rate as a Function of Particle Size as Modeled by Equation (4).

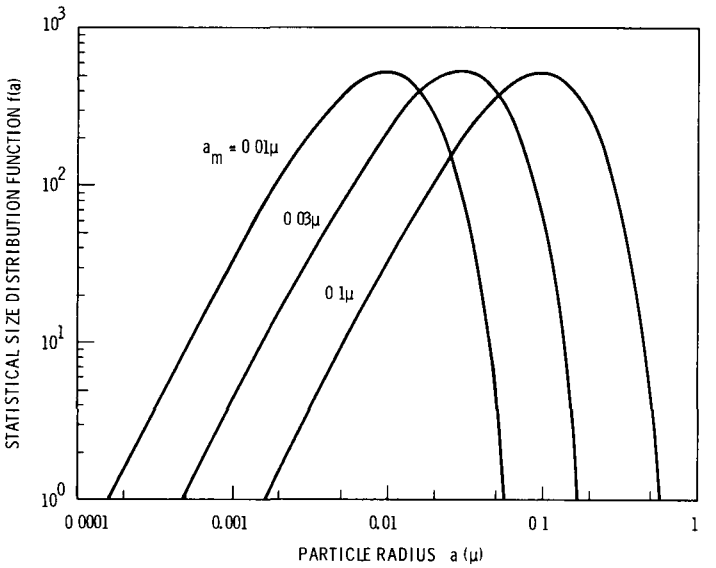

Neg 710973-4

FIGURE 2. Typical Aerosol Particle Size Distributions Used in the Modeling (the units on the ordinate are arbitrary).

particles of radii a to a + da is $\mathcal{Q}(a)$ f da the total radioactivity per unit volume is then

$$A(t) = \int_0^\infty \mathcal{Q}(a)\ f(a,t)\ da. \qquad (6)$$

If initially the total radioactivity per unit volume is A(o) and if the attachment function is proportional to a^n, where usually n = 1, 2 or 3, then from (6) we have that the airborne radioactivity at time t would be

$$A(t) = A(o)\ \frac{\langle a^n(t)\rangle}{\langle a^n(o)\rangle} \qquad (7)$$

$$\text{where } \langle a^n(t)\rangle = \int_0^\infty a^n\ f(a,t)\ da. \qquad (8)$$

The final step toward applying these results is to recognize that the number of aerosol particles of each radius is reduced by rain scavenging, according to

$$f(a,t) = f(a,t = o)\ e^{-\Lambda(a)t} \qquad (9)$$

Thus, upon substituting (9) into (7) we obtain that the airborne radioactivity per unit volume which is attached to aerosol particles, is reduced by washout in the manner

$$A(t) = \frac{A(o)}{\langle a^n(o)\rangle} \int_0^\infty a^n\ f(a,o)\ e^{\Lambda(a)t}\, da. \qquad (10)$$

In (10), f(a,o) would be given by an expression similar to (5).

There are a great number of potential applications of the theoretical framework presented above. Unfortunately, because of the complicated dependence of the washout rate on the particle size [see (4)], the equations must be integrated numerically. Partially just to illustrate these potentials, we have evaluated a limited number of test cases.

Figure 3 demonstrates the slow reduction of airborne radioactivity [according to (10) and using (4) and (5)] when the radioactivity is attached ($\mathcal{Q} \alpha\ a^3$) to aerosol particles of mean radius 0.03 μ. Different mean raindrop radii are considered.

Figure 4 shows the variation in the reduction of airborne radioactivity, as the "rainfall" rate (more realistically, the "spray" rate, such as from a nozzle) changes. For this case, R_m = 0.1 mm and we have explored the case where the radioactivity on an individual aerosol particle is proportional to its radius: $\mathcal{Q} \alpha\ a^1$. The type of results represented by Figures 3 and 4 should permit a comparison of theory with experimental results such as those recently obtained by Beilke[7] on the washout of Aitken particles.

Another type of prediction available from this analysis is concerned with the radioactivity of individual rainfalls. During dt, a raindrop of radius R picks up an amount of radioactivity equal to

$$\pi R^2\ E(a,R)\ V\ dt\, \mathcal{Q}(a)\ f(a,t)\ da.$$

Integrating this over the flight path of the drop and over all particle sizes and assuming that the velocity of the drop is a constant and that f(a,t) is independent of altitude leads to the result for the activity of a single drop:

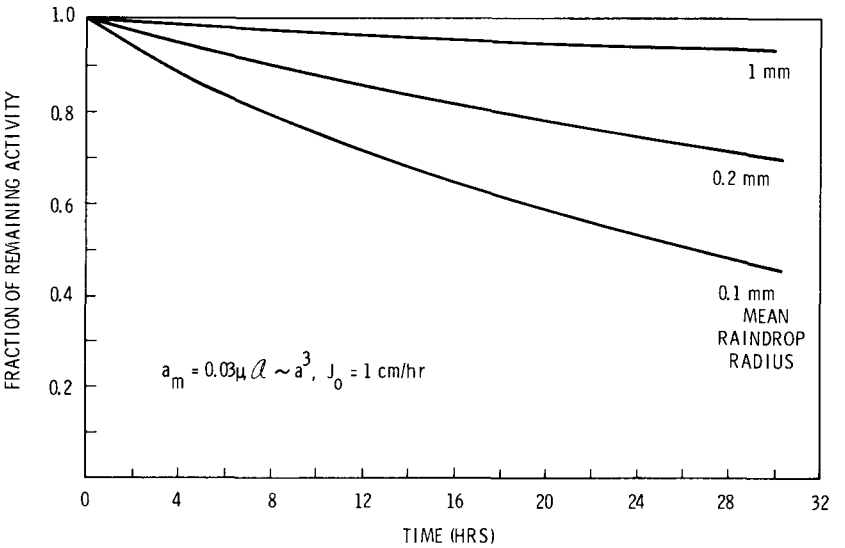

Neg 710973-5

FIGURE 3. The Reduction in the Airborne Radioactivity Attached to Aerosol Particles of Mean Radius 0.03 μ by a 1 cm-hr Rainfall Rate of Different Mean Raindrop Sizes.

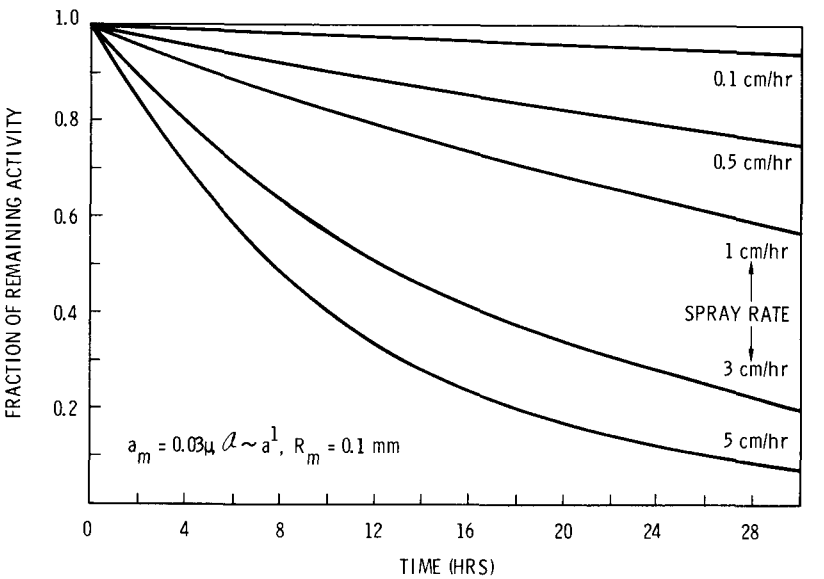

Neg 710973-6

FIGURE 4. Similar to Figure 3 Except that the Activity on an Individual Particle Is Assumed to be Proportional to its Radius and the "Rainfall" Rate Is Varied at Fixed r_m.

$$\pi R^2 H \int_0^\infty \mathcal{A}(a)\ f(a)\ E(a,R)\ da. \quad (11)$$

where H is height through which the drop has fallen. The flux of radioactivity to the ground (under the above restrictive assumptions which, however, can easily be removed) is then

$$H \int_0^\infty dR\ N(R)\ V(R)\ \pi R^2 \int_0^\infty da\ \mathcal{A}(a)\ f(a)\ E(a,R) \quad (12)$$

Dividing (12) by the flux of water to the ground, ρJ_o, where ρ is the density of water, leads to the prediction for the below-cloud scavenging concentration ratio {i.e., the ratio of the concentration of the radioactivity in the precipitation κ(dpm/g H_2O) to the concentration in air [see Equation (6)], χ (dpm/m^3 in air)} the result:

$$\frac{\kappa}{\chi} = \frac{H\ (10^{-6}\ m^3\ cm^{-3})}{A\ \rho J_o} \int_0^\infty da\ \mathcal{A}(a)\ f(a)\ \Lambda(a,R_m). \quad (13)$$

A sample calculation based on (13) is shown in Figure 5. Since κ/χ ratios for in-cloud nucleation scavenging are typically $\mathcal{O}(1)$,* it is interesting to notice the relatively inefficient scavenging by rain of aerosol particles of radii near 0.03μ. It is also interesting to observe the dependence of κ/χ on mean raindrop size. Experimental results obtained by Makhon'ko[8] of a similar effect are discussed in a companion paper in this volume.*

In conclusion, the purpose of this report has been to illustrate some of the directions in which precipitation scavenging research can proceed, toward assisting safety analyses. The computations displayed were chosen to illustrate the potential applications of this modeling.

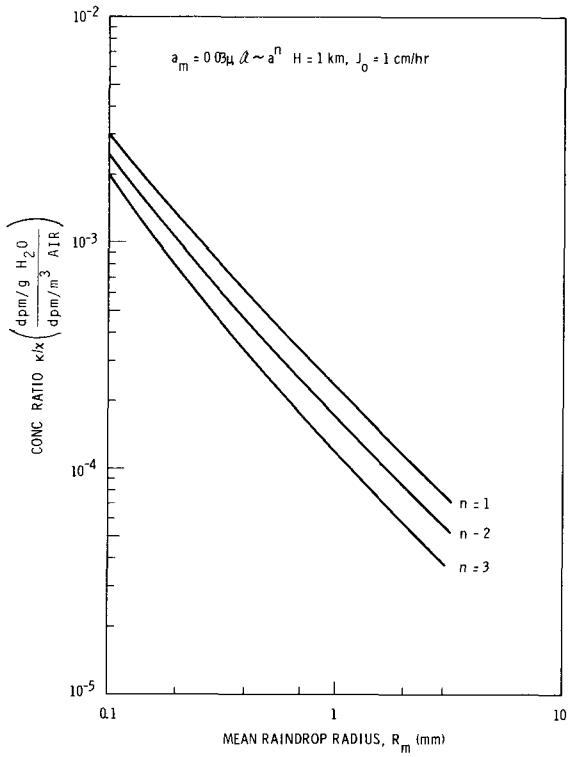

Neg 710973-2

FIGURE 5. The Ratio of the Concentration of Radioactivity in Precipitation (dpm/g H_2O) to the Concentration in Air (dpm/m^3, air) as a Function of a Mean Raindrop Radius for a Fall Height of 1 km and a Rainfall Rate of 1 cm/hr.

*See the contribution in this volume entitled "An Inquiry Into the Causes of the Variations in the Bomb Debris Scavenging Ratios" by the same author.

REFERENCES

1. A. G. Zimin. Mechanisms of Capture and Precipitation of Atmospheric Contaminants by Clouds and Precipitation." Problems of Nuclear Meteorology, edited by I. L. Karol' and S. G. Malakhov. Translated from a publication of the State Publishing House, Moscow, 1962. AEC-tr-6128, 1964.

2. K. P. Makhon'ko. "Spontaneous Removal of Radioactive Dust from the Lower Troposphere (Review)," Izv. Atmos. and Oceanic Phys., Vol. 2, pp. 508-522 (transl. pp. 304-313), 1966.

3. R. J. Engelmann. "The Calculation of Precipitation Scavenging," in Meteorology and Atomic Energy 1968, D. H. Slade, ed., U. S. Atomic Energy Commission, Division of Technical Information, available as TID-24190 from the Clearinghouse, 1968.

4. Precipitation Scavenging (1970), R. J. Engelmann and W.G.N. Slinn, coords., AEC Symposium Series, No. 22. Available from NTIS as CONF-700601. 1970.

5. Atmospheric Scavenging of Radioisotopes, B. Styra, C. Garbaliauskas and V. Lujanas, eds. Akademiya Nauk Litovskoi SSR, available from NTIS, TT 69-55099. 1970.

6. M. T. Dana. "Olympic Peninsula Rain: Characterization of Size and Electric Charge," Pacific Northwest Laboratory Annual Report for 1969, Vol. II: Physical Sciences, Part 1. Atmospheric Sciences, BNWL-1307, Battelle-Northwest, Richland, Washington, June, 1970.

7. S. Beilke. Untersuchungen Über Das Auswachen Atmosphärischer Spurenstoffe Durch Niederschläge Nr. 19, Berichte Des Institutes Für Meteorologie Und Geophysik Der Universität Frankfurt/Main. Frankfurt-Main, Feldergstrasse 47. Translation as APTIC TR-0901, Environmental Protection Agency. 1970.

8. A. S. Avramyenko and K. P. Makhon'ko. "Radioactivity of Raindrops," Izv. Atmos. and Oceanic. Phys., Vol. 5, pp. 647-648 (transl. pp. 375-376). 1969.

PRECIPITATION SCAVENGING OF TRITIUM AND TRITIATED WATER

J. M. Hales and L. C. Schwendiman

A method is being developed, based upon reversible gas-scavenging theory, to enable the estimation of rain-scavenging rates of tritium and tritiated water. This method will be applicable to problems involving scavenging in plumes as well as in the general atmosphere.

A project has been initiated to develop a reliable method of calculating deposition of tritium gas and tritiated water through natural atmospheric washout processes. This method, which is applicable to systems involving tritium compounds in plumes as well as those dispersed in the atmosphere, is based primarily upon a theory of reversible gas scavenging developed and presented in an earlier report.[1]

The present analysis focuses upon a single raindrop of diameter D falling through a region of known pollutant concentration. Washout of pollutant may occur by two mechanisms:

1. Scavenging of gaseous pollutant by the falling drop.
2. Capture of pollutant-containing fog-droplets by the falling drop.

Pollutant captured by the drop can be released subsequent to pick-up through desorption, depending upon concentration levels in the ambient gas.

The analysis is facilitated greatly by the fact that solubility equilibrium between tritium gas, tritiated water, and water follow a linear relationship (Henry's law), which can be expressed as

$$P_A = H X_A; \; H = \text{constant}, \qquad (1)$$

where P_A and X_A are the partial pressure and liquid-phase mole-fraction of pollutant A at equilibrium. Applying this analysis to estimate dC/dz, the rate of concentration change of a raindrop falling through a polluted atmosphere, where y_{Ab} is the gas-phase mole fraction and m the mass-concentration of suspended fog droplets, gives the result

$$\frac{dC}{dz} \simeq - \frac{3\,E(d)\,m\,y_{Ab}}{2\,D\,\rho_w\,H'} + \frac{6\,K_y}{v_t\,D}\,(y_{Ab} - H'C). \qquad (2)$$

This may be integrated to give

$$C(D,O) = \xi \int_o^{z_o} e^{\zeta z}\, y_{Ab}\, dz \qquad (3)$$

$$\xi = \frac{-6\,K_y}{D\,v_t} + \frac{3\,E(D)\,m}{2\,D\rho_w\,H'} \qquad (4)$$

$$\zeta = \frac{6\,K_y\,H'}{v_t\,D}. \qquad (5)$$

Here the nomenclature is defined as follows:

D = drop diameter
$E(D)$ = average collection efficency for cloud droplets
H' = H/molar concentration of condensed water
K_y = overall mass-transfer coefficient
ρ_w = density of water
v_t = terminal velocity of drop, dz/dt
y_{Ab} = gas-phase pollutant concentration.

Equation (2) et seq. is based upon the following assumptions:

1. Collection of pollutant by the mechanisms of particulate and gaseous scavenging in any differential element of plume is an additive function,
2. m is independent of z,
3. Suspended fog droplets are at equilibrium with gas-phase pollutant levels.

To determine ground-level deposition, y_{Ab} must be specified and the concentrations predicted by (3) must be distributed according to the rain size spectrum. If the Pasquill equation[2] is used for y_{Ab}, then upon the assumption of vertical rainfall, Equation (3) may be expressed as follows:

$$C(x,y,a) = \frac{\xi Q}{2\, u\sqrt{2\pi}\,\sigma_y} \exp - \left[1/2(y/\sigma_y)^2\right] \cdot \exp\left(\sigma_z^2\, \zeta^2/2\right).$$

$$\left\{\exp(-\zeta h)\ \left\{\operatorname{erf}\left[\ \sqrt{2}\ \sigma_z \left(\frac{\zeta}{2} - \frac{h}{2\sigma_z^2}\right)\right] + \operatorname{erf}\left[\frac{z_o - \sigma_z^2\,\zeta + h}{\sigma_z\sqrt{2}}\right]\right\}\right.$$

$$\left.\exp(\zeta h)\left\{\operatorname{erf}\left[\ \sqrt{2}\ \sigma_z \left(\zeta/2 + \frac{h}{2\sigma_z^2}\right)\right] + \operatorname{erf}\left[\frac{z_o - \sigma_z^2\,\zeta - h}{\sigma_z\sqrt{2}}\right]\right\}\right\}. \qquad (3a)$$

This may subsequently be distributed over the rain-size spectrum to predict deposition at any location(x, y) beneath the plume. The parameters h, Q, σ_i in (3a) designate emission height, source-strength, and standard deviation in accordance with Pasquill's original result.

It should be noted that this treatment is not restricted to Pasquill-type plumes, Equation (3) being applicable to any geometry of y_{Ab}. In particular, this equation can be used to estimate scavenging behavior in the atmosphere in general as long

as the vertical distribution of pollutant is known.

It is expected that this project shall be completed in the near future, culminating in a publication containing illustrative distributed solutions of (3a) for a variety of atmospheric conditions, and including a recommended procedure for the general estimation of tritium deposition rates.

REFERENCES

1. *J. M. Hales, J. M. Thorp and M. A. Wolf. Field Investigation of Sulfur Dioxide Washout and Rainout from the Plume of a Large Coal-Fired Power Plant by Natural Precipitation, Final Report to Environmental Protection Agency, Air Pollution Control Office, Contract CPA 22-69-150, March 1971.*

2. *F. A. Gifford. "An Outline of Theories of Diffusion in the Lower Layers of the Atmosphere," in Meteorology and Atomic Energy 1968, D. H. Slade, ed., U.S. AEC, 1968.*

THE EFFECT OF WIND ON RAIN SCAVENGING

W. G. N. Slinn and B. C. Scott

A preliminary theoretical evaluation is made of the effect of wind on rain scavenging. The theory is compared with a recent calculation by Berg on the influence of the mean wind on experiment R15 performed by Engelmann. In agreement with Berg's, the results show that even in this extreme case of variable mean wind experienced by the raindrops, the effect of reasonable variations of aerosol particle mass density is more important than the variations of the mean wind. It is proposed that the calculations be extended to study the influence of atmospheric turbulence on scavenging.

Berg[1] has recently made an interesting study of the effect of wind on rain scavenging of large ($\sim$10 μ) aerosol particles. Specifically, he has analyzed the influence of the wind on experiment R15 performed by Engelmann,[2,3] who released artificial rain from a height of approximately 30 m and determined the precipitation's efficiency for scavenging ZnS particles from a controlled plume. In Figure 1, the solid curves show the measured air concentration of ZnS particles in the plume, and the pertinent wind profile. In the present report we shall present a re-evaluation of Berg's analysis of R15, with the objective of constructing a basis for the future study of the effect on scavenging of atmospheric turbulence. For convenience in the

numerical analysis we shall use for the "observed" profiles, the analytic curves which are given by the dashed lines of Figure 1.

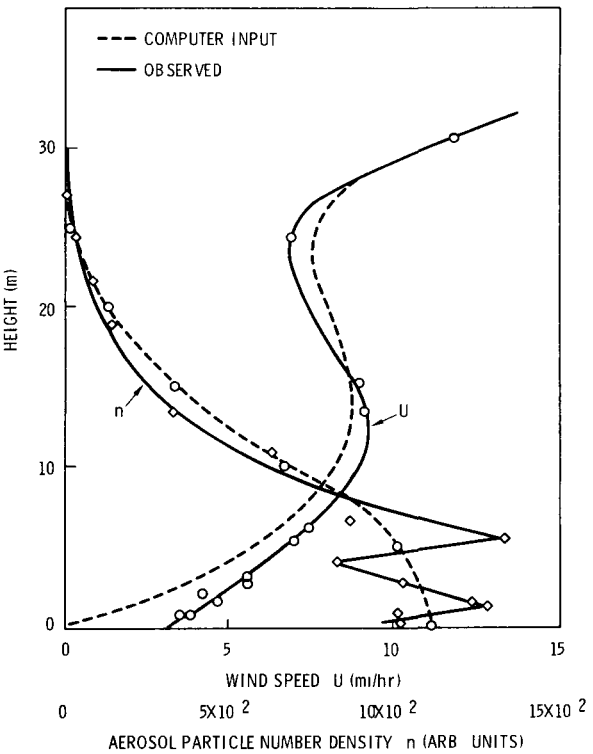

Neg 710972-6

FIGURE 1. The Measured Profiles of the Mean Wind, U(mi hr^{-1}) and Aerosol Particle Number Density, n (arbitrary units) for R15 as Obtained by Engelmann.(2) For convenience in the numerical calculations, use was made of analytical expressions for the profiles, which are plotted as the dotted curves.

To determine the number of particles collected by a raindrop of mass M and diameter D, its trajectory must be found. To this end, we introduce the symbols defined in Figure 2 and

$\vec{V}$ = velocity of drop (cm sec^{-1})
$\vec{U}$ = velocity of wind (cm sec^{-1})
$\vec{V}-\vec{U} \equiv \vec{v}$ = relative velocity (cm sec^{-1})
$v = |\vec{v}|$ = relative speed (cm sec^{-1})
D = drop diameter = 1.56 mm
M = drop mass (g)
d = particle diameter = 15 μ
n = particle number density (cm^{-3})
ρ_p = particle density (g cm^{-3})
ρ_a = air density (g cm^{-3})
ν = kinematic viscosity of air (cm^2 sec^{-1})
g = acceleration of gravity (cm sec^{-2})

The equations of motion for the drop are

$$\frac{d\vec{R}}{dt} = \vec{V} \qquad (1)$$

$$\frac{d\vec{V}}{dt} = M\,g\,(-\hat{k}) - \vec{D} \qquad (2)$$

in which the drag force is

$$\vec{D} = \frac{1}{2}\,\rho_a\,v^2\,\frac{\pi D^2}{4}\,C_D\,\frac{\vec{v}}{v}\,. \qquad (3)$$

A semi empirical expression for the drag coefficient derived by Abraham[4] is

$$C_D = C_o\left[1 + \frac{\delta_o}{Re^{1/2}}\right]^2 \qquad (4)$$

where the constants have the values

$$C_o \delta_o^2 = 24$$

$$\delta_o = 9.06$$

and Re is the Reynolds number based on the drop diameter: $Re = Dv/\nu$. The set of Equations (1) to (4) is sufficient to determine the drop's trajectory.

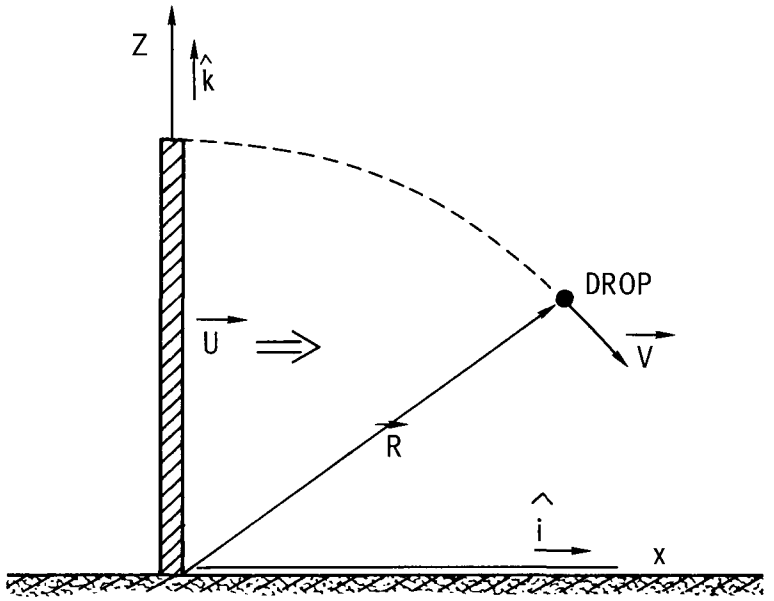

Neg 710973-7

FIGURE 2. Notation Used in the Calculation of the Drop Trajectory.

An interesting result of the calculation of the trajectory is shown in Figure 3 where the relative speed between the drop and the air is plotted as a function of time. When the drop is released from the top of the tower, there is a large (∿10 mph wind) relative speed, since it is assumed that the velocity of the drop with respect to the tower is initially zero. During the first (approximately) tenth of a second, the relative speed falls since the drop is accelerated by the wind. Thereafter, between 0.1 and 1 second, the relative speed increases due to the gravitational acceleration of the drop. During the remaining portion of the drop's flight, the relative speed varies slightly from the terminal speed of

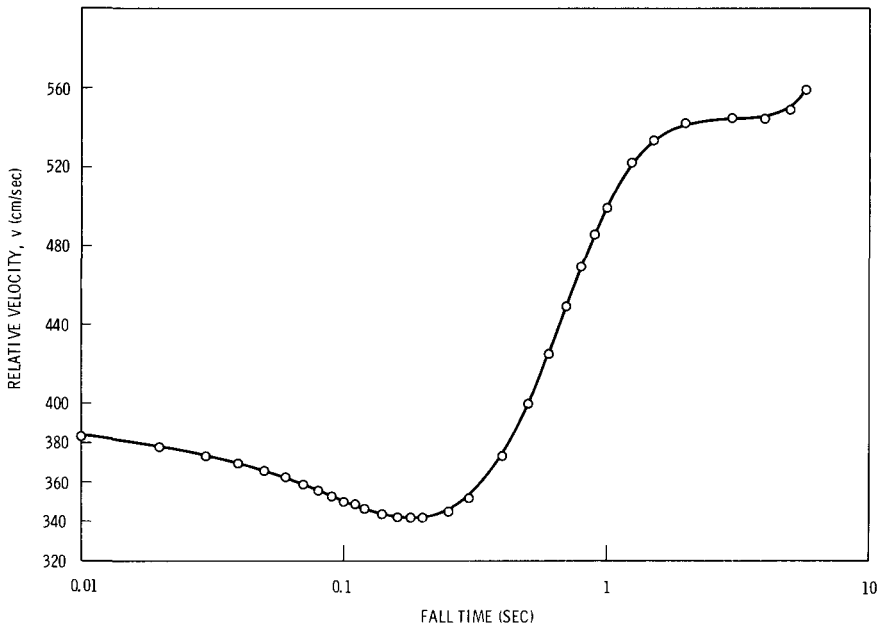

Neg 710972-11

FIGURE 3. Computed Results for the Time Dependence of the Relative Speed Between a 1.56 mm Drop and Air. The initial velocity of the drop with respect to the ground was assumed to be zero, and the mean wind profile was as shown in Figure 1.

the drop, because of the variation in the wind speed (see Figure 1).

To calculate the number of aerosol particles scavenged by the drop, we use the relation that during each time interval, dt, the number picked up is

$$\frac{\pi D^2}{4} \; E(K) \; v \; n(z) \; dt \qquad (5)$$

where E(K) is the collection efficiency of the drop, which for particles larger than about 1 μ depends on the Stokes' impact parameter

$$K = \frac{\rho_d}{\rho_a} \frac{d^2}{D^2} \frac{R_e}{9}. \qquad (6)$$

Since E(K) is not known accurately, even for nonaccelerating flow fields around a drop,[2,5] we believe it to be representative of the state-of-the-art, to use the following semi-empirical expression* for the collection efficiency[6]

$$E(K) = [1 - e^{-K/2}]. \qquad (7)$$

It is not proposed that this expression necessarily describes the true collection efficiency very accurately, but it is expected that it contains sufficient accuracy to allow us to

*See the contribution in this volume entitled "Numerical Explorations of Washout of Aerosol Particles."

explore the effects of wind on rain scavenging. In Figure 4 is shown the variation of the collection efficiency [as given by Equation (7)] during the fall time of the drop for the case where $\rho_p = 1$ g cm^{-3}. The variation of E in this case is more pronounced than for the case $\rho_p = 4$ g cm^{-3}.

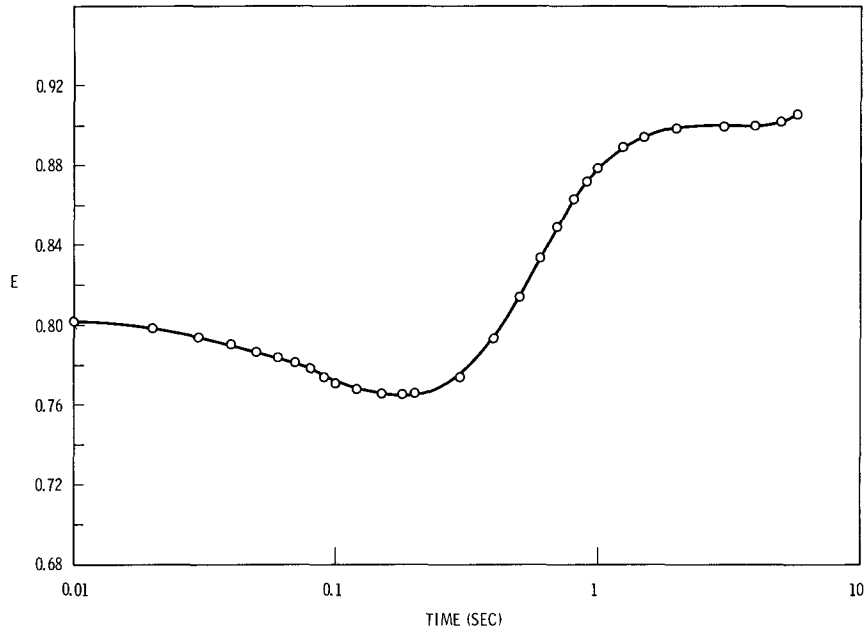

Neg 710972-12

FIGURE 4. The Variation in the Collection Efficiency for a 1.56 mm Drop Falling Through the Observed Mean Wind Profile for R15, Assuming Aerosol Particle Density of 1 g cm^{-3} and Diameter of 15 μ.

To determine the number of ZnS particles collected by the drop, we integrated (5) using (6), (7) and the relative velocity as obtained above (e.g., see Figure 3). Results of these calculations are shown in Figure 5 which demonstrates the number of ZnS particles scavenged by the drop as a function of height. Since n(z), the number density of particles in the air, is given in arbitrary units, there is no significance to the absolute values on the abscissa of Figure 5. However, viewed as a statistical average over many drops, a number such as 10^{-1}

particles collected by one drop, after falling 8 meters, would mean that one in 10 drops would have collected one ZnS particle.

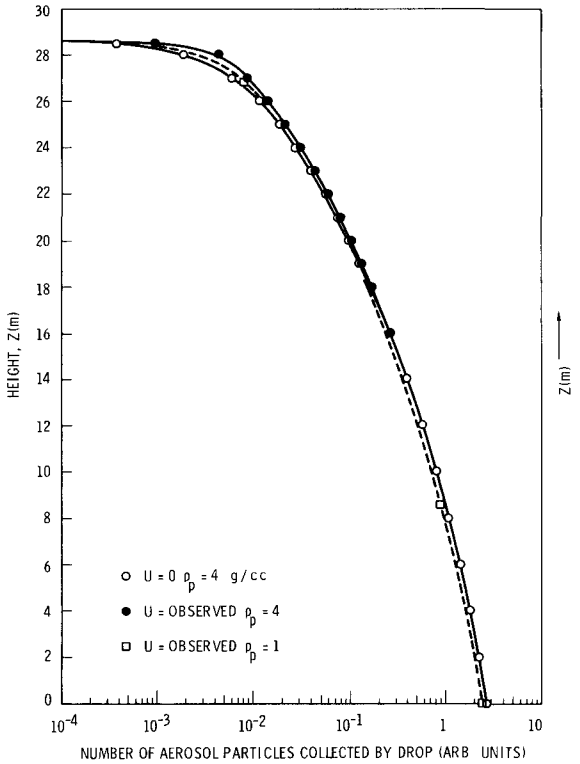

Neg 710972-10

FIGURE 5. Computed Results Showing the Effect of Variation of the Mean Wind on the Rain Scavenging by 1.56 mm Drops, of 15 μ Aerosol Particles.

The major result shown on Figure 5 is that for R15, the wind did not significantly influence the scavenging. This can be seen from Figure 5 by comparing the curve for the case of zero wind speed with the curve derived using the observed wind profile. From this result one should not necessarily infer that the influence of atmospheric turbulence on scavenging is negligible, since the results in Figure 5 are definitely responsive to the experimental conditions of R15, wherein the most concentrated region of the plume was apparently low enough so that the drop had essentially reached its terminal velocity. On the contrary, the differences in the curves of Figure 5 in the first few meters suggest that turbulence effects should be investigated.

Other results of these calculations are shown by a few data points on Figure 5, and more explicitly on Figure 6, where the results are magnified for the first few meters of the drop's trajectory. The effect explored was the consequence of different mass densities of the ZnS particles and therefore, different impact parameters [see Equation (6)]. It is seen in Figure 6 that if the mass density of the ZnS particles was 1 rather than 4 g cm^{-3}, then the number of particles scavenged by the drop would be smaller. The computed point at the end of the trajectory of the drop (shown on Figure 5) reflects the prediction that there is about a 10% reduction in the number of ZnS particles scavenged by the drop, if ρ_p = 1 instead of 4 g cm^{-3}. Figure 6 further emphasizes the small effect of the wind on the scavenging, where plots for the cases: U = 0, 3.576 m sec^{-1}, and the observed wind profile, are shown.

In conclusion, this has been an exploratory study of the effect of

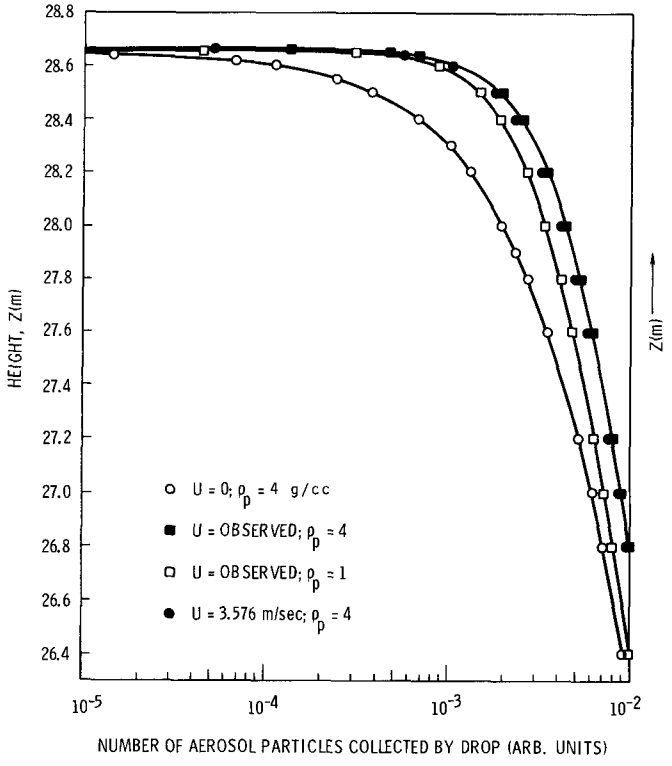

Neg 710972-7

FIGURE 6. The Variation in the Washout Rate During the First Few Meters of the Drop's Trajectory.

wind on rain scavenging. It is proposed that future studies of the influence of turbulence on scavenging will use the above analysis as a theoretical base. For example, we propose to add fluctuating components to the mean wind, and vary the amplitude of these fluctuations to model the observed energy spectral density of atmospheric turbulence.

We wish to express our appreciation to T. G. Owe Berg for providing us with a preprint of his manuscript and to R. J. Engelmann for his assistance in identifying R15 as a useful test case.

REFERENCES

1. *T. G. Owe Berg. "The Effect of Wind on Washout by Rain," submitted for publication in J. Atmos. Sci., 1970.*

2. *R. J. Engelmann. Rain Scavenging of Particulates, HW-79382. Hanford Atomic Products Operation Richland, Washington. 1963.*

3. *R. J. Engelmann. "Rain Scavenging of Zinc Sulphide Particles," J. Atmos. Sci., vol. 22, pp. 719-727. 1965.*

4. *F. F. Abraham. "Functional Dependence of Drag Coefficients of a Sphere on Reynolds Number," Phys. Fluids, vol. 13, pp. 2194-2195. 1970.*

5. *A. G. Zimin. "Mechanisms of Capture and Precipitation Contaminants by Clouds and Precipitation," Problems of Nuclear Meteorology, Moscow, 1962. (Transl. AEC-TR-6128, p. 139).*

6. *D. H. Michael and P. W. Norey. "Particle Collision Efficiencies for a Sphere," J. Fluid Mech., vol. 37, pp. 565-575. 1969.*

RAINDROP ELECTRIC CHARGE: CONTINUOUS VERSUS SHOWERY RAINFALL

M. T. Dana

Sensitive measurements of electric charges on Pacific Northwest coastal raindrops show that there exist significant differences in the characteristics of the charge distributions between rains of different synoptic types. The continuous rain (generally pre-frontal) is always positively charged, with little time variation in the distribution parameters; but instability showers are apt to have net charges of either sign with frequent switching and greater magnitudes.

Extensive data on precipitation characteristics have been collected at the Olympic Peninsula field site over the past four winter seasons. Raindrop charges were previously examined[1,2] on a gross basis; that is, by collecting many rain charge samples and characterizing them in terms of the accompanying rainfall intensity. Further analyses of the data, and of some additional showery rain charge samples, has revealed some basic differences in raindrop charge spectra between continuous and showery rain.

A selection was made of groups of raindrop charge samples, taken both during continuous (generally pre-frontal) and unstable showery conditions. The samples were considered representative of the trends in rainfall intensity and of the general electric polarity and magnitude of the complete raindrop charge record. The samples were divided into positive and negative components and distributed statistically. In most cases, the unipolar distributions are lognormal; consequently, the number median charge magnitude determined from a sample is nearly the geometric number median value.

CONTINUOUS RAIN

Results of measurements of rain drop electric charges during a period of continuous rain, typical of those associated with frontal activity at the Quillayute site, are shown in Figures 1 through 3. This period of rain occurred about 1100 to 1200 PST 7 December 1968, several hours in

advance of a frontal passage. In Figure 1, the positive and negative median charges are shown as cross-hatched bars flanking the time axis; superimposed is the rainfall intensity record. The net charge for each sample -- which here is the mean of the positive and negative medians, weighted by their relative numbers -- is shown as a solid black bar. The net charge is positive throughout, and the positive fraction of the total number of pulses varied from 0.64 to 0.93, averaging 0.79 for all the samples.

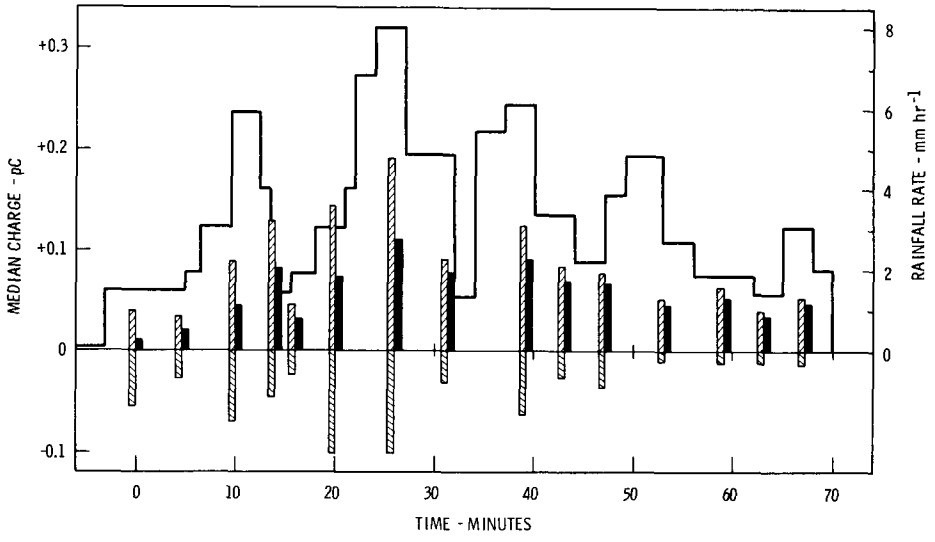

Neg 704303-6

FIGURE 1. Time Evolution of the Rainfall Rate and Median Raindrop Charge Values for the Rain Period ca. 1100-1200 PST, December 7, 1968. See text for explanation of symbols.

Figures 2 and 3 show the time evolution of the bipolar distribution of raindrop charges for the same time period as Figure 1. The charge scale is linear but, for compactness in displaying the extremities of the distributions, the scale is compressed by a factor of ten beyond a charge magnitude of 0.15 pC (picocoulomb). Dashed lines, parallel to the time axis, indicate the point of change of scale. The ordinate of the distributions, the "frequency" $F_{\pm i}$ is given by

$$F_{\pm i} = \frac{\frac{n_{\pm i}}{\Delta_i}}{\frac{n_{\pm i}}{\Delta_i}} \frac{n_{\pm i}}{(n_{+i} + n_{-i})} \qquad (1)$$

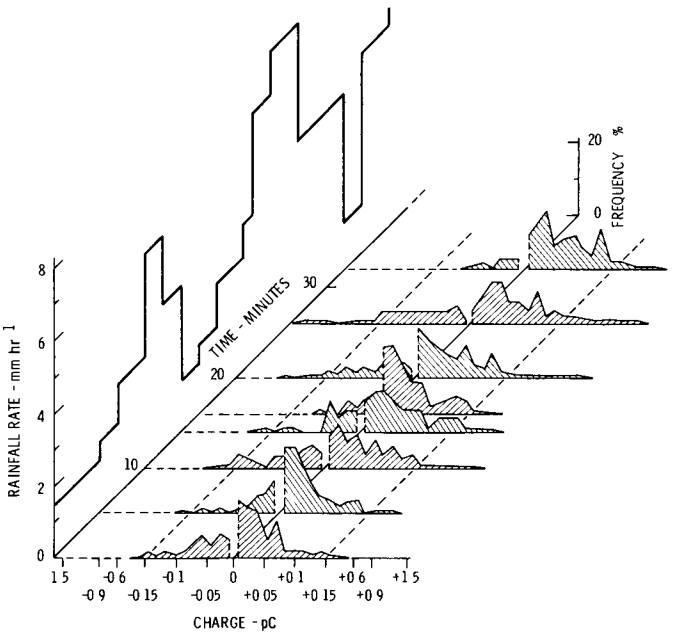

Neg 704303-4

FIGURE 2. Time Evolution of the Raindrop Charge Distribution for the Rain Period 1100-1200 PST, December 7, 1968. See text for explanation of scale units.

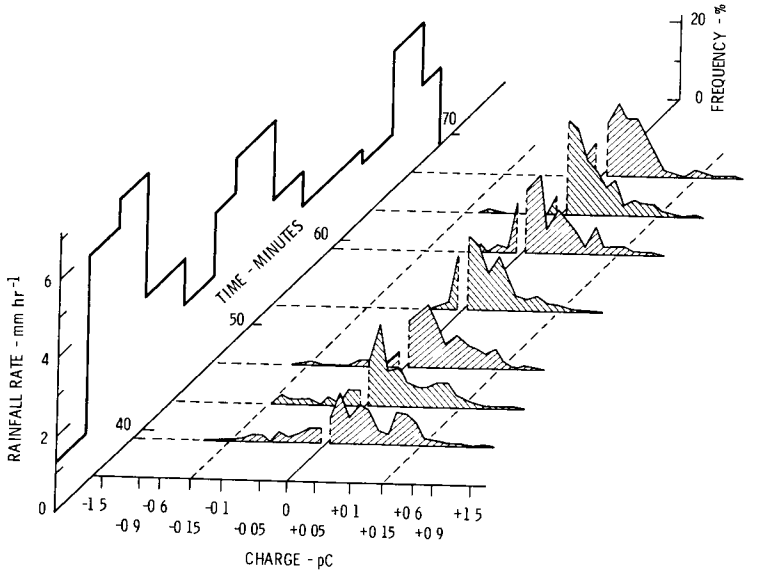

Neg 704303-5

FIGURE 3. Continuation (in time) of Figure 2.

where Δ_i is the width of the charge interval in pC (picocoulomb), and $n_{\pm i}$ are the numbers of pulses of each sign in the interval. With the frequency expressed in this way, the areas under the distribution curves are equal, and the areas of the positive and negative components of any given distribution are proportional to the relative numbers of positive and negative pulses. The value of Δ_i for charge magnitudes less than 0.15 pC is 0.015 pC, and for magnitudes greater than 0.15 pC, Δ_i is 0.15 pC. For clarity in presentation, the curves are shown as lines connecting the midpoints of the intervals, rather than as histograms. The gap in the distributions about zero charge indicates the lower limit of measurement sensitivity -- about 0.01 pC in this case.

For this rain period, the positive charges predominate, but at the higher rainfall intensities the distributions are broader, with a greater proportion of negative charge. The latter stage of the rain period (Figure 3) shows increasing positivity of the charge distribution, and a decrease of magnitudes.

SHOWERY RAIN

Unlike the continuous (pre-frontal) rain, showery rain brings charges which are apt to be of either polarity and of greater magnitude. Figures 4 and 5 are time evolution graphs of a rain period ca. 1600 PST 13 December 1968, at approximately one hour after frontal passage. The net charge swings rapidly between positive and negative, but the second rainfall intensity peak, much like the first, showed more consistency in magnitude, despite the polarity shifts. The three consecutive charge samples about minute 20 (see Figure 5) show a sudden spurt of negatively charged rain immersed in a generally positive shower. The values for Δ_i in Figure 5 are 0.03 pC (magnitudes less than 0.3 pC) and 0.30 pC (magnitudes greater than 0.3 pC).

Another example of shower rain charge measurements is presented in Figures 6 and 7. This was an isolated period of rain on 16 March 1970, an instability shower following significant frontal activity the day before. The region was dominated by a moist unstable air mass; a strong westerly flow contributed to well developed convective precipitation. The charge magnitudes are much higher than previous samples (note the charge scale in Figure 6 -- a factor of ten greater than that of Figure 4) and the net charge changed twice during the period of most intense rain. The predominant sign was negative, but toward the end, as Figure 7 shows, a distribution characteristic of continuous rain is approached. The values for Δ_i in Figure 7 are 0.2 pC (magnitudes less than 2.0 pC) and 2.0 pC (magnitudes greater than 2.0 pC).

DISCUSSION

With very few exceptions, the samples taken from charge records in continuous rain show a net positive electrification, with the ratio

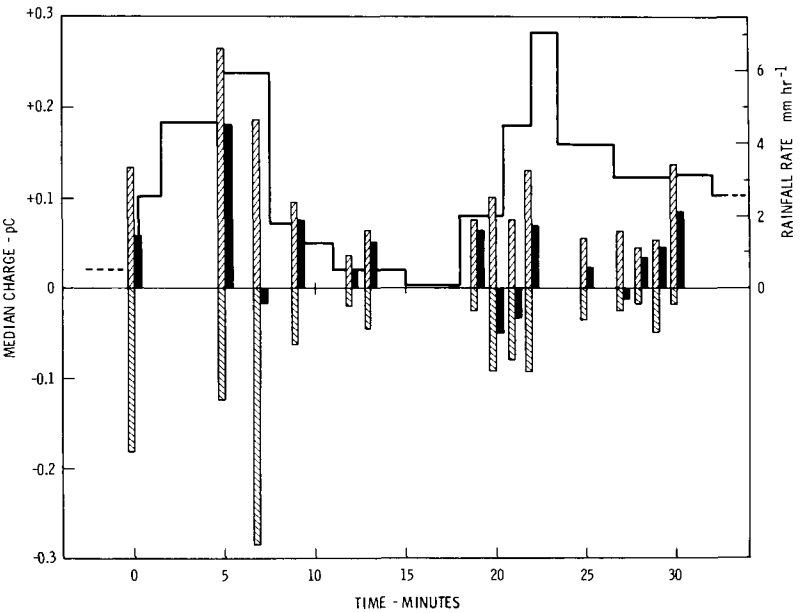

Neg 704303-3

FIGURE 4. Time Evolution of the Rainfall Rate and Median Raindrop Charge Values for the Showery Rain Period of December 13, 1968.

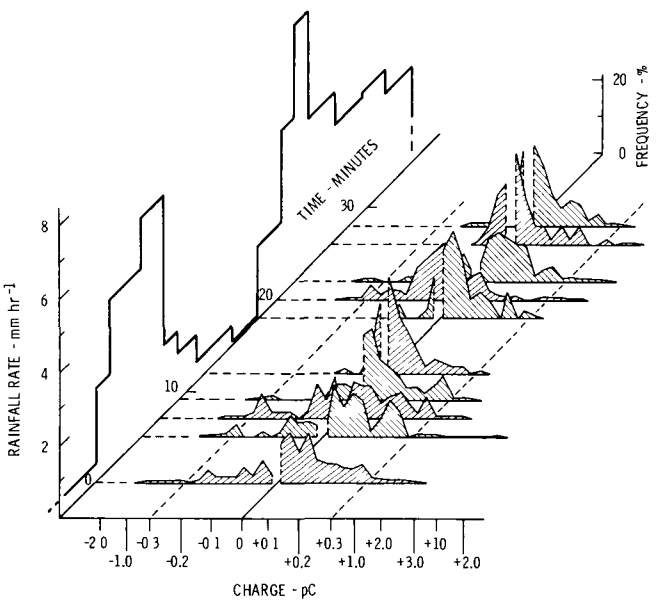

Neg 704303-2

FIGURE 5. Time Evolution of the Raindrop Charge Distribution for the Showery Rain Period of December 13, 1968.

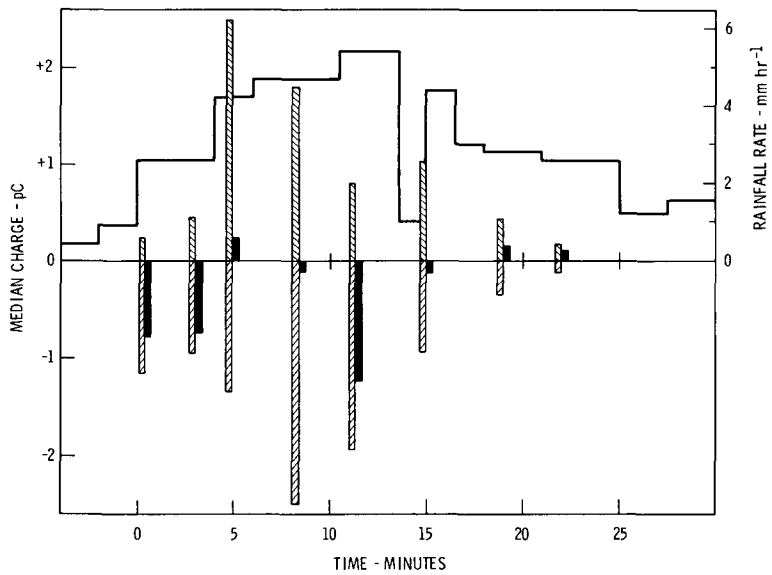

Neg 704303-8

FIGURE 6. Time Evolution of the Rainfall Rate and Median Raindrop Charge Values for the Showery Period of March 16, 1970.

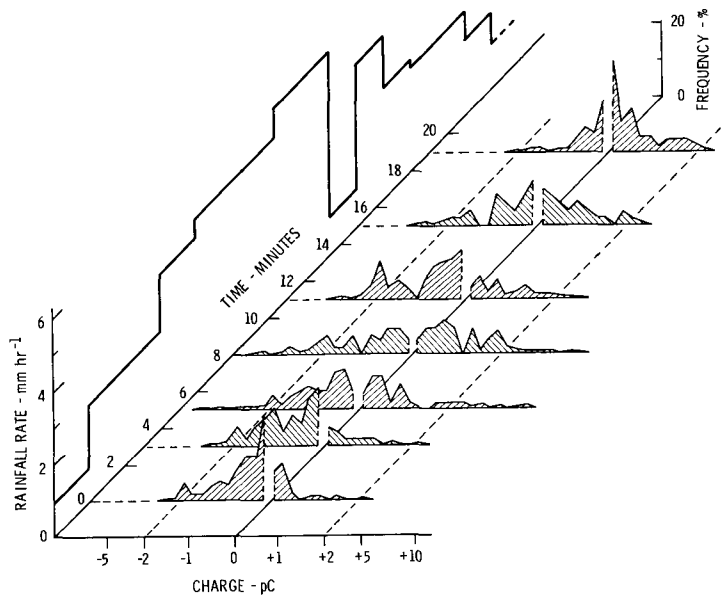

Neg 704303-1

FIGURE 7. Time Evolution of the Raindrop Charge Distribution for the Showery Rain Period of March 16, 1970.

of numbers positive to negative at least 2:1. The shape of the distributions, such as those in Figures 2 and 3, are rather uniformly representative of the gross distributions for the appropriate rainfall intensity. In general, the distributions are modified only slightly by an increase in intensity: the medians increase slowly and the distributions broaden, mainly on the positive side, because of small increase in the number of more highly charged raindrops. At the highest intensities, i.e., at the peak intensity of rain periods, the negative side of the distribution broadens as well. The general positivity of the net electrification is in agreement with the observations of Reiter,[3,4] whose voluminous records show the predominance of positive precipitation current in situations of continuous rain.

A near-neutral or unstable atmosphere, conductive to convective activity, appears to be accompanied by a greater chance for negatively charged rain, frequent and sometimes rapid changes in polarity, and -- in the results herein -- raindrop charges of significantly higher magnitude. These results compliment Reiter's[3] findings of near equal probability of either polarity for the atmospheric potential gradient and precipitation current during shower precipitation, and support his view that the electrical characteristics at a given time may be used as a rather accurate indicator of the general synoptic situation.

REFERENCES

1. *M. A. Wolf and M. Terry Dana. "Experimental Studies in Precipitation Scavenging," Pacific Northwest Laboratory Annual Report for 1968, Vol. II: Physical Sciences, Part 1. Atmospheric Sciences, BNWL-1051-1, pp. 24-25, Battelle-Northwest, Richland, Washington, November 1969.*

2. *M. Terry Dana. "Olympic Peninsula Rain: Characterization of Size and Electric Charge," Pacific Northwest Laboratory Annual Report for 1969, Vol. II: Physical Sciences, Part 1. Atmospheric Sciences, BNWL-1037-1, pp. 86-91, Battelle-Northwest, Richland, Washington, June 1970.*

3. *R. Reiter. "Precipitation and Cloud Electricity," Quart. J. Roy. Meteor. Soc., Vol. 91, pp. 60-72. 1965.*

4. *R. Reiter. "Results of Investigations of Precipitation and Cloud Electricity Based on 15 Years of Observations," Arch. Met. Geoph. Biokl., Ser. A, Vol. 17, pp. 17-29. 1968.*

CALIBRATION OF AN ULTRASONIC NOZZLE FOR AEROSOL GENERATION

M. T. Dana

Particle size measurements were made of the aerosol output of an ultrasonic nozzle. Dispersal of a 1.0 g/l solution of rhodamine B in methanol resulted in dry particles with mass median diameter about 0.2 micron and geometric standard deviation of 1.8. For liquid flow rates from 77 to 275 ml/min, and at an air pressure of 80 lb/in.^{2}, this size was essentially constant. Lower operating pressures resulted in larger particles. The initial droplet diameter of about 2.5 microns represents a considerable improvement over previous generation methods.

A convenient and versatile means of dispensing aerosol particles for precipitation scavenging experiments is through atomization of a methanol solution of a fluorescent dye. Subsequent evaporation of the solvent results in the formation of a spherical particle. Equating the mass of dye in the spherical particle to the mass of dye in the methanol droplet leads to the following size relationship:

$$d' = D\,(C/\rho)^{1/3}, \qquad (1)$$

where d' is the particle diameter, D is the solution droplet diameter, C is the dye solution concentration (mass per unit volume), and ρ is the density of the dry tracer particle. With a particular tracer, such as rhodamine B, and an atomizer which provides a fixed value of D, the particle size is dependent on $C^{1/3}$. This is a severe limitation for field use, because C is limited by the finite solubility of the tracer, but must be sufficiently high such that the mass of tracer released during an experiment is enough for detectability of the scavenged tracer in the collected rainwater. The generator used during recent field research seasons was a simple air-jet atomizer (Solo agricultural sprayer),[1] whose spray droplet diameter (mass median) D was determined to be about 40 microns. Thus in practice, particle diameters were limited to the range 1-15 microns.

In an effort to reach the submicron particle size range more conveniently, a generator was sought which would provide a smaller initial droplet diameter. Selected for testing and calibration was a commercially available ultrasonic nozzle (Astrospray 1700 Series). The nozzle configuration includes an adjustable resonator cavity into which a flow of air (typically 12 ft^3/min at 80 lb/in.^{2}) is directed. The resulting ultrasonic field finely atomizes a stream of liquid which is introduced at low pressure. The droplet size distribution is ostensibly affected by the

selection of air pressure, liquid flow rate, and resonator gap setting. Since the smallest droplets were sought, the gap was set for the finest spray. Usable air pressures were limited by the air delivery system (manifolded compressed air cylinders in the field), and were varied between 60 and 100 lb/in.^{2}. Initial trials at these pressures indicated that the most promising variable for control of droplet size was the liquid feed rate, with air pressure as a secondary parameter.

An aerosol generation chamber was constructed in the laboratory for the calibration trials. The chamber, the volume of which was about 170 ft^3, was exhausted by a blower, which moved about 140 ft^3/min. No attempt was made to establish a uniform tracer concentration in the chamber; the nozzle was aimed away from the outlet such that the plume circulated well before being exhausted. Sampling was through ports in the wall to one side of the aerosol plume. The primary sampler was a simple point-to-plane electrostatic precipitator which deposited particles on electron microscope grids for subsequent photography and manual graticular sizing.

Some use was made of an Anderson cascade impactor, which sizes particles according to aerodynamic properties, and provides samples of several size ranges for mass analysis by fluorometry. It was hoped that some comparison of the results of the two methods could be made, both for calibration of the Anderson and, to some extent, for confirmation of the precipitator results. The complexity of the process of conversion of the actual size -- determined by electron microscopy -- to an aerodynamic size appropriate to the impactor, and the fact that the predominance of the mass of the impactor samples was in the lower stages of the Anderson, caused postponement of this problem until time permits.

For the calibration runs, a solution concentration of 1.0 g/l was used; this concentration is that most convenient for field use. A typical electron micrograph of the resulting particles is shown in Figure 1. The grid was shadowed with gold prior to examination; the particle shadows reveal the remarkable sphericity of most of the particles.

Table 1 lists the operational details and particle size results for the runs for which time has permitted full analysis. Inasmuch as the particle size distributions are closely lognormal, the geometric number median diameter d_g' and the geometric standard deviation σ_g' are indicated. The mass median diameter d_3' was computed with the well-known Hatch[2] formula:

$$\ln d_3' = \ln d_g' + 3 (\ln \sigma_g')^2. \quad (2)$$

The primes are to indicate actual particle size distribution parameters. Mass distributions were computed directly and mass medians derived for the samples, but these were scattered and considered to be quite inaccurate, since much of the mass of a particular sample is contained in relatively few particles.

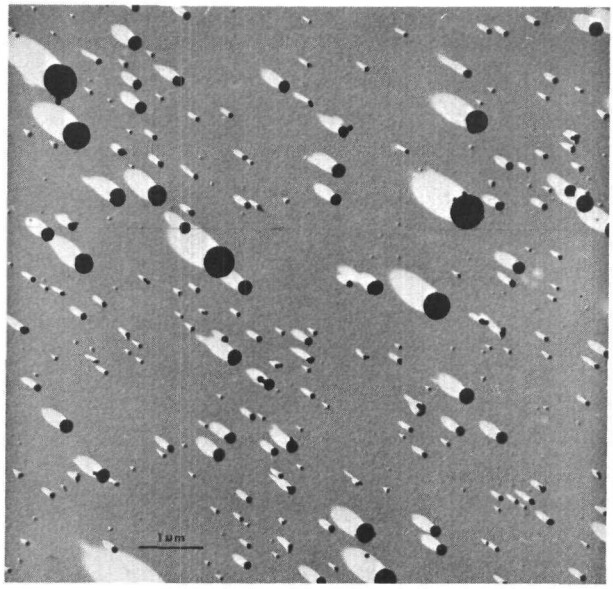

FIGURE 1. Rhodamine B Particles, from Ultrasonic Nozzle.

TABLE 1. Particle Size Results

Run	Solution Feed Rate (ml min^{-1})	Air Pressure (psi)	Photo Magnification	Number of Particles Sized	d_g' (μ)	σ_g'	d_3' (μ)	d_g (μ)	σ_g	d_3 (μ)
17	77	80	21000	542	0.06	2.01	0.25	0.13	1.59	0.25
33	131	80	22500	655	0.06	1.78	0.17	0.14	1.45	0.21
23	140	80	21000	777	0.07	1.72	0.16	0.15	1.44	0.22
24	275	80	21000	427	0.07	1.83	0.21	0.15	1.52	0.25
9	80	75	21000	478	0.09	1.88	0.28	0.18	1.57	0.32
21	68	70	21000	610	0.08	1.62	0.16	0.16	1.40	0.23
28	131	70	22500	463	0.09	1.83	0.28	0.18	1.55	0.32
20	236	65	22500	358	0.07	2.12	0.40	0.16	1.69	0.35
41	105	80	8000	1158	0.13	1.55	0.24	0.23	1.39	0.32
38	105	80	8000	959	0.11	1.50	0.18	0.20	1.35	0.27
42	131	80	8000	963	0.12	1.56	0.22	0.22	1.39	0.30
39	147	80	8000	1244	0.11	1.56	0.20	0.20	1.39	0.28

In view of the consistency of the σ_g' values obtained, the method of mass median computation is deemed more appropriate.

A convenient means of expressing particle size, for the purposes of standardizing between materials of different density, is in terms of aerodynamic diameter.* The aerodynamic parameters are listed in Table 1 by unprimed symbols.

Unexpectedly, the particle size did not appear to vary with liquid feed rate, at constant air pressure. But in the limited number of runs made with pressure below 80 lb/in.^{2}, there was a tendency toward larger particles and broad spectra, making the lower acceptable pressure about 70 lb/in.^{2}.

The size results were affected by the magnification of the photograph sized. The lower magnification pictures resulted in a larger median size, but a narrower distribution, such that the mass median was not very different. The expectation is natural that, at lower magnification, some smaller particles will be lost, but most of the mass resides in the larger particles. At any rate, the high magnification, which allowed easier sizing of the full size range, is deemed most appropriate.

It appears that a satisfactorily narrow distribution may be generated with the nozzle operating at a pressure of 80 lb/in.^{2}, and with liquid rate between 70 and 275 ml/min. Putting C = 1.0 g/l and ρ = 1.38 g/cm^3 into Eq. (1) leads to an initial droplet diameter D of about 2.5 microns, a vast improvement over the 40 micron air-jet atomizer droplet. Unfortunately, the particle size was not widely variable by adjustment of nozzle operating parameters, at least in the limited range of them explored here. Operation is possible at higher pressures, and when practicable to do so, particle sizing characterization will be extended.

REFERENCES

1. *M. A. Wolf and M. T. Dana. "Experimental Studies in Precipitation Scavenging," Pacific Northwest Laboratory Annual Report for 1968, Vol. II: Physical Sciences, Part 1. Atmospheric Sciences, BNWL-1051-1, pp. 18-25. Battelle-Northwest, Richland, Washington, November 1969.*

2. *T. F. Hatch and S. Choate. "Statistical Description of the Size Properties of Non-Uniform Particulate Substances," J. Franklin Inst., Vol. 207, p. 369. 1933.*

*See Equation (1) of "Washout of Soluble Dye Particles," this report.

AN ALTERNATIVE DERIVATION OF THE CONVECTIVE DIFFUSION EQUATION*

W. G. N. Slinn**

A new and more convincing derivation is given of the generalized Smoluchowski-Kramers equation from the Fokker-Planck equation describing the motion of Brownian particles in a nonequilibrium environment. A solution to the Fokker-Planck equation is sought in the form of a Chapman-Enskog expansion. The first moment of the first two terms in this asymptotic expansion is sufficient to obtain the Smoluchowski-Kramers equation. The new convective diffusion equation is found to be identical to the previously reported results obtained by extending Kramers' method.

Previously we reported on studies of Brownian diffusion in a nonuniform gas.[1-4] The analyses are restricted to Brownian particles (B particles) whose Knudsen number is large compared to unity. The genesis of the work is the problem of the precipitation scavenging of submicron particles.[5,6] For this problem, one of the fundamental objectives is to obtain the equation which describes the motion of a B particle in the nonuniform environment of the hydrometeor. Another objective, of course, is to solve the resultant equation. This is essentially done in References 3 and 5.

However, there were certain unsatisfying features of our earlier derivation of the fundamental equation - the convective diffusion equation - from the new Fokker-Planck equation. In the earlier report, Kramers' method was extended and then applied. Professor Mazo, University of Oregon, called our attention to an alternative derivation of the classical diffusion equation from the usual Fokker-Planck equation. The essentials of the method are described by Lebowitz et al.[7] although there are a number of errors in that paper arising from their improper identification of the collisional invariants of the Fokker-Planck collision operator. In this report we shall extend and then apply the method as presented by Resibois.[8]

THE FOKKER-PLANCK EQUATION

The new Fokker-Planck equation for B particles in a nonuniform gas was shown to be[(2)]

$$\frac{\partial f}{\partial t} + u_i \frac{\partial f}{\partial r_i} = \beta_I \frac{\partial}{\partial u_i}\left[c_i f + \frac{kT_I^*}{M}\frac{\partial f}{\partial u_i}\right] \quad (1)$$

---

* *This report is based on a portion of an article accepted for publication in the Journal of Statistical Physics.*

** *A part of the financial support for this work was obtained from Battelle Memorial Institute's Physical Sciences Program.*

where f is the number, probability density function in the $(\vec{r},\vec{u})$ phase space for the B particles. In Eq. (1), the summation convention, with no summation over capital letter indices, is used. Also,

$$\beta_I = \beta\left(1 - \frac{\tau_I}{5p}\right) \tag{2}$$

where β is the Epstein drag coefficient per unit mass; p is the pressure, and τ_I is the Ith principal axis component of the viscous stress tensor. Other definitions are

$$c_i = u_i - \bar{u}_i \tag{3}$$

$$\bar{u}_i = \frac{f_i^{(e)}}{\beta_I} + \frac{q_i}{5p} + V_i^{(f)} \tag{4}$$

in which $\vec{f}^{(e)}$ is the external force per unit mass; $\vec{q}$ is the heat flux and $\vec{v}^{(f)}$ is the fluid velocity and finally,

$$\frac{kT_I^*}{M} = \frac{kT}{M}\left(1 - \frac{2\tau_I}{5p}\right) \tag{5}$$

in which k is Boltzmann's constant; T is the temperature and M is the mass of the B particle.

Since the collision operator, the right hand side of Eq. (1), conserves the number of B particles (but not momentum or energy, as was assumed by Lebowitz et al.[7]) then integrating Eq. (1) over all velocity leads to

$$\frac{\partial N}{\partial t} + \frac{\partial}{\partial r_i}\int u_i f\, d^3u = 0 \tag{6}$$

in which we have used that the number density of B particles is given by

$$N = \int f\, d^3u. \tag{7}$$

If Eq. (6) is rewritten in the form of a conservation equation,

$$\frac{\partial N}{\partial t} = -\nabla\cdot\overrightarrow{(\text{Flux})} \tag{8}$$

then it is seen that we are already near our desired result of deriving a convective-diffusion equation from the Fokker-Planck (F-P) equation.

CHAPMAN-ENSKOG EXPANSION

To obtain a convective diffusion equation which should provide an adequate description of the motion of a B particle during time intervals long compared to β^{-1}, the first step is to seek a solution to the F-P equation in the form of an asymptotic series:

$$f = f^{(o)} + \beta^{-1} f^{(1)} + \mathcal{O}(\beta^{-2}). \tag{9}$$

Substituting Eq. (9) into the F-P equation, and equating coefficients of the same power of β^{-n}, leads to

$$0 = \left(1-\frac{\tau_I}{5p}\right)\frac{\partial}{\partial u_i}\left[c_i f^{(o)} + \frac{kT_I^*}{M}\frac{\partial f^{(o)}}{\partial u_i}\right] \tag{10}$$

$$\frac{\partial f^{(o)}}{\partial t} + u_i\frac{\partial f^{(o)}}{\partial t} = \left(1-\frac{\tau_I}{5p}\right)\frac{\partial}{\partial u_i}\left[c_i f^{(1)} + \frac{kT_I^*}{M}\frac{\partial f^{(1)}}{\partial u_i}\right] \tag{11}$$

and so on.

An appropriate solution to Eq. (10) is what was obtained earlier[2] using an entirely different approach:

$$f^{(o)} = N \prod_{I=1}^{3} \left(\frac{M}{2\pi kT_I}\right)^{1/2} \exp\left\{\frac{-c_I^2}{2kT_I/M}\right\}. \quad (12)$$

It will be seen that, in fact, Eq. (11) need not be solved.

Substituting Eqs. (12) and (9) into (8) leads to

$$\frac{\partial N}{\partial t} = -\frac{\partial}{\partial r_i}\left[N\bar{u}_i + \beta^{-1}\int u_i\, f^{(1)}\, d^3u + \mathcal{O}(\beta^{-2})\right]. \quad (13)$$

Thus, to terms of order β^{-2}, we need evaluate only the first moment of $f^{(1)}$. This can be obtained from Eq. (11) without solving the equation.

However, first we make use of the fundamental, Chapman-Enskog-type, assumption. It is assumed that for time intervals large compared to β^{-1}, the time dependence of f is implicit, through the dependence of the density, etc., on time. Thus, a "normal" solution is assumed, wherein

$$\frac{\partial f^{(0)}}{\partial t} = \frac{\partial f^{(0)}}{\partial N}\frac{\partial N}{\partial t} + \frac{\partial f^{(0)}}{\partial T}\frac{\partial T}{\partial t} + \frac{\partial f^{(0)}}{\partial \bar{u}_i}\frac{\partial \bar{u}}{\partial t}\, i + \ldots. \quad (14)$$

Some terms in Eq. (14) can be ignored since they lead to terms which are of second order in fluid gradients. The other terms, such as $\partial N/\partial t$, can be obtained from Eq. (13) and the fluid equations:

$$\frac{\partial N}{\partial t} \approx \frac{\partial}{\partial r_i} N\bar{u}_i \quad (15)$$

$$\frac{\partial T}{\partial t} \approx -V_i^{(f)}\frac{\partial T}{\partial r_i} - (\gamma-1)\, T\frac{\partial V_i^{(f)}}{\partial r_i} \quad (16)$$

$$\frac{\partial V_i^{(f)}}{\partial t} \approx -V_j^{(f)}\frac{\partial V_i^{(f)}}{\partial r_j} - \frac{1}{\rho}\frac{\partial p}{\partial r_i} \quad (17)$$

in which the approximate, Euler-type, conservation equations are used, to be consistent with the order of gradients which are retained.

Now, to obtain the second term on the right hand side of Eq. (13), Eq. (14) is substituted into Eq. (11) and the latter is multiplied through by u_j and integrated over all $\vec{u}$. As a result, we obtain

$$\left[\frac{\partial N}{\partial t}\frac{\partial}{\partial N} + \frac{\partial T}{\partial t}\frac{\partial}{\partial T} + \frac{\partial V_k^{(f)}}{\partial t}\frac{\partial}{\partial V_k^{(f)}} + \frac{\partial p}{\partial t}\frac{\partial}{\partial p} + \frac{\partial f_k^{(e)}}{\partial t}\frac{\partial}{\partial f_k^{(e)}} + \ldots.\right](N\bar{u}_j)$$

$$+ \frac{\partial}{\partial r_i}\int u_i u_j\, f^{(0)}\, d^3u = \left(1-\frac{\tau_I}{5p}\right)\int u_j \frac{\partial}{\partial u_i}\left[c_i f^{(1)} + \frac{kT_I^*}{M}\frac{\partial f^{(1)}}{\partial u_i}\right] d^3u. \quad (18)$$

Integrating the right hand side of Eq. (18) by parts and utilizing that, by construction,

$$\int f^{(1)}\, d^3u = 0 \qquad (19)$$

then the right hand side becomes

$$-\left(1-\frac{\tau_I}{5p}\right)\int u_j\, f^{(1)}\, d^3u$$

which is exactly what is desired for Eq. (13).

Finally, substituting Eqs. (15-17) into the left hand side of Eq. (18), ignoring terms of second order in gradients or terms which correspond to changes in quantities during time intervals small compared to β^{-1}, and substituting the result into Eq. (13) leads to

$$\frac{\partial N}{\partial t} = \nabla \cdot [\tilde{D} \cdot \nabla N - N\vec{v}_d] \qquad (20)$$

where

$$\tilde{D} = D\left[\tilde{I} - \frac{\tilde{\tau}}{5p}\right], \qquad (21)$$

where D is Einstein's diffusion coefficient and $\tilde{I}$ is the identity or metric tensor, and where

$$\vec{V}_d = \vec{V}^{(f)} + \frac{\vec{q}}{5p} + \frac{\vec{f}^{(e)}}{\beta} \cdot \left(\tilde{I} + \frac{\tilde{\tau}}{5p}\right)$$

$$+ D\left(\frac{2}{5p}\nabla\cdot\tilde{\tau} - \frac{\nabla T}{T}\right). \qquad (22)$$

These results are exactly the same as the results obtained previously[2] by modifying Kramers' method.

REFERENCES

1. *W.G.N. Slinn. "The Convective Diffusion Equation for the Scavenging of Submicron Particles," Pacific Northwest Laboratory Annual Report for 1967, Vol. II: Physical Sciences, Part 3. Atmospheric Sciences, BNWL-715-3. Battelle-Northwest, Richland, Washington, October 1968.*

2. *W.G.N. Slinn. Brownian Diffusion of Submicron Particles in Air Under Nonequilibrium Conditions, BNWL-987. Battelle-Northwest, Richland, Washington, February 1969.*

3. *W.G.N. Slinn and S. F. Shen. "Anisotropic Brownian Diffusion and Precipitation Scavenging of Submicron Particles," J. Geophys. Res., Vol. 75, pp. 2267-2270, 1970.*

4. *W.G.N. Slinn. "Anisotropic Brownian Diffusion in Free-Molecule Couette Flow," Pacific Northwest Laboratory Annual Report for 1967, Vol. II: Physical Sciences, Part 1. Atmospheric Sciences, BNWL-1307. Battelle-Northwest, Richland, Washington, June 1970.*

5. *W.G.N. Slinn. "Precipitation Scavenging of Submicron Particles: A Theoretical Analysis," USAEC Meteorological Information Meeting, Chalk River, Ontario, AECL-2787. September 1967.*

6. *W.G.N. Slinn and J. M. Hales. "Phoretic Processes in Scavenging," Precipitation Scavenging (1970), R. J. Engelmann and W.G.N. Slinn, eds., AEC Symposium Series, 1970.*

7. *J. L. Lebowitz, H. L. Frisch and E. Helfand. "Nonequilibrium Distribution Functions in a Fluid," Phys. Fluids, Vol. 3, pp. 325-338, 1960.*

8. *P.M.V. Resibois. Electrolyte Theory, Pergamon Press, New York. 1968.*

BLANK

DIFFUSION AND TURBULENCE STUDIES

The seriousness of pollutant releases to the atmosphere is strongly influenced by the diffusive capacity of the atmosphere and the ability of the atmosphere to cleanse itself. Consequently, studies of dispersion and deposition, and of turbulence affecting these processes are of considerable importance. Turbulence studies have aimed at modeling the power spectra of the three wind components in various wind speeds and stabilities and at various heights. Ultimately, the goal is the understanding of the interrelation between turbulence and dispersion to the extent that diffusion models can be developed without input from "turbulence measurements," since turbulence should be described by the same parameters necessary to describe diffusion.

Recent turbulence and diffusion field experiments carried out at the Hanford site have been restricted to the planetary boundary layer. Diffusion experiments have involved instantaneous and point source tracer releases, investigation of source height effects through simultaneous tracer releases at two elevations and, by virtue of real time tracer concentration measurements, the investigation of the contribution of meander and diffusion to the crosswind concentration distribution of the time integrated plume. Continuing intensive field measurements in the turbulence area have permitted the modeling of wind component spectra, the effects of atmospheric stability on atmospheric turbulence spectra and momentum flux.

Studies resulting from data generated during the experimental phase of the Barbados Oceanographic and Meteorological Experiment continued with the development of a system for processing of BOMEX turbulence data and refinements in studies involving measurement of the air-sea interchange by means of radioactive tracers.

Fallout studies concerned with describing the behavior of pollutants transported over large distances and at elevations well above the planetary boundary layer also were pursued. Close agreement was found between observed effluent (Phoebus 1B) trajectories and diabatic trajectories employing data from a computerized radiational cooling model. Another study compares the reliability of current computerized prognostic trajectories with isobaric trajectories based on observed 850 mb surface data.

COMPARISON OF MAXIMUM EXPOSURES AT GROUND LEVEL RESULTING FROM SIMULTANEOUS RELEASE OF TRACERS FROM ELEVATIONS OF 2 AND 26 METERS

P. W. Nickola

Atmospheric tracers were simultaneously released from elevations of 2 m and 26 m for periods ranging from 30 to 60 min. The seventeen dual releases took place during a variety of atmospheric stabilities. Ground-level field sampling took place between distances of 0.1 and 12.8 km from the source. After normalization to unit mass emitted, ratios of exposures resulting from the two levels of release were formed. The magnitude of these ratios was strongly related to atmospheric stability at distances relatively close to the sources, but the reduction of exposure due to the aloft release was minimal beyond 3 km for all stabilities encountered.

Generally, experimental investigation of the effects of source height on the ground-level concentration of atmospheric pollutants entails release of a tracer from one elevation under a specific meteorological condition, and then a repeat release from a different elevation at a time when the meteorology is similar to the conditions existing during the first release. Unfortunately, the free atmosphere is an uncooperative laboratory which never precisely repeats itself, and thus the effects of such a variable as source height can be somewhat obscured by the changes in meteorology between experiments. The simultaneous release from more than one elevation of atmospheric tracers with identical aerodynamic properties overcomes the problem.

Simultaneous field releases of the tracers fluorescein and zinc sulfide FP 2210 began at Hanford in 1964. This dual tracer technique[1] involves simultaneous collection of the tracers on a common set of filters, and subsequent noninterfering assays for each tracer.

In order to test the compatibility of these tracers in the field, early experiments involved release of both tracers from the same source.[2] On the average, good agreement was found. When the masses of tracer collected on field filters were normalized to the masses dispersed, the mean ratio of masses of fluorescein to FP 2210 at plume centerline was found to be 1.01. The range embraced by one standard deviation about the mean ratio was from 0.69 to 1.45. A total of nine field releases with sampling between 0.2 and 3.2 km from the sources was involved in this investigation. At the 95% confidence level, there was no difference in the fluorescein to FP 2210 ratio from sampling arc to sampling arc.

From 1966 through 1969, a series of dual tracer releases was made from different elevations of the Hanford 122-m Meteorology Tower. Assay of the FP 2210 tracer was readily accomplished, and some analysis of these data has been reported in earlier annual reports of this series.[3,4,5] Various difficulties delayed much of the fluorescein assay until 1970.

A total of 17 experiments was conducted in which tracers were released simultaneously from elevations of about 2 and 26 m. Thirty to sixty minute duration releases were made at both night and day, and under a variety of atmospheric conditions. Atmospheric stabilities, as indicated by the Richardson number (Ri), for the layer between 2 and 15 m varied from -0.59 to 0.24. Sampling was accomplished on 15 sampling arcs concentric about the source tower at distances ranging from 0.1 to 12.8 km. Not all sampling arcs were used with each experiment.

Figure 1 presents plume centerline exposures (E_p) for field tests during the most stable (Test U-57 with Ri = 0.24) and least stable (Test U-55 with Ri = -0.59) conditions observed. The data have been normalized to mass of tracer emitted (Q), but not to wind speed since the intent here is to emphasize the difference in exposures actually observed with equal releases. Also, the incorporation of a normalizing wind speed requires somewhat arbitrary decisions in the selection of the elevation of wind speed effective in transporting tracer from the release point to the sampler.

Note on Figure 1 that in the case of less stable Test U-55, the advantage of reduced exposures due to increased release height (H) is lost before reaching a distance 0.3 km from the source. In the case of more stable Test U-57, the benefit of the 26-m release height is in evidence to a distance of about 3 km.

For each sampling distances of each test, ratios were formed by dividing the normalized centerline exposure (E_p/Q) resulting from the 26-m release by E_p/Q resulting from the 2-m release. Rank correlation tests were made between Ri and the exposure ratios at 400 m from the source. The correlation between the ratio and Ri was significant at the 0.005 confidence level. (Similar rank correlation between exposure ratio and $\sigma_\theta \bar{u}$ also showed significance, but only at the 0.05 level. Wind direction standard deviation (σ_θ) and mean wind speed ($\bar{u}$) measured at the 15-m elevation were used in this computation.)

The high correlation between exposure ratio at 400 m and Ri led to a decision to group the tests on the basis of Ri for analysis. Arbitrary groupings of moderately stable (Ri > 0.10), slightly stable (0.10 > Ri > 0), slightly unstable (0 > Ri > -0.10), and moderately unstable (-0.10 > Ri) were formed. Logarithms of the ratios were averaged and the resulting means were converted again to exposure ratios and plotted.

Figure 2 presents the results. If the experiments are presumed to

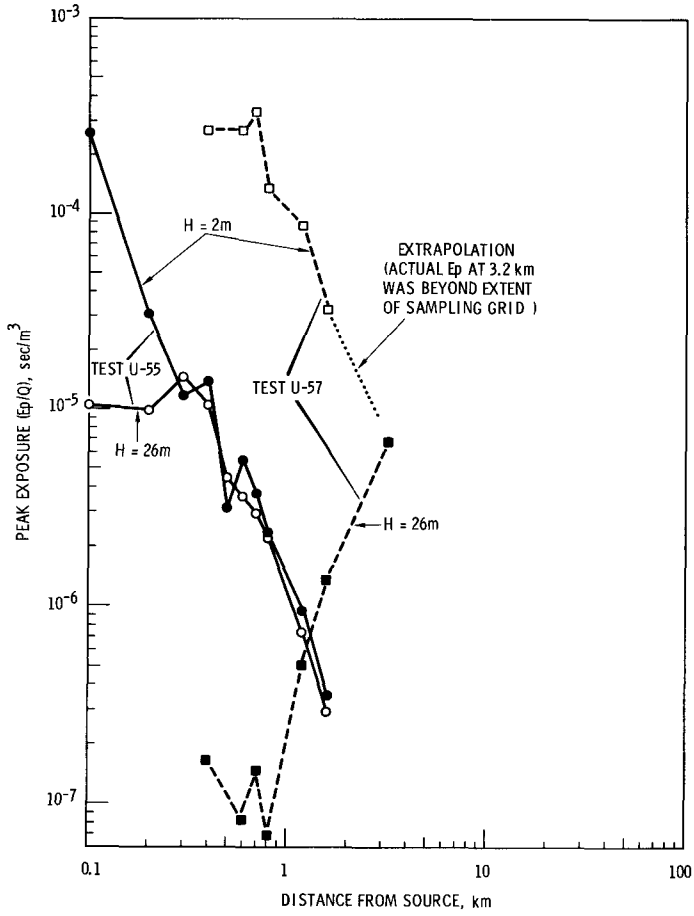

Neg 710923-9

FIGURE 1. Plume Centerline Exposures for Most Stable (U-57) and Most Unstable (U-55) Atmospheres of Test Series. H is release height.

embrace the range of "typical" conditions within each stability class, the graph suggests that 90% of the benefits of the H = 26 m release over the H = 2 m release are gone in moderately unstable atmospheres by the time the plumes travel 0.6 km. For slightly unstable atmospheres, the benefits are missing beyond 1.2 km; and for slightly stable atmospheres, beyond 3 km. There is obviously an anomaly in either the slightly stable or moderately stable curves as the ratio exceeds 0.3. Since six field experiments contributed to the slightly stable data, whereas only three experiments were incorporated in the moderately stable data, the slightly stable category should be more valid.

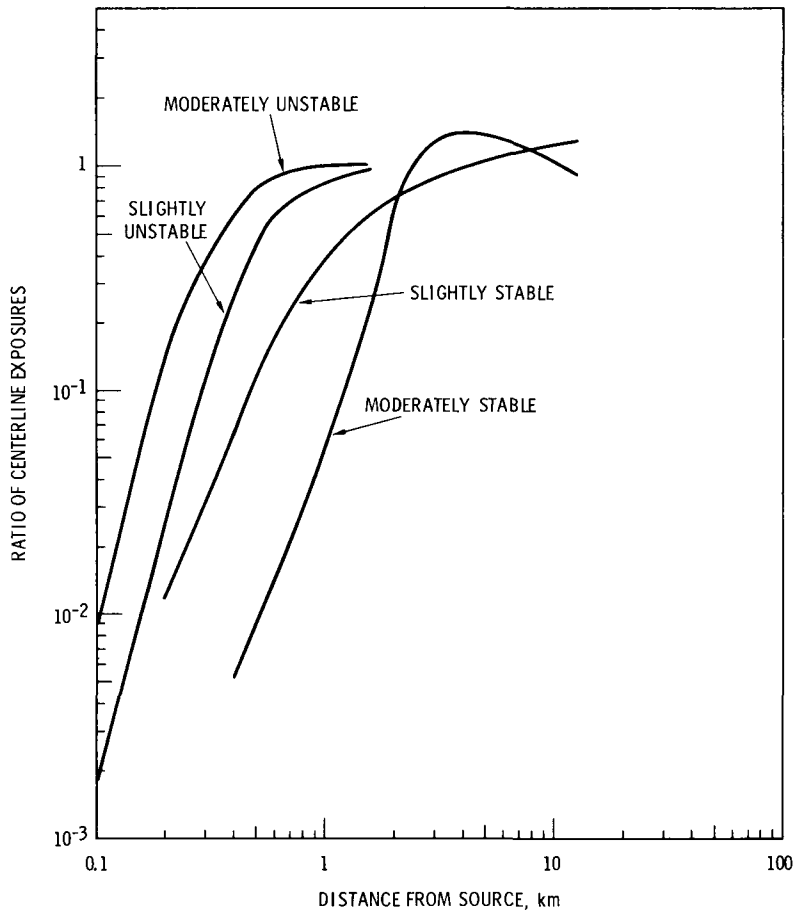

Neg 710923-8

FIGURE 2. Centerline Exposure Ratio (H = 26-m Release to H = 2-m Release) Versus Distance.

A somewhat different approach to Figure 2 can be made. If the interest lay in reducing pollution at a distance of, for example, 1 km from a source, erection of a 26-m stack could be said to offer no advantage over surface level release during moderately unstable conditions. Under slightly unstable conditions, erection of the 26-m stack would only reduce maximum exposures by 15%. In slightly stable atmospheres, the exposure reduction would be to 40% of the ground level release, and in moderately stable atmospheres the reduction would be to about 0.5%.

REFERENCES

1. J. D. Ludwick. Dual Atmospheric Tracer Techniques for Diffusion Studies Using Phosphorescence-Fluorescence Analysis, HW-70892. General Electric Company, Richland, Washington, March 1961.

2. P. W. Nickola. Field Testing of a Fluorescein-Zinc Sulfide Dual Atmospheric Tracer Technique, BNWL-103. Battelle-Northwest, Richland, Washington, August 1965.

3. C. E. Elderkin, W. T. Hinds, and J. W. Sloot. "Elevated Source Diffusion Studies," Pacific Northwest Laboratory Annual Report for 1966 to the USAEC Division of Biology and Medicine, Volume II Physical Sciences, Part 1 Atmospheric Sciences, BNWL-481 1, pp. 5-8, Battelle-Northwest, Richland, Washington, October 1967.

4. P. W. Nickola. "Results of Field Investigations of Source Height and Stability on Atmospheric Exposure," Pacific Northwest Laboratory Annual Report for 1968 to the USAEC Division of Biology and Medicine, Volume II Physical Sciences, Part 1 Atmosperic Sciences, BNWL-1051 1, pp. 1-4, Battelle-Northwest, Richland, Washington, November 1969.

5. P. W. Nickola. "The Effects of Source Height and Stability on Plume Centerline Exposure," Pacific Northwest Laboratory Annual Report for 1969 to the USAEC Division of Biology and Medicine, Volume II Physical Sciences, Part 1 Atmospheric Sciences, BNWL-1307 1, pp. 2-6, Battelle-Northwest, Richland, Washington, June 1970.

MEASUREMENTS OF THE MOVEMENT, CONCENTRATION, AND DIMENSIONS OF INSTANTANEOUSLY GENERATED PUFFS OF AN INERT GAS TRACER

P. W. Nickola

Data generated during eight field puff releases of ^{85}Kr were analyzed. Information specifying effective speed and height, magnitude of short-period concentration, magnitude of crosswind and downwind concentration integrations, and dimensions of the puffs were generated. Perhaps the most significant conclusion reached was that the effects of atmospheric stability on puff dimensions were best shown when dimensions were considered as a function of time rather than of distance from source.

During the fall of 1967, a series of releases of the inert gas ^{85}Kr was made on the Hanford atmospheric diffusion grid. Descriptions of the ^{85}Kr field grid and instrumentation have been given in these annual reports[1-3] and elsewhere.[4,5] A data volume[6] has been published, and several research papers[7-11] have been generated from the krypton tracer data.

Although the ^{85}Kr releases were of both continuous (plume) and instantaneous (puff) varieties, the

results summarized in this note deal only with the puffs. This summary is a much condensed version of a paper recently submitted for journal publication.[12]

Field measurements of puff releases have received little attention when contrasted with the considerable investigations associated with plume releases. The emphasis on plumes stems partially from concern with the great number of industrial stacks which emit pollutants on a more or less continuous basis. Further, field generation and measurement of puffs are technically more difficult than the similar procedures for plumes. Nevertheless, there are infrequent or accidental pollutant releases which are better simulated by tracer puff releases. Explosions or rocket launch-pad accidents are examples.

Eight puffs of ^{85}Kr were released at surface level and permitted to drift through the three-dimensional field grid of 64 Geiger-Müller sensors. The grid extended to a height of 21 m and to a distance of 800 m from the source. Concentrations were recorded as a series of 4.8-sec duration mean concentrations for each of the 64 sensors. This history of concentration at 64 known field locations, and the accompanying meteorology measurements made on towers near the source, permitted specification of the movement, concentration, and dimensions of the puffs.

The effective speed with which a puff moved as it intersected the plane 1.5 m above the surface increased as the distance from source (or time following release) increased. Since wind speeds increased with height, the effective height at which the puffs were moved also increased with distance (or time). At 800 m, the effective transport height was greater than 1.5 m in two of seven cases. The effect of atmospheric stability on the effective height was not obvious.

At the 1.5-m elevation, peak values of short-period concentration, exposure, and crosswind integrated concentration increased with increasing atmospheric stability. Figure 1 presents maximum exposures for seven puffs as a function of distance from source, and as a function of travel time. Tests P2 and P8 were conducted in stable atmospheres, Test P7 in an unstable atmosphere, and the remainder of the tests in near neutral conditions. The shaded area on the exposure versus distance portion of the graph embraces the measurements made by other investigators as reported in Meteorology and Atomic Energy 1968.[13]

Measurements made at the 1.5-m elevation showed that within 800 m of the source and for locations near the puff centroid, crosswind integrated concentrations exceeded integrations made in the downwind direction regardless of stability. Thus, a person who moved rapidly (relative to wind speed) crosswind through a puff would have breathed a greater amount of contaminant than a person moving up or downwind.

The standard deviation (σ_I) of the concentration distribution through

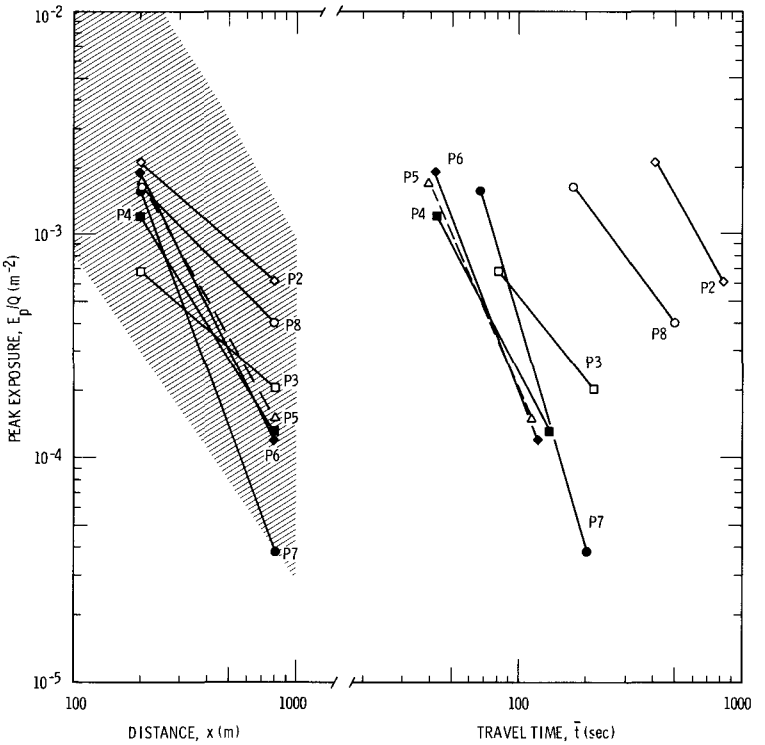

Neg 710200-3

FIGURE 1. Peak Exposure Versus Distance and Versus Travel Time

a puff in the downwind (x), crosswind (y), and vertical (z) directions were employed to specify puff dimensions. The fact that the magnitude of these σ_{xI}, σ_{yI}, and σ_{zI} values was dependent upon the plane of measurement in the puff suggested that tracer concentration within the puffs was not trivariant normal in distribution. Even though the trivariant normal distribution may have been approximated shortly after puff generation, the effects of wind speed and direction shear deformed the puffs before they travelled a distance of 200 meters.

Regardless of atmospheric stability, $\sigma_{xI} > \sigma_{yI} > \sigma_{zI}$ within the 800 m extent of the field grid. In stable atmospheres, the ratio σ_{yI}/σ_{xI} decreased slightly as the puffs travelled from 200 m to 800 m - i.e., downwind elongation continued. However, for the single release into an unstable atmosphere, the σ_{yI}/σ_{xI} ratio increased from 0.30 to 0.72 during puff travel from 200 m to 800 m. The ratio σ_{zI}/σ_{xI} decreased with distance (or time) regardless of stability.

Although it is common practice to present diffusion parameters such as peak concentration, peak exposure, or puff and plume dimensions as functions of distance from source, Taylor[14] and many others have employed the concept of travel time

as the independent variable. The appeal of this approach with the subject puff data is exemplified in Table 1. When puff dimensions are considered as functions of distance, releases in stable atmospheres are seen to result in puff dimensions at least as large as those in less stable atmospheres. In fact, the wind speeds during the stable tests happened to be much less than those during the less stable tests. Thus the processes of diffusion were taking place over a much greater time interval while puffs were travelling to a given distance during the stable tests. Presentation of the puff dimensions as a function of travel time results in the intuitively more appealing result at the right in Table 1 - namely, that when atmospheric turbulence is minimized, puff dimensions are also minimized.

TABLE 1. Averaged Puff Dimensions Versus Distance and Versus Travel Time

Atmospheric Stability	Observed Wind Speeds	Distance from Source						Travel Time					
		200 m			800 m			1 min			5 min		
		σ_{xI}	σ_{yI}	σ_{zI}	σ_{xI}	σ_{yI}	σ_{zI}	σ_{xI}	σ_{yI}	σ_{zI}	σ_{xI}	σ_{yI}	σ_{zI}
	(mps)	(m)	(m)	(m)	(m)	(m)	(m)	(m)	(m)	(m)	(m)	(m)	(m)
Unstable to Neutral	4 to 8	37	11	6	92	46	12	40	13	6	170	130	17
Stable	1 to 2	55	13	6	180	46	16	6	2	2	60	14	10

REFERENCES

1. *J. D. Ludwick, J. J. Lashock, R. E. Connally and P. W. Nickola. "Automatic Real-Time Air Monitoring of ^{85}Kr Utilizing the 4096 Memory of a Multiparameter Analyzer." Pacific Northwest Laboratory Annual Report for 1967 to the USAEC Division of Biology and Medicine. Volume II: Physical Sciences, Part 3. Atmospheric Sciences, BNWL-715 3, pp. 58-62. Battelle-Northwest, Richland, Washington, October 1968.*

2. *J. J. Lashock. "Electronic Design and Construction of a Noble Gas Atmospheric Tracer System." Pacific Northwest Laboratory Annual Report for 1967 to the USAEC Division of Biology and Medicine. Volume II: Physical Sciences, Part 3. Atmospheric Sciences, BNWL-715 3, pp. 54-57. Battelle-Northwest, Richland, Washington, October 1968.*

3. *P. W. Nickola, J. V. Ramsdell, Jr. and J. D. Ludwick. "Real Time Histories of Diffusing Plumes and*

Puffs Determined from Use of an Inert Gas Tracer System." Pacific Northwest Laboratory Annual Report for 1969 to the USAEC Division of Biology and Medicine. Volume II: Physical Sciences, Part 1. Atmospheric Sciences, BNWL-1307 1, pp. 6-10. Battelle-Northwest, Richland, Washington, June 1970.

4. *J. D. Ludwick, J. J. Lashock, R. E. Connally and P. W. Nickola. "Automatic Real-Time Air Monitoring of ^{85}Kr Utilizing the 4096 Memory of a Multiparameter Analyzer." Review of Scientific Instruments, Volume 39, pp. 853-859, 1968.*

5. *P. W. Nickola, J. D. Ludwick and J. V. Ramsdell, Jr. "An Inert Gas Tracer System for Monitoring the Real-Time History of a Diffusing Plume or Puff." J. Appl. Meteor., Volume 9, pp. 621-626, August 1970.*

6. *P. W. Nickola, J. V. Ramsdell, Jr. and J. D. Ludwick. Detailed Time-Histories of Concentrations Resulting from Puff and Short-Period Releases of an Inert Radioactive Gas: A Volume of Atmospheric Diffusion Data, BNWL-1272. Battelle-Northwest, Richland, Washington, February 1970.*

7. *P. W. Nickola and J. D. Ludwick. "The Measurement of Particulate Plume Depletion in the Atmosphere by Comparison with an Inert Gaseous Tracer." Pacific Northwest Laboratory Annual Report for 1967 to the USAEC Division of Biology and Medicine. Volume II: Physical Sciences, Part 3. Atmospheric Sciences, BNWL-715 3, pp. 65-73. Battelle-Northwest, Richland, Washington, October 1968.*

8. *J. V. Ramsdell and W. T. Hinds. "Concentration Fluctuations and Peak-to-Mean Concentration Ratios in Plumes from a Continuous, Ground-level Point Source," BNWL-SA-2915. Manuscript submitted to Atmospheric Environment, June 1970.*

9. *P. W. Nickola. "Measurements of the Transport Speed and Physical Dimensions of a Diffusing Puff of a Gaseous Tracer in the Atmosphere." Pacific Northwest Laboratory Annual Report for 1969 to the USAEC Division of Biology and Medicine. Volume II: Physical Sciences, Part 1. Atmospheric Sciences, BNWL-1307 1, pp. 10-14. Battelle-Northwest, Richland, Washington, June 1970.*

10. *J. V. Ramsdell. "Modeling Peak-to-Mean Concentration Ratios in Diffusing Plumes." Pacific Northwest Laboratory Annual Report for 1969 to the USAEC Division of Biology and Medicine. Volume II: Physical Sciences, Part 1. Atmospheric Sciences, BNWL-1307 1, pp. 21-25. Battelle-Northwest, Richland, Washington, June 1970.*

11. *J. V. Ramsdell. "Concentration Fluctuations in Diffusing Plumes." Pacific Northwest Laboratory Annual Report for 1969 to the USAEC Division of Biology and Medicine. Volume II: Physical Sciences, Part 1. Atmospheric Sciences, BNWL-1307 1, pp. 27-29. Battelle-Northwest, Richland, Washington, June 1970.*

12. *P. W. Nickola. "Measurements of the Movement, Concentration, and Dimensions of Clouds Resulting from Instantaneous Point Sources." Manuscript submitted to J. Appl. Meteor., January 1971.*

13. *Atomic Energy Commission. Meteorology and Atomic Energy 1968. USAEC Division of Technical Information, TID 24190, Clearinghouse for Federal Scientific and Technical Information, NBS, U.S. Dept. of Commerce, Springfield, Virginia, July 1968.*

14. *G. I. Taylor. "Diffusion by Continuous Movements." Proceedings of the London Mathematical Society, ser. 2, 20, pp. 196-211, 1921.*

ADVANCEMENTS IN CAPABILITIES OF THE HANFORD INERT GAS TRACER SYSTEM FOR FIELD DIFFUSION STUDIES

P. W. Nickola and J. D. Ludwick*

The Hanford prototype inert gas field diffusion tracer system has been improved and the field grid has been extended. Sampling previously included 64 field detectors which were arrayed to a maximum height of 21 m on 6 towers and to a distance of 800 m from the tracer release point. The revised array of 128 sensors extends to a height of 42 m on 10 towers and to a distance of 1600 m. Remotely activated protective covers on the field sensors replace the manually removable covers of the prototype system. A capability for continually recording concentration fluctuations in fine detail replaces the intermittent recording with less detail associated with the prototype system.

A ^{85}Kr field tracer system was first installed on the Hanford diffusion grid in 1967. A series of thirteen ^{85}Kr releases was made on this prototype grid in the summer and fall of 1967. Documentations of this inert gas tracer system and of the results of these prototype releases are referenced in the immediately preceding article** of this annual report. Modifications and additions to this prototype system are nearing completion. These advances will enhance the versatility of the system and extend the range over which measurements can be made.

Location of sensors on this revised field grid is diagrammed schematically on Figure 1. This revised installation is contrasted with the prototype installation in Table 1. A total of 64 sensors was employed in the prototype system, with sampling heights extending to 21.3 m. The maximum distance at which the Geiger counter sensors were installed was 800 m from the source. The revised installation arrays 128 sensors to a height of 42 m and to a distance of 1600 m from the source. Current plans do not include samplers above the 1.5-m basic level at 1600 m.

Each of the 128 field sensors requires an individual coaxial cable to link it to a programmer located in a trailer near the tracer source. The sensors added in the revised system required about 40 miles of cable to accomplish this linking. Early experience with the prototype system in which coaxial cables were placed directly on the ground revealed that

---

*Radiological Sciences Department.

**P. W. Nickola. "Measurements of the Movement, Concentration, and Dimensions of Instantaneously Generated Puffs of an Inert Gas Tracer."

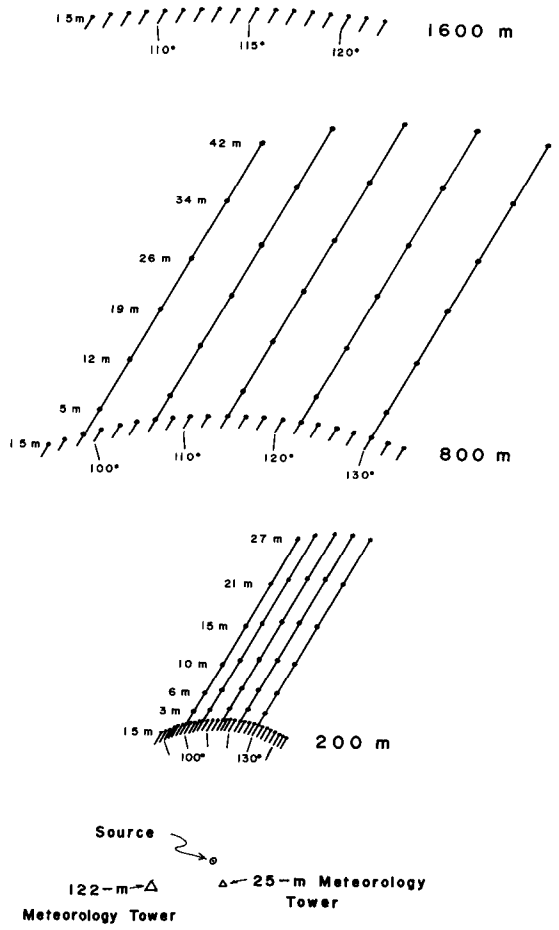

Neg 704920-1

FIGURE 1. The Revised Field Grid of the Inert Gas Tracer System

desert rodents found the cable insulation quite appetizing. To avoid cable damage, all cables have been suspended from a series of metal fence posts. Bridging of vehicle access roads on the field grid was necessary at six field locations. Although these coaxial cables are an unglamorous portion of the field system, their acquisition and installation represented a considerable expenditure of funds and manpower.

Leaving the mica windows of the Geiger counter field detectors continually exposed to weathering would result in relatively rapid deterioration and tube failure. The prototype field technique entailed replacing a plastic cap over each sensor subsequent to each field experiment, and removing it again prior to the next experiment. This procedure was rather time consuming - particularly with respect to the tower-mounted sensors. This difficulty has been overcome in the revised system with the installation of remotely activated covers. The primary

TABLE 1. Comparison of Field Instrumentation on Prototype and Revised Field Diffusion Grid

	Prototype Installation		Revised Installation	
Sensor Location	No. of Sensors	Sampling Extent	No. of Sensors	Sampling Extent
200-m arc at 1.5-m level	20	94° to 132°	30	86° to 144°
200-m arc on towers	4 sensors/tower, 3 towers, total of 12	0.8 to 10.7 m	6 sensors/tower, 5 towers, total of 30	3 to 27 m
800-m arc at 1.5-m level	20	94° to 132°	21	94° to 134°
800-m arc on towers	4 sensors/tower, 3 towers, total of 12	0.8 to 21.3 m	6 sensors/tower, 5 towers, total of 30	5 to 42 m
1600-m arc at 1.5-m level	None		17	106° to 122°
Total	64 sensors		128 sensors	

component of these covers is an electrically activated valve. A field detector equipped with a remotely activated cover is shown on Figure 2.

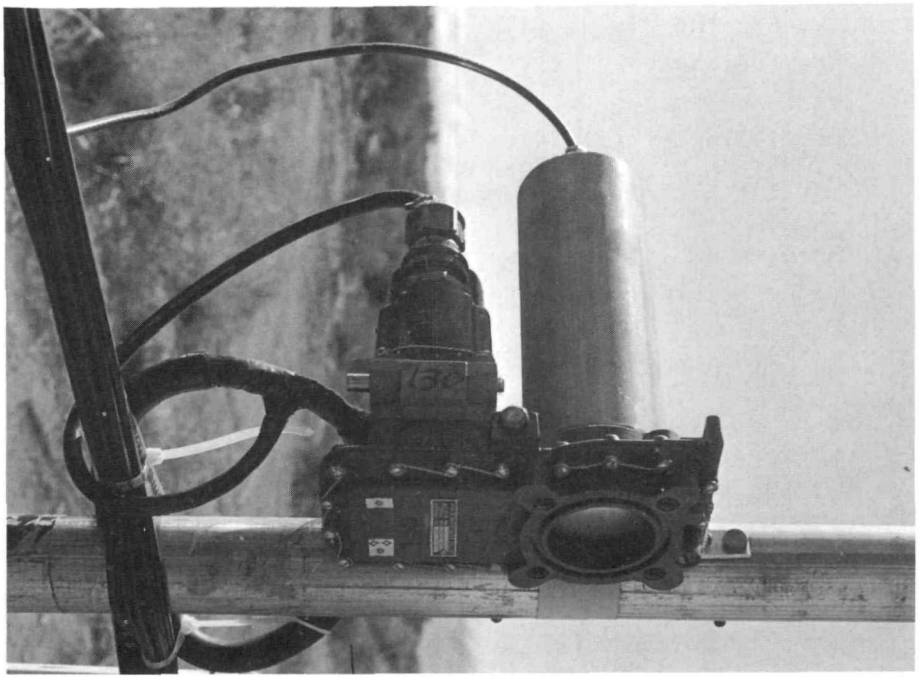

Neg 711162-5

FIGURE 2. Field Detector Equipped with Remotely Activated Weather Cap

The prototype system incorporated a 4096 address memory which was programmed to accept information from the 64 field detectors for a total of 64 time increments. At the completion of the 64 time increments, the memory was completely filled, and had to be read to magnetic tape (a procedure requiring about 40 sec) before the memory was cleared and able to accept additional information. So as to avoid loss of tracer concentration data during the memory readout process, it was necessary to

estimate the length of time it would take for a plume or puff of tracer to clear the field array, and to program the length of the time increments accordingly. This procedure frequently resulted in the choice of time increments of relatively long duration (about 40 sec during 15 min plume releases) and a loss of much of the detail of the fluctuating concentration within the plume. Furthermore, poor estimates of the duration of tracer passage sometimes resulted in the filling of all 64 memory time channels before tracer had cleared the field grid.

A marked improvement in recording technique is being incorporated into the revised system. The prime improvement is the addition of a second memory unit. Detector signals can then be read into one memory unit while the second unit is dumping stored data to a magnetic tape. This procedure will permit uninterrupted sampling with short sampling time increments for extended periods of time. The limiting factor will be length of magnetic tape rather than number of addresses in the memory.

Data reduction will be facilitated by use of computer-compatible tape recording procedures.

TECHNOLOGY DEVELOPMENT FOR DUAL ATMOSPHERIC TRACER STUDIES ON AN INSTRUMENTED METEOROLOGICAL GRID

J. D. Ludwick*

Nuclear techniques are useful in studies of air pollution problems including the dispersion of material from a source and its subsequent distribution throughout the environment. A noble-gas-tracer grid system has been developed and used in the quantitative measurement on a real time basis of the transport and diffusion of ^{85}Kr released as a puff or continuous source out to distances of 800 meters.

This developed ^{85}Kr monitoring system has been modified to allow continuous recording of real time data differentiated into 1 second time intervals. Each downwind detector was modified to include a remotely operated cover plate which can also be used as an absorber or energy discriminator between the ^{85}Kr beta particles and other airborne radionuclides. Thus, it is adaptable to the measurement of reasonably high and low energy beta emitters in the presence of ^{85}Kr (0.7 MeV). Typically, a high energy beta could originate from a

*Radiological Sciences Department

radioactive particulate in the micron size range where unwanted effects from self-absorption would be negligible. Two techniques which have been considered for the generation of a 0.1 to 1 micron aerosol are the vaporization of a low-boiling solid material and the ignition of solid propellent-type materials.

Several factors must be considered in dispersing tracer radionuclides such as ^{85}Kr to the environment. The downwind radiation hazard must be reduced to a negligible factor. This can be accomplished by using least possible quantities of a short-lived radioisotope. In addition, the dispersal study must be conducted at a controlled location insuring that no detectable quantities of radiation leave the test site. For dual tracer experiments the beta energy of the particulate must be at least 50% different from that of the 0.7 MeV ^{85}Kr beta particle (or of the 0.35 MeV ^{133}Xe). Several radioisotopes prepared by neutron activation meet this criterion; these include ^{56}Mn, ^{31}Si, ^{64}Cu and ^{24}Na. Another convenient method for the preparation of such radioisotope sources would be in the use of a long-lived parent, short-lived daughter combination where a daughter of moderate strength could be separated from its parent at a time convenient to the field experiment needs.

The field experiments would be initiated by vaporization or ignition of the particulate tracer at the same time as the krypton vial burst. As the plumes traveled downwind, each monitor station's cover plate would be synchronously opened and closed at 1 second intervals. The thickness of the cover plate in the area over the detector surface would be adjusted to allow passage of only the harder beta particle. Thus data accumulated while the cover was open would represent the total air concentration of both the gaseous and the particulate tracer. During the closed cycle, however, only information from the harder beta tracer would be collected. In this way, not only would the unique real time particulate air concentrations be obtained but also, by comparison with the simultaneous noble gas concentrations measured, a quantitative measure of the depleting character of the particulate would be available.

THE REAL PLUME AND ITS RELATIONSHIP TO THE APPARENT PLUME

J. V. Ramsdell

The real plume and its relationship to the time integrated or apparent plume are discussed. The crosswind concentration in the real plume is shown to be asymptotically Gaussian. The variance of the crosswind concentration distribution of the apparent plume is shown to be equal to the sum of the crosswind concentration variance and the meander variance of the real plume. The relative contributions of the diffusion and meander of a real plume to the diffusion of an apparent plume are discussed.

Until comparatively recently most data on diffusion in plumes were obtained using sampling devices which integrated the plume behavior over relatively long periods of time. By the very nature of the averaging inherent in the experimental techniques, many details of the diffusion process were lost. Thus, the plume described by most of the standard diffusion models has little resemblance to the plume actually observed by the eye. For the past 3 years diffusion data collected at Hanford using the ^{85}Kr Tracer System[1] have been analyzed in an attempt to fill in some of the missing details. During the last year attention has been focused on description of the real plume and its relationship to the plume described by previous data. The latter of these plumes has been previously termed the mean plume but will hencefore be referred to as the apparent plume.

The ^{85}Kr Tracer System was designed in such a manner that relatively short averaging intervals would be available for data collection. As a result, data collected during prototype tests for the System are suitable for description of real plume characteristics. Data from the 1958 diffusion tests at Round Hill Massachusetts[2] were also found to be suitable.

The first four moments of the crosswind concentration distribution were computed for each real plume cross-section. The moments of particular interest were the third and fourth which describe the skew and peakedness of the distribution. To facilitate determination of the mean characteristics of the real plume, coefficients of skewness and kurtosis were computed and averaged. The expected coefficient of skewness for a symmetrical distribution is zero with the probability of positive and negative values being equal. Therefore, arithmetic averaging was used to determine the mean value for real plumes. On the other hand, the coefficient of kurtosis is bounded from below by zero. The observed values of the coefficient of kurtosis ranged from

somewhat less than 2 to well over 10 with a mode and median of the order of 3. To avoid placing excessive weight on high values, the mean coefficient of kurtosis for the real plume was determined using geometric averaging. The mean values of these coefficients are listed in Table 1. None of the coefficient values in the table is significantly different from the corresponding values for the Gaussian distribution, i.e., a coefficient of skewness of 0 and coefficient of kurtosis of 3. The conclusion that the mean concentration in the real plume is at least asymptotically Gaussian follows from this comparison.

TABLE 1. Average Coefficients of Skewness and Kurtosis for the Crosswind Concentration Distribution in Real Plumes

Location	Tracer	Distance (Meters)	Coefficient of Skewness	Coefficient of Kurtosis	Number of Observations
Hanford. 1967	^{85}Kr	200	0.02	3.03	70
		800	-0.08	2.79	67
Round Hill. 1958	SO_2	50	-0.32	3.28	10
		100	0.09	3.30	12
		200	0.15	3.46	7

Assuming that the concentration distribution in the apparent plume is also at least asymptotically Gaussian leads to the conclusion that the variances of the concentration distributions in the two plumes are related in following manner:[3]

$$\overline{Y^2} = \overline{D^2} + \overline{M^2}$$

where, $\overline{Y^2}$ is the variance in the apparent plume; $\overline{D^2}$ is the variance in the real plume, and $\overline{M^2}$ is the variance of distribution of the positions of the center of mass of the real plume. In effect, $\overline{D^2}$ represents true diffusion within and $\overline{M^2}$ represents the meandering of the real plume. During two of the ^{85}Kr prototype tests sufficient data were obtained at 200 and 800 meters to permit direct computation of each of the terms in this relationship. Figure 1 shows the results of these computations as well as some previous computations involving somewhat less tenable assumptions.[4]

Accepting the foregoing relationship as correct, attention was directed toward determining the relative magnitudes of the contribution of real plume diffusion and meander to the

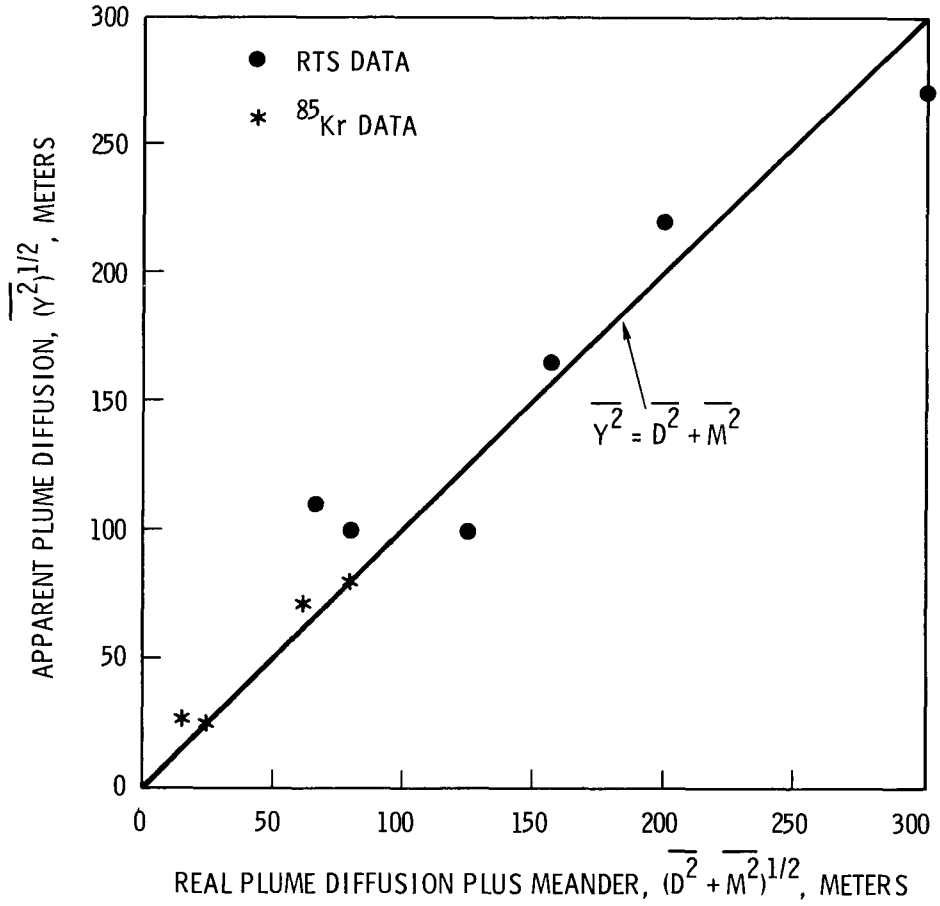

Neg 710972-5

FIGURE 1. Comparison of the Standard Deviation of the Cross-wind Concentration Distribution in the Apparent Plume with an Approximation Using Real Plume Measurements.

diffusion of the apparent plume. Figure 2 shows the decrease in the ratio of the variances of the cross-wind concentration distribution as a function of the ratio of observation times for one of the ^{85}Kr plumes. T is the time period during which the plume was examined and is associated with the apparent plume. It is constant. The time t is associated with plume segments of shorter duration and was variable in length in multiples of 38.4 sec up to T. The larger the ratio T/t, the closer the approximation of the ratio $\overline{D^2}/\overline{Y^2}$. Figure 2 indicates that the real plume diffusion accounted for about 20 percent of the apparent plume diffusion at 200 meters and about 10 percent at 800 meters. There is no reason to expect that these ratios are universal.

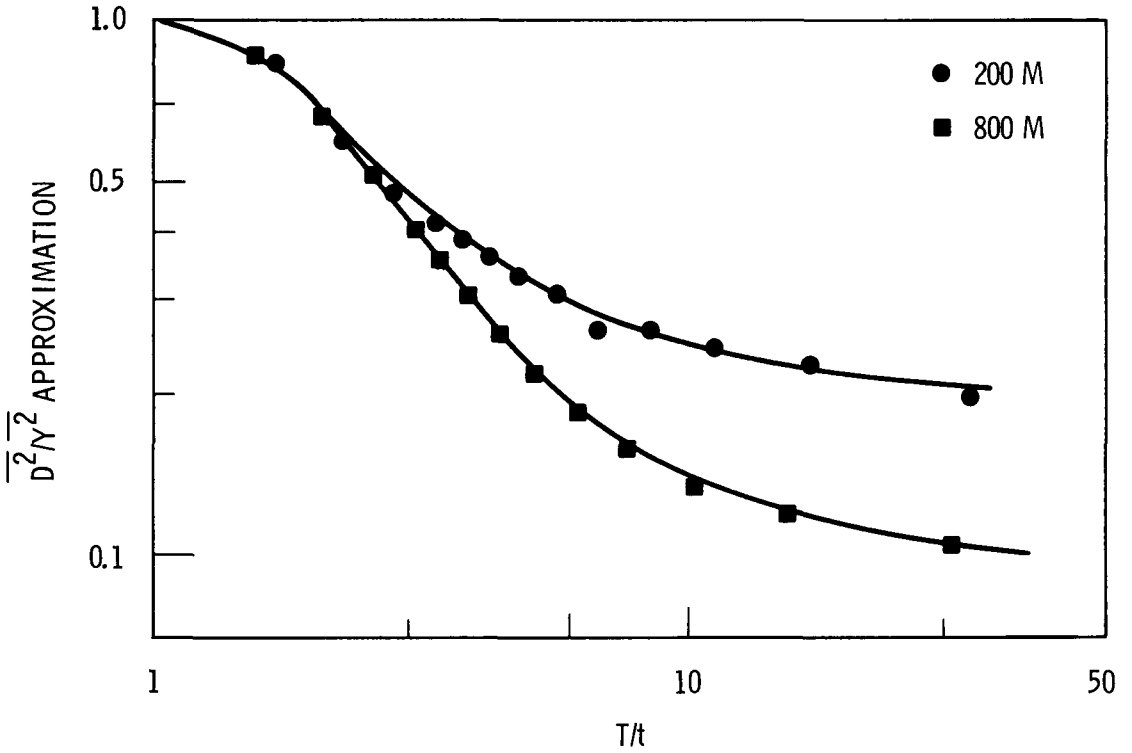

Neg 710972-1

FIGURE 2. The Ratio of Diffusion in Plume Segments to Diffusion in the Apparent Plume as a Function of the Ratio of Observation Times, where T is the Observation Time for the Apparent Plume and t for the Plume Segment (t min = 38.4 sec).

Complete descriptions of the real plume and its growth parameters will require more data. However, the present data do raise the question of the advisability of basing hazards analysis upon apparent plume parameters.

REFERENCES

1. *J. D. Ludwick, J. J. Lashock, R. E. Connally and P. W. Nickola. "Automatic Real-Time Monitoring of ^{85}Kr Utilizing the 4096 Memory of a Multiparameter Analyzer," Pacific Northwest Laboratory Annual Report for 1967, to the USAEC Division of Biology and Medicine, Volume II: Physical Sciences, Part 3. Atmospheric Sciences, BNWL-715-3. Battelle-Northwest, Richland, Washington, October 1968.*

2. *H. E. Cramer, F. A. Record and H. C. Vaughan. The Study of the Diffusion of Gases or Aerosols in the Lower Atmosphere, Final Report, M.I.T. AFCRC-TR-59-207. January 1959.*

3. *F. Gifford. "Statistical Properties of a Fluctuating Plume Dispersion Model;" Adv. in Geophysics, 6, New York, Academic Press, p. 471. 1959.*

4. *J. V. Ramsdell. "The Use of Instantaneous Plume Measurements to Approximate a Mean Plume," Pacific Northwest Laboratory Annual Report for 1967 to the USAEC Division of Biology and Medicine, Volume II: Physical Sciences, Part 3. Atmospheric Sciences, BNWL-715-3. Battelle-Northwest, Richland, Washington, October 1968.*

A COMPARISON OF 12-HOUR PROGNOSTIC ISOBARIC TRAJECTORIES WITH CALCULATED TRAJECTORIES FROM HANFORD, WASHINGTON FOR OCTOBER 1970

W. E. Davis and J. M. Thorp

A comparison of isobaric trajectories, calculated versus prognostic, indicated a correlation of 0.78 for distance traveled in 12 hours. A similar comparison of calculated trajectories versus isobaric trajectories based on persistence gave a correlation of 0.92 for a 12-hour movement. However, the 12-hour azimuthal difference between trajectory end points showed the prognostic trajectory to be superior to the persistence trajectory in anticipating the direction traveled from Hanford.

Prognostic trajectories are of interest in connection with air pollution problems, since they can indicate where the pollutant is expected to go, at what level it will be found, as well as where the pollutant will be removed from the atmosphere by precipitation. This report has been addressed in particular to the question of how reliable are present-day prognostic trajectories.

The isobaric trajectories were forecast using the computer results of the Primitive Equations (P.E.) model[1]. These isobaric trajectories were then compared with isobaric trajectories calculated on the observed 850 mb surface for a 12-hour

period. The 800 mb level, rather than the 850 mb level, was provided to the authors for use in order to lessen the terrain effects inherent in the P.E. model. The reason the 850 mb was used to verify the trajectories was that data were readily available at that level. In the mean, the two trajectories should be similar with 800 mb level trajectories moving at a higher speed. Trajectories based on persistence were assumed to require the least data, construction time and effort of any useful method. They have been used here as standard trajectories for evaluating the P.E. prognostic trajectories. For the first six hours, persistence and calculated trajectories are approximately coincident. With this in mind, the distances traveled in 12 hours as prognosticated through the P.E. model were correlated with distances determined from calculated trajectories and the distances expected on a persistence basis were also correlated with calculated trajectories. Table 1 indicates a comparison of distance traveled.

TABLE 1. Mean Travel Distance (Degrees of Latitude at 12 Hours)

Persistence	Calculated	Prognostic
3.5	3.5	2.9

Table 2 indicated linear regression results of $x = ay + b$ where x is calculated and y is persistence for the first column and y prognostic in the second column, where r is the correlation coefficient, a slope, b intercept, σ_a is variation of the slope, σ_b is variation of the intercept. Instead of increasing with height, we see that the distance traveled is less for the 800 mb P.E. prognostic than the calculated or persistence 850 mb distance. This may to some extent be due to smoothing of the wind field in the P.E. model, except that the same smoothing should also occur in the individual trajectories for a representative sample. In general, the intensity of the wind appears to be underestimated by about 3 knots (0.6° latitude in 12 hours) if we accept the October 1970 data as representative. For the same period, the deviations in azimuth showed the prognostic trajectory to be superior with a standard deviation of 16° from the calculated trajectory while persistence had a standard deviation of 25° from the calculated.

Table 3 indicates the result of comparing the distance separation between the calculated versus persistence and calculated versus

TABLE 2. Linear Regression Results

	Persistence	Prognostic
r	0.92	0.79
a	0.97	0.86
b	0.04	0.01
σ_a	0.04	0.08
σ_b	0.30	0.52

TABLE 3. Δ Distances

Δd (° lat.)	Distance from Prognostic to Calculated		Distance from Persistence to Calculated	
	N	Cumulative %	N	Cumulative %
0.0-0.4	2	5	6	14
0.5-0.9	10	32	20	62
1.0-1.4	9	55	6	76
1.5-1.9	6	71	5	88
2.0-2.4	5	84	4	98
2.5-2.9	5	97	1	100
3.0-3.4	1	100		

prognostic where $\Delta d = [(x_1 - x_2)^2 + (y_1 - y_2)^2]^{1/2}$. In general, the three tables indicate that, at least for the Hanford Area, persistence trajectories do a better job of forecasting distance traveled by air parcels at twelve hours. The prognostic P.E. model, however, forecasts the angular movement better than persistence. Thus some improvement may be readily expected in using the P.E. model for angular movement with greater reliance on the existing isotach patterns for 12-hour trajectories. Consideration is now being given to this as well as to using isentropic trajectories rather than isobaric in an evaluation of the prognostic trajectories for the P.E. model. The use of isentropic trajectories will give a better evaluation of prognostic trajectories since vertical movement may be considered as part of verification.

REFERENCE

1. *J. Heffter. Unpublished data, NOAA, Silver Springs, Maryland, 1970.*

RADIATIONAL COOLING OF AIR PARCELS FOLLOWING THE EFFLUENT OF PHOEBUS 1B EP-IV, FEBRUARY 24, 1967

W. E. Davis and B. C. Scott

An updated radiational cooling model predicted diabatic results consistent with airplane measurements of plume height. The computer model produced diabatic cooling results which were in approximate agreement with results derived from previous hand calculations.

Prior to 1970, the authors have computed radiational cooling through the use of the Elsasser diagram.[1] Since these computations were time consuming, a computer program was developed by Scott.[2]

Computed values of radiational cooling in a partially cloudy atmosphere were then utilized in a diabatic trajectory analysis of the effluent released from a Phoebus 1B reactor test. Comparisons between the measured effluent path and the computed path suggested that the values of radiational cooling incorporated into the trajectory analysis were erroneous. The radiation computer program was reevaluated and improved. New diabatic trajectories, utilizing data from the updated radiational model, were then constructed and found to be in close agreement with the observed trajectories of the effluent.[1]

Table 1 presents the cumulative radiational cooling effects in the cloudy atmosphere along the effluent's path. The initially predicted values (OLD) of radiative change showed a cumulative heating while the actual plume was observed to be cooling. The updated values of radiational cooling were found to be consistent with previously obtained values from an Elsasser diagram, thus lending further support for the accuracy of the present numerical model.

TABLE 1. Cumulative Cooling with Clouds

February	Elsasser	Scott Updated	Scott Old	Derived Measurements Δθ*	Sky Cover for the Plume
	°C	°C	°C	°C	
23 22Z-24 12Z	-0.4	-0.4	+0.5	-0.5	overcast
24 12Z-25 00Z	-0.7	-0.8	+1.0	-1.2	overcast
25 00Z-25 12Z	-1.1	-1.5	+1.2	-1.7	clear to overcast
25 12Z-26 00Z	-1.4	-2.5	No		clear to overcast
26 00Z-26 12Z	-2.0	-3.5	data		clear to overcast

*Averaged from aircraft measurements.

In general, the radiational model yielded higher cooling rates than the hand calculations on an Elsasser diagram for times greater than H + 21:30 hours, and thus enabled the centerline of the predicted plume path[1] to be lowered to an altitude near where the actual plume was measured. Aircraft measurements indicated a "hot spot"[3] at H + 32 hours with the potential temperature (θ) of the plume approximately 1/2 °C cooler than the θ predicted for the center of plume by the diabatic trajectory. However, there is no indication that the aircraft actually measured the center of the plume since a vertical temperature and concentration sounding was not taken at this time.

To summarize, the updated numerical model appears to describe accurately the radiational cooling in a cloudy atmosphere and will thus enable its incorporation into a real time diabatic trajectory analysis scheme.

REFERENCES

1. *W. E. Davis and B. C. Scott. "Diabatic Trajectories and a Trajectory Case Study of the Effluent from Phoebus 1B EP-IV February 23, 1967," Pacific Northwest Laboratory Annual Report for 1968 to the USAEC Division of Biology and Medicine, Vol. II: Physical Sciences, Part 1. Atmospheric Sciences, BNWL-1051. Battelle-Northwest, Richland, Washington, November 1969.*

2. *B. C. Scott. "RAFLUX - A Numerical Model for Calculating the Long Wave Radiative Transfer in the Troposphere," Pacific Northwest Laboratory Annual Report for 1969 to the USAEC Division of Biology and Medicine, Vol. II: Physical Sciences, Part 1. Atmospheric Sciences, BNWL-1307. Battelle-Northwest, Richland, Washington, June 1970.*

3. *J. E. Hand and V. F. Weissman. Phoebus 1B EP-IV Effluent and Ground Deposition Surveys, Addendum II, EGG 1183-1321, April 21, 1967.*

PROJECT BOMEX STUDIES OF ATMOSPHERIC AND OCEANIC MIXING AND AIR-SEA INTERCHANGE USING RADIOACTIVE TRACERS

J. A. Young and W. B. Silker*

The activities of cosmogenic ^{7}Be and several bomb-produced radionuclides were measured in air, seawater, and rain samples during the Barbados Oceanographic and Meteorological Experiment (BOMEX). Because of its relatively short 53 day half-life, ^{7}Be was confined primarily to the top 50 meters of the sea, so its inventory in the sea could be determined from samples collected between the surface and 100 meters. The inventories of ^{7}Be and the other radionuclides in the sea varied by a factor of about 2.5 during BOMEX, with

*Radiological Sciences Department

most of the variation occurring in the top 30 meters. The observed changes were not due to rain, since the addition of ^{7}Be by rainfall during the experimental period was only 10 to 15% of the ^{7}Be decay in the sea. The rapid variations in concentration were probably caused by horizontal transport of water masses of different activities through the BOMEX array (Figure 1).

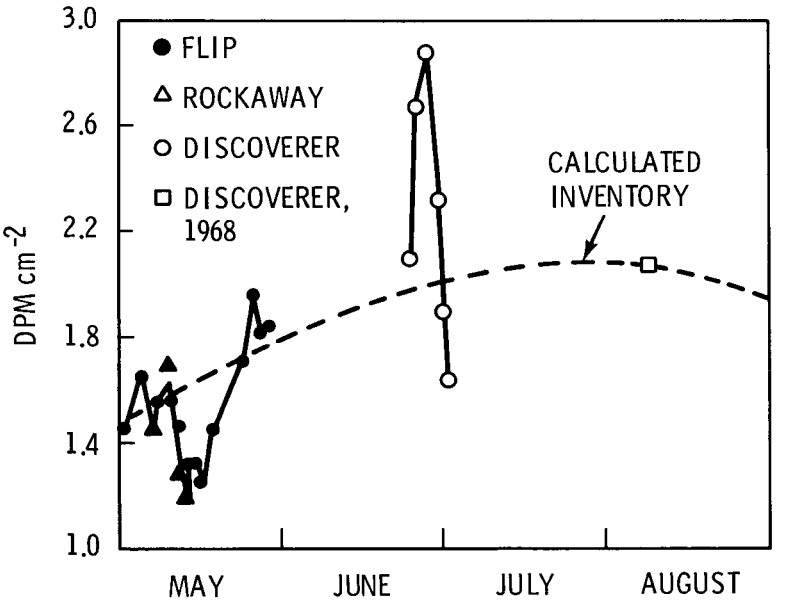

Neg 710080-3

FIGURE 1. ^{7}Be Inventory in a 1 cm^2 Column of Seawater

During the second two weeks of May large amounts of fresh water, presumably Amazon River water, entered the southeast corner of the BOMEX array. Measured surface salinities decreased from around 35% at the USCGS Rockaway during the first two weeks of May to as low as 31% at the USCGS Discoverer during the last two weeks of June, indicating the presence of around 12% fresh water. The large changes in ^{7}Be activity could have been caused by intrusions of river waters having high ^{7}Be activity. Beryllium-7 activities were generally higher when salinities were low. However, the ^{7}Be activity was not directly proportional to the amount of fresh water present, so the intrusion of fresh water was probably not the only cause of the variation in ^{7}Be activity. The variations in

activity may indicate that ^{7}Be activities in the ocean are generally not uniform over large horizontal areas, due to differences in the amount of ^{7}Be transferred across the sea at different locations resulting from different rainfall patterns, air concentrations, and wind speeds.

Air filter samples have been collected on the Island of Barbados since May 1969 (Figure 2). These samples indicate that the air concentration of ^{7}Be varies seasonally by an order of magnitude at this location, with maximum concentrations occurring around May and June and minimum concentrations occurring in November and December. Therefore, ^{7}Be inventories in the sea should also change with the time of year. If one assumes that the rate of transfer of ^{7}Be across the sea surface is proportional only to the air concentration, one can calculate the variation of seawater inventory with time by choosing the proportionality constant so that the calculated inventories agree with the measured inventories. A rate of transfer of 9.52 atoms of $^{7}Be/cm^{2}$ of sea surface/day/dpm of ^{7}Be in 10^{3} standard cubic meters (SCM) of air gives calculated seawater inventories which agree with measured inventories. These calculations indicate that the maximum and the minimum in the seawater inventory should both occur 2 or 3 months after the maximum and the minimum in the air concentration.

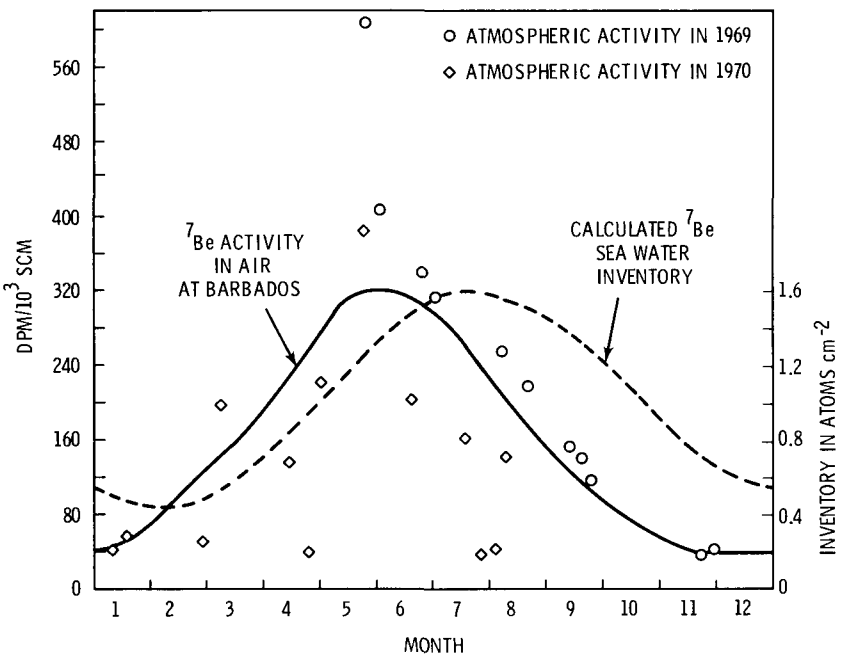

Neg 710080-1

FIGURE 2. ^{7}Be Disintegration Rate in Air at Barbados and the Calculated Seawater ^{7}Be Inventory

During the BOMEX period the ^{7}Be inventory in the sea was increasing, on the average, by 0.010 atom cm^{-2} sec^{-1}. The rate of addition to the sea was 35% greater than the rate of decay in the sea. Dividing the rate of addition by the average atmospheric concentration gives a value of 0.7 cm sec^{-1} for the deposition velocity. The vertical diffusion coefficients in the surface layers of the ocean can be calculated from the flux across the sea surface and the vertical concentration gradient. The vertical profile measured on May 11, 1969 gives the following values for the vertical diffusion coefficient, K_Z.

Depth, meters	K_Z, $cm^2 sec^{-1}$
0-15	4.3
15-30	4.8
30-50	0.82
75-100	0.60

The activities of ^{7}Be and the nuclear-weapons-produced radionuclides in air filter samples collected by aircraft during BOMEX did not increase significantly between 0.3 and 9.1 km altitude. On the average there was a minimum in the activity of the radionuclides at 1.5 km, probably because of rainout. Many of the vertical profiles showed a minimum for the activity of the bomb-produced radionuclides but not for ^{7}Be at some altitude, often 9.1 km. These minimums probably resulted from intrusions of southern hemispheric air, since the activities of the bomb-produced radionuclides were considerably lower in the southern hemisphere at this time, but the ^{7}Be activity should be about the same in the two hemispheres. Other profiles showed minimums in both ^{7}Be and the bomb-produced radionuclides at around 9 km and were therefore not due to intrusions of southern hemispheric air. Probably these minimums resulted from recent precipitation scavenging of the air. It is possible that air which was scavenged in the cumulonimbus of the intertropical convergence zone moved northward into the BOMEX array.

Often there were large increases in radionuclide activity with time at some altitude and location. The increases at 12 km during the first 2 weeks of June were particularly large. Back trajectories were calculated for many of the air masses showing high radionuclide activities. It was found that these air masses had originated within the previous few days at latitudes of 30° N or greater. Activities of ^{7}Be and the bomb-produced radionuclides are generally considerably greater at these higher latitudes.

During the BOMEX experiment, air samples were collected at five elevations from 1 ft to 70 ft above the sea surface aboard Flip, the Rockway and the Discoverer. Many of these profiles showed increasing radionuclide activities with height, due to the removal of the radionuclides at the sea surface. On some of the profiles, however, the increase in activity with height was too small to be measured. When the vertical eddy diffusion coefficients measured by

other investigators become available the rate of transfer of ^{7}Be and other radionuclides across the sea surface as a function of time will be calculated to determine the effect of meteorological parameters such as wind speed upon the flux across the sea surface. The calculated fluxes will also be compared with the average fluxes determined from the measured seawater inventories.

THE DEVELOPMENT OF A SYSTEM FOR PROCESSING DIGITAL TURBULENCE DATA OBSERVED DURING BOMEX AND TEST DATA RESULTS

R. K. Woodruff

Participation in the Barbados Oceanographic and Meteorological Experiment required the development of a digital data processing capability for the turbulence data collected. Hardware modifications have been accomplished and software developed to permit reading data on field tapes directly into a computer. Additional programs have been written to restore the continuity of the data series, scale and edit the data and determine gross statistics. Test results from data collected from Barbados are comparable with oceanic data collected elsewhere by other investigators.

As reported previously,[1] the Atmospheric Resources Department (ARD) of BNW and the Department of Oceanography, Florida State University (FSU), jointly undertook the preparation, deployment and operation of the TRITON spar buoy for the Barbados Oceanographic and Meteorological Experiment in 1969. BNW's major efforts were in the development, testing and operation of a high capacity thermoelectric generator power source and a sensor and data recording system for measuring the turbulent fluctuations of the wind vector, moisture and heat.

A Geodyne digital data recording system (Model 985) was selected as the data recorder because it satisfied the data recording requirements and the requirement for interface compatibility with existing buoy recording equipment operated by FSU. BOMEX was the first experiment in which the ARD has used digital field recorders for the acquisition of turbulence data. Previous recording has been done using analog recorders. This situation has required the development of a digital data processing system analogous to that currently used for processing analog recorded turbulence data collected for other purposes.

That which follows briefly discusses the steps that have been and are being taken to complete the Geodyne digital data recording and processing capability and specifically for processing the data collected

from the TRITON buoy and the island of Barbados as part of the BOMEX.

The processing of the Geodyne recorder data is being accomplished in the following steps:

1) Cassette Tape Reader Modification and Translation Software Development,
2) Data Processing Software Development,
3) Software Interfacing.

CASSETTE TAPE READER MODIFICATION AND TRANSLATION SOFTWARE DEVELOPMENT

The Geodyne tape recorder uses one-quarter inch magnetic tape cassettes holding 1200 feet of continuous loop tape. These cassettes are convenient for field use; however, before the data can be processed they must be translated into IBM standard format and placed on one-half inch tape.

Although a commercial translator was available, considerations of expense and versatility led to modification of a less expensive model and its direct interfacing with the BNW SEL 840A computer. This will allow more extensive error checking procedures to be undertaken than are normally available. Generally, translators provided only for the tape-to-tape translation and a gross accumulation of record bit count errors. In the present system each 480-bit data record (32 words of 15 bits each) is checked for the correct bit count. If the record is distorted its data are voided, but its position is maintained such that an interpolated or substitute record can be entered at a later time and the continuity of the real-time data series maintained. Each of these blank record position is, of course, flagged such that it can be relocated for appropriate processing. A count of the number of distorted records is printed out for approximately every 4 minutes of real-time data. This makes it possible to determine sections of a data tape that are not suitable for processing because of recording malfunctions. Normally, this would not be a necessary function; however, it was included in the initial translation process as it was known that recording transients caused some malfunctions during the at-sea phases of the BOMEX operation.

Future improvements or expansion of this translation process will include expansion of the error checking function by including a parity check for each data word. This has not been done to date as the Geodyne recorder did not initially record parity. This feature is being added to upgrade recording quality.

The translator system hardware modification and software development was accomplished by personnel of the BNW Computer Systems Development Section. The hardware modification involved the replacement of pulse return-to-zero logic recording circuits with circuitry for reading data recorded with the nonreturn-to-zero phase shift logic of the Geodyne recorder. These modifications are the subject of BNW Computer Systems Development Memorandum 71-1, dated January 1971.

DATA PROCESSING SOFTWARE DEVELOPMENT

Programs have been written to read the half-inch IBM standard tape generated by the translation process, perform various conversions, editing and statistical summarization functions and write the edited data on magnetic tape for more detailed analyses. These programs accomplish the following operations in the order listed:

1) Missing data substitution,
2) Conversion to engineering units, calibration scaling, and the determination of x, y and z wind components,
3) Raw data statistics calculation,
4) Reasonableness editing, and
5) Statistical summarization of edited data.

The first function of the data processing software is to restore the continuity of the data series by placing representative data in the data records that were found by the translation software to be distorted. This is accomplished by substituting a good data record that was observed a short time (a few seconds) before or after the missing data record. If the data are distorted continuously for 10 seconds real time, a data discontinuity is noted such that these sections of a record can be avoided in subsequent detailed analyses.

When the continuity of the data series has been restored, the decimal equivalents of the octal numbers representing the data are converted to the appropriate engineering units and scaled according to the sensor calibrations. The wind vectors measured by the two wind turbulence sensors are orthogonalized to common x, y and z components.

The following raw data statistics are determined for each parameter:

1) 5-minute real-time means;
2) For the total run length:
   (a) Standard deviations and means, and
   (b) Standard deviation and mean of the population of successive sample differences.

The reasonableness editing logic assumes that the data populations are Gaussian and utilizes the raw data statistics to establish criteria for rejection of individual data values. Data points are rejected if they do not satisfy either of the following criteria:

1) The point does not appear to be a member of the population of raw data points as determined from the calculated statistics of that population, and
2) The difference between the value of the point in question and the previous one does not appear to be a member of the population of successive difference values determined from the raw data. If the data point fails either test, its value is reduced until it satisfies the above criteria.

With the completion of the reasonableness editing, the means and standard deviations for successive five-minute real time intervals are determined. These statistics can

tnen be used to determine which sections of the data satisfy the requirements for various types of special analyses.

SOFTWARE INTERFACING

At this point in the programming sequence, the data will be put into a format compatible with programs which have been previously developed for the analysis of turbulence data on a UNIVAC 1108 as part of other ARD research efforts. This will provide access to a library of several useful statistical analyses such as power, cross, and bi-spectra, auto and cross-correlation functions, second, third and fourth moments of the individual distributions and the second and third moments of joint distributions.

TEST DATA RESULTS

With the completion of a basic data processing system, it is necessary to verify the reasonableness of the final output before further processing. This was accomplished with a data tape collected on the island of Barbados.

By virtue of the close proximity of the observation location to the shoreline and the persistent onshore winds, it would appear most reasonable to compare the observed data to data typical of oceanic conditions. Table 1 compares some statistics by Miyake, et al. (1970)[2] University of British Columbia with one set of test data.

It is expected that stability conditions were reasonably similar in both cases. The times over which the statistics were determined, however, should contribute to some small differences in the data. The UBC statistics were determined for periods of 33-63 minutes while the BNW statistics are for 5-minute periods. The comparison obtained, however, is sufficient to demonstrate the reasonableness of the data and reinforces the initial assumption that the data observed at the island location may be representative of oceanic conditions.

The verification of other data sets will be accomplished in the future, as well as the comparison of the power spectra obtained with those of other oceanic data before more extensive analysis is initiated.

TABLE 1. Comparison of Data

	σ_u cm/sec		σ_v cm/sec		σ_w cm/sec		σ_t °C	
	UBC	BNW	UBC	BNW	UBC	BNW	UBC	BNW
Max	74	65	64	51	42	42	0.21	0.73
Mean	52	42	44	33	26	25	0.15	0.30
Min	32	27	29	19	17	17	0.07	0.19

REFERENCES

1. *R. K. Woodruff and A. G. Dunbar. "The Development and Testing of a Stable Buoy and Instrument System for Studies at the Sea-Air Interface," Pacific Northwest Laboratory Annual Report for 1969, Vol. II: Physical Sciences, Part 1: Atmospheric Sciences, BNWL-1307, pp. 46-53. Battelle-Northwest, Richland, Washington, June 1970.*

2. *M. Miyake, R. W. Stewart and R. W. Burling (1970). "Spectra and Cospectra of Turbulence over Water." Quarterly Journal of the Royal Meteorological Society, 96, pp. 138-143.*

MODELING OF WIND COMPONENT SPECTRA

C. E. Elderkin, D. C. Powell and T. W. Horst

Modeling of turbulence spectra in neutral conditions shows a linear scaling with height to at least 60 meters for the vertical component with the normalized frequency of the peak somewhat higher than previously reported. The longitudinal component spectra also scale proportional to height above a frequency of 0.01 hertz and exhibit a second, low frequency peak, which does not depend on height. The low frequency portion of the lateral component shows no consistent modeling characteristics. The inertial subrange was found above 7.5 meters in the normalized frequency range above a value of about one. The expected -5/3 power dependence on frequency and the 4/3 ratio between either vertical or lateral component spectra and the longitudinal spectra are reasonably well demonstrated. The theoretical nondimensional form of the inertial subrange was closely followed when the generally accepted value of 0.146 for Kolmogoroff's constant and the recently adjusted value of 0.35 for Von Karman's constant are used.

An understanding of the spectral structure of atmospheric turbulence is important in developing dependable methods for estimating diffusion of pollutants released to the atmosphere. Consequently, spectral models for the turbulent fluctuations of each wind component under various conditions of wind speed, atmospheric stability, and height are of interest. Efforts in this direction are represented by the summary of turbulence spectral results presented by Busch and Panofsky,[1] which show that, for the vertical velocity component, the Monin-Obukhov similarity theory is followed with good agreement between spectra from Hanford, Round Hill, and Cedar Hill. The spectra are scaled directly proportional to height up to about 50 meters.

The longitudinal spectra, however, show less agreement between the three sites at lower frequencies. There

appears to be a scaling of the spectra which is not directly proportional to height and strict agreement between sites for the frequency of maximum energy was not found.

It is clear that additional high quality turbulence data from towers are needed to adequately model turbulence spectral structure. Experiments were conducted during the summer of 1970 at Hanford to measure turbulence with sonic anemometers simultaneously at three levels: 7 1/2 meters, 15 meters and 60 meters; and Gill three-propeller anemometers at three other heights: 1 7/8 meters, 3 3/4 meters and 30 meters. Twelve experiments were conducted in unstable, near neutral, and stable conditions as well as transitional states. Data from three tests, originally recorded on analog magnetic tape recorders, have been digitized and processed on the UNIVAC 1108 computer yielding moments, Reynolds stresses, heat flux, spectral, and cross spectral distributions.

VERTICAL COMPONENT SPECTRA

One 55-minute period of neutral data was analyzed. The recording was from 1910 to 2005 P.S.T., July 28, 1970. The three spectra for w' from the sonic anemometers at 60, 15 and 7.5 meters, respectively, follow the nondimensional scheme very well. The maximum nondimensional spectral value was found to be 0.46 at the nondimensional frequency 0.46. The frequency is somewhat higher than the value, 0.32, given by Busch and Panofsky.[1] The difference may, in part, be due to using $\bar{U}$, the mean longitudinal component, in normalizing the frequency in the present work, whereas the mean horizontal wind speed was used in the studies cited by Busch and Panofsky.

An analytical expression of the form used by Fichtl and McVehil[2] was used to model the Hanford spectra for w'. The form used by Busch and Panofsky

$$\frac{nS_w(n)}{u_*^2} = \frac{1.075\left(\frac{f}{0.32}\right)}{1 + 1.5\left(\frac{f}{0.32}\right)^{5/3}}, \qquad (1)$$

a special case of the more complicated Fichtl and McVehil form, is simpler and was found to fit the Hanford spectra as well when the constants determining the predicted value for maximum energy and the predicted frequency of maximum energy were appropriately adjusted. The expression fitting the Hanford spectra is

$$\frac{nS_w(n)}{u_*^2} = \frac{1.15\left(\frac{f}{0.46}\right)}{1 + 1.5\left(\frac{f}{0.46}\right)^{5/3}} . \qquad (2)$$

Values from this expression may be compared to those from a theoretical expression for the inertial subrange, based on Kolmogoroff's similarity theory and the further assumption that the dissipation is equal to the mechanical production. This expression is

$$\frac{nS_w(n)}{u_*^2} = \frac{4}{3} A k^{-2/3} \left(\frac{nz}{\bar{U}}\right)^{-2/3} \qquad (3)$$

where A is the Kolmogoroff constant, generally accepted as 0.146, and k is the Von Karman's constant, recently re-evaluated at 0.35. In the inertial

subrange, the values from (3) are between those of (1) and (2); the difference between expression (2) and (3) is about 15%, as seen in Figure 1. To assure that the conditions associated with the assumption of neutral stability were met, the energy budget was analyzed for the same data which indicated that there was negligible convection and flux divergence at 7.5 meters and at 15.0 meters. But between 30 and 60 meters, slight instability and a small positive flux divergence are noted.

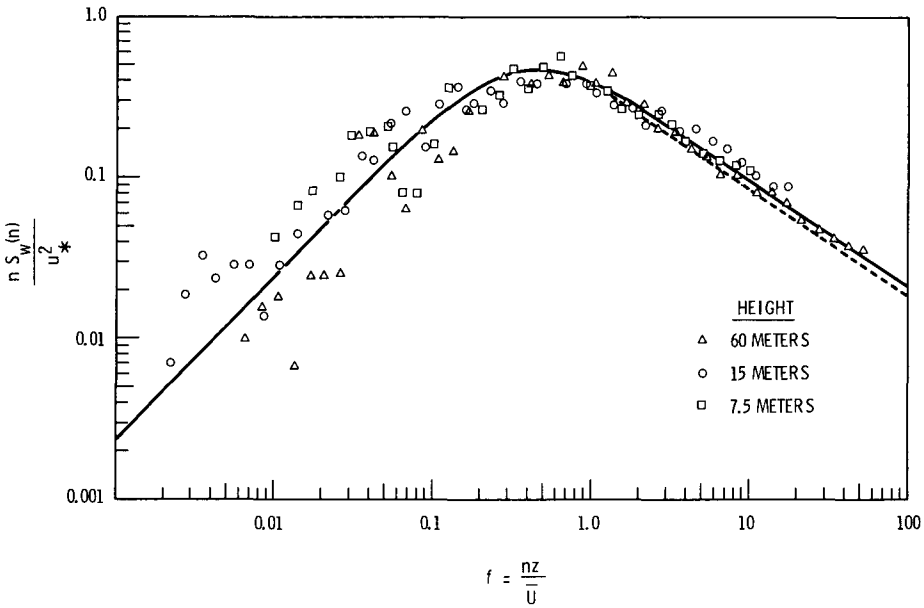

Neg 711160-5

FIGURE 1. Nondimensional w Spectra for 3 Heights - Neutral Case

HORIZONTAL COMPONENT SPECTRA

Previous difficulty in defining the frequency of maximum energy for the longitudinal component may be due to interference by mesoscale turbulence, which may differ significantly from one site to another, or even from one data collection period to another.

The longitudinal spectra for the present Hanford neutral data show two peaks separated by a trough at about 0.01 hertz. Other data collected at Hanford for TOLCAT analysis[3] have shown the same feature. One of the peaks is scaled frequency-wise as a linear function of height, and the other peak is at the same frequency at all heights (see Figure 2).

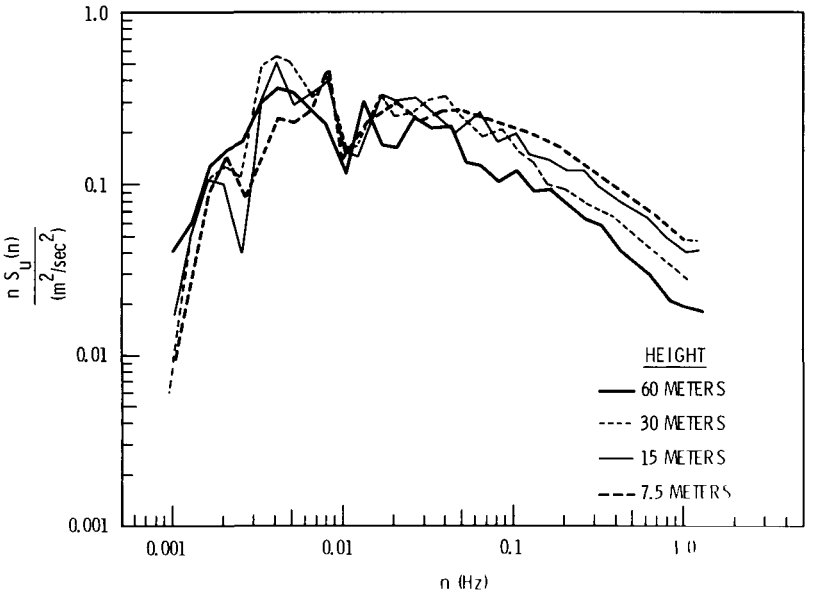

Neg 711160-1

FIGURE 2. Dimensional u Spectra for 4 Heights - Neutral Case

The higher frequency peak, modeled proportional to height, shows maximum energy occurring at a frequency about an order of magnitude lower than for the w' spectra, and exhibits the -2/3 slope in the inertial sub-range. The 4/3 ratio expected between the energy in the two components in the inertial subrange is reasonably well verified, being observed as 3 to 2, rather than 4 to 3, as predicted by theory. An empirical expression derived to match the u' spectra in the high frequency peak is

$$\frac{nS_u(n)}{u_*^2} = \frac{3.00\ (\frac{f}{0.056})}{1 + 1.5(\frac{f}{0.056})^{5/3}} \qquad (4)$$

and is shown in Figure 3.

The agreement between this expression and the theoretical expression for the inertial subrange is excellent, being within 1%. The theoretical expression is given by (3) with the 4/3 factor removed.

The spectra for the lateral velocity component also show a reasonable verification of the inertial subrange for normalized frequencies greater than about f = 1 above the 7.5 meter height. Both the -2/3 slope and the 4/3 ratio are fairly well approximated. At 7.5 meters, however, the lateral component spectrum did not exceed the longitudinal spectrum throughout the highest decade of frequencies measured showing that the inertial subrange does

not truly exist there. At lower frequencies, below the inertial subrange, the lateral component also does not demonstrate a constant spectral shape suitable for good modeling. The lowest frequency portion of the lateral spectra does not appear to scale according to height, to show a peak at a common frequency, or to show a gap at a common frequency for the different heights. Additional data will be required to define the best model of the lateral spectra and to show the scatter to be expected.

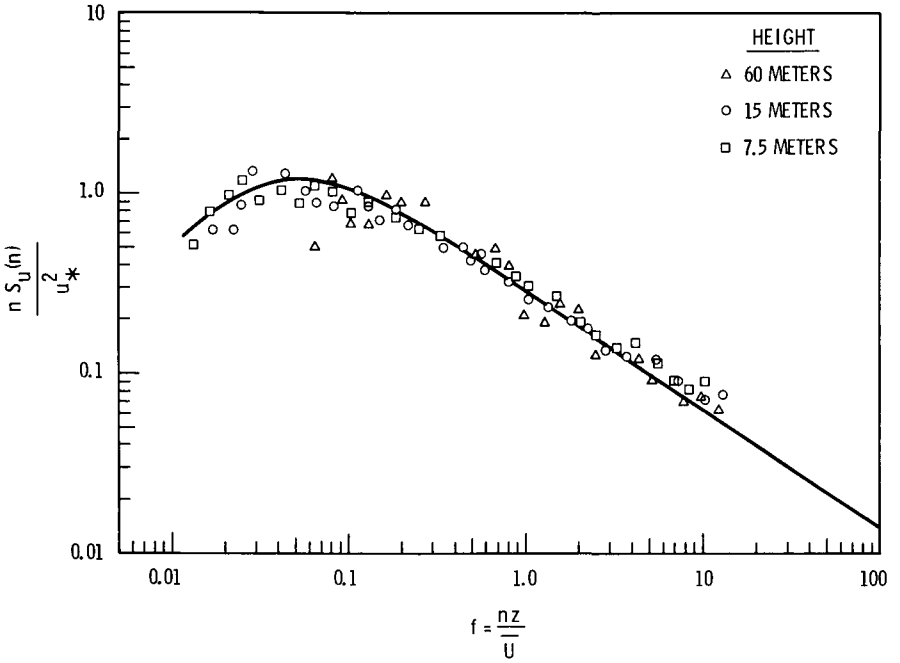

Neg 711160-2

FIGURE 3. Nondimensional u Spectra for 3 Heights - Neutral Case

REFERENCES

1. *N. E. Busch and H. A. Panofsky. "Recent Spectra of Atmospheric Turbulence," Royal Met. Society Qtrly. Journ., Vol. 94, 1968.*

2. *George H. Fichtl and George H. McVehil. "Longitudinal and Lateral Spectra of Turbulence in the Atmospheric Boundary Layer at the Kennedy Space Center," Journ. of Appl. Met., Vol. 9, No. 1, February 1970.*

3. *C. E. Elderkin, D. C. Powell, A. G. Dunbar and T. W. Horst. Take-off and Landing Critical Atmospheric Turbulence (TOLCAT) Experimental Investigation - Interim Report, Battelle Memorial Institute, Pacific Northwest Laboratory Techn. Report AFFDL-TR-70-117, November 1970. (In press.)*

BNWL-1551
Part 1

DIABATIC EFFECTS ON ATMOSPHERIC TURBULENCE SPECTRA

C. E. Elderkin

The turbulence spectrum for the vertical velocity component in diabatic conditions is shifted in frequency from the spectrum for the neutral case. The data for unstable conditions are shifted to lower frequencies and the data for stable conditions to higher frequencies. When stability is included in the scaling of the nondimensional frequency, as predicted in the inertial subrange by Kolmogoroff's expression with the dissipation determined through the turbulent energy budget equation, the spectra are all reasonably coincident and agreement with the inertial subrange theory was generally within 10%. This was accomplished by assuming that convective production equals the flux divergence of turbulent energy. The assumption that the flux divergence is zero, used in earlier spectral modeling work, does not organize the data so well. In addition, direct evaluation of the flux divergence demonstrates that it was definitely nonzero. However, it also does not precisely balance the convective production and appears to lag in its adjustment from one stability condition to another.

It has previously been shown from turbulence results at various sites (see Busch & Panofsky)[1] that for the vertical wind component, in addition to being scaled proportional to height, the spectra exhibit a stability dependence. For stable conditions, the spectra are shifted to higher frequencies than for neutral and unstable conditions. It was concluded in that study that the stability dependence observed appeared to be consistent with the results suggested in the inertial subrange of the longitudinal component spectra, that the dissipation of turbulent energy is balanced by the total production, i.e., mechanical plus convective. This implies that the divergence of the turbulent energy flux is approximately zero.

However, recent results of very comprehensive turbulence experiments performed by AFCRL (Haugen, et al.)[2] were analyzed and reported by Wyngaard and Cote,[3] which showed that the flux divergence was not negligible. Indeed, direct measurements of this quantity appeared to approximately balance the convective production. However, the dissipation was not balanced by the mechanical production alone and possibly the unmeasured pressure transport term is significant.

Recently, improved turbulence measurements in diabatic conditions have been possible at Hanford. Particularly, more definitive information is available on the stability and Reynolds stress and their variations with height than with those data included in the summary cited above and evaluated in previous studies at Hanford.[4]

Sonic anemometer data from 7.5, 15 and 60-meter heights were analyzed for two almost adjacent 28-minute periods of unstable data. The periods investigated were 1537-1605, July 20, 1970 and 1619-1647, July 20, 1970.

These data were from the most stationary periods within the 70-minute interval under consideration. The Reynolds stress, which was relatively constant across the vertical space of the array during neutral conditions in the same series of tests, decreased significantly with height during the two unstable periods considered here - more so during the first than during the second. The comparison is shown as below:

TABLE 1.

	$\overline{-u'w'}$ $(mps)^2$		
Height,m	Neutral case	1st unstable case	2nd unstable case
60.00	0.19	0.07	0.31
30.00	0.23	0.19	0.46
15.00	0.23	0.37	0.51
7.50	0.22	0.48	0.40
3.75	0.21	0.40	0.36

Because of the large change through the vertical profile of the Reynolds stress, it is surprising that the vertical component spectra for the unstable cases model as a function of height as well as they do. This resulted, however, only when a single, near surface value of u_*^2, was used to normalize spectra from all heights. Ratios across the span of values for $nS_w(n)/u^*_o{}^2$ were seldom greater than 1.6 at any given frequency within the inertial subrange. However, some stratification according to height (or according to the stability, varying as a function of height) was still detectable.

When the stability dependence is included in the scaling of the spectrum for the vertical component, within the inertial subrange (see C. E. Elderkin),[4] the theoretical description takes the form

$$\frac{n\,S_w(n)}{u_*^2} = \frac{4}{3}\,Ak^{-2/3}\left(\frac{1}{\phi_\varepsilon}\frac{nz}{\bar{U}}\right)^{-2/3} \qquad (1)$$

where ϕ_ε is the normalized dissipation,

$$\phi_\varepsilon = \frac{\varepsilon}{u_*^3/kz}\,. \qquad (2)$$

It has been assumed by Busch and Panofsky[1] and in previous work at Hanford[2], that

$$\phi_\varepsilon = \phi_M - \frac{z}{L} \qquad (3)$$

where the nondimensional form of the turbulent energy budget equation has been used with the flux divergence of turbulent energy set equal to zero. Here ϕ_M is the dimensionless wind shear and L the Monin-Obukhov stability lengthy scale. Averaging together the measurements from 7.5 meters and from 15.0 meters, the representative values of L for the two periods considered in the present analysis were calculated to be -98 meters and -225 meters.

At the 60-meter height, the first period was therefore considerably more unstable than those cases included in the studies referenced above and a better evaluation could be made of the assumption that dissipation equals the sum of mechanical and convective energy inputs. It was clear that this assumption, when used in Equation (1), did not produce as good a comparison with the spectral data within the inertial subrange as would the assumption that convective energy production and flux divergence are equal. With the latter assumption, the spectral wave lengths are scaled not only by height but also by the dimensionless wind shear (as proposed earlier by Berman[5]), i.e., in Equation (1), we let $\phi_\varepsilon = \phi_M$.

Therefore, the spectral estimates of the vertical component for the two unstable periods, normalized to u_*^2 determined near the surface, are plotted in Figure 1 as a function of the normalized frequency, $\frac{1}{\phi_M}\frac{nz}{\bar{U}}$. These are compared with the theoretically expected curve in the inertial subrange (the dashed line) and the empirical curve determined from the spectral data for neutral stability (where $\phi_M = 1$).

The modeled expression for neutral conditions is appropriate here if the dependent variable is further normalized by dividing f by ϕ_ε as specified by Busch and Panofsky;[1] however, we assume here that $\phi_\varepsilon = \phi_M$ where ϕ_M is determined from the KEYPS formulation of the diabatic wind profile.

The expression for the neutral case, given in a complementary Annual Report discussion,[6] with the additional normalization becomes

$$\frac{n\,S_W(n)}{u_*^2} = \frac{1.15\ (f/0.46\ \phi_\varepsilon)}{1 + 1.5\ (f/0.46\ \phi_\varepsilon)^{5/3}}$$

$$\text{where } f = \frac{nz}{\bar{U}} . \qquad (4)$$

It can be seen from Figure 1 that there is a slight shift to lower frequencies for the unstable cases but the shape of the spectrum is reasonably well preserved. It is also apparent that for the two unstable cases plotted there is no distinction between them when their respective stabilities are incorporated into the scaling through $\phi_\varepsilon = \phi_M$. In addition, the slight separation of the data for different heights has now disappeared as the varying stability with height has been taken into account. The comparison with the theoretical curve within the inertial subrange is even

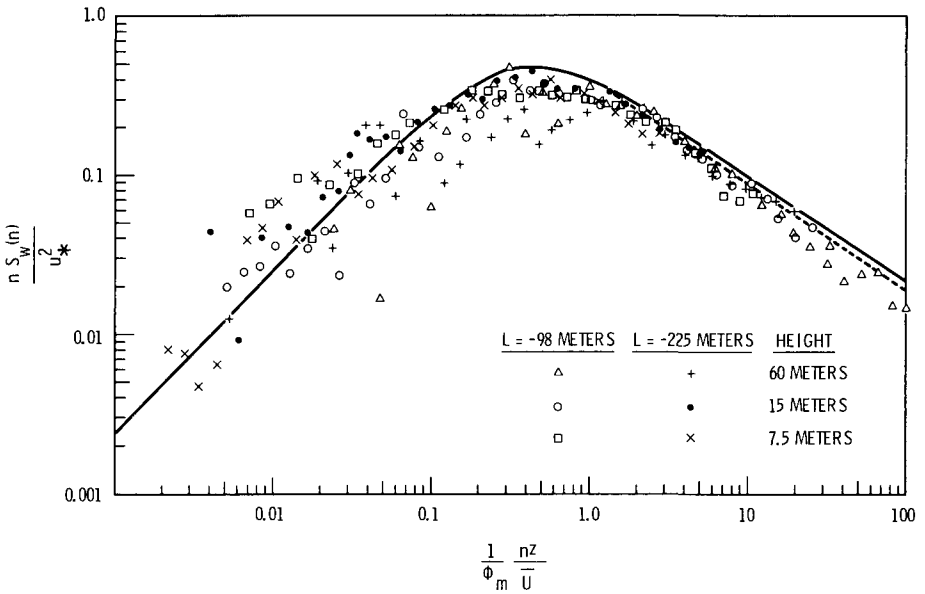

Neg 7111160-3

FIGURE 1. Nondimensional w Spectra for 3 Heights - Two Unstable Cases

more striking, the data being generally less than 10% lower.

Similarly for the stable case shown in Figure 2, in the inertial subrange, the theoretical expression is virtually coincident with the data (from an experiment on July 23, 1970 at 2143 to 2238 PST) when frequency is scaled inversely proportional to $\phi_\varepsilon = \phi_M$. However, these data were only very slightly stable, with L = 4400, so that data with greater stability must be obtained for this evaluation. Nevertheless, it can be seen that for the greater stability at the 60-meter level, the low frequency end of the spectrum is considerably lower than the model for neutral conditions, suggesting that the neutral spectral shape may not be appropriate, through a simple stability scaling, to the stable case.

Much of the uncertainty in modeling diabatic turbulence is in understanding the energy budget, particularly the magnitude of the vertical flux divergence of turbulent energy. The analysis of the two 28-minute periods of unstable data (separated by 14 minutes) shows the magnitude of the flux divergence to be definitely nonzero. However, a one-to-one relationship with -z/L was not found.

Although -L was half as great in the first 28-minute period as in the last period (and, therefore, -z/L greater in the first period), the flux divergence increased sharply with height during the last period,

being less than -z/L through the lowest half of the tower and greater than -z/L in the upper portion. During the first period, there was a consistent increase in the divergence with height up to about 11 meters, and no increase from 11 meters to 45 meters, dropping below -z/L in the upper portion. It appears that adjustments in the flux divergence term to stationary values do not occur in phase with nor as rapidly as in the energy levels themselves and would consequently complicate the modeling of the diabatic spectra.

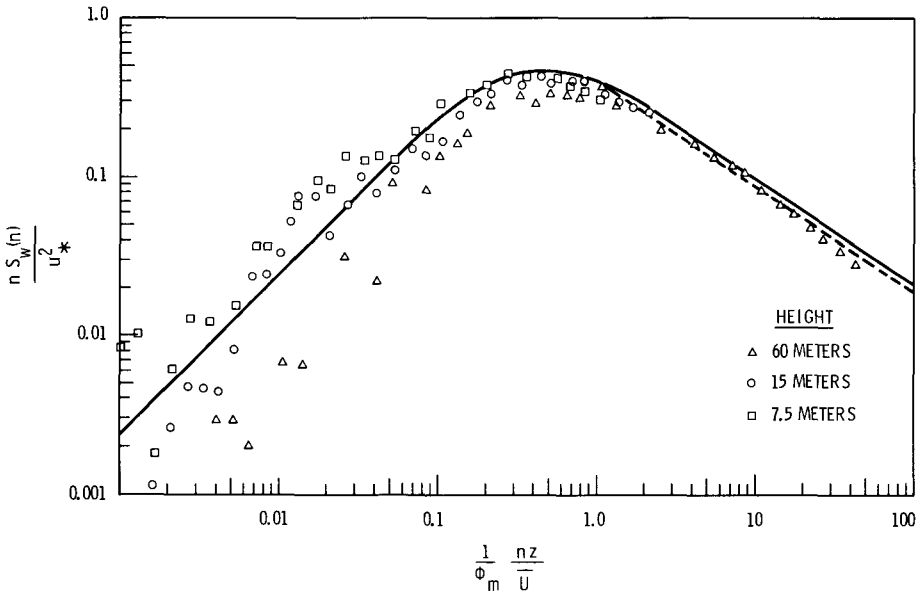

Neg 711160-4

FIGURE 2. Nondimensional w Spectra for 3 Heights - Stable Case

REFERENCES

1. *N. E. Busch and H. A. Panofsky. "Recent Spectra of Atmospheric Turbulence," Royal Met. Society Qtrly. Journ., Vol. 94, 1968.*

2. *D. A. Haugen, J. C. Kaimal and E. F. Bradley. "An Experimental Study of Reynolds Stress and Heat Flux in the Atmospheric Surface Layer," submitted to Royal Met. Society Qtrly. Journ., 1971.*

3. *J. C. Wyngaard and O. R. Cote. "The Budgets of Turbulent Kinetic Energy and Temperature Variance in the Atmospheric Surface Layer," submitted to the Journal of Applied Sciences, 1971.*

4. *C. E. Elderkin. "Atmospheric Turbulence Studies," Pacific Northwest Laboratory Annual Report for 1967 to the USAEC Division of Biology and Medicine, Volume II:*

Physical Sciences, Part 3. Atmospheric Sciences, BNWL-715 3, October 1968.

5. *S. Berman. "Estimating the Longitudinal Wind Spectrum Near the Ground," Royal Met. Society Qtrly. Journ., 91 p. 302, 1965.*

6. *C. E. Elderkin, D. C. Powell and T. W. Horst. Pacific Northwest Laboratory Annual Report for 1970 to the USAEC Division of Biology and Medicine, BNWL 1551, Part 1 (To be published in 1971).*

DIABATIC EFFECTS ON PROFILES OF THE SHEAR STRESS

D. C. Powell

Analysis of two periods of unstable data show the Reynolds stress correlation, $-\overline{u'w'}$, to vary markedly with height across the layer commonly designated as the constant flux layer for the neutral case. Vertical similarity is exhibited when the profiles are plotted versus z/L. By deleting Von Karman's constant from L, a new length, $L_* = kL$, was defined because L_* seemed to be a better measure of the approximate height at which the transition from mechanical turbulence to convective turbulence takes place. Since none of the terms in the standard equation of mean motion were found to be of sufficient magnitude to balance the observed decrease of height of the Reynolds stress, the inclusion of large order advective correlations, in particular, $\overline{w\partial U/\partial z}$ is proposed. In the layer immediately adjacent to the surface roughness elements where the Reynolds stress was observed to increase with height, the distinction between the mean flow and the turbulence deteriorates. Therefore, the applicability of the above equation to this type of turbulence is questioned.

When the temperature lapse rate across the atmospheric boundary layer is unstable, the physical characteristics of the turbulence are known to exhibit a certain transition with height - the transition from so-called mechanical turbulence to so-called convective turbulence. The two correlations that are characteristic of these two types, but not in the same way, are $\overline{u'w'}$ and $\overline{w'T'}$, respectively. The first correlation is intrinsically associated with the vertical shear of the mean wind, which is caused by the presence of the boundary. The second correlation is intrinsically associated with the unstable temperature lapse rate. This correlation induces rotational movements internally and locally, which may be of a scale comparable with the scale of the eddies or mechanical turbulence, or may be of a larger scale.

Consider a low level in the turbulent boundary layer - low enough that $-\overline{u'w'}$ is at or near its maximum absolute value, but high enough that the mean wind $\bar{U}$ is at least an order of magnitude greater than $\sqrt{-\overline{u'w'}}$. At this level, we assume that the value of $-\overline{u'w'}$ is characteristic and call it u^{*2}. Now, at this level the ratio of the magnitudes of $\overline{w'T'}$ and u^{*2} will vary, and obviously the greater the ratio when the first is compared to the second, the shorter the vertical span required for the transition from mechanical to convective turbulence.

A length, L, containing these two terms is found in the buoyancy term of the nondimensional turbulence energy equation:

$$kzg/\bar{T}\left(\frac{\overline{w'T'}}{u_*^3}\right) \equiv \frac{z}{L} \qquad (1)$$

where k is Von Karman's constant, z is the height, g is gravity, and $\bar{T}$ is the mean temperature. The L is the Monin-Obukhov length. The purpose of this paper is to examine the variation with L of the profile of $\overline{u'w'}$. Admittedly, the data sample analyzed is not large enough to make the conclusions more than tentative. Therefore, future analysis will test the same ideas.

PHYSICAL DISCUSSION OF L

Physically, it makes sense to expect the magnitude of L to be such that most of the transition takes place across the layer where z and L are of the same order of magnitude. In order to bring this about, it was found necessary to redefine L without Von Karman's constant.

$$L^* \equiv \frac{-u_*^3}{(g/T)\,\overline{w'T'}} = kL \qquad (2)$$

This appears physically justifiable for the following reason. The simplest boundary layer equation containing k applies strictly to mechanical turbulence:

$$\frac{d\bar{U}}{dz} = \frac{u_*}{kz} \qquad (3)$$

which simply states that the change of mean wind speed with height is the quotient of a characteristic turbulence velocity by a characteristic length. Now, which quantity does k belong with - with z or with u_*? If it belongs with z, its place in L seems inappropriate since L is not a function of z. On the other hand, if it belongs with u_*, inclusion of k to the minus third power in L seems appropriate, since u_*^3 is in L. By using the former assumption, L* of the desired physical characteristics is obtained.

MEASUREMENT ARRAY

The data from which the following analysis was taken were recorded from five logarithmically spaced sensors mounted on one tower, at heights of

60, 30, 15, 7.5 and 3.75 meters. The instruments at 60, 15 and 7.5 meters were sonic anemometers. Stress calculations from the Gill anemometer data have been reconciled with determinations from sonic anemometer data in other studies.

ANALYSIS OF THE DATA

The data were recorded in two almost consecutive 28-minute periods:

1st period 1537-1605, 20 July 1970
2nd period 1619-1647, 20 July 1970

The sky was clear, the temperature in the upper nineties, and the mean wind speed at 7.5 meters about 8 mps. The periods chosen were the most stationary periods over the 70-minute interval of the most unstable data available.

Richardson numbers for the two periods were about -0.3 and -0.1, respectively.

When $-\overline{u'w'}$ is given by height for each period, the values at 30 and 60 meters differ markedly from the 1st to the 2nd period (Table 1).

TABLE 1.

z	$-\overline{u'w'}$ (mps)^2 1st period	$-\overline{u'w'}$ (mps)^2 2nd period
60.00	0.07	0.31
30.00	0.19	0.46
15.00	0.37	0.51
7.50	0.48	0.40
3.75	0.40	0.36

Better correspondence may be achieved if the values are plotted as functions of z/L*. The values of L* for the two periods turn out to be -34 meters and -79 meters, respectively (Table 2).

TABLE 2.

Period	1st	1st	2nd	1st	2nd	1st	2nd	1st	2nd	2nd
-z/L*	1.75	0.87	0.76	0.44	0.38	0.22	0.19	0.11	0.10	0.05
$-\overline{u'w'}$	0.07	0.19	0.31	0.37	0.46	0.48	0.51	0.40	0.40	0.36

The curve for each period is shown in Figure 1.

From Table 2 and the Figure 1, we note the following:

1. The change of the correlation takes place over the height range where z and L* are of the same order of magnitude,
2. The two curves showing the correlation as a function of z/L* for each period are strikingly similar,
3. The correlation is greater during the period of less instability. Since the mean wind speed is also about a half mps greater during the less unstable period, the result implies that the instability may interfere with both the mean wind speed and the $-\overline{u'w'}$ correlation.

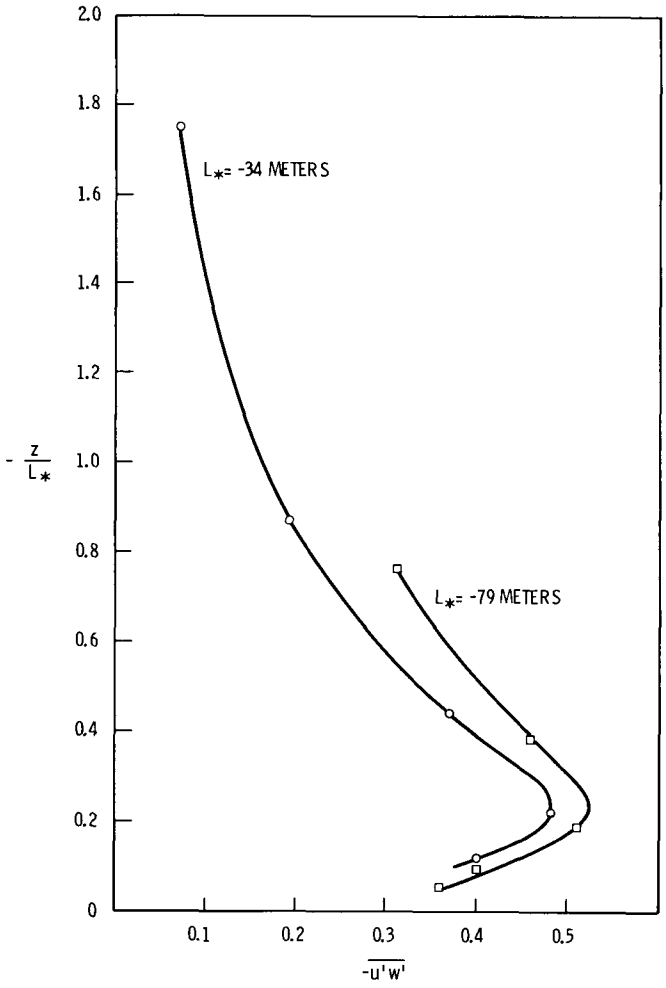

Neg 711160-6

FIGURE 1. Shear Stress as a Function of z/L

APPLICATION OF THE EQUATION OF MOTION

The change of height of $\overline{u'w'}$ is one of the terms in the equation of the mean motion in the longitudinal direction. Since none of the terms in this equation contain any heat flux quantities, explicitly, the arguments of the preceding section must be reviewed in connection with this equation.

The derivation of the usual equation for the mean flow containing the Reynolds stresses requires assuming that there is no correlation between the variation of the mean flow and the variation of the turbulence fluctuation. Otherwise, additional terms would appear in the equation. The assumption is usually taken to mean that the variation of the two parts of the flow is over vastly different time scales.

Using this assumption and also assuming incompressible flow in a nonrotational system, and ignoring the diffusion term, the equation of mean motion in integrated form may be written:

$$\int_{t_o}^{t} \frac{\partial U}{\partial t}\, dt = -\int_{t_o}^{t} \left[U\frac{\partial U}{\partial x} + V\frac{\partial U}{\partial y} + W\frac{\partial U}{\partial z} + \frac{1}{\rho}\frac{\partial P}{\partial x} + \frac{\partial}{\partial z}(uw)\right] dt \qquad (4)$$

where the total instantaneous velocity $U_i(t)$ has been divided into two uncorrelated components, $U_i(t) + u_i'(t)$; $i = 1, 2, 3$. This may be rewritten:

$$\frac{u(t) - u(t_o)}{t - t_o} = -\overline{U\frac{\partial U}{\partial x}} - \overline{V\frac{\partial U}{\partial y}} - \overline{W\frac{\partial U}{\partial z}} - \frac{1}{\rho}\frac{\partial \overline{P}}{\partial x} - \frac{\partial}{\partial z}\overline{u'w'} \qquad (5)$$

where the overscore is a time average over a time period considerably greater than that of the turbulent fluctuations.

The decrease with height of the Reynolds stress ($-\overline{u'w'}$) has been compared numerically with the acceleration term on the left and with the pressure gradient term. For the two 28-minute periods, the acceleration term was calculated to be roughtly -0.54×10^{-3} and -1.44×10^{-3} m sec^{-2}. Since the wind direction was approximately from 320°, the pressure term was computed by selecting stations roughly northwest and southeast of Hanford and using pressure figures on surface maps for the nearest time. This calculation yielded a pressure gradient term on the order of 1.0×10^{-3} m sec^{-2}. Comparing these numbers with values of the decrease with height of the stress term, from Table 1, it is found that values for the latter for the first period are as great as -12×10^{-3} and -15×10^{-3} m sec^{-2}. The greatest value from the second period data is -5×10^{-3} m sec^{-2}. Clearly, at least during the first period, when the instability was the greatest, conditions prevailed that are inconsistent with the assumptions used in deriving Equation (5).

The apparent trouble lies in the assumption that the physics can be meaningfully explained by dividing the total flow into a mean flow and a turbulent flow which are not correlated. The instability could very well induce correlation between the scales of the mean motion and those of the turbulent motions such as $\overline{w\,\partial U/\partial z}$. Physically this term would refer to intermediate scale bursts of positive w that stretch the profile and are thus correlated with lower values of $\partial U/\partial z$. Therefore the term, $\overline{-w\partial U/\partial z}$, added to the right side of Equation (5), should make a positive contribution to the acceleration term on the left, and this could be the necessary convective balance for the change of height of the Reynolds stress.

Plots of the velocities also show considerable meandering of the lateral component during the first period. If this is correlated with $\partial U/\partial y$, the term $\overline{v\partial U/\partial y}$ could also be important.

Figure 1 shows that near the surface the Reynolds stress increases with height up to a certain level. Physically, this can be associated with the increase of the vertical variance with height through the same layer; however, the vertical variance is not one of the terms in the equation of mean motion (5).

In this case the inadequacies of Equation (5) seem even greater than for the layers above, where the Reynolds stress was decreasing with height. This equation, and in fact all classical boundary layer turbulence equations, are derived by assuming that the total flow consists of two characteristic velocities that remain physically distinct, and also distinct, magnitude-wise. These are the advective velocity, $\overline{U}$, and a characteristic turbulence velocity, u*. As a boundary consisting of thickly scattered sagebrush plants (not a canopy) on the order of one-meter height is approached, there is a level at which the two velocities are no longer distinct. This description appears to apply particularly to the unstable case.

Two conclusions, both tentative, may be drawn from the analysis of the data.

1. The Reynolds stress, $\overline{-u'w'}$, is not constant over a constant flux layer during periods of marked instability. The height at which the deterioration of the correlation takes place is related to the Monin-Obukov L, but is much better approximated by L* = kL, where k is Von Karman's constant.
2. The change of height of the Reynolds stress for the most unstable case is not balanced by the appropriate component of the pressure gradient term nor by the acceleration term. Therefore, an equation of mean motion derived by dividing the total motion into a rapidly varying motion superimposed over a slowly varying motion is not applicable when further assumption is made that the motions in the two scales are uncorrelated.

BNWL-1551
Part 1

A NEW EXPRESSION FOR THE LOGARITHMIC WIND LAW

D. C. Powell

The logarithmic wind profile law is the physical result of interactions between the mean flow, characterized by $\bar{U}$, and the turbulence, characterized by u. Although this is mathematically expressed by the logarithmic wind equation, from a physical point of view the equation is somewhat unsatisfying because none of the terms in it are of a form appropriate to express the physical interaction. Seemingly this can be remedied if Von Karman's constant is physically regarded as a function of $\bar{U}$ and u*. Such a function is proposed and presented in this paper although analytical justification of the idea has not been completed.*

The simplest meteorological phenomenon resulting from the interaction between boundary layer turbulence and the mean flow is the logarithmic wind profile. The differential equation expressing this is

$$\frac{d\bar{U}}{dz} = \frac{u_*}{kz} \qquad (1)$$

where $\bar{U}$ is the mean wind speed; u* is a characteristic velocity of the turbulence, assumed invariant across the vertical span to which the law applies; z is a height within this range, and k is Von Karman's constant. By using basic boundary layer theory, it can be shown that $\bar{U}$ and u* are separated by at least one order of magnitude.

Spectral models of turbulence in the neutral boundary layer show the turbulence scaling as a linear function of height. Physically, this means that the characteristic length of the turbulence at height z is directly proportional to z. Therefore, the right side of the logarithmic wind equation expresses the shear as the quotient of the characteristic velocity of the turbulence by the characteristic length of the turbulence, adjusted by what appears to be an empirical scaling factor.

Using u* and z in this manner on the right provides a dimensionally correct equation from the simplest possible arrangement of characteristic values of identical dimension to the dimensional quantities on the left. The physics of the situation is such that the simplest dimensional arrangement suffices. But, from a physical point of view, there must also be a term expressing the physical interaction between the mean flow and the turbulence, without which there would be no logarithmic wind profile. Mathematically, such a term must be dimensionless. All this is obviously present, mathematically it is Von Karman's constant, which is variously evaluated in the neighborhood of 0.35 to 0.40.

The purpose of this paper is to propose a replacement for Von Karman's constant that has the following properties:

1. The expression is a dimensionless function of $\overline{U}$ and u*.
2. The expression is of the appropriate form to express interaction between the flows characterized by the two velocity scales.
3. The expression is either constant or quasi-constant even though the quantity $u^*/\overline{U}$ is a function of height.
4. The expression, which will be in the numerator, will have a numerical value that is included in the range of the reciprocals of 0.35 and 0.40. That is, the numerical value should be from 2.50 to 2.86.

Such an expression is readily available. Mathematically the requirement that $\overline{U}$ and u* remain separated by at least one order of magnitude is equivalent to requiring

$$2.59 < \left(\frac{\overline{U} + u_*}{\overline{U}}\right)^{\overline{U}/u_*} < e < 2.72 \qquad (2)$$

This expression meets all the above requirements. Perhaps, no more than numerical coincidence is involved, but, on the other hand, there may be some physical reason why the logarithmic wind law may be written:

$$\frac{d\overline{U}}{dz} = \left(\frac{\overline{U} + u_*}{\overline{U}}\right)^{\overline{U}/u_*} \left(\frac{u_*}{z}\right) \qquad (3)$$

On the right, the dimensionality is given by the simplest possible arrangement of characteristic values, and the physical interaction is expressed by a classical function of contrasting magnitudes (in this case scales of motion) associated with a mathematical limit. The whole expression appears quite fundamental, and, if it were known a priori, there would be temptation to look for a physical process to which it corresponds. The equation predicts a minimum value of 0.368 for Von Karman's constant, and a maximum value less than 0.40. As such it is, of course, empirically verifiable.

Further heuristic attempts to justify the equation can be made. In boundary layer flow fluid is subjected to two opposing tendencies. It is required to obey the no-slip boundary condition at the boundary and to follow a free-stream velocity at some height above the friction layer. The primary expression of the adjustment is the sheared profile of the mean wind, $d\overline{U}/dz$. However, when the turbulent motions are considered, the instantaneous wind profile is found to consist not only of the primary shear, but also of secondary shears on a much smaller scale corresponding to the largest scale of the turbulence. But these secondary patterns may also break into tertiary patterns of turbulence on a still smaller scale, also contributing to the shear. Physically, there is a limit to how many such smaller scales can be formed, and this limit is imposed by the viscosity of the fluid, which damps out motions smaller than a certain scale. In turbulent flows, the effective viscosity is not the molecular viscosity, but is the eddy viscosity, which is a function of u*, i.e., is a function of the turbulence.

Now look once more at Equation (3). The formation of several succeeding smaller scales of motion with smaller characteristic velocities

corresponds mathematically to the successive powers of $u^*/\bar{U}$ generated by expanding the interaction term. The limit to such expansion, imposed by the eddy viscosity, corresponds to the exponent, $\bar{U}/u^*$. Appropriately the exponent decreases as the turbulence becomes of greater magnitude.

Since no real proof has been offered, counter-examples must be sought. It may be argued that the ratio $\bar{U}/u^*$ may become arbitrarily large, in which case the fluid may no longer be regarded as turbulent. Mathematically, this is true. But physically, the onset of turbulence is known to occur with the breaking of the flow into large eddies, which in turn break into smaller ones as the Reynolds number of the flow is increased. Batchelor[1] writing about homogeneous turbulence states:

"In the early stages of the generation of a field of turbulence of whatever kind, only the smaller wave-numbers of the eventual spectral distribution of energy are excited. These smaller wave-numbers are those which are of the order of magnitude of the reciprocal of the various linear dimensions of the mechanical system generating the turbulence.... Then, as we have seen, the action of the inertia force is to transfer energy to other (and, in general higher) wave numbers and to direct it to the sink provided by viscous dissipation."

This statement means that the turbulence phenomenon itself places an upper limit on the ratio $\bar{U}/u^*$, which complements the lower limit earlier cited.

Finally, it may be remarked that the height at which the correlation $-\overline{u'w'}$ drops significantly below u^{*2} may be expected to be the height beyond which the logarithmic law no longer holds. Also, if at some intermediate height, z_c, in the constant flux layer, the ratio $\bar{U}(z_c)/u^*$ is considered, this ratio is seen to suggest a quotient of inertial forces by viscous forces, and suggests a new form of Reynolds number that is a function of eddy viscosity rather than molecular viscosity.

REFERENCE

1. *G. K. Batchelor. The Theory of Homogeneous Turbulence, Cambridge University Press, Cambridge, England, 1953.*

RADIOISOTOPES AS PARTICLES AND VOLATILES

An objective of this research is to establish the capability to predict particle deposition velocities for atmospheric conditions. This capability is presently being established by measuring particle behavior in the controllable conditions in a wind tunnel. Theory and experiments are leading to the development of models which correctly relate the variables influencing particle deposition.

BNWL-1551
Part 1

DEPOSITION VELOCITIES

G. A. Sehmel and L. C. Schwendiman

Deposition velocities of monodispersed particles were measured for deposition onto a 0.7 cm high plastic grass surface and a smooth electrically grounded brass surface. These deposition velocities range from 0.06 to 12 cm/sec and show a rapid increase with particle diameter. The velocities are a function of the type of deposition surface as well as particle diameter (2 to 28 μm) and friction velocity (11 to 144 cm/sec). The average air velocity does not correlate the deposition velocities, but as a first approximation the deposition velocities are correlated by the friction velocity.

Wind tunnel studies were conducted to measure the deposition velocity of uniform diameter particles from turbulent air flow. The deposition velocity is defined as the particle deposition flux to a surface divided by the concentration above the surface. The initial deposition surfaces, a plastic grass 0.7 cm high and an electrically grounded, smooth brass shim stock, were placed on the floor of the 2 ft × 2 ft cross-section wind tunnel. These surfaces were initially chosen because of their uniformity, difference in surface roughness, dif, ference in electrical properties, and the ease with which the material deposited on them could be determined.

An important objective of this work is to determine the diffusional contribution to particle transport across the boundary layer region near the surface. Particle diffusion can cause the deposition velocity for a smooth surface to be either much greater than or equal to the particle terminal settling velocity. If the surface were rough, the deposition would be even greater than for the smooth surface. This increase for the rough surface would be attributable to particle interception by the protruding elements of surface roughness as well as the increased eddy diffusion. Consequently, the deposition velocity to the smooth surface is considered to be the lower limit for particle transport rates from the atmosphere to earth surfaces.

The deposition velocities of monodispersed uranine particles from 2 to 28 μm in diameter were measured at nominal air velocities of 5, 15 and 30 mph. As shown in Table 1, these velocities yield much different friction velocities, u_*, for the two different surfaces. The friction velocity, an important index to turbulence conditions near the surface, is derived from the velocity profile near the surface. It is defined by the expression

$$u = \frac{u_*}{k} \ln\left(\frac{y + y_o}{y_o}\right), \qquad (1)$$

in which k is Von Karman's constant of 0.4, y_o is an experimentally determined roughness height, and y is the height above the surface at which the velocity, u, is measured.

TABLE 1. Friction Velocities

Air Velocity mph	Friction Velocity, cm/sec Grass	Smooth Brass
5	19	11
15	70	34
30	144	73

Deposition velocities, K_1, are defined as the particle deposition flux divided by the airborne particle concentration 1 cm above the surface. The experimental deposition velocities range from 0.06 to 12 cm/sec. The deposition velocities are compared for the two different surfaces in Figure 1. The average deposition velocities for the grass surface are represented by the solid curves while the deposition velocities for the smooth brass surface are represented by the non-solid line curves. Conclusions drawn from this comparison are the following:

1. The increase in the deposition velocity over the terminal settling velocity, v_t, is caused by eddy diffusion for the smooth surface and both eddy diffusion plus impaction for the grass surface. A comparison of the ratio of K_1/v_t would show that K_1/v_t is a function of surface type as well as of particle diameter. The maxima in this ratio form "bumps" in the curves. As will be discussed in the next section, these "bumps" are caused by the relative importance of eddy diffusion and the terminal settling velocity.
2. The deposition velocity is not simply correlated by the average air velocity.
3. The deposition velocity as a first approximation can be correlated by the friction velocity, u_*.
4. Particle re-entrainment was not observed for the grass surface since the deposition velocity continuously increased with both friction velocity and particle diameter.
5. Particle re-entrainment did occur from the smooth brass surface for the 28 μm diameter particles, but not for the 14 μm diameter particles, at a friction velocity of 73 cm/sec. Indeed, the resulting deposition velocities are even less than would be predicted by the terminal settling velocity.

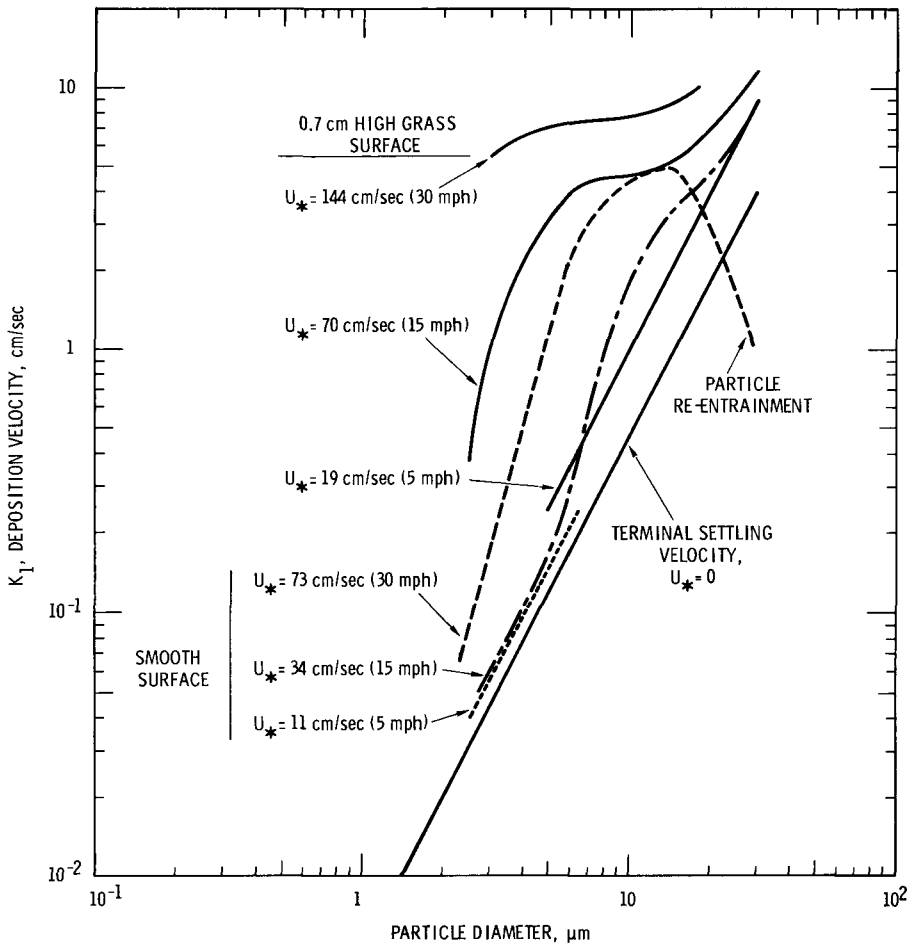

Neg 710293-1

FIGURE 1. Comparison of Experimental Deposition Velocities to Surfaces with Different Roughness

PARTICLE EDDY DIFFUSIVITIES

G. A. Sehmel and L. C. Schwendiman

Particle effective eddy diffusion coefficients, ε/ν, [(Inertial + diffusion)/viscous forces], were calculated from experimental deposition fluxes to a smooth horizontal surface. The ε/ν values are a function of both particle inertia (τ^+), the distance from the surface (y^+), and the air friction velocity (u_*) which is contained in both dimensionless terms. These ε/ν values are greater than those for particle deposition along a vertical surface. Deposition velocities predicted from the correlation show minima of 1.8×10^{-4} to 7.7×10^{-3} cm/sec for particle sizes from 0.066 to 0.54 μm. The minima as well as all deposition velocities are equal to or much greater than predicted from gravitational settling.

A model was developed and evaluated to predict deposition velocities for the lower limit of deposition velocities which might be expected in the atmosphere. This is the case of deposition onto a smooth surface. We have chosen cold rolled brass to represent this surface. The model states that the particle deposition flux, N, is defined by

$$N = -(\varepsilon/\nu + D/\nu)\, u_* \frac{dC}{dy^+} - v_t C, \quad (2)$$

in which ε is the particle diffusivity, D is the Brownian diffusivity, ν is the kinematic viscosity of air, $y^+ = yu_*/\nu$ is the dimensionless distance above the surface, and v_t is the terminal settling velocity. Previously, the problem in using this equation was that the particle eddy diffusivity could not be predicted. The current research progress now permits particle eddy diffusivities to be predicted for the non-isotropic turbulence conditions in the boundary layer over a smooth surface.

Particle eddy diffusivities at a 1 cm height above the grass were calculated using a rearranged form of Equation (2) in which the diffusivities are a function of the experimental particle concentration profile and the experimental deposition flux. The resulting diffusivity ratios, ε/ν, show data scatter, but can be represented reasonably well by a constant $\varepsilon/\nu = 140$ for $y^+ > 350$. These ε/ν values are similar to those for air momentum transfer.

For heights of less than 1 cm, particle effective eddy diffusion coefficients, ε/ν, [(inertial + eddy diffusion)/viscous forces], were calculated from the experimental deposition velocities to the smooth brass surface. For the calculation, Equation (2) was rearranged and integrated to predict deposition velocities from an explicit correlation of the unknown eddy diffusivities. The adjustable parameters in this explicit correlation were adjusted to minimize

the sum of squares between the predicted and experimental deposition velocities. As a test of the final explicit correlation for eddy diffusivities, the predicted deposition velocities are compared with the experimental deposition velocities in Figure 1. The comparison shows that the data fall along the solid line which would indicate perfect agreement. These experimental deposition velocities cover a wide range from 0.06 to 5 cm/sec and represent uranine particle diameters from 2 to 14 μm. The friction velocities were 11, 34 and 73 cm/sec which correspond to nominal air velocities of 5, 15 and 30 mph in the center of the wind tunnel over the smooth brass surface.

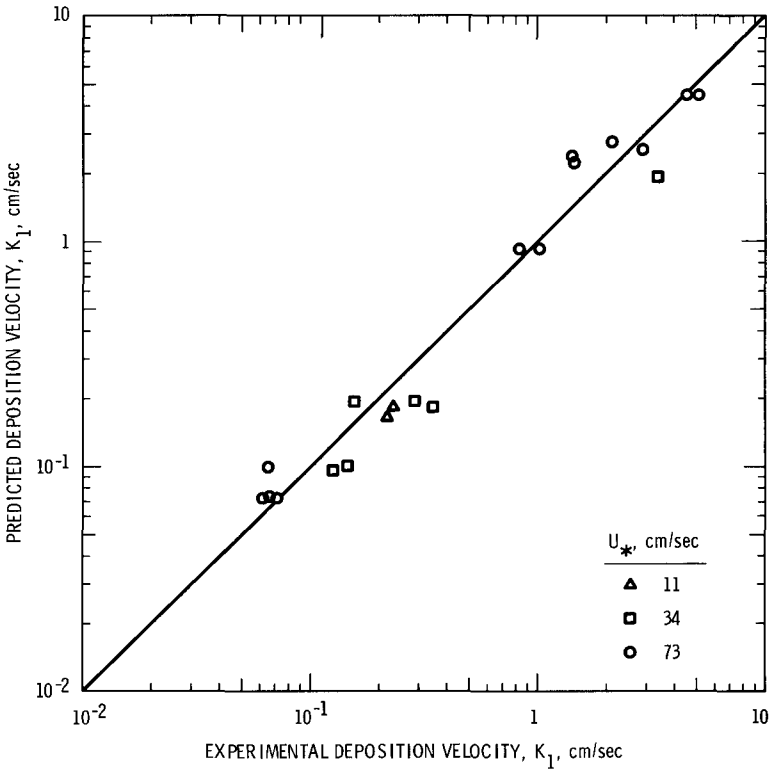

Neg 710273-7

FIGURE 1. Comparison of Predicted and Experimental Deposition Velocities Over a Smooth Horizontal Surface

The correlation for the effective eddy diffusivities is

$$\varepsilon/\nu = 0.018\ (y^+)^{2.0}\ (\tau^+)^{1.7}\ . \quad (3)$$

The effective eddy diffusivities are thus a function of both particle inertia (τ^+), the distance from the surface (y^+), and the air friction velocity which is contained in both dimensionless terms. The dimensionless term τ^+ is equal to $(\rho d^2/18\mu)(u_*^2/\nu)$ in which ρ is the particle density, d is the particle diameter, and μ is the air viscosity. These ε/ν values are greater than the previously reported ε/ν values for particle deposition along a vertical surface. Both correlations show that particle eddy diffusion coefficients are much greater than the eddy diffusion of air momentum for distances from the surface of $y^+ < 20$.

The eddy diffusivity correlation has been used in Equation (2) to predict particle deposition velocities for particle sizes from 10^{-3} to 10^2 μm diameter and for particle densities from 0.5 to 10 g/cm^3. The results show that the deposition velocities can be controlled by either diffusion or the terminal settling velocity. These regions have been identified. For instance, in Figure 1 (see page 160) the deposition velocities first increase rapidly with particle size and then form a "bump" in which the increase is less rapid. This "bump" is caused by a decreasing influence of diffusion and a subsequently more controlling influence of the terminal settling velocity.

Deposition velocities have been known to exhibit an ill-defined minimum region. These minimum deposition velocities are now defined in Figure 2 as a function of friction velocity and particle density. These minimum deposition velocities range from 1.8×10^{-4} to 7.7×10^{-3} cm/sec for particle diameters from 0.066 to 0.54 μm. An extrapolation beyond the friction velocity curve for 145 cm/sec is interpreted to indicate that about a 0.3 μm diameter particle would have minimum deposition at even greater friction velocities.

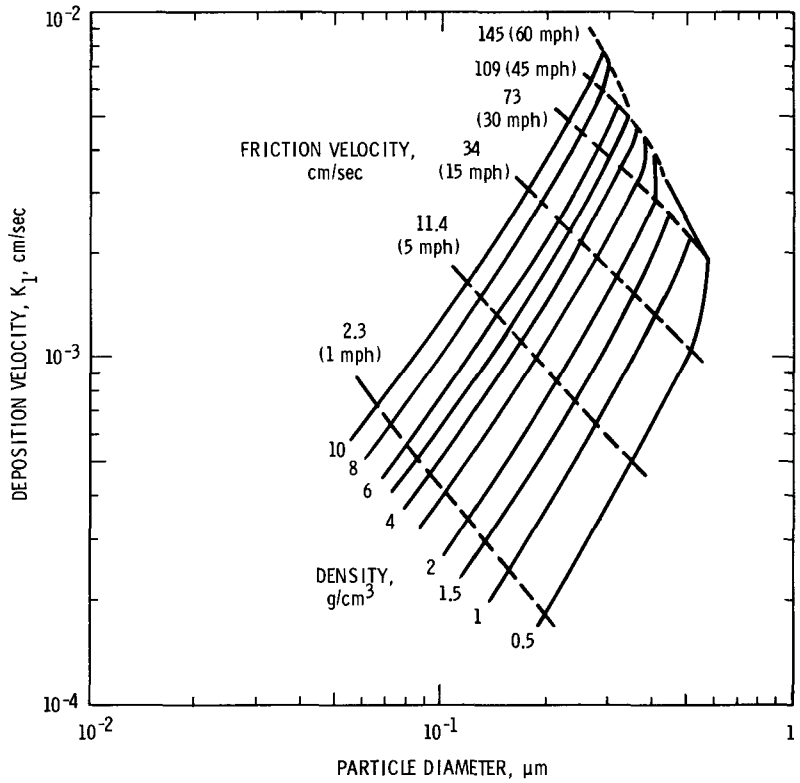

Neg 710273-8

FIGURE 2. Particle Diameter for Minimum Deposition Velocity Over a Smooth Horizontal Surface

ECOLOGICAL MICROMETEOROLOGY AND CLIMATOLOGY

Energy from the sun penetrates the earth's atmosphere in a spectrum of wave lengths. A portion of this energy is reflected and re-radiated back to space; a portion is absorbed by the soil and a portion is transferred to the atmosphere from soil and vegetation through processes of vegetative transpiration, and turbulent heat and moisture exchange. The interactions between soil, vegetation and atmosphere provide a controlling factor in ecosystem developmentt and phenological responses. Micrometeorological investigations attempt to define quantitatively some of these basic interactions.

The interaction between atmosphere and ecological systems can be investigated in a broader sense through the regional climatology. Once the small scale micrometeorological and microclimatological relationships are understood it becomes possible to relate the general input of precipitation, temperature, evaporation and radiation to ecological responses.

Micrometeorological and climatological investigations continue to probe the effect of atmospheric processes on the ecosystems of the Arid Lands Ecology Reserve.

PRECIPITATION PATTERNS ON THE ALE RESERVE

W. T. Hinds* and J. M. Thorp

A network of 26 rain gages was placed on the ALE Reserve in 1968. During the past bioyear (the moisture accumulation and growth season, from October through May), the gages were visited regularly, leading to the pattern of total rainfall and snowfall (in centimeters) on the Reserve shown in Figure 1. The precipitation is strongly influenced by the crosswind obstruction of Rattlesnake Hills, leading to a pronounced maximum in total precipitation below the crest. It is not known at this time whether this maximum is artificially introduced by wind errors, or is in fact real. Likewise, it is not known whether a similar maximum exists on the windward slopes of the Rattlesnake Hills, where successful wheat and grazing operations are numerous.

*Ecosystems Department

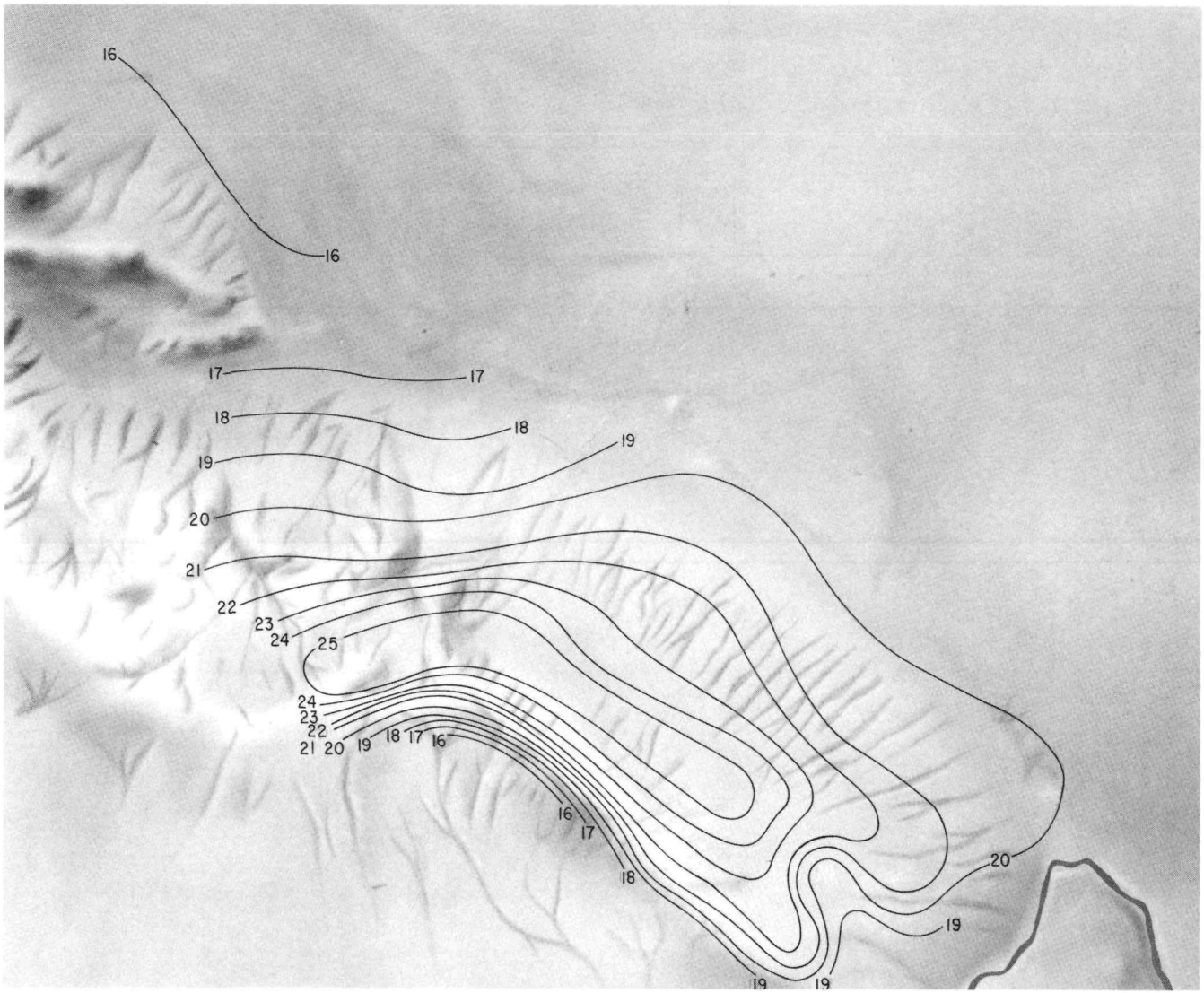

FIGURE 1. Pattern of Total Rainfall and Snowfall on the ALE Reserve, October 1969 Through May 1970, in cm of Water

PRECIPITATION ON THE ALE RESERVE FROM A SUMMER THUNDERSTORM SERIES

J. M. Thorp

A climatological measurement period during the summer of 1970 coincided with a period in which the only precipitation falling on the Arid Lands Ecology (ALE) Reserve was from a series of thunderstorms, thus offering the possibility of a study of precipitation distribution from a thunderstorm.

During the period June 25 to July 14, 1970, weather observers at the Hanford Meteorology Station, located 4 1/2 miles north of the ALE Reserve northern boundary, reported thundershowers over the ALE Reserve on June 26, July 4 and July 13. Precipitation data collected from the ALE network of climatological stations on July 14 have been plotted to show the distribution of total precipitation for the period (Figure 1). Total precipitation for the same period at the Hanford Meteorology Station was less than 0.01 inch.

It is a common observation at the Meteorology Station that the majority of thunderstorms passing over the Hanford Project approach from the southwest quadrant and move off in the northeast quadrant. The thunderstorms originating over these semiarid steppe lands are smaller in dimension, have shorter lives and release smaller amounts of precipitation than the typical midwestern thunderstorm. Isohyets drawn on Figure 1 show that the precipitation swath from all three thunderstorms can easily be delineated by the ALE climatology network, thus permitting an estimate of thunderstorm cell diameter of 3 to 6 miles. The angular shape of the isohyet pattern suggests that two primary storm tracks are responsible for the precipitation pattern. These probable tracks (shown by arrows on Figure 1) agree very well with the thunderstorm observations recorded by the duty forecaster at the Meteorology Station.

Though 5 per cent or more of the total annual precipitation on the ALE Reserve (see "Precipitation Patterns on the ALE Reserve," Hinds and Thorp, in this publication) may fall in a single thundershower, wetted areas are so limited, evaporation rates are so great and showery periods so infrequent during the summer months that available soil moisture from such showers can remain only a few days. Thus, it is doubtful that plants on the ALE Reserve can make significant use of precipitation from summer thundershowers.

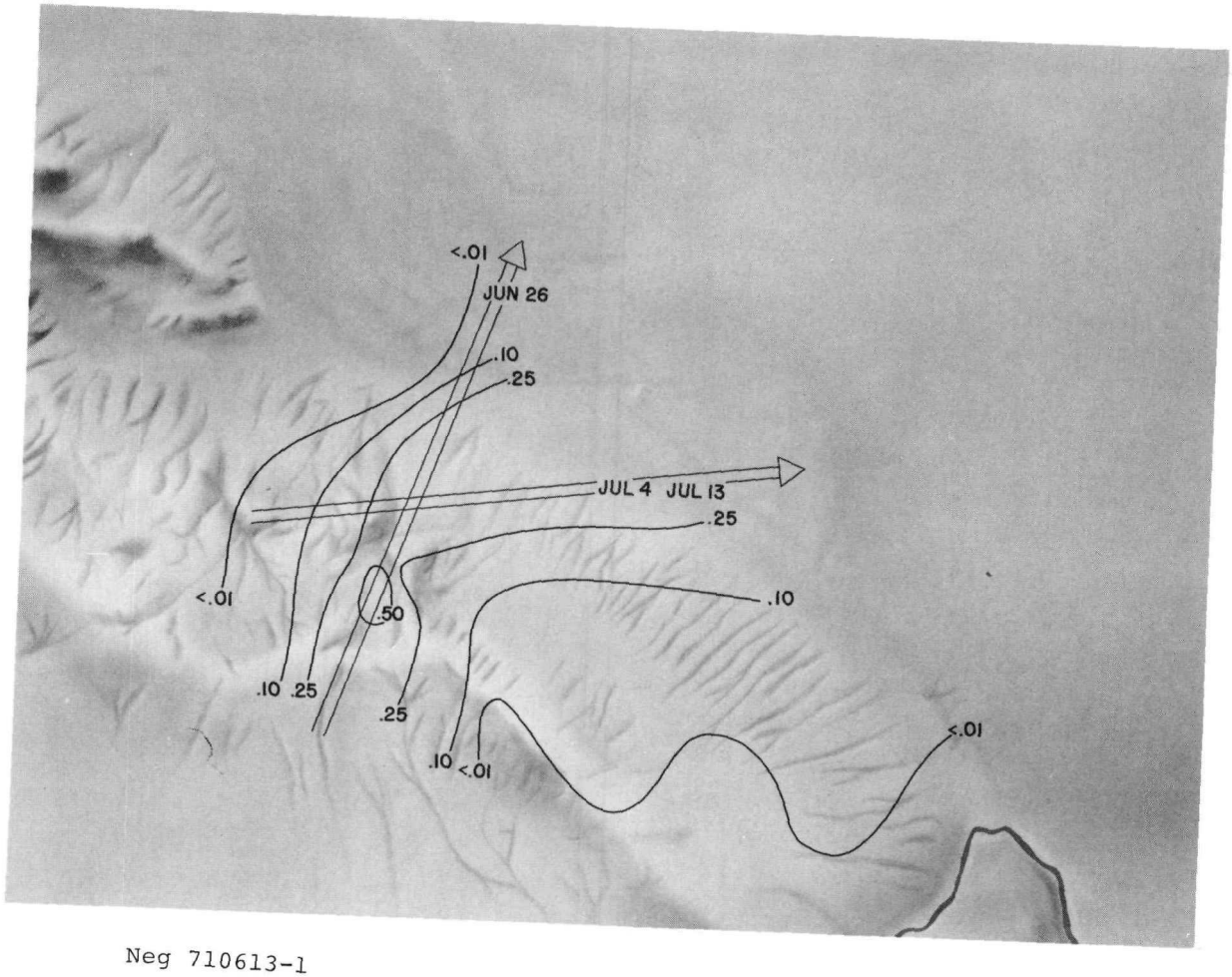

Neg 710613-1

FIGURE 1. Thunderstorm Tracks and Precipitation (Inches of Water) on the ALE Reserve, June 25 to July 13, 1970.

BNWL-1551
Part 1

EVAPORATION FROM BARE AND VEGETATED LYSIMETERS AT DIFFERENT ELEVATIONS

W. T. Hinds*

Small weighing lysimeters, 137 cm^2 in area and 60 cm deep, were placed in two old fields, at elevations of 600 and 1700 ft. At each elevation 33 lysimeters were installed: 21 planted to cheatgrass, and 12 bare. The lysimeters were emplaced February 27, 1970, and weighed at weekly or semiweekly intervals, allowing estimation of evaporation and transpiration between weighings. The results, shown as cumulative totals in Figure 1, indicate a substantial and important difference in cumulative moisture use between the two elevations. At the 1700 ft elevation, more moisture was lost from bare soil than at the 600 ft elevation; but, for most of the spring growing season, a higher rate of transpiration was observed at 600 ft than at 1700 ft. Only after the death of the plants at 600 ft did the transpiration at 1700 ft elevations surpass the lower. The higher evaporation from the bare soil at 1700 ft indicates that at least part of the precipitation excess at the higher elevation (relative to the lower) was biologically unavailable, even during the growing season. A further point noted was that a larger proportion of soil moisture was transpired at the lower elevation (about 37%) than at the higher elevation (about 23%). Thus, these data indicate that the lower elevation provided a more efficient environment for moisture usage by cheatgrass than the higher elevation, partially offsetting the advantages of the higher precipitation totals measured at the higher elevations.

*Ecosystems Department

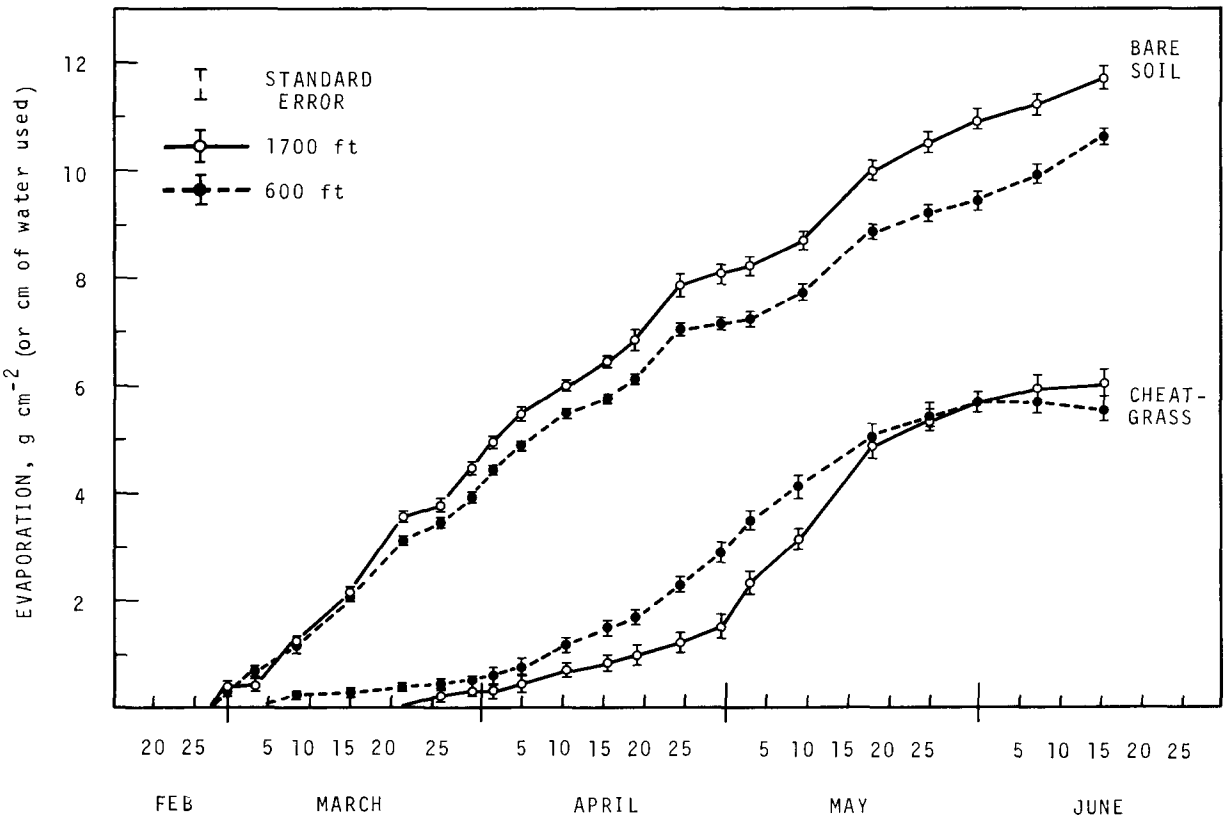

FIGURE 1. Moisture Use of Bare Soil and Cheatgrass Lysimeter Study, Spring 1970.

CLIMATOLOGICAL INSTRUMENTATION ON THE ALE RESERVE - 1970

J. M. Thorp and W. T. Hinds*

The initial climatological network on the Arid Lands Ecology (ALE) Reserve was described in the 1968 Annual Report. Several additions to the network were made in 1970.

Two-point soil thermographs and strip chart hygrothermographs are now in operation at 600 feet, 1600 feet, 2900 feet and 3400 feet (all heights MSL). Propane-heated recording precipitation gages have been placed at the eastern and western extremities of a drainage basin. Other propane gages are at 660 feet and 3400 feet. A standard Weather Bureau type precipitation gage has been placed at 2900 feet. Two portable anemometers with recorders and a portable short wave pyranometer are available for short term micrometeorological and microclimatological investigations.

*Ecosystems Department

BLANK

ATMOSPHERIC RESOURCES DEPARTMENT STAFF

C. L. Simpson - Manager
R. F. Lee - Clerical

R. L. Conley, Jr. - Specialist

Consultants

F. I. Badgley
University of Washington
Seattle, Washington

P. E. Church
University of Washington
Seattle, Washington

M. Miyake
University of British Columbia
Vancouver, B. C., Canada

J. Rosinski
National Center for Atmospheric Research
Boulder, Colorado

ATMOSPHERIC PHYSICS SECTION

C. E. Elderkin - Manager
L. L. Carratt - Clerical

Professional Staff

W. E. Davis
J. C. Draper
A. G. Dunbar
F. O. Gladfelder
T. W. Horst
F. D. Lloyd
P. W. Nickola
D. C. Powell
J. M. Thorp
R. K. Woodruff

Technical Staff

O. B. Abbey
V. T. Henderson
D. M. Hughey

ATMOSPHERIC ANALYSIS SECTION

M. A. Wolf - Manager
H. A. Garner - Clerical

Professional Staff

H. G. Daubek
E. W. Lusty
J. V. Ramsdell

Technical Staff

D. W. Glover
R. E. Wheeler

SYNOPTIC METEOROLOGY SECTION

E. H. Phinney - Manager

Professional Staff

O. P. Gifford
D. E. Jenne
R. E. Kerns
D. J. Newland
W. A. Stone

AIR POLLUTION CHEMISTRY SECTION

L. C. Schwendiman - Manager
D. L. Barrett - Clerical

Professional Staff

L. A. du Plessis
J. M. Hales
J. Mishima
G. A. Sehmel

Technical Staff

S. L. Sutter

PRECIPITATION PHYSICS SECTION

W.G.N. Slinn - Manager
H. A. Garner - Clerical

Professional Staff

M. T. Dana
B. C. Scott
J. W. Sloot

Technical Staff

M. C. Miller

ASSOCIATED PERSONNEL

W. T. Hinds - Soil Relationships Section, Ecosystems Department
J. D. Ludwick - Radiological Chemistry Section, Radiological Sciences Department
R. W. Perkins - Radiological Chemistry Section, Radiological Sciences Department
H. G. Rieck, Jr. - Radiological Chemistry Section, Radiological Sciences Department
D. E. Robertson - Radiological Chemistry Section, Radiological Sciences Department
W. B. Silker - Radiological Chemistry Section, Radiological Sciences Department
C. W. Thomas - Radiological Chemistry Section, Radiological Sciences Department
K. E. Willis, Jr. - Finance Department, assigned to Environmental and Life Sciences Division
J. A. Young - Radiological Chemistry Section, Radiological Sciences Department

GENERAL MAINTENANCE SERVICES

G. G. Matthews - Foreman

Carpenter - E. C. Bolin

Instrument - J. D. Hughes
R. D. Jensen
R. N. Martin
H. M. Osborn

Electrical - H. E. Jones

Pipefitter - R. R. Brodaczynski

Millwright - L. F. Conley

BLANK

PUBLICATIONS AND PRESENTATIONS

DOCUMENTS

P. W. Nickola, J. V. Ramsdell, Jr. and J. D. Ludwick. Detailed Time-Histories of Concentrations Resulting from Puff and Short-Period Releases of an Inert Radioactive Gas: A Volume of Atmospheric Diffusion Data. BNWL-1272. February, 1970

W. E. Davis and B. C. Scott. Diabatic Trajectories in the Lower Atmosphere. BNWL-SA-2465. March, 1970.

Staff of the Atmospheric Resources Department. Pacific Northwest Laboratory Annual Report for 1969 to the USAEC Division of Biology and Medicine, Volume II: Physical Sciences, Part 1. Atmospheric Sciences, BNWL-1307. Battelle-Northwest, Richland, Washington, June, 1970.

PUBLICATIONS

A. P. Wehner, G. A. Sehmel, L. C. Schwendiman and J. G. Harter. "Unipolarly Charged Aerosols: Effect on Deposition in Tubes and on Droplet Size," Arch. Environ. Health, vol. 20, pp. 28-36. January, 1970.

J. V. Ramsdell, Jr. and W. T. Hinds. "Concentration Fluctuations and Peak-to-Mean Concentration Ratios in Plumes from a Ground Level Continuous Point Source," BNWL-SA-2909. February, 1970. Accepted for publication in Atmospheric Environment, 1971.

G. A. Sehmel. "Particle Deposition from Turbulent Air Flow," J. of Geophysical Research, vol. 75, no. 9, pp. 1766-1781. March 20, 1970.

W.G.N. Slinn and S. F. Shen. "Anisotropic Brownian Diffusion and Precipitation Scavenging of Submicron Particles," J. Geophys. Res., vol. 75, no. 12, pp. 2267-2270. April, 1970.

J. D. Ludwick and C. L. Simpson. "Grass and Ground Deposited Zinc Sulfide During Atmospheric Diffusion Tests Using Phosphorescence Decay Analysis," BNWL-SA-3192. Submitted for publication in Environmental Science and Technology, April, 1970.

P. W. Nickola, J. D. Ludwick and J. V. Ramsdell, Jr. "An Atmospheric Tracer Technique Employing ^{85}Kr and Use of this Technique in Defining Puff Dimensions and Transport Speed." BNWL-SA-3359. May, 1970. Accepted for publication in Issue 8(4) of Isotopes and Radiation Technology. 1971.

P. W. Nickola, J. D. Ludwick and J. V. Ramsdell, Jr. "An Inert Gas Tracer System for Monitoring the Real-Time History of a Diffusing Plume or Puff," Journal of Applied Meteorology, vol. 9, no. 4, pp. 621-626. August, 1970.

M. T. Dana. "The Electric Charges on Raindrops in Continuous and Showery Rainfall," submitted to J. Atmos. Sci., September, 1970.

W.G.N. Slinn and J. M. Hales. "A Re-evaluation of the Role of Thermophoresis as a Mechanism of In- and Below-Cloud Scavenging," BNWL-SA-3367. Submitted for publication in J. Atmos. Sci., October, 1970.

G. A. Sehmel. "Particle Sampling Bias Introduced by Anisokinetic Sampling and Deposition within the Sampling Line," Amer. Ind. Hyg. Assoc. J., vol. 31, pp. 758-771. Nov.-Dec., 1970.

G. A. Sehmel. "Complexities of Particle Deposition and Re-entrainment in Turbulent Pipe Flow," Aerosol Science, vol. 1, December, 1970.

W.G.N. Slinn and A. G. Gibbs. "The Stochastic Growth of a Rain Droplet," BNWL-SA-3547. Accepted for publication in J. Atoms. Sci., December,]970.

G. A. Sehmel. "Particle Deposition from Turbulent Air Flow," International Symposium on Atmospheric Trace Constituents and Atmospheric Circulation, Edited by E. A. Martell, K. K. Turekian, American Geophysical Union, Washington, D.C., pp. 1766-1781. 1970.

W.G.N. Slinn and S. F. Shen. "Brownian Diffusion in a Nonuniform Gas," BNWL-SA-2091. Accepted for publication in J. Stat. Phys. vol. 3. 1971.

W.G.N. Slinn, S. F. Shen and R. M. Mazo. "A Kinetic Theory of Diffusely Reflecting Brownian Particles," J. Stat. Phys., vol. 2, no. 3, pp. 251-265, 1970.

W. T. Hinds. "Diffusion Over Coastal Mountains of Southern California," Atmospheric Environment, vol. 4, pp. 107-124. 1970.

PRESENTATIONS

W.G.N. Slinn. "The Equipartition and Fluctuation-Dissipation Theorems, Revisited," presented at the 1970 Regional SIAM Meeting, Portland State University, March, 1970. (To be abstracted in SIAM Review.)

The following presentations were made at the Precipitation Scavenging (1970) Symposium, Richland, Washington, June 2-4, 1970 and published in Precipitation Scavenging (1970). R. J. Engelmann and W.G.N. Slinn, Coordinators. AEC Symposium Series No. 22. Available from NTIS as CONF-700601. December, 1970.

R. W. Perkins, C. W. Thomas, J. A. Young and B. C. Scott. "In-Cloud Scavenging Analysis from Cosmogenic Radionuclide Measurements."

M. T. Dana. "Scavenging of Soluble Dye Particles by Rain."

J. M. Hales, J. M. Thorp and M. A. Wolf. "Washout of SO_2 from the Plume of a Coal-Fired Power Plant."

W.G.N. Slinn and J. M. Hales. "Phoretic Processes in Scavenging."

G. A. Sehmel. "Turbulent Deposition of Monodispersed Particles on Simulated Grass," BNWL-SA-3214. Presented at the Third Rochester International Conference on Environmental Toxicity, University of Rochester, June 18-20, 1970. (To be published in Assessment of Airborne Particles.)

G. A. Sehmel. "Particle Collection Efficiencies for 0.035 Inch Diameter Wires," BNWL-SA-3251. Presented at the Third Rochester International Conference on Environmental Toxicity, University of Rochester, June 18-20, 1970. (To be published in Assessment of Airborne Particles.)

J. Mishima. "Some Observations on Noble Gas Partitioning in Dynamic Air-Water Systems." 11th Air Cleaning Conference, Richland, Washington. August 28, 1970.

M. T. Dana. "The Electric Charge on Olympic Peninsula Raindrops," Pacific Northwest Regional Meeting, American Geophysical Union, Tacoma, Washington, October 14-16, 1970.

DISTRIBUTION

OFFSITE

No. of Copies	
1	AEC Chicago Patent Group G. H. Lee
17	AEC Division of Biology and Medicine N. F. Barr T. M. Beasley H. D. Bruner W. W. Burr R. Cooper C. W. Edington R. J. Engelmann J. D. Goldstein J. Z. Holland J. S. Kirby-Smith S. A. Lough W. F. Marlow J. E. Miller C. L. Osterberg J. R. Totter H. Wasson R. W. Wood
1	AEC Division of Production W. L. Lennemann
1	AEC Division of Reactor Development & Technology Chief, Environmental & Sanitary Engineering Branch
194	AEC Division of Technical Information
2	Argonne National Laboratory P. F. Gustafson J. Kline
2	Atomic Energy of Canada Limited Chalk River, Ontario C. A. Mawson I. Ophel
1	Atomic Energy Establishment Trombay Bombay 73, India A. K. Ganguly
1	Atomic Energy Research Establishment Harwell, Berks, England Librarian
1	Australian AEC Post Office Coogee New South Wales, Australia A. W. R. Wilson
3	Brookhaven National Laboratory L. P. Hatch M. E. Smith G. M. Woodwell
5	Commissariat a l'Energie Atomique Centre d' Etudes Nucleaires de Cadarache BP n°, 13- St Paul les Durance, France C. Gailledreau
4	Centre d' Etudes Nucleaires de Saclay P. O. Box 2, Saclay Gif-sur-Yvette (S & O) France A. Barbreau F. Duhamel A. Menoux P. Slizewicz
1	Comision Nacional de Energia Atomica Buenos Aires, Argentina E. Vander Elst
1	Commonwealth Scientific and Industrial Research Organization Aspendal, Victoria, Australia B. B. Hicks
1	Commonwealth Scientific & Industrial Research Organization 314 Albert Street, P. O. Box 89 East Melbourne, Victoria Australia 3002 Librarian
2	du Pont Company, Aiken B. C. Rusche W. B. Scott
1	du Pont Company, Wilmington V. R. Thayer
1	ENEA (OECD) Health & Safety Office 38, Blvd. Suchet Paris XVI, France E. Wallauschek

No. of Copies

1 Eurochemic Library
Mol, Belgium
Librarian

1 Geological Survey of the United Kingdom, Water Division
Stevenson Buchan

1 Geological Survey of the United States
Washington 25, D.C.
M. King Hubbert

1 George Washington University
Washington, D.C.
C. R. Naeser

1 Geotechnical Corporation
Box 28277
Dallas 28, Texas
W. B. Heroy

1 Gesellschaft Kernforschung mbH
Karlsruhe 5, West Germany
H. Krause

1 Health & Safety Laboratory
New York City
John Harley

1 International Atomic Energy Agency
Vienna 1, Kaerntnerring 11, Austria
Director, Division of Health, Safety and Waste Management

2 Lawrence Radiation Laboratory
Livermore
G. H. Higgins
J. B. Knox

1 Los Alamos Scientific Laboratory
J. W. Healy

5 Ministry of Agriculture, Fisheries, & Food Laboratory
Lowestoft, Suffolk, England
Librarian

2 National Institute of Radiological Sciences
250, Kurosuna Cho,
Chiba-shi, Japan
M. Saiki
M. Suzuki

No. of Copies

3 Oak Ridge National Laboratory
S. I. Auerbach
K. Z. Morgan
E. G. Struxness

1 World Health Organization
Geneva, Switzerland
R. L. Dobson

1 World Meteorological Organization
Geneva, Switzerland
Librarian

ONSITE

1 AEC Chicago Patent Group
R. M. Poteat

8 AEC Richland Operations Office
N. W. Fraser
W. E. Lotz
C. R. Qualheim
M. R. Schneller
M. W. Tiernan
D. G. Williams
Technical Information Library (2)

1 Atlantic Richfield Hanford Company
D. J. Brown

2 Douglas United Nuclear
P. C. Jerman
DUN Files

1 Hanford Environmental Health Foundation
P. A. Fuqua

286 Battelle-Northwest
F. W. Albaugh
E. L. Alpen
W. J. Bair
N. E. Ballou
C. A. Bennett
W. J. Clarke
G. L. Culp
G. M. Dalen
R. L. Dillon
C. E. Elderkin (30)
S. J. Farmer
R. F. Foster
J. J. Fuquay (25)
W. A. Haney
J. C. Hampton
A. J. Haverfield

No. of
Copies

Battelle-Northwest (Continued)

J. F. Honstead
V. G. Horstman
F. P. Hungate
D. R. Kalkwarf
L. J. Kirby
H. A. Kornberg
H. V. Larson
J. M. Nielsen
T. P. O'Farrell
D. E. Olesen
R. F. Palmer
J. F. Park
R. S. Paul
D. W. Pearce
R. W. Perkins
E. H. Phinney
P. M. Potter
W. D. Richmond
W. C. Roesch

Battelle-Northwest (Continued)

L. C. Schwendiman
A. J. Scott
W. G. N. Slinn (75)
W. H. Swift
C. L. Simpson (100)
J. A. Strand
M. F. Sullivan
W. L. Templeton
R. C. Thompson
C. J. Touhill
C. M. Unruh
B. E. Vaughan
W. R. Wiley
W. E. Wilson
N. A. Wogman
M. A. Wolf
Biology Library (2)
Technical Information (5)
Technical Publications (2)